Towards Sustainable Materials: Earth Abundant Elements for Transformations of CO_2 and Epoxides

by

© Kori A. Andrea

A Thesis submitted to the School of Graduate Studies in partial fulfillment of the
fulfillment of the requirements for the degree of

Doctor of Philosophy

Department of Chemistry
Memorial University of Newfoundland

June 2021

St. John's Newfoundland and Labrador

Abstract

The utilization of carbon dioxide (CO_2) as a renewable C-1 feedstock has received significant attention in recent years. In particular the coupling and/or polymerization of epoxides and CO_2 to yield cyclic and/or polycarbonates is a growing area of research leading to the production of sustainable materials. Due to the high thermodynamic stability of CO_2 these reactions typically proceed in the presence of a metal catalyst, while in the recent literature organocatalysts have found promising results. In this thesis, both iron and boron containing catalytic systems are reported that have shown excellent activity for these reactions. In **Chapter 2**, a series of iron(III) chloride and iron(III) μ-oxo compounds supported by tetradentate amino-bis(phenolate) ligands containing a homopiperazinyl backbone were prepared and characterized by electronic absorption spectroscopy, magnetic moment measurement, and MALDI-TOF mass spectrometry. We provide evidence that an epoxide deoxygenation step occurs when employing monometallic iron(III) chlorido species as catalysts. This affords the corresponding μ-oxo compounds which can then enter their own catalytic cycle. Deoxygenation of epoxides during their catalytic reactions with carbon dioxide is frequently overlooked and should be considered as an additional mechanistic pathway when investigating catalysts. Through extensive studies of the iron systems reported herein, we have shown a structure/geometry of the catalyst and product selectivity relationship. This study (reported in **Chapter 3**) demonstrated that the highly modifiable aminophenolate ligands can be tailored to yield iron complexes for both CO_2/epoxide coupling and ring-opening copolymerization activity.

Metal-free catalysts have gained interest in the recent years as alternatives for these transformations but is still in its infancy compared to transition metal-based systems. In **Chapter 4**, we have shown that arylboranes can be used as catalysts in these transformations to produce either cyclic or polycarbonates. Kinetic studies revealed a process that was first-order in all reagents with the exception of CO_2, where an inverse dependence was shown. Building upon this report and taking into account the extensive research focused on Frustrated Lewis pairs and their ability to catalyze a range of transformations such as hydrosilylations I chose to combine these two ideas. Via assisted tandem catalysis BPh_3 could first catalyze the copolymerization of epoxides and CO_2 to give polycarbonates and then with the addition of a silane could catalyse the hydrosilylation of these materials. This work is reported in **Chapter 5**.

Finally, **Chapter 6** reports the same arylborane systems as a catalyst for the block copolymerization of epoxides, CO_2 and anhydrides in a controlled fashion. Further, by switching from BPh_3 to the more Lewis acidic BCF, the carbonate block in the obtained polymer could be selectivity degraded to the corresponding cyclic carbonate. This is the first report of an arylborane for both the polymerization of epoxides, anhydrides, and CO_2 as well as the first for the selective depolymerization of these materials.

Acknowledgements

First and foremost, I would like to thank my supervisor, Dr. Francesca Kerton for her support, guidance and encouragement throughout my degree. I am so grateful for all she has done for me over the past 5 years and I have learned so much under her guidance and supervision. I would not be the scientist I am today without her. Secondly, I would like to thank my committee members Dr. Christopher Kozak and Dr. Stephanie MacQuarrie for their guidance, feedback and support throughout my doctoral studies. I truly believe the key to a successful research career is to have a strong support system of mentors behind you. I would also like to thank Dr. Andrew Weller and his research team (University of Oxford, now York University, UK) for allowing me to spend time in his research group at the University of Oxford as a Michael Smith Foreign study exchange student from June-December 2019. This was one of the best experiences of my life and allowed me to build friendships that will last a lifetime.

A special thank you to Dr. Céline Schneider for NMR training, experiments and data interpretation, Dr. Stefana Egli and Linda Windsor for MALDI-TOF training, Nick Ryan for IR training, and Dr. Michael Katz for X-ray crystallography discussions and life advice.

A heartfelt thanks to all members of the Green Chemistry and Catalysis group at Memorial University both past and present who have made this experience so memorable. Special thanks to Jennifer Murphy, Kenson Ambrose, Tim Anderson, Erika Butler, Hart Plommer, Juliana Vidal, and Dakshita Jagota for all the laughs, coffee breaks and pub nights. I'm so thankful for your friendship and support over the years, you all have not only made this a successful but an enjoyable experience. Special thank you to all co-authors on my published work. While for those papers included in this thesis, I am the principal author, the work was completed with the help of a strong team of researchers that I was fortunate to work alongside.

I would also like to thank NSERC (Canada Graduate Scholarship-Masters, Vanier Canada Graduate Scholarship and Michael Smith Foreign Study Supplement and Dr. Kerton's research grant), Department of Chemistry, School of Graduate Studies (SGS), Graduate Student's Union (GSU) and Memorial University for funding. The funding obtained through these organizations have allowed me to focus entirely on my research without the added financial burden.

Lastly, I would like to thank my strong support system composed of my family and close circle of friends. To my parents (Paul and Rhonda) and younger brother Vincent, thank you for always believing in me and being an ear to listen.

Table of Contents

List of Tables

List of Figures

List of Schemes

List of Abbreviations and Symbols

(°): degrees

1,3-CHDO: 1,3-cyclohexadiene oxide

1,4-CHDO: 1,4-cyclohexadiene oxide

α-Me7CC: 4-methyl-1,3-dioxepan-2-one

β-Me7CC: 5-methyl-1,3-dioxepan-2-one

μ_{eff}: magnetic moments

χ_m: magnetic susceptibility

Å: Ångstrom (10^{-10} m)

AGE: allyl glycidol ether

AIBN: azobisisobutyronitrile

AN: acceptor number

BCF: tris(pentafluorophenyl)borane

BPh_3: triphenylborane

BO: 2-benzyloxirane

CDA: *cis*-4-cyclohexene-1,2-dicarboxylic anhydride

$CDCl_3$: deuterated chloroform

CHC: cyclohexene carbonate

CHO: cyclohexene oxide

CO_2: carbon dioxide

COS: carbonyl sulfide

Đ: dispersity (M_w/M_n)

DBU: 1,8-diazobicyclo[5.4.0]undec-7-ene

DMAP: 4-dimethylaminopyridine

DMAEMA: dimethylaminoethyl methacrylate

DOSY: diffusion ordered spectroscopy

DOX: doxorubicin

DSC: differential scanning calorimetry

DTMeAB: N,N,N-trimethyl-1-dodecana-minium bromide

ECH: epichlorohydrin

EO: ethylene oxide

Fc: ferrocene

FIA: fluoride ion affinity

FLP: frustrated Lewis pair

FTIR: fourier transform infrared (spectroscopy)

GC: gas chromatography

GL: glycidol

GPC: gel-permeation chromatography

GPE: glycidol phenyl ether

h: hour

HIA: hydride ion affinity

LO: limonene oxide

MA: malic anhydride

MALDI-TOF: matrix assisted laser desorption/ionization time of flight

MHS: Mark-Houwink Sakurada

NMR: nuclear magnetic resonance (spectroscopy)

PAH: phthalic anhydride

PCHC: polycyclohexene carbonate

PEG: polyethylene glycol

PO: propylene oxide

PPC: polypropylene carbonate

PPO: polypropylene oxide

PPNCl: bis(triphenylphosphine)iminium chloride

PS: polystyrene

PVCHC: poly(vinylcyclohexene) carbonate

ROAC: ring-opening alternating copolymerization of epoxides and cyclic anhydrides

ROCOP: ring-opening copolymerization

ROP: ring-opening polymerization

RSC: redox-switchable catalysis

SA: succinic anhydride

scCO_2: supercritical carbon dioxide

SO: styrene oxide

T: temperature

t: time

TBAB: tetrabutylammonium bromide

TIP: temperature independent paramagnetic contribution

T_g: glass transition temperature

TBD: 1,5,7-Triazabicyclo[4.4.0]dec-5-ene *t*BGE: *tert*-butyl glycidol ether

TOF: turnover frequency

TON: turnover number

TPAT: phenyltrimethylammonium tribromide

UV-vis: ultraviolet-visible (spectroscopy)

VCHO: vinylcyclohexene oxide

ZROP: zwitterionic ring-opening polymerization

List of Appendices

Overall Thesis Co-authorship Statement

The majority of this thesis has been peer reviewed by experts in the field and published in well-respected scientific journals. Throughout the thesis, prior to each chapter, a co-authorship statement is included, explaining each author's contribution to the chapter. Only works that contributed to a first author paper are included herein. In addition to these 6 publications, during my time as a doctoral student at Memorial University, I have also been a co-author on the following publications below.

In 2019, I was awarded an NSERC Michael Smith Foreign Study Supplement. Through this scholarship I spent 6 months in the group of Prof. Andrew S. Weller at the University of Oxford (June 2019-December 2019). At Oxford, I worked on the development of cobalt and rhodium catalysts for the synthesis of polyaminoboranes. My time at Oxford resulted in co-authorships on the following papers:

D. E. Ryan, **K. A. Andrea**, J. J. Race, T. M. Boyd, G. C. Lloyd–Jones and A. S. Weller* Amine-Borane Dehydropolymerization using Rh-based Pre-Catalysts: Resting State, Chain-Control and Efficient Polymer Synthesis. *ACS Catal.*. **2020**, 10, 7443

T. M. Boyd, **K. A. Andrea**, K. Baston, A. Johnson, D. E. Ryan, A. S. Weller,* A Simple Cobalt–Based Catalyst System for the Controlled Dehydropolymerisation of $H_3B{\cdot}NMeH_2$ on the Gram-Scale *Chem. Commun.*. **2020**, 56, 482.

I was also a co-author on a paper from a collaborative project between Dr. Glen Briand (Mount Allison University) and Dr. Francesca Kerton studying indium complexes as catalysts for coupling reactions between carbon dioxide and epoxides:

K. A. Andrea, A. R. Beckett, G. G. Briand*, S. A. Martell, J. Masuda, K. M. Morrison, E. M. T. Yammine. Synthesis and Structural Characterization of Methylindium Imino/Aminophenolates: Comparison to Aluminum Analogues and Reactivity Toward the Coupling Reactions of Carbon Dioxide with Epoxides. *J. Organomet. Chem.*. **2020**, 919, 12130

Co-authorship Statement

Chapter 1: Introduction and Literature Review

A significant portion of this chapter has been published in the following two review articles:

Ring-Opening Polymerizations and Copolymerizations of Epoxides using Aluminum- and Boron-Centered Catalysts
European Polymer Journal, **2019**, 120, 109202
Special Issue: Ring-Opening Polymerization

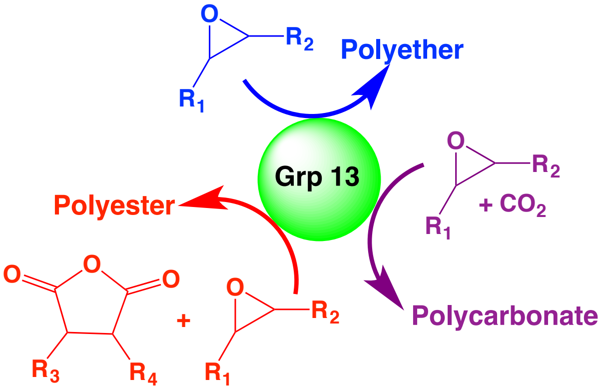

Authors: Kori A. Andrea†, Hart Plommer†, and Francesca M. Kerton*
†Each author contributed equally

K. A. Andrea was responsible for the introduction of this paper, along with all sections discussing literature on boron-centered catalysts for these transformations, while H. Plommer wrote the sections focused on aluminum-centered systems. F. M. Kerton oversaw, edited and directed the completion of this manuscript.

Iron-Catalyzed Reactions of CO_2 and Epoxides to Yield Cyclic and Polycarbonates
Polymer Journal, **2021**, 53, 29-46
Special Issue: CO_2: Capture of, utilization of and degradation into

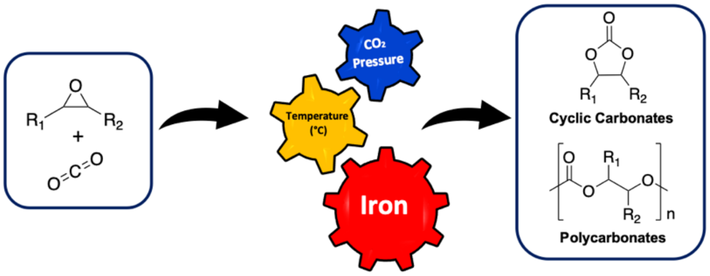

Authors: Kori A. Andrea and Francesca M. Kerton*

K. A. Andrea was responsible for all literature review and drafting the initial manuscript.
F. M. Kerton oversaw, edited and directed the completion of this manuscript.

Chapter 1 Introduction and Literature Review

1.1 Green Chemistry

Green Chemistry is an initiative that aims to design new chemical processes and modify existing ones in an attempt to reduce waste and unwanted hazardous reagents and by-products. This concept began to emerge in the late 1990s, largely due to the need to develop chemical processes that are both environmentally benign and economically feasible.[1] In 1998, Paul Anastas and John Warner published the 12 Principles of Green Chemistry, which are essentially a set of 'rules' researchers can use as a guide, allowing them to be conscious of potential waste and hazards prior to designing new chemicals or processes.[2] Although in most cases it is nearly impossible to obey all principles at once, it is important for researchers to be aware and plan accordingly. Research in the field of catalysis continues to play a central role in Green Chemistry. Catalysis is often employed as a means of providing a more energy efficient process while also aiming to improve selectivity and apply the principle of atom economy.

1.2 CO_2 as a renewable feedstock

The use of CO_2 as a renewable C-1 (single carbon) building block is driven by the potential to create a renewable carbon economy.[3] Although CO_2 is an essential component of the Earth's natural carbon cycle, atmospheric levels of CO_2 are constantly rising and are contributing to abnormal increases in global atmospheric temperatures and climate change. This rise is largely due to anthropogenic activities such as the burning of fossil fuels to meet society's high energy demands. CO_2 use in the preparation of commercially viable chemicals in a 'green' manner is an attractive application due to its low toxicity and cost, while being a highly abundant starting material.[2] However, activation and utilization of CO_2 remains difficult due to its high thermodynamic stability. Often extreme reaction conditions such as high temperatures and pressures along with reactive substrates must be employed to overcome this inherent stability.[4]

1.3 Reactions of carbon dioxide and epoxides

Epoxides, otherwise known as oxiranes, are widely used monomers in ring-opening polymerization reactions (ROP) due to the significant ring-strain in their three-membered rings.[5-6] They can be polymerized in a number of ways but a metal initiator or catalyst is often used in order to obtain polymers or copolymers with narrow dispersities via controlled or living polymerization reactions. Epoxides can also be copolymerized with carbon dioxide to yield polycarbonates and with cyclic anhydrides to yield polyesters.[7-9]

The most commonly used epoxides in this field are propylene oxide (PO) and cyclohexene oxide (CHO). The ring-opening copolymerization (ROCOP) of CHO and CO_2 to give polycyclohexene carbonate (PCHC) has been thoroughly investigated for many years, through the use of metal-based catalysts including chromium, cobalt, zinc, iron and aluminum complexes.[7] ROCOP of PO and CO_2 on the other hand is more susceptible to backbiting leading to the formation of propylene carbonate. Systems capable of catalyzing the copolymerization to yield polypropylene carbonate (PPC) have been reported, but careful ligand design, along with choice of reaction conditions remain important to suppress backbiting reactions.[7, 10] Several other epoxides, including functionalized monomers such as vinylcyclohexene oxide (VCHO), have been screened by researchers in this area (**Figure 1.1**),[8] but have been less explored in comparison.

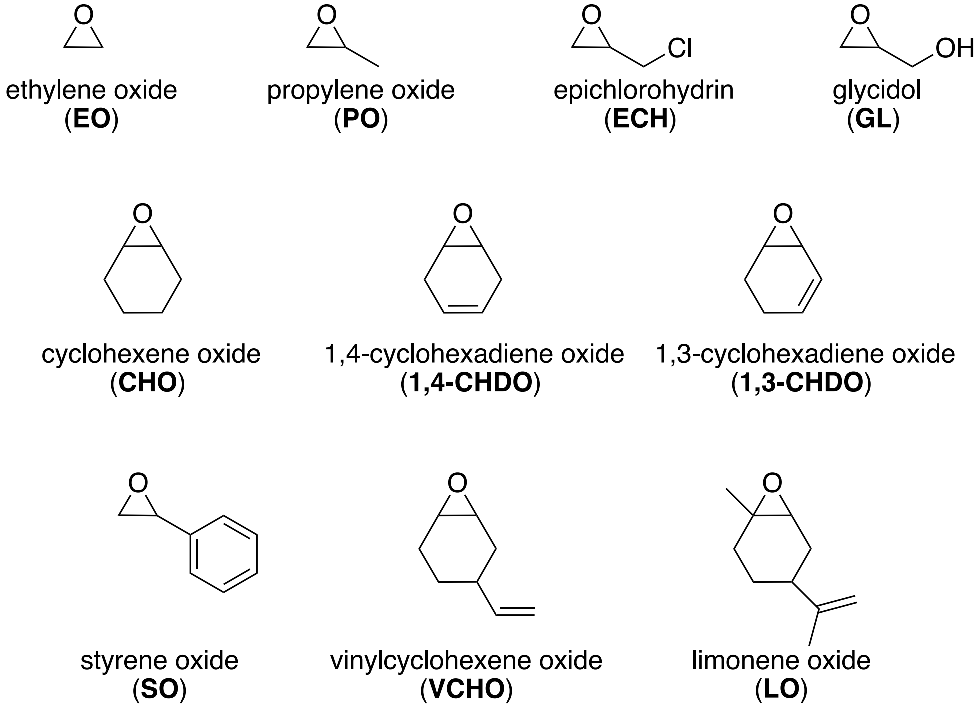

Figure 1.1. Selective representation of commonly used epoxides in ring-opening polymerization and copolymerization reactions.

A general reaction scheme for the reactions of CO_2 and epoxides (using CHO as an example) is shown in **Scheme 1.1**. The reaction begins with ring-opening of the coordinated epoxide by an appropriate nucleophile (anionic or neutral) to form an alkoxide species. This can then undergo CO_2 insertion to form a metal-carbonate species or insertion of a second epoxide unit leading to polyether linkages. The metal carbonate species can serve as a nucleophile to ring-open a second coordinated epoxide followed by insertion of a second CO_2 molecule, leading to carbonate containing linkages within a polymer chain. At any point during polymer growth, 'backbiting' may occur to form cyclic carbonates.[10] There are two possible metal-mediated pathways (**Scheme 1.1**) – path A via a metal-alkoxide intermediate and path B via a metal-carbonate species, and two potential displaced anionic polymer chain pathways – via an anionic alkoxide species as shown or an anionic carbonate species. In most cases, backbiting is more likely to occur at elevated temperatures and lower pressures, and probably occurs when the anionic growing polymer chain is displaced from the metal centre due to a lower activation energy for this process i.e. backbiting is not metal-mediated. Furthermore, higher molecular weight polymer is often obtained when a bifunctional catalyst bearing pendant ionic functionalities are used in these reactions. It is thought that the ionic groups present within the designer catalyst systems (e.g. ammonium, phosphonium, imidazolium) stabilize the growing polymer chain and help reduce the tendency for anionic polymer displacement.[10] When polymerization does occur, if the rate of epoxide ring-opening is faster than the rate of CO_2 insertion, the resulting polycarbonate can contain a mixture of both ether and carbonate linkages. The presence of ether linkages is not detrimental if it can be controlled i.e. the amount of ether linkages in the copolymer can be tuned. One advantage is that ether linkages are thermodynamically stable to backbiting depolymerization of the copolymer.[11]

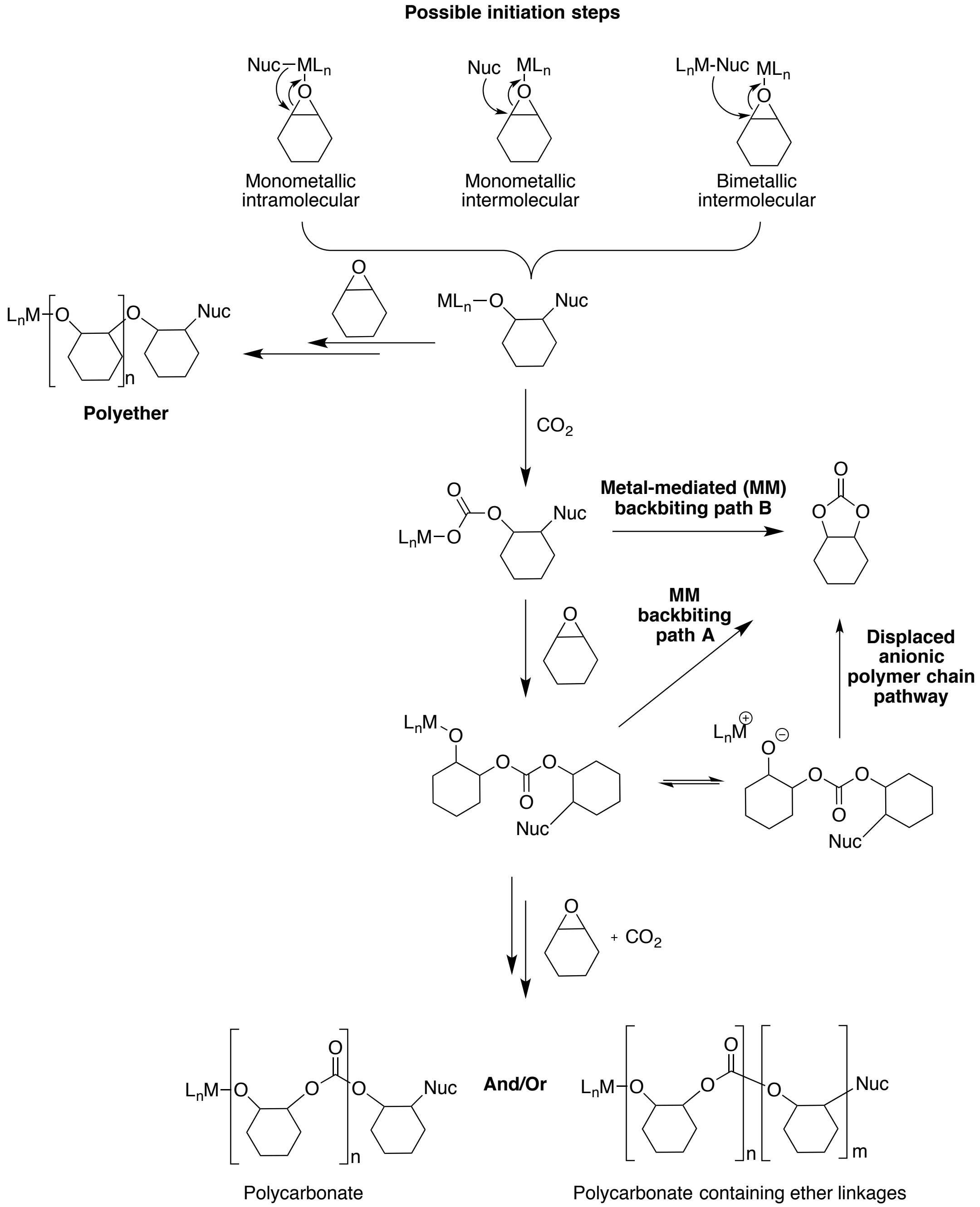

Scheme 1.1. General mechanistic scheme for the catalytic copolymerization of CO_2 and cyclohexene oxide

1.4 In situ Reaction Monitoring

The ability to monitor reactions in situ as they progress can provide insight into mechanistic steps, reaction intermediates, and the influence of different reaction parameters on overall reaction outcomes. For reactions utilizing CO_2 as a substrate, in situ infrared spectroscopy for reaction monitoring is a powerful technique. Due to the strong characteristic absorbance of carbonyl groups in the infrared spectrum, CO_2/epoxide coupling reactions can be monitored in real time as either the cyclic and/or polycarbonate product is formed. As these reactions are completed under high CO_2 pressures, a modified Parr stainless steel reactor vessel can be fitted with a Si ATR sensor probe connected to a ReactIR base unit allowing real-time reaction monitoring. ReactIR is a brand of Mettler Toledo, and consists of a suite of instruments and tools for monitoring reactions using infrared spectroscopy. Researchers have shown that the intensity of typical infrared absorbance bands for epoxides, cyclic carbonates and polycarbonates are directly proportional to their concentrations according to Beer-Lambert Law.[12]

Darensbourg et al. were the first group to report this method of in situ monitoring for epoxide/CO_2 reactions in 2003.[13] Using chromium salen based catalysts they compared the kinetics of the copolymerization of CHO and PO with CO_2. By monitoring reactions at various temperatures, they were able to determine activation energies for both reactions. In particular, they found that for CHO/CO_2 coupling reactions the activation energies for cyclic cyclohexene carbonate and poly(cyclohexene carbonate) were 133 and 46.9 kJ mol^{-1} respectively. These data help explain why in the case of CHO/CO_2 reactions the polymer product often times is more readily formed in preference to the cyclic product. Similar studies have been performed since using cobalt based catalysts.[14]

Our group has reported a similar experimental set-up to these groups for our own investigations. In 2018, Kozak and Ni reported kinetic studies for the copolymerization of CHO and CO_2 using a diamino-bis(phenolate) chromium(III) complex and determined the polycarbonate formation to have an activation energy of 62 kJ mol^{-1}.[12] Most recently we have used this technique to study our BPh_3/PPNCl catalytic system and were able to determine a detailed rate law for the catalytic coupling of PO and CO_2 to yield propylene carbonate.[15] This work has been published in *ACS Catal.* **2019**, 9(3), 1799-1809 and is discussed in detail in **Chapter 4**.

1.5 Iron catalyzed reactions of CO_2 and Epoxides

While to date these transformations have been driven by metal-based catalysts centered on Cr, Co, Zn and Al, in the past decade the use of iron-based catalysts has begun to emerge.[16] The concept of using iron as a catalyst in organic transformations is not new, for decades it has been widely employed within catalysts for the Haber process to produce ammonia. Iron is an attractive alternative to heavier transition metals due to its high earth abundance, relatively low cost and long-term sustainability. In addition, iron is present in many biological/metabolic processes in nature. Iron can exist in oxidation states ranging from -2 to +5, which contributes to its wide range of applications (i.e. lower oxidation states lead to a more nucleophilic nature, while higher oxidation states result in a higher Lewis acidity and electrophilicity).

Along with its use in cross-coupling, oxidations, hydrogenations and cyclizations, iron has played a key role in polymerization catalysts, with one of the most famous being the Brookhart-Gibson catalysts for olefin polymerization.[17-19] As well, an emerging class of 'switchable' catalysts revolving around the incorporation of a ferrocene unit in the ligand backbone or iron serving as the active catalytic center have recently reported by several groups (an example is shown in **Figure 1.2**) and these have been particularly effective in ring-opening copolymerization reactions.[20-27]

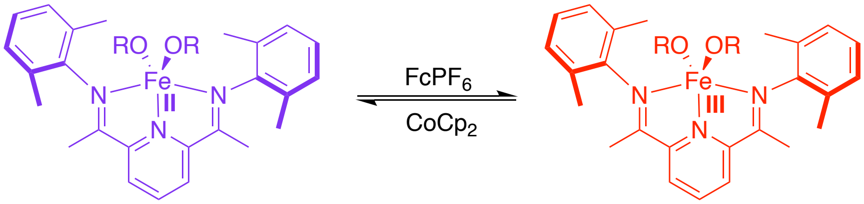

Figure 1.2. Redox-switchable iron catalysts reported by Byers et al. for chemoselective ring opening of cyclic diesters (purple, iron(II) system) and epoxides (red, iron(III) system)[16]

Iron catalysts in CO_2 chemistry have been reported for CO_2 reduction and hydroformylation reactions; however, the use of iron catalysts in CO_2/epoxide chemistry has been less explored. There were early patents reporting the ability of iron halides to promote polymerization of PO and double metal cyanides composed of zinc hexacyanoferrate and zinc ferricyanide to copolymerize CO_2 and epoxides,[28-31] in the latter examples the epoxide is activated by the zinc center rather than iron. Most advancements in this area have occurred in the past ~10 years (**Figure 1.3**).

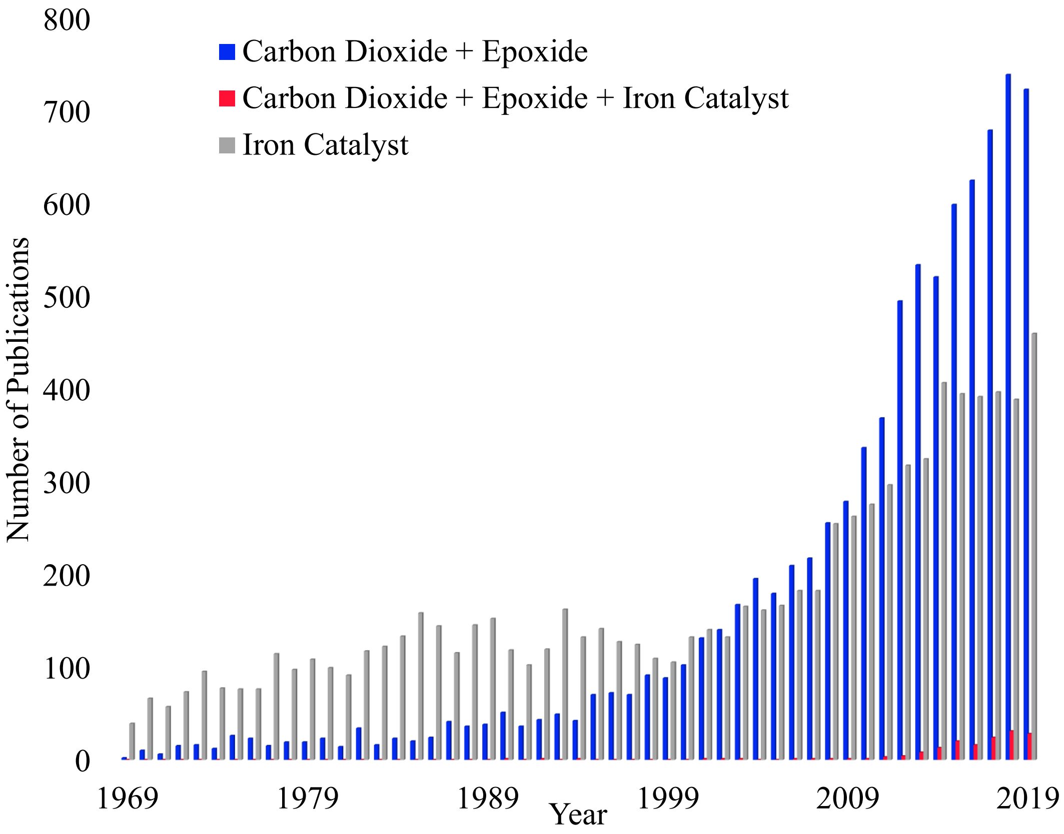

Figure 1.3. Number of articles (journal, review, patents) published since 1969-present. (Note: search was conducted using SciFinder using keywords carbon dioxide, epoxide and iron catalyst.

1.5.1 Iron Catalysts for Cyclic Carbonate Formation

Cyclic carbonates find commercial applications as green solvents, additives to gasoline and in the preparation of electrolyte solutions for lithium-ion batteries. In addition to this, cyclic carbonates can also be used as monomers for polymerizations either through ring-opening polymerization (**Scheme 1.2**) or transesterification reactions. Although they have much potential, on an industrial scale cyclic carbonates are normally formed using harsh reaction conditions. Thus, the drive to develop sustainable efficient catalysts to allow their production under milder conditions is desired.[32-33] In terms of their use as starting materials for polycarbonate synthesis results reported in the recent scientific literature have been somewhat limited, however some of these are highlighted in **Scheme 1.2 B**. In 2010, Carpentier, Guillaume et al. reported the synthesis and ROP of 7-membered cyclic carbonates (4-methyl- and 5-methyl 1,3-dioxepan-2-one; α-Me7CC and β-Me7CC respectively).[34] The polymerization of these organic carbonates was studied with well-established Al, Zn and Y based catalysts alongside several organocatalysts. Polymers could be obtained with modest molecular weights and T_g values ranging from –11 to 36 °C depending on the substrate used and obtained molecular weight. Prior to this report previous examples had focused on ROP of the related unsubstituted 7-membered cyclic monomer.

In 2019, Satoh, Isono et al. demonstrated the ability of trimethyl glycine, a naturally sourced product, as an effective catalyst for the ROP of the 5-membered cyclic monomer trimethylene carbonate (**Scheme 1.2 C**).[35] This system showed high catalytic activity yielding polymers with narrow dispersities ($Đ$ = 1.2) and moderate molecular weights (~4000 g mol^{-1}). A very novel and promising aspect of this study involved the use of functional catalytic initiators leading to materials with various potential industrial applications. For example, the use of 6-azide-1-hexanol, which contains a terminal azido group, as an alcohol initiator led to a polymer material which can be further functionalized via ‘click’ chemistry leading to the production of block copolymers and macromolecular architectures.

Finally, to demonstrate the potential applications of these materials, Cao, Chen et al. reported a nitric oxide functionalized polycarbonate (**Scheme 1.2 D**).[36] The cyclic monomer could be ring-opened in the presence of a polymeric alcohol initiator (mPEG-OH). This polymer in the presence of doxorubicin (DOX), a commonly employed chemotherapeutic drug, formed a self-assembled biodegradable polymer/DOX micelle. Incorporation of the NO donors was shown to improve drug release under physiological conditions. This example highlights one of the many potential applications for polymers produced via ROP of cyclic carbonate monomers.

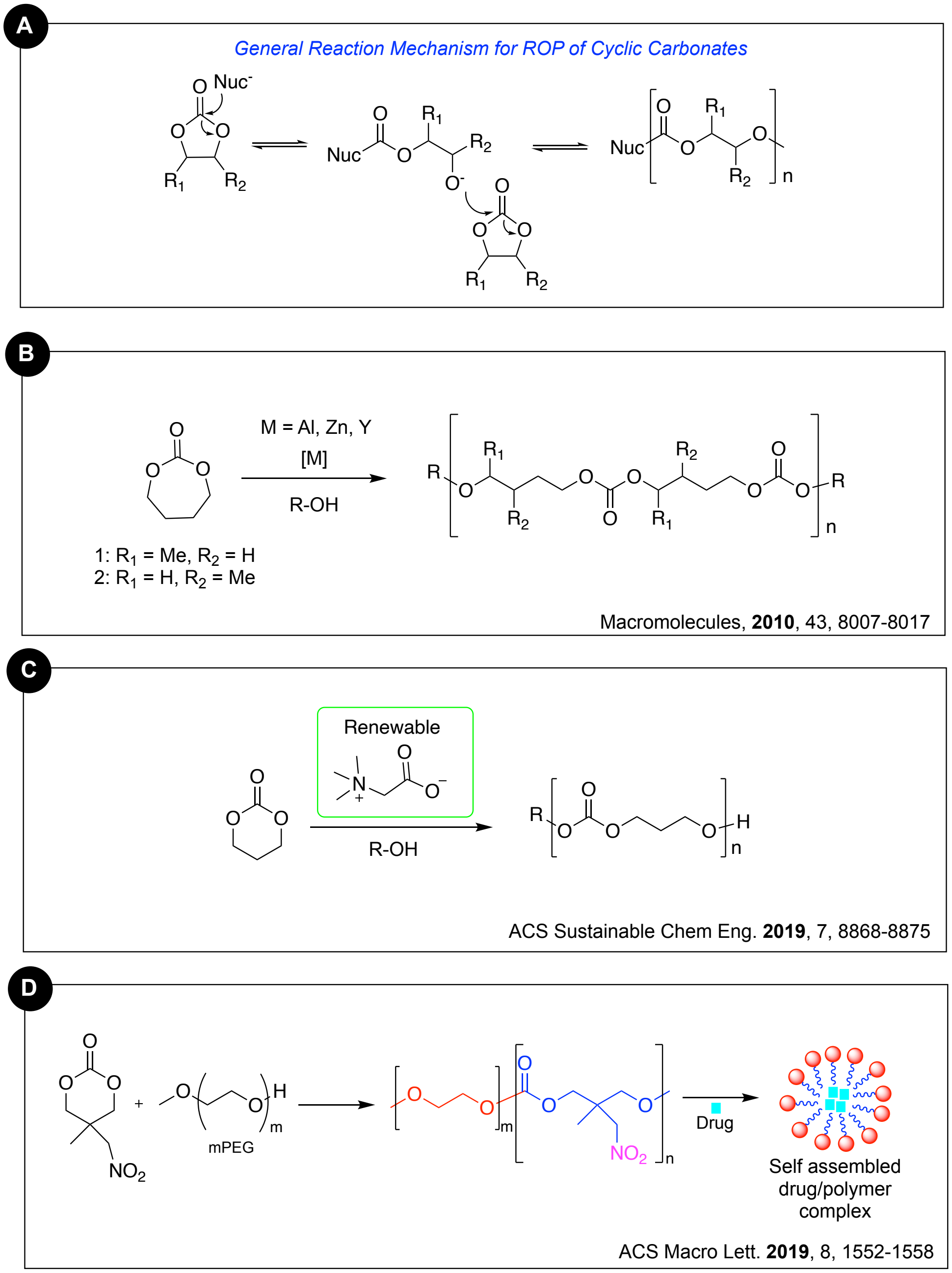

Macromolecules, **2010**, 43, 8007-8017

ACS Sustainable Chem Eng. **2019**, 7, 8868-8875

ACS Macro Lett. **2019**, 8, 1552-1558

Scheme 1.2. Anionic ring-opening of cyclic carbonates as monomers to form polycarbonates and select examples in the literature.

The first report of an iron catalyst for cyclic carbonate formation came from a patent in 1994 from the Texaco Chemical Company.[37] Complex **1.1** (**Figure 1.4**) was active for the coupling of PO and CO_2 to give propylene carbonate without the use of a cocatalyst. Good conversions were obtained (~80%) but reaction rates were slow (TOF = 58 h^{-1}) and harsh reaction conditions were required (180 °C, ~100 bar CO_2). Following this, He et al. reported a series of metal phthalocyanines as catalysts for the coupling of CO_2 and terminal epoxides.[38] The presence of a base, tributylamine, was needed in excess (4.5 equiv. per Fe) for the reaction to proceed. Similar to the previous report, harsh reaction conditions (140 °C, 43 bar CO_2) were used. In 2007, Jing et al. reported an iron porphyrin complex **1.3** for the coupling of PO and CO_2.[39] This paper mainly focused on the analogous cobalt porphyrin complexes for the same reaction, but the iron analog was synthesized for a comparison. The systems were active for cyclic carbonate formation at 25 °C and 7 bar CO_2 in the presence of 2 equiv. phenyltrimethylammonium tribromide (TPAT). However, in comparison to the cobalt analogs, the iron complexes were far less reactive, only giving a conversion of 10% after 3 h.

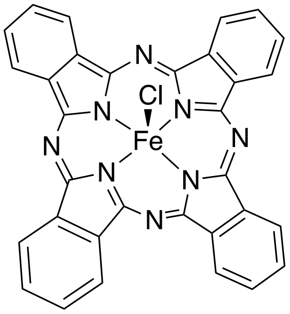

1.1 (Marquis, Sanderson, 1994)

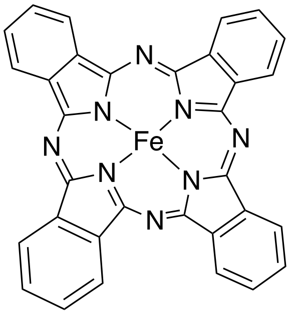

1.2 (He, 2000)

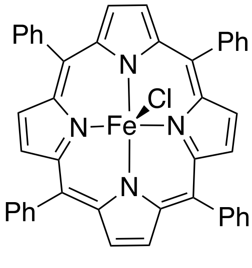

1.3 (Jing, 2007)

Figure 1.4. Early iron catalysts for the production of cyclic and polycarbonates.

A major breakthrough in the field of iron catalyzed CO_2/epoxide chemistry came from the Williams group in 2011,[40] and focused on polycarbonate formation so will be discussed in detail in the sections below. Shortly after this, Rieger et al. reported tetraamine and diimine-diamine iron(III) complexes active towards the coupling of CO_2 and PO to form propylene carbonate (**Figure 1.5**).[41] Complexes **1.4.1** and **1.4.2** were active for cyclic carbonate formation without the addition of an external cocatalyst, but showed higher conversions upon the addition of 1 equiv. of TBAB. Complex **1.5** was inactive alone but could obtain conversions >80% with the addition of TBAB. Kinetic studies on these systems, utilizing in situ IR spectroscopy, revealed a second order dependence on iron concentration and thus a bimetallic reaction pathway involving two separate iron centers was proposed. For example, in the absence of cocatalyst, the mechanism for complex **1.4.1** begins by the dissociation of a weakly bound Cl^-, resulting in a vacant binding site for epoxide coordination. Next, a Cl^- from a second catalyst molecule ring-opens the coordinated epoxide. CO_2 insertions occur at the iron-alkoxide bond, followed by back-biting to yield the cyclic carbonate and regenerate the active catalytic species.

Building upon this work, Wang et al. reported similar tetraamine and diimine-diamine iron (III) complexes active towards the coupling of PO, ECH and CHO with CO_2.[42] Both complexes were highly active catalysts and unlike the previously reported Rieger complex **1.5**, **1.7** was active without the addition of a cocatalyst, but conversions remained low. Although a direct comparison cannot be made as reaction conditions differ slightly. Regardless, in the presence of 1 equiv. of TBAB, high activity was achieved. Further, these systems were also active for the coupling of CO_2 with ECH and CHO. For CHO, no evidence of copolymer formation was seen. Instead, exclusively the *cis*-isomer was formed in moderate conversions.

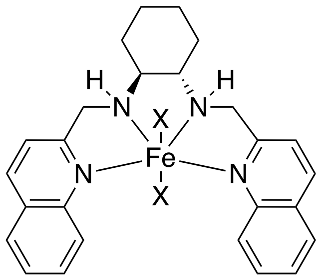

1.4.1: X = Cl
1.4.2: X = OTf
1.4 (Rieger, 2011)

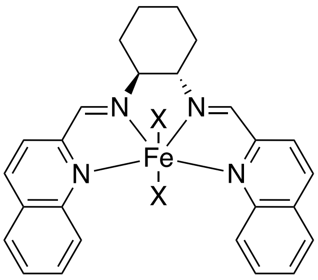

X = Cl

1.5 (Rieger, 2011)

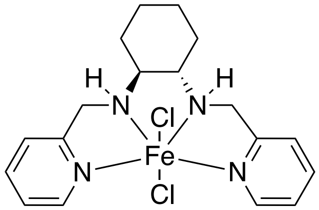

1.6 (Wang, 2014)

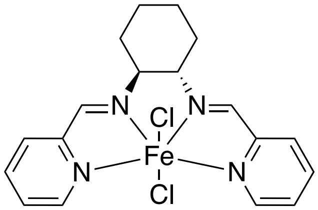

1.7 (Wang, 2014)

Figure 1.5. Tetraamine and diamine-diamine iron(III) complexes for the coupling of CO_2 and propylene oxide.

Zevaco et al. published a family of iron(III) complexes using N_4 and N_2O_2 chelating ligand frameworks for the coupling and copolymerization of epoxides and CO_2 (**Figure 1.6**). The first complexes, **1.8.1** and **1.8.2,** were screened as catalysts for the formation of propylene carbonate.[43] **1.8.1** with chloride groups in the axial positions was quite active (78% conv. after 20 h) while the derivative complex with acetate groups (**1.8.2**) gave 8% conv. under identical conditions. Modification of the aryl backbone in the ligand framework gave rise to complexes **1.9.1**-**1.9.4** which again were all highly active catalysts towards the coupling of PO and CO_2 for propylene carbonate formation.[44] In 2013, Zevco et al. expanded to N_2O_2- iron(III) (**1.10**) and iron(II) (**1.11**) systems that were active catalysts for the coupling of PO and 9 other substituted epoxides with CO_2 to yield cyclic carbonates.[45] It was found that the iron(II) system (**1.11**) was only active in the presence of a cocatalyst (TBAB) and required higher catalyst loadings to achieve high conversions. On the other hand, the iron(III) complex, **1.10**, was active without an external cocatalyst and required lower catalyst loadings to achieve similar conversions. This complex was also screened for reactivity with a range of other epoxides demonstrating the diverse applicability of this system.

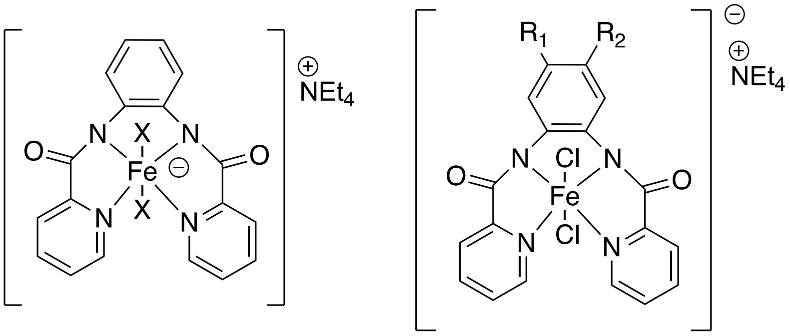

1.8.1: X = Cl
1.8.2: X = OAc

1.9.1: $R_1 = R_2 = H$
1.9.2: $R_1 = R_2 = Cl$
1.9.3: $R_1 = R_2 = Me$
1.9.4: $R_1 = H$, $R_2 = NO_2$

1.8 (Zevaco, Döring, 2012)

1.9 (Zevaco, 2014)

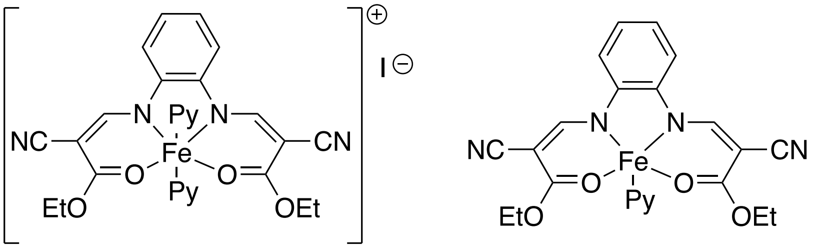

1.10

1.11

(Zevaco, 2013)

Figure 1.6. Iron(III) complexes repoted by Zevaco et al. for coupling and polymerization reactions of CO_2 and epoxides.

In 2012, Kleij et al. reported iron(III) amine triphenolate complexes for the coupling of epoxides and CO_2.[46] Following their initial report, they published a follow-up study eluding to the possibility of the complexes existing as monomeric or dimeric species (**Scheme 1.3**, top).[47] The ability of dimer-formation was attributed to *ortho*-position substitution of the phenolate backbone leading to stability in the case of dimer formation. That is, complexes bearing *tert*-butyl or phenyl groups in the *orth*o-position favored the monomeric structure, while hydrogen and methyl groups in the *ortho*-position favored the dimeric species. In all cases the monomeric species were far more active as catalysts for coupling reactions. In addition, during reactions, higher temperatures and the use of a coordinating solvent favored the dissociation of the dimer complex into its monomeric form.

An interesting study on these complexes came a year later demonstrating the ability of these complexes to control the stereochemistry of the final product when 2,3-epoxybutane was used as the substrate.[48] It was found that when starting with either pure *cis*- or *trans*-2-BO the stereochemistry of the final product was dependent on the relative amount of cocatalyst used. For example, when **1.13.2** was used as a catalyst with *cis*-2-BO as a substrate, >95% of the corresponding *cis*-product was achieved when 10-16 equiv. of TBAB was present as a cocatalyst. However, once less than 2.5 equiv. of TBAB was present in solution, selectivity began to switch towards the *trans*-product, with 89% *trans*-product being produced in the presence of 0.5 equiv. TBAB. The authors explained this reactivity through two separate ring-closing mechanisms, leading exclusively to one product over the other (**Scheme 1.3**). The mechanism begins in a similar manner to other reported systems. That is ring-opening of the coordinated epoxide by an external nucleophile by S_N2 attack, resulting in inversion of stereochemistry at this carbon atom. This is then followed by CO_2 insertion leading to a metal-bound carbonate species. In the ring-closing pathway leading to the *cis*-product (high TBAB concentrations), there is competition between the metal-bound carbonate and excess Br^- anions for the vacant Fe binding site. This results in dissociation of the metal bound carbonate, which can then back-bite through an outer sphere ring-closure mechanism leading to the *trans*-product. On the other hand, under low concentrations of TBAB, the carbonate species is more likely to be bound to the iron center and hence the metal center controls inversion of stereochemistry. The bound bromide anion that ring-opened the initial epoxide, interacts with the vacant *cis*-coordination site on iron, and the partially positive sp^2 carbon undergoes a pseudo-S_N1 type ring-closure mechanism.

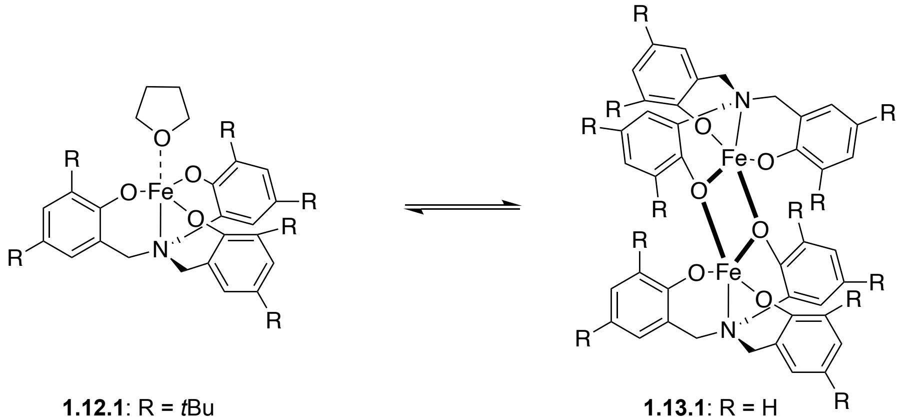

1.12.1: R = *t*Bu
1.12.2: R = Ph

1.13.1: R = H
1.13.2: R = Me

(Kleij, 2012)

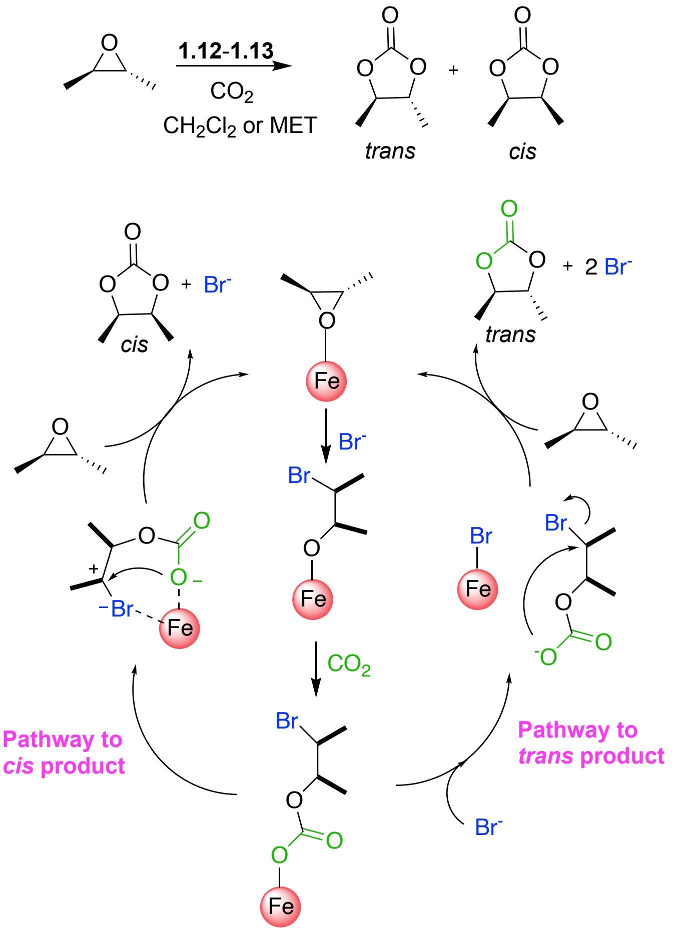

(Kleij, 2013)

Scheme 1.3. Proposed ring-closure mechanisms proposed by Kleij et al. for the inversion or stereo-retention of *trans*-2,3-epoxybutane.

Recently, a bimetallic iron(III) thioether-triphenolate complex reported by the Capacchione group showed exceptional activity towards the coupling of PO and CO_2 to form cyclic carbonates under neat conditions producing a high TOF of 580 h^{-1} (**Figure 1.7**).[49] Upon optimizing reaction conditions the catalyst (0.025 mol%) with 2 equiv. TBAB as a co-catalyst at 100 °C and 20 bar CO_2, 87% conversion of PO to the cyclic product was achieved in only 6 h. Other tested co-catalysts including PPNCl and 4-dimethylaminopyridine (DMAP) proved less active. The authors attribute the high reactivity of their system to the favored coordination of the epoxide to the iron center as a result of the soft donor sulfur atoms on the chelating ligand being weakly bonded. DFT studies shed light on the importance of the hemilabile Fe-S bond and demonstrated only one iron center is reactive in the catalytic cycle. The functional group tolerance and substrate scope of the catalyst was also assessed by testing its activity against a series of epoxide substrates. When the methyl group of PO was replaced with a chloride or hydroxyl (substrates being epichlorohydrin and glycidol respectively) very similar or higher conversions were obtained. In the case of CHO, only 13% conversion to the cyclic product was obtained yielding the *cis*-isomer with no evidence of polycarbonate formation.[49]

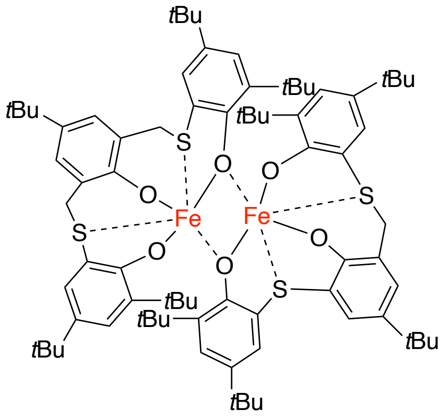

1.14 (Capacchione, 2015)

Figure 1.7. Bimetallic iron(III) thioether-triphenolate catalyst for propylene carbonate formation.

In 2016, Repo et al. reported a bifunctional Schiff base iron(III) complex for cyclic carbonate formation in the absence of a cocatalyst.[50] Reactions proceeded at low pressures (10 bar CO_2) and although active without an additional cocatalyst, small amounts of TBAB were shown to improve yields. In addition to PO, the bifunctional system was also active towards the coupling of CO_2 and ECH, SO, CHO and 1-hexene oxide. Kinetic studies were performed via in situ IR spectroscopy and revealed an overall first-order dependence on iron supporting the intramolecular catalytic process. The imidazole group of the ligand serves to activate CO_2 producing an anionic carbonate species which can then ring open a coordination epoxide at the iron center (**Scheme 1.4**). Intramolecular ring-closing releases the final product while regenerating the active catalytic species.

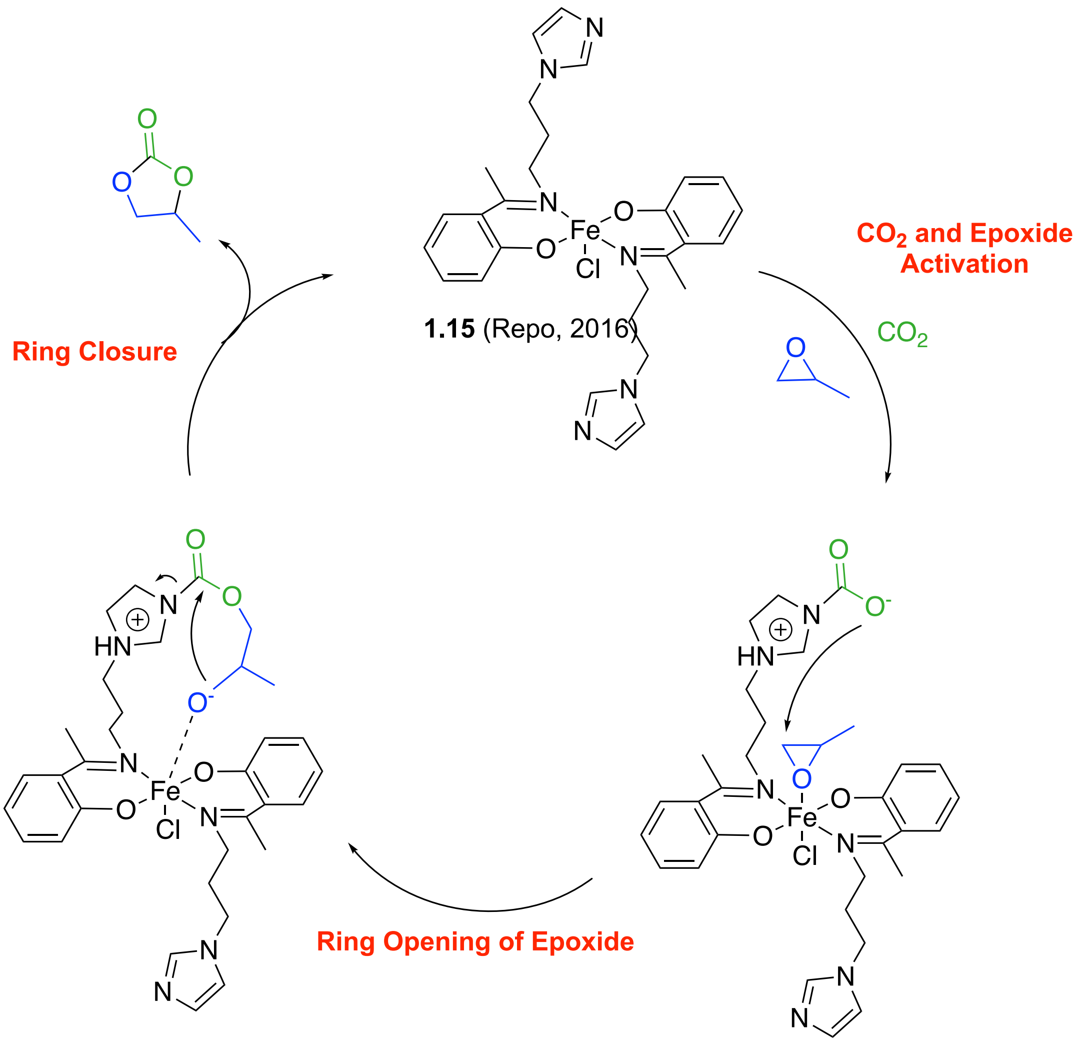

Scheme 1.4. Proposed intramolecular mechanism reported by Repo et al. for the synthesis of propylene carbonate

In 2016, our group reported a family of iron(III) complexes supported by tetradentate amino-bis(phenolate) ligands that were active towards the coupling of CO$_2$ and a range of terminal epoxides in the presence of a suitable cocatalyst.[51] Electron-withdrawing substituents on the phenolate rings led to complexes with the highest catalytic activity. However, during coupling reactions we observed reaction mixtures changing from intense purple to a red-orange color over the course of the reaction and postulated the idea that an oxo-bridged species formed in situ during the reaction. Hence, in a follow-up report, we synthesized the corresponding oxo-species and tested them as catalysts. This work has been published in *Inorg. Chem.* **2018**, 57 (21), 13494-13504 and discussed in detail in **Chapter 2**.[52] Following this study, we reported an in-depth study of iron complexes bearing aminobis(phenolate) ligands in varying coordination geometries. This work has been published in *Inorg. Chem.* **2019**, 58, 11231-11240. and discussed in detail in **Chapter 3**.[53]

In 2018, Garden et al. reported phenoxyimine iron(III) complexes containing varying ortho substituents in the ligand backbone (**1.20.1**-**1.20.3**) as catalysts for cyclic carbonate formation (**Figure 1.8**).[54] All complexes were found to be highly active for the selective coupling of PO and CO_2 to give propylene carbonate under relatively mild conditions (20 bar) and low catalyst loading (0.05 mol%) with excess TBAB. It was found that complexes of ligands containing electron-withdrawing substituents (**1.20.3**) showed the highest activity which was attributed to the increased Lewis acidity of the iron(III) center. These air-stable, robust systems were also active towards a selection of commonly employed epoxides and in the case of CHO, exclusively the *cis*-cyclic product was obtained.

Building upon their previous report in 2015, Capacchione et al. reported the synthesis of mononuclear iron(III) complexes bearing sulphur atoms in the ligand backbone (**1.21.1-1.21.4, Figure 1.8**).[55] In terms of cyclic carbonate formation, these systems were very active even under very mild reaction conditions (35 °C, 1 bar CO_2), with **1.21.4** proving to be the most active catalyst. Without the addition of a cocatalyst no conversion was obtained, however, excess TBAB resulted in an efficient binary catalytic system. Kinetic studies revealed a process that was first order with respect to iron concentration and suggested that the rate determining step was epoxide ring-opening. These systems demonstrated a wide epoxide scope, and at 1 bar CO_2, demonstrated the highest initial TOF (290 h^{-1} in the case of PO) for a homogeneous catalytic system at this pressure. In addition, these systems were also active for polycarbonate formation and will be discussed in more detail below.

Salen, salan and salalen ligands have been long studied in CO_2/epoxide coupling and polymerization reactions, particularly with chromium and cobalt based systems. However, their complexation with iron for these transformations has been less explored. In 2018, Lamberti et al. reported a selection of such complexes (**1.23.1-1.23.4**) based on iron(III) (**Figure 1.9**).[56] In the case of PO, all complexes were active and selective towards the formation of propylene carbonate with good conversions. Out of the four complexes screened, complex **1.23.4** showed the highest activity, followed closely by **1.23.1**, then **1.23.2** and **1.23.3**. The authors attributed this trend in reactivity due to an enhanced flexibility in the ligand backbone in **1.23.4** compared to **1.23.3** and highlighting the importance of a flexible backbone in improved catalytic activity. This may be due to increased ability to coordinate and activate the requisite reagents for this catalyzed reaction.

To the best of our knowledge, there have been only two reports of iron catalysts for cyclic carbonate formation in 2019. The first came from Pescarmona and Otten who reported six different formazanate ferrate(II) complexes bearing labile halide ligands which were active without the addition of a cocatalyst (**Figure 1.8**).[57] Changing the ancillary ligand (**1.22.1-1.22.3**) resulted in a reactivity trend from most active to least active catalyst with regards to the halide present: $Br^- > I^- > Cl^-$. From a mechanistic viewpoint, this makes sense as reactivity depends on the leaving group ability and thus access to a vacant site for epoxide coordination. In addition, the effect of substituents in the ligand backbone was also investigated. Changing the aromatic group from a *p*-tol to the more electron withdrawing C_6F_5 group, or more electron-donating *p*-OMe (in attempts to modify the Lewis acidity of the iron center) did not afford significant changes in reactivity and conversions remained similar.

Following this report, Jones et al. reported a collection of air-stable iron(III) acetate complexes bearing salan, salen and salalen ligand frameworks (**Figure 1.9**).[58] These complexes exhibited activity towards the coupling of CHO and CO_2 to give in the majority of cases exclusively *cis*-CHC. Comparing the diverse group of complexes, the iron salan acetate complex **1.24.10** showed the highest activity. Increasing the flexibility of the aminopiperidine ligand backbone (i.e. **1.24.4** to **1.24.5**) resulted in improved activity which is consistent with findings by Garden et al. as discussed above.[54] In addition, **1.24.10** was also screened as a catalyst against a range of terminal epoxides with varying electronic/sterics effects giving moderate to high conversions in all cases. These systems were also active towards the ring-opening polymerization of *rac*-lactide but will not be discussed in detail here as it is outside the scope of this thesis. Interestingly, the authors also noted observing a distinct color change from purple to red of reaction mixtures over the course of coupling reactions. Upon future investigation through UV-vis studies, this was attributed to the formation of a μ-oxo bridged species formed through an epoxide deoxygenation, which is consistent with our earlier studies on similar systems.[52]

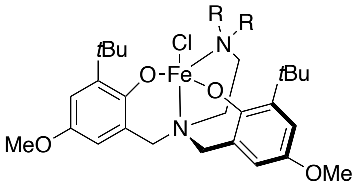

1.18.1: R = Et
1.18.2: R = *i*Pr
1.18.3: R = *n*Bu

1.18 (Kerton and Kozak, 2019)

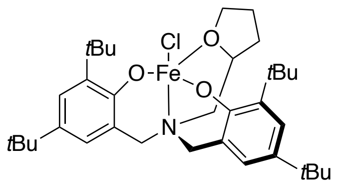

1.19 (Kerton and Kozak, 2019)

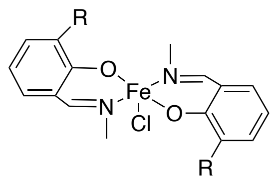

1.20.1: R = H
1.20.2: R = *t*Bu
1.20.3: R = Cl

1.20 (Garden, 2018)

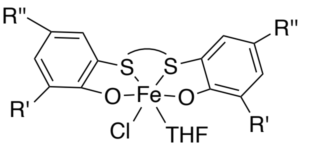

1.21.1:) = $(CH_2)_2$, R' = CPh_3, R" = Me
1.21.2:) = $(CH_2)_2$, R' = R" = $C(CH_3)_2Ph$
1.21.3:) = $(CH_2)_2$, R' = R" = Me
1.21.4:) = c-Hex, R' = R" = *t*Bu

1.21 (Capacchione, 2018)

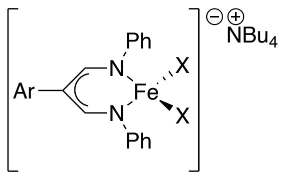

1.22.1: Ar = *p*-tol, X = Cl
1.22.2: Ar = *p*-tol, X = Br
1.22.3: Ar = *p*-tol, X = I
1.22.4: Ar = C_6F_5, X = Br
1.22.5: Ar = C_6F_5, X = I
1.22.6: Ar = C_6H_4(*p*-OMe), X = Br

1.22 (Pescarmona and Otten, 2019)

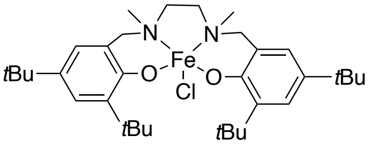

1.23.1

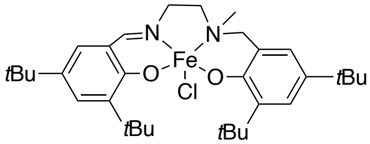

1.23.2

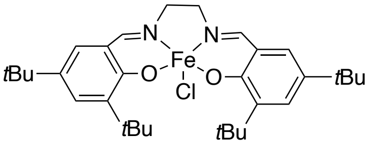

1.23.3

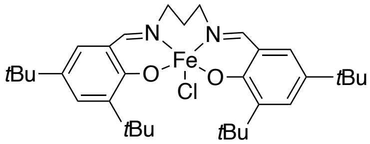

1.23.4

1.23 (Lamberti, 2018)

Figure 1.8. Selection of recent iron catalysts reported for cyclic carbonate formation.

1.24 (Jones, 2019)

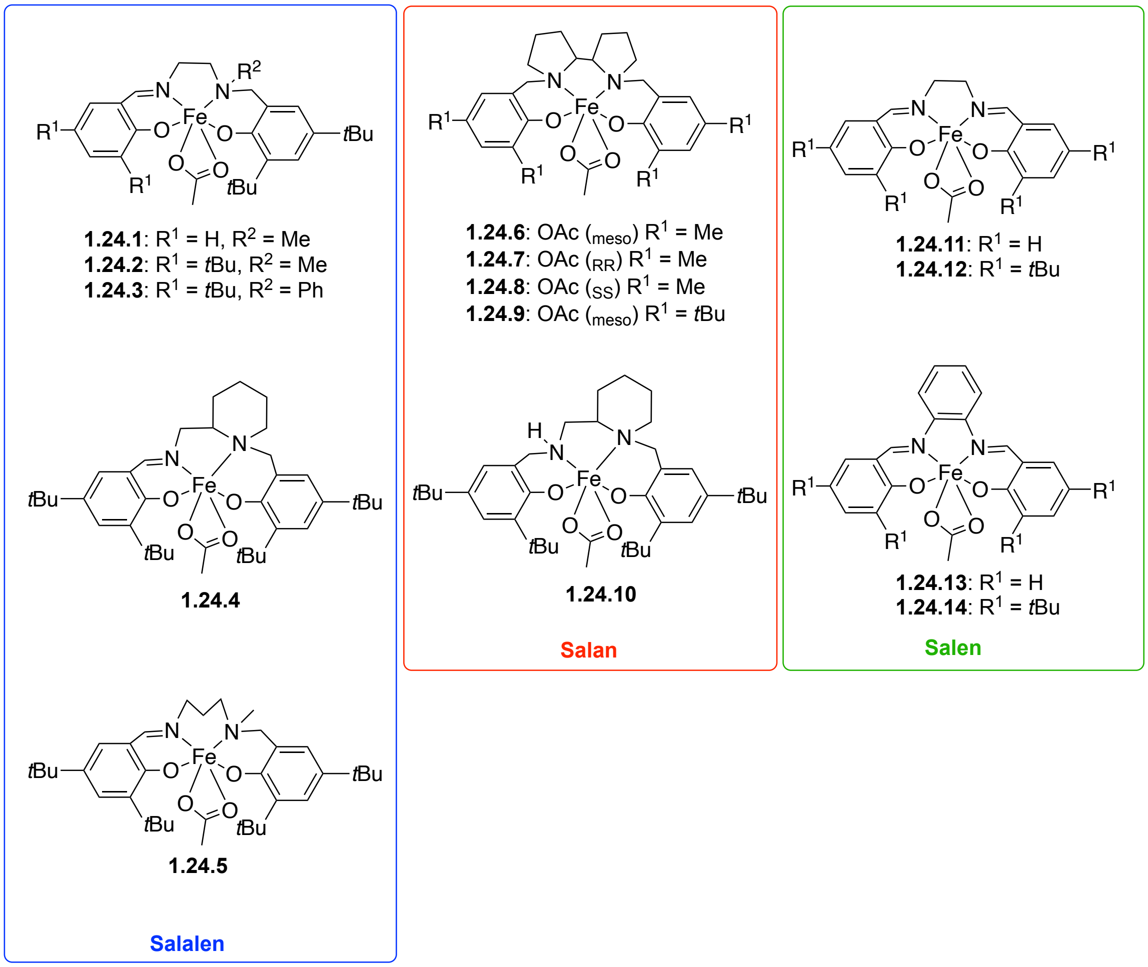

Figure 1.9. Iron(III) acetate complexes reported by Jones et al. for the selective coupling of CO_2 and several terminal epoxides.

Table 1.1 provides a summary of those systems discussed in the sections above for the coupling of CO_2 and epoxides to yield cyclic carbonates. In most cases the addition of an external cocatalyst is needed to obtain high activity. In the majority of cases high reaction temperatures and moderate CO_2 pressures are employed. By far to date PO has been the most explored substrate for these transformations, but in the recent years, researchers have been expanding the substrate scope to other terminal and more challenging internal epoxides.

Table 1.1. Summary of iron catalysts for coupling of CO_2 and epoxides to give cyclic carbonates.

Entry	Complex (mol% Fe) [Ref.]	Substrate	Cocatalyst	P_{CO_2} (bar)	T. (°C)	t (h)	% Conv.
1	**1.1** (0.5) [Marquis, Sanderson, 1994][37]	PO	-	100^a	180	2	80
2	**1.2** (0.1) [He, 2000][38]	PO	Tributylamine (4.5 equiv.)	43^a	140	5	6
3	**1.2** (0.1) [He, 2000][38]	ECH	Tributylamine (4.5 equiv.)	43^a	140	0.5	91
4	**1.3** (0.1) [Jing, 2007][39]	PO	PTAT (2 equiv.)	7	25	3	10^b
5	**1.4.1** (1.0) [Rieger, 2011][41]	PO	-	15	100	2	80
6	**1.4.2** (1.0) [Rieger, 2011][41]	PO	-	15	100	2	41
7	**1.5** (1.0) [Rieger, 2011][41]	PO	-	15	100	2	Trace
8	**1.5** (1.0) [Rieger, 2011][41]	PO	TBAB (1 equiv.)	15	100	2	82
9	**1.6** (0.1) [Wang, 2014][42]	PO	TBAB (1 equiv.)	40	130	4	>99
10	**1.7** (0.1) [Wang, 2014][42]	PO	TBAB (1 equiv.)	40	130	4	>99
11	**1.6** (0.1) [Wang, 2014][42]	ECH	TBAB (1 equiv.)	40	100	4	97
12	**1.6** (0.2) [Wang, 2014][42]	CHO	TBAB (1 equiv.)	40	100	12	47 (>99% *cis*-CHC)
13	**1.8.1** (0.5) [Zevaco, Döring, 2012][43]	PO	-	35	80	20	78
14	**1.8.2** (0.5) [Zevaco, Döring, 2012][43]	PO	-	35	80	20	8
15	**1.9.4** (0.5) [Zevaco, 2014][44]	PO	-	35	80	20	92
16	**1.10** (0.2) [Zevaco, 2013][45]	PO	-	50	80	20	99
17	**1.11** (1.0) [Zevaco, 2013][45]	PO	TBAB (1 equiv.)	50	80	20	91
18	**1.10** (0.2) [Zevaco, 2013][45]	SO	-	50	80	20	96
19	**1.12.2** (1.0) [Kleij, 2012][47]	PO	TBAB (5 equiv.)	10	25	18	$88^{b,c}$
20	**1.13.2** (0.25) [Kleij, 2013][48]	*cis*-2-BO	TBAB (16 equiv.)	10	80	18	>99 *cis* isomer
21	**1.13.2** (0.25) [Kleij, 2013][48]	*cis*-2-BO	TBAB (0.5 equiv.)	10	80	18	89 *trans* isomer

22	**1.14** (0.025) [Capacchione, 2015][49]	PO	TBAB (2 equiv.)	20	100	6	87
23	**1.15** (0.12) [Repo, 2016][50]	PO	TBAB (8 equiv.)	10	100	3	66[d]
24	**1.16.1** (0.025) [Kerton, 2018][52]	PO	PPNCl (4 equiv.)	20	100	22	40
25	**1.17.1** (0.025) [Kerton, 2018][52]	PO	PPNCl (4 equiv.)	20	100	22	29
26	**1.29.1** (0.025) [Kerton, Kozak 2019][53]	PO	PPNCl (4 equiv.)	20	100	22	>99
27	**1.20.3** (0.05) [Garden, 2018][54]	PO	TBAB (2 equiv.)	20	120	2	76
28	**1.21.4** (0.1) [Capacchione, 2018][55]	PO	TBAB (5 equiv.)	1	35	6	65
29	**1.22.2** (0.25) [Pescarmona, Otten, 2019][57]	PO	-	12	90	18	>99
30	**1.23.1** (0.025) [Lamberti, 2018][56]	PO	TBAB (4 equiv.)	20	100	16	85
31	**1.24.4** (0.08) [Jones, 2019][58]	CHO	TBAC (8 equiv.)	10	80	24	46 (>99 *cis*-CHC)
32	**1.24.10** (0.08) [Jones, 2019][58]	CHO	TBAC (8 equiv.)	10	80	24	66 (>99 *cis*-CHC)
33	**1.24.14** (0.08) [Jones, 2019][58]	CHO	TBAC (8 equiv.)	10	80	24	59 (84% *cis*-CHC, 16% polyether)

[a]Actual pressure not reported. Value in table was determined using the ideal gas law with the given temperature, autoclave volume and mol of CO_2 reported. [b]Value reported as an isolated yield of carbonate instead of conversion of epoxide. [c]Solvent used methylethylketone. [d]Solvent used methylene chloride.

1.5.2. Iron Catalysts for Polycarbonate Formation

Ring-opening polymerizations and copolymerizations of epoxides, cyclic carbonates and other cyclic monomers is generally driven by the reduction in bond and/or angle strain of the cyclic monomer. Polycarbonates find many industrial uses due to their desirable properties including low-weight, durability, transparency and high-impact resistance. The majority of industrially produced polycarbonates today are petroleum-derived and not sustainable i.e. the carbonate group is provided through use of phosgene or other reagents. The synthesis of polycarbonates via the copolymerization of epoxides with CO_2 leads to potentially renewable incorporation of CO_2. While this has been studied widely in recent years the majority of examples focus on chromium and cobalt; iron has been less explored, with limited examples reported to date (**Figure 1.10**).

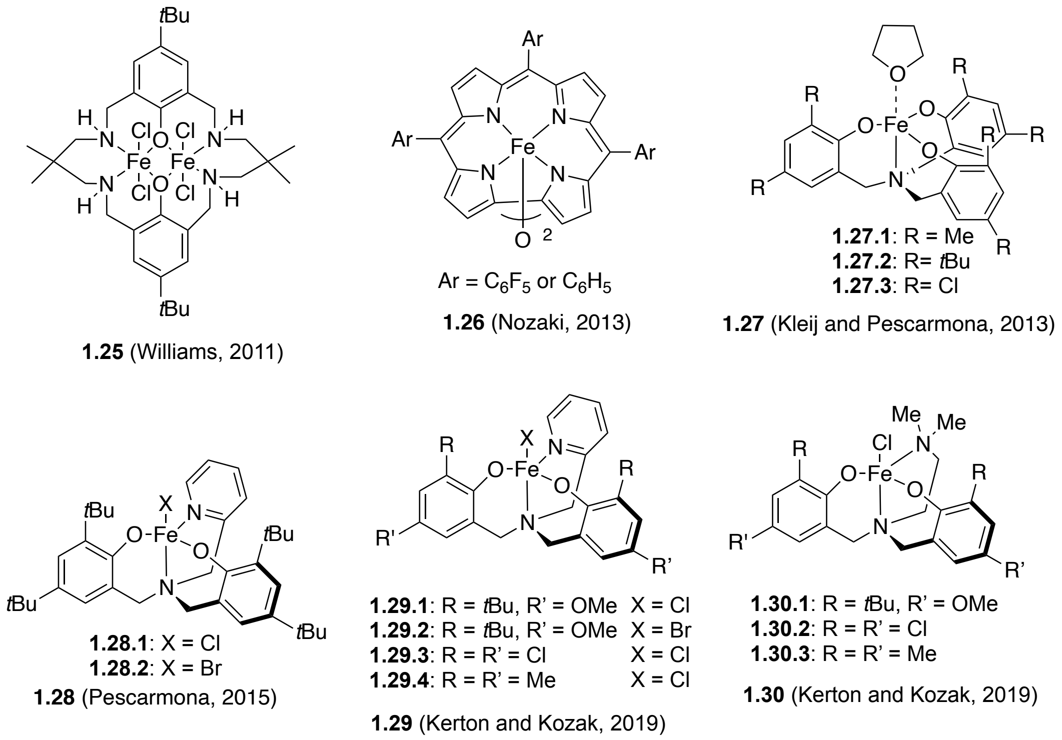

Ar = C_6F_5 or C_6H_5

1.25 (Williams, 2011)

1.26 (Nozaki, 2013)

1.27.1: R = Me
1.27.2: R= *t*Bu
1.27.3: R= Cl

1.27 (Kleij and Pescarmona, 2013)

1.28.1: X = Cl
1.28.2: X = Br

1.28 (Pescarmona, 2015)

1.29.1: R = *t*Bu, R' = OMe X = Cl
1.29.2: R = *t*Bu, R' = OMe X = Br
1.29.3: R = R' = Cl X = Cl
1.29.4: R = R' = Me X = Cl

1.29 (Kerton and Kozak, 2019)

1.30.1: R = *t*Bu, R' = OMe
1.30.2: R = R' = Cl
1.30.3: R = R' = Me

1.30 (Kerton and Kozak, 2019)

Figure 1.10. Iron catalysts used for CO_2/epoxide copolymerization.

A major breakthrough in iron catalysis for both selective polycarbonate and cyclic carbonate formation was reported by Buchard et al. in 2011.[40] The system was based on an air-stable di-iron(III) complex, **1.25**, in which the selective formation of either poly(cyclohexene carbonate) or *cis*-cyclohexene carbonate could be controlled by the amount of bis(triphenylphosphine)iminium chloride (PPNCl) present in the reaction (**Scheme 1.5**). In terms of polycarbonate formation, CHO could be copolymerized with

CO_2 under neat conditions with a catalyst loading of 0.1 mol%, 80 °C and CO_2 pressures <10 atm. Although active at 1 atm CO_2, the produced polycarbonate contained only 66% carbonate linkages. However, upon increasing pressures to 10 atm CO_2, polycarbonates with >99% carbonate linkages could be produced within 5 h.

The ability of this system to selectively form the *cis*-cyclic product is quite impressive. While in general, cyclic cyclohexene carbonate is more difficult to produce than the polycarbonate, when it is formed it is often the *trans*-isomer produced due to the back-biting mechanism. In order to produce the *cis*-isomer a double-inversion of stereochemistry must occur at the chiral centers of CHO. The authors in this case observed that by increasing the amount of anionic co-catalyst (PPNCl in this case) to two equiv. with respect to the catalyst, *cis*-cyclohexene carbonate was selectively produced. They suggested that the presence of excess Cl^- favours the formation of the anionic carbonate species (**Scheme 1.5**, bottom right). This species would be more nucleophilic than the carbonate bound to the Fe center in the initial steps, which would then undergo an intramolecular nucleophilic substitution (S_N2-like), leading to an inversion of stereochemistry and producing the *cis*-product. In addition, this catalyst was active for the cyclization of propylene oxide and styrene oxide under 1 atm CO_2 to yield the cyclic carbonates at conversions of 91% and 98% respectively.

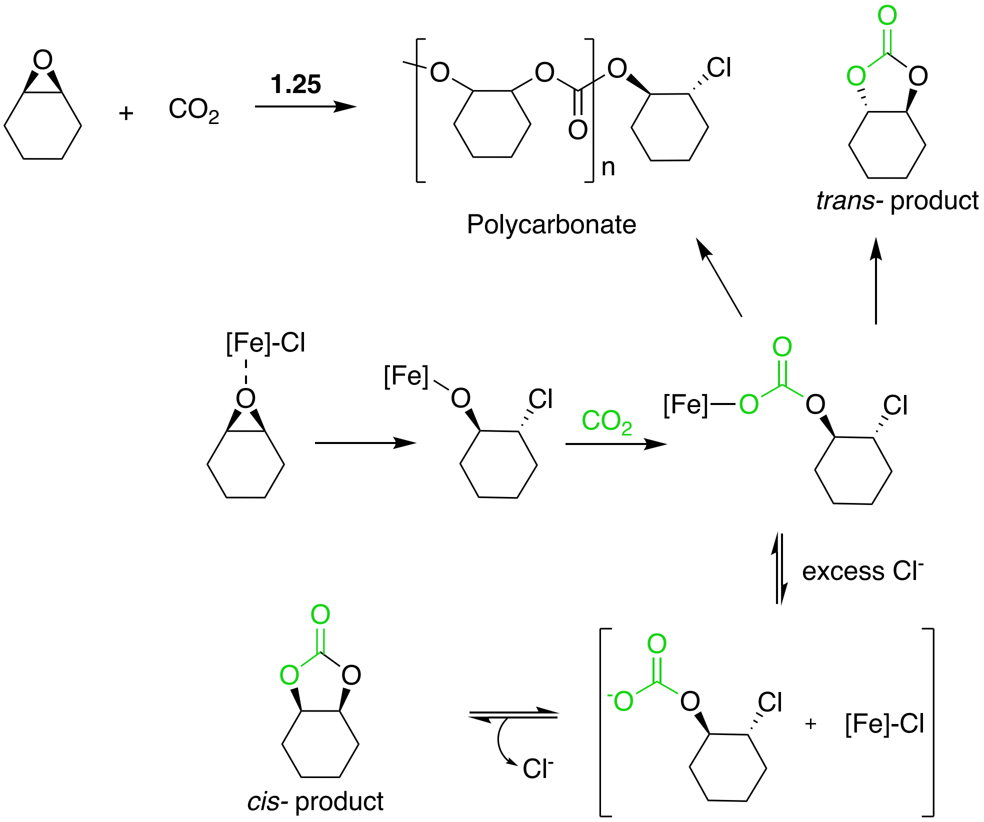

Scheme 1.5. Proposed reaction intermediates leading to the exclusive formation of *cis*-cyclohexene carbonate.

The first report of a PO/CO_2 iron-catalyzed copolymerization was reported by the Nozaki group in 2013.[59] Their system was composed of an iron-corrole complex, **1.26**, with bridging oxo axial ligands, combined with PPNCl as a co-catalyst. The copolymerization of PO with CO_2 was achieved at 60 °C and 20 bar CO_2 pressure with a catalyst loading of 0.05 mol% iron and 0.5 equiv. PPNCl with respect to iron. These conditions gave an impressive TOF of 1004 h^{-1}; however, in all cases the % carbonate linkages in the obtained copolymer were quite low, never reaching values >30%. Increasing the amount of PPNCl decreased the selectivity and large amounts of propylene carbonate was observed. When the bimetallic iron species was replaced with a monomeric iron complex with chloride as the axial ligand, catalytic activity diminished. When an iron(III) species supported by tetraarylporphyrin ligands was used only the cyclic carbonate product was produced. This demonstrated that the combination of bimetallic iron species supported by a corrole ligand was essential in producing poly(propylene carbonate).

In 2013, Kleij, Pescarmona and coworkers reported iron amino triphenolate catalysts that were active for cyclic carbonate (discussed above) and polycyclohexene carbonate formation under supercritical CO_2 ($scCO_2$) conditions.[60] By carefully tuning the nature and relative amount of co-catalyst in relation to catalyst they were able to switch the selectivity of their system to produce either the cyclic or polymeric product when CHO was used as a substrate. They note that in order to control selectivity the intermediate in the catalytic cycle where back-biting or further epoxide insertion can occur (similar to what was shown in **Scheme 1.3** above) is very important. That is, back-biting to form the cyclic product is favoured if the nucleophile X^- is a good leaving group or if the metal-bound carbonate can easily dissociate and/or is displaced by another equivalent of X^-, preventing further epoxide insertion leading to polycarbonate formation. The authors screened a series of both tetrabutylammonium halides and bis(triphenylphosphine)iminium halides and saw that in general at higher ratios of co-catalyst to catalyst (10:1) formation of the cyclic product was favored and only the *cis* isomer was formed. This discovery was shown to be similar to work by Williams et al. as discussed previously, suggesting a displacement of the metal-bound carbonate before ring-closure.[29] Comparing the three complexes studied, similar activity was observed in complexes bearing either methyl or *tert*-butyl substituents (**1.27.1** and **1.27.2**) suggesting sterics had no major influence on the reaction mechanism.

The chloride substituted complex (**1.27.3**) showed lower activity which was attributed to its lower solubility in $scCO_2$. In all cases obtained polymers gave broad GPC traces which could be deconvoluted resulting in two separate molecular weight fractions. Glass transition temperatures of polycarbonates were in the range of 70-80 °C, and ^{13}C NMR analysis revealed that the polymer samples contained both isotactic and syndiotactic diads.

Following this report, Pescarmona et al. reported an iron(III)aminobis(phenolate) complex (**1.28**) as a catalyst for the copolymerization of CHO and CO_2 in $scCO_2$ (60 °C, 80 bar CO_2) in combination with a suitable cocatalyst (PPNCl or tetrabutylammonium salts- $[Bu_4N][X]$, where X = Cl, Br or OAc).[61] By fine-tuning the relative amounts of catalyst:cocatalyst >99% selectivity towards *cis*-CHC could be obtained but for PCHC formation conversions were good, but only up to 88% selectively for the polymeric product could be achieved. Polymers produced were of an oligomeric nature (740-1600 g mol^{-1}) with narrow dispersities. When the substrate was switched from CHO to VCHO the selectivity towards PVCHC increased to 98% at optimized conditions, however overall epoxide conversion remained low at 48%. Molecular weights also showed an overall increase up to 3800 g mol^{-1}. The microstructure of these materials were also investigated. In the case of both CHO and VCHO $^{13}C\{^1H\}$ NMR analysis revealed atactic polycarbonates. The obtained PVCHC could also be cross-linked using a radical initiator azobisisobutyronitrile (AIBN) and 1,3-propanedithiol leading to an overall increase of 55 °C in the original polymer glass transition temperature (T_g). This cross-linking resulted in lower solubility in a range of organic solvents alluding to improved chemical resistance of the cross-linked materials. SEM images showed a distinct difference in morphology between PVCHC and the corresponding cross-linked PVCHC which was attributed to possible nucleation and particle growth differences in ethanol between the two materials.

The Zevaco group have also published two reports of iron complexes containing a N,N-bis(2-pyridinecarboxamide)-1,2-benzene ligand framework (**1.8** and **1.9**) as catalysts for both cyclic carbonate and PCHC formation. In general, these complexes showed higher activity towards cyclic carbonates (discussed above) however, for reactions of CHO and CO_2, PCHC was obtained with very low molecular weights ranging from 760-2700 g mol^{-1}.[43-44]

In 2018 Capacchione et al. reported [OSSO]-type iron (III) complexes (**1.21.1-1.21.4**) that were active for cyclic carbonate (discussed above) and polycarbonate formation in the case of CHO/CO_2 copolymerization.[55] In all cases, bimodal molecular weight distributions were observed for the resulting polymers via GPC analysis which was in large part attributed to trace amounts of water in reaction mixtures. In an attempt to minimize this the epoxide was distilled twice over CaH_2 which resulted in both improved catalytic activity and nearly unimodal molecular weight distributions. As mentioned above in the case of cyclic carbonates, kinetic studies revealed a process first order in iron. However, in the case of polycarbonate formation, kinetic studies revealed a process second order in iron concentration suggesting the involvement of two iron centers in the catalytic cycle. DFT studies revealed, in the case of CHO, that the energy barrier for chain propagation is lower than that of the ring-closing step explaining polycarbonate selectivity in the case of CHO.

We have recently reported a family of iron(III) amino-bis(phenolate) complexes varying in phenolate substituents within the ligands and coordination geometries, and our attempts to establish structure-activity relationships for CO_2-epoxide reactions (**1.29-**

1.30).[53] This work has been published in *Inorg. Chem*. **2019**, 58, 11231-11240. and is discussed in detail in **Chapter 3**. **Table 1.2** summarizes data for those systems discussed above, which are active towards the copolymerization of CO_2 and epoxides to yield polycarbonates. In comparison to cyclic carbonate formation there are fewer reports of iron catalysts for polycarbonate formation; however, this area has advanced significantly in recent years. Comparing the systems in **Table 1.2**, it is worth noting for obtained polycarbonates the difference in % CO_3 linkages. For example, while the Nozaki iron corrole system gave the highest molecular weight polymer to date, the degree of carbonate linkage incorporation was quite low (**Table 1.2**, entry 3). In addition, in the case of CHO, controlling selectivity towards either PCHC or the cyclic product is crucial and can often be controlled by the relative amount of cocatalyst to iron.

Table 1.2. Summary of iron catalysts for copolymerization of CO_2 and epoxides.

Entry	Complex (mol% Fe) [Ref.]	Substrate	Cocatalyst	P_{CO_2} (bar)	T (°C)	t (h)	% Conv.	CO_3 links (%)	Mn [Đ]
1	**1.25** (0.1) [Williams, 2011][40]	CHO	-	10	80	24	70	99	11700 [1.1]
2	**1.25** (0.1) [Williams, 2011][40]	CHO	PPNCl (4 equiv.)	1	80	48	41 (*cis*-CHC)	-	-
3	**1.26** (0.05) [Nozaki, 2013][59]	PO	PPNCl (0.5 equiv.)	20	60	1	51[a]	17	29000 [1.3]
4	**1.27.1** (0.1) [Kleij, Pescarmona, 2013][60]	CHO	PPNCl (1 equiv.)	80	85	3	56[a]	99	1509 [1.3]; 6022 [1.1]
5	**1.28.1** (0.5) [Pescarmona, 2015][61]	CHO	TBACl (1 equiv.)	80	60	18	60 (82% PCHC; 18% cis-CHC)	96	1400 [1.1]
6	**1.9.3** (0.5) [Zevaco, 2014][44]	CHO	-	50	80	20	33 (100 selective)	100	2200 [1.2]
7	**1.21.2** (0.1 mol%) [Capacchione, 2018][55]	CHO	(TBACl 1 equiv.)	10	80	1	34	>99	23 200 [1.0], 1100 [1.0]
8	**1.29.1** (0.5) [Kerton, Kozak 2019] [53]	CHO	PPNCl (1 equiv.)	60	60	22	99	>99	9200 [1.1]
9	**1.29.1** (0.5) [Kerton, Kozak 2019][53]	CHO	PPNCl (4 equiv.)	60	60	22	99 (*cis*-CHC)	-	-

[a] Value reported as an isolated yield of carbonate instead of conversion of epoxide.

Compared to the numerous catalytic systems employing chromium and zinc in particular the examples of iron catalysts are limited. Consequently, there is still tremendous scope and space in the literature for further expansion on iron systems for these transformations.

1.6 The Power of Boron

1.6.1 Lewis Acidity of Boron

Traditionally boron-based reagents are employed as a Lewis acid in reactions due to their strong electrophilic nature due to a vacant p-orbital that is ideal for accepting electrons. Many neutral boranes exist such as trialkyl- and triaryl- in which their Lewis acidic nature can be easily tuned by modifying the alkyl- or aryl- substituents with electron withdrawing groups (**Figure 1.11**). Increasing the amount/nature of these groups can lead to the altering of the electrophilic nature of the central borane atom.[62-63] Perhaps the most famous example of a Lewis acidic borane is tris(pentafluorophenyl)borane, $[B(C_6F_5)_3]$ or commonly referred to as BCF, well-known for its strong Lewis acidity due to three fluorinated phenyl rings. This compound was first synthesized in the 1960s and since many different versions of this borane have been reported. The un-halogenated version of BCF, triphenylborane, BPh_3, exhibits a much lower Lewis acidity due to the absence of these fifteen fluorine atoms.

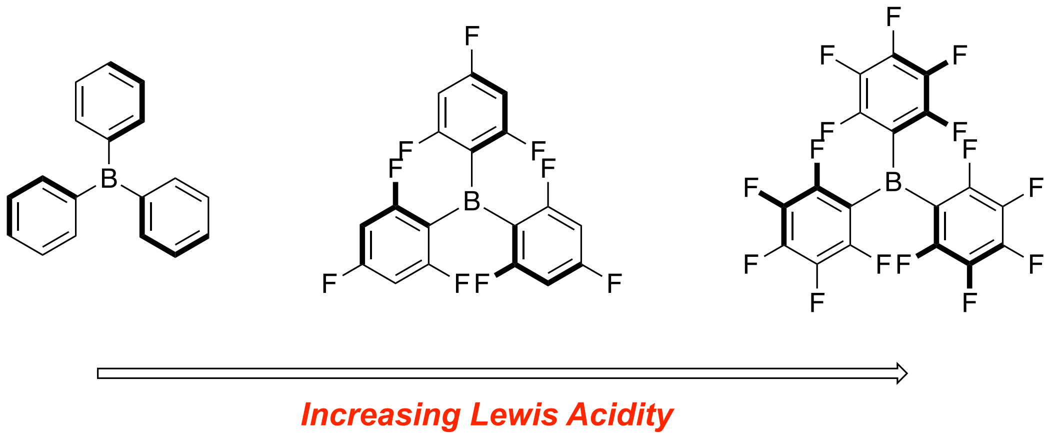

Figure 1.11. Boranes arranged in increasing Lewis acidic strength

It is possible to determine the Lewis acidity of a borane experimentally using various different methods (**Figure 1.12**). The first two methods in **Figure 1.12**, Gutmann-Beckett and the Childs Method are spectroscopic techniques that measure the effect of adding a probe molecule on the Lewis acidity of the borane in question. The Gutmann-Beckett method involves the addition of triethylphospine (Et_3PO) to the borane in question.[64] The borane will then undergo coordination of the oxygen atom in Et_3PO resulting in a shift of the ^{31}P NMR spectrum due to a deshielding effect on the phosphorus atom. This shift can be used to determine the acceptor number (AN) of the borane of interest. The AN can be defined as follows:

$$AN = \left\{ \frac{\delta complex - \delta(1)}{\delta(2) - \delta(1)} \right\} * 100$$

Where $\delta_{complex}$ represents the ^{31}P NMR shift of the Et_3PO coordinated to the complex of interest, $\delta_{(1)}$ and $\delta_{(2)}$ are the ^{31}P chemical shifts of Et_3PO dissolved in hexane (41.0 ppm, AN = 0) and $SbCl_5$ (86.1 ppm, AN = 100) respectively. The larger the AN value the more Lewis acidic the compound of interest is. For example, BCF has an AN of 76 while BPh_3 has an AN of 55.[65] Similar to the Gutmann-Beckett method, the Childs Method uses NMR spectroscopy to correlate Lewis acidity of an unknown compound. The Childs Method however, measures the change in ^{1}H NMR shift of the proton adjacent to the methyl group in crotonaldehyde upon its coordination to a Lewis acid.[66]

On the other hand, Fluoride Ion Affinity (FIA) and Hydride Ion Affinity (HIA) are computationally derived metrics. Fluoride ions, due to their small size and high electronegativity react readily with a Lewis acid. The reaction enthalpy of this interaction (fluoride ion affinity) can be measured and related to the strength of the Lewis acid. COF_2

is often used as a model substrate rather than F^- alone as its electron affinity is easier to calculate.[67] HIA uses computational methods to study a series of isodesmic reactions which allows the determination of the relative x hydride affinity of the Lewis acid being examined.[68]

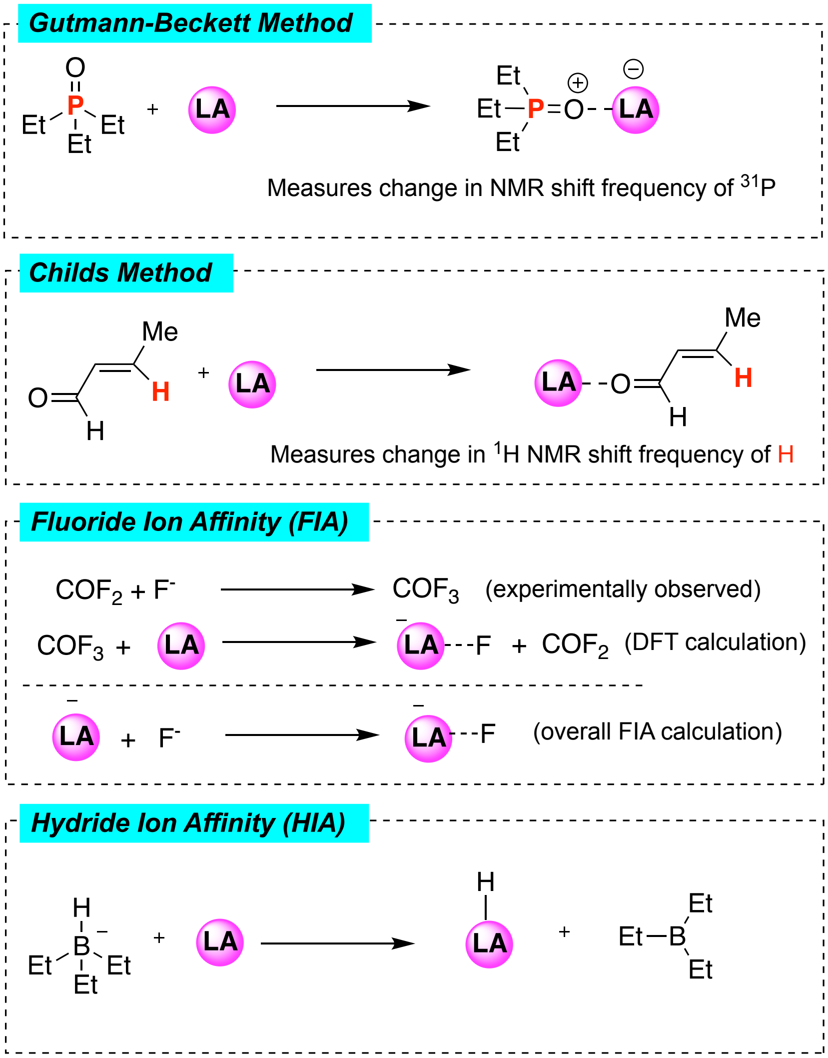

Figure 1.12. Common methods used for determining the Lewis acidic strength of boranes.

1.6.2 Boranes in Frustrated Lewis Pair chemistry

A Frustrated Lewis Pair (FLP) is defined as a compound containing both a Lewis acid and base that are unable to come together and form a traditional adduct due to increased steric hinderance. The first example of a FLP was reported by Stephan and coworkers in 2006. This example was based on a sterically encumbered phosphine and borane ($Mes_2PC_6F_4B(C_6F_5)_2$; Mes = 2,4,6-$Me_3C_6H_2$).[69] This system was capable of reversibly activating H_2. Since this report there has been an explosion of research in this area, applying the idea of FLP chemistry to many different catalytic transformations such as hydrogenations, hydrosilylations, hydroborations, aminations, hydroarylations, polymerizations and CO_2 reductions.[70-76] These breakthroughs have inspired chemists to future explore this area and has revealed the importance of boranes in FLP chemistry as the Lewis acid component of the ‘frustrated’ adduct. The Lewis acidic strength of the borane has a direct influence on the reactivity of the FLP of interest, which can be quantitively measured using methods mentioned above.

While there are several commercially available boranes, researchers have moved towards synthesizing boranes with varying electronic properties. This is especially true in the case of aryl boranes in which their Lewis acidic properties can be varied by modifying aryl substituents on the phenyl rings with various groups (i.e. different halogens for example).[77]

Trace amounts of water in FLP reactions can be problematic, resulting in catalyst poisoning and eventual borane degradation. Due to the strong Lewis acidity of these boranes, they exhibit a high oxophilicity. This leads to water coordination to the borane and formation of a [Ar_3-OH_2] Lewis acid/base adduct, which can, upon the elimination of C_6H_6 leads to borane decomposition.[78]

1.6.3 ^{11}B NMR as a Spectroscopic tool

There are two stable isotopes of boron, ^{10}B and ^{11}B, accounting for approx. 20% and 80% natural abundance respectively. ^{11}B is studied more extensively in NMR spectroscopy due to its higher sensitivity, abundance and resolution. Both nuclei are quadrupolar (^{11}B spin of 3/2 and ^{10}B spin of 3) and thus typically give quite broad signals. ^{11}B NMR shifts usually fall within the range of +100 to -120 ppm and spectra are referenced to $BF_3 \cdot OEt_2/CDCl_3$.

Use of traditional NMR tubes can lead to interferences in ^{11}B NMR spectra as they contain large quantities of borosilicate glass. This results in a broad hump in the spectrum between -30 to +30 ppm. As a result, researchers studying boron chemistry will often use quartz NMR tubes to eliminate this background signal. However, these tubes are more fragile and costly than traditional tubes.

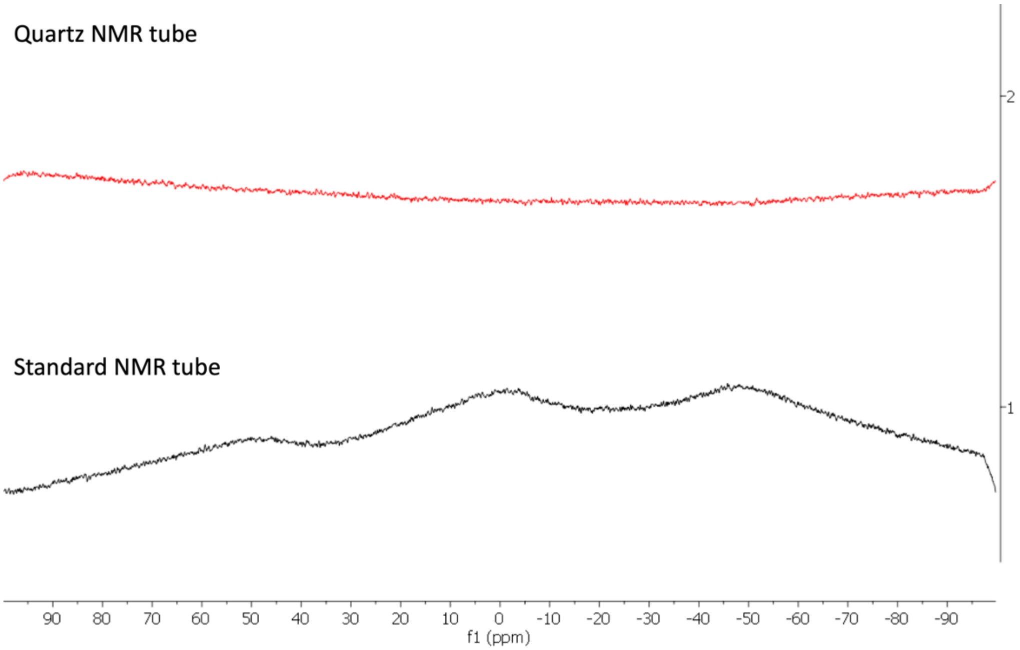

Figure 1.13. NMR spectra showing background signal vs. quartz tube

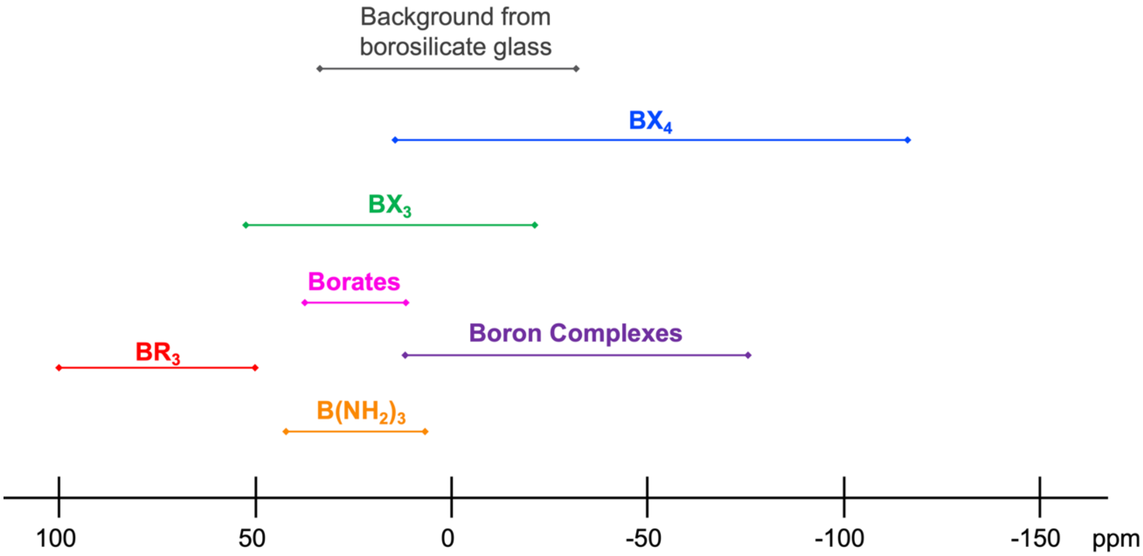

Figure 1.14. ^{11}B NMR shift ranges of common borane reagents and compounds.

1.7 Boron-containing Catalysts

1.7.1 Borane catalyzed ring-opening polymerizations of epoxides

There have been several borane systems, both alkyl and aryl boranes, reported for catalyzing ROP of epoxides. In 2003, Chen and co-workers reported the catalytic ROP of PO by both organoboranes and aluminum Lewis acids.[79] They evaluated the reactivity of six aryl boranes with varying Lewis acidity (**Figure 1.15**). It was found that the ROP of PO to form PPO was highly dependent on the Lewis acidity of the borane. That is, as the Lewis acidity of the borane decreased, so did the yield of PPO. Weakly Lewis acidic boranes (e.g. BPh_3 and $B(OC_6F_5)_3$) did not produce isolable amounts of PPO, while BCF proved to be the most active of the boranes studied. In addition to requiring a highly Lewis acidic borane, hydroxyl-containing initiators having high Brønsted acidity led to higher M_n polymers.

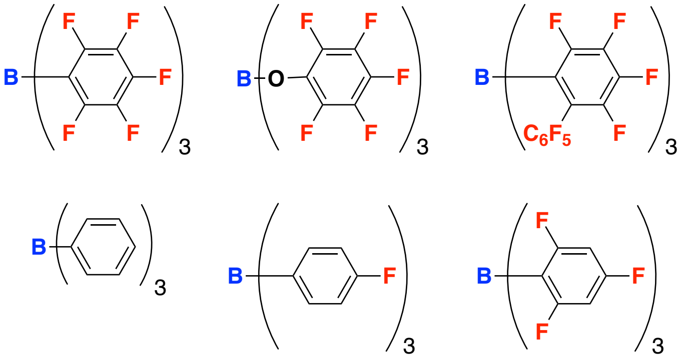

Figure 1.15. Aryl boranes evaluated for the catalytic ROP of PO by Chen and co-workers.

In 2014, Barroso-Bujans and co-workers reported BCF catalyzed zwitterionic polymerization of glycidol monomers to yield cyclic polyethers.[80] In comparison to their linear form, cyclic polyethers are attractive as they introduce new hydrodynamic, thermal, mechanical and chemical properties.[81-83] While zwitterionic ring-opening polymerization

(ZROP) is a known strategy to yield cyclic polymers, this was the first report of a borane catalyst for this transformation. BCF alone was able to catalyse the ZROP of glycidol phenyl ether (GPE), among other glycidol monomers, under anhydrous conditions to form cyclic polymers as studied via MALDI-TOF MS (**Scheme 1.6**). The mechanism was proposed based on both detailed experimental and DFT studies.[80] It was found that the presence of water in the reaction mixture led to the formation of linear hydroxyl-terminated chains rather that the desired cyclic product.

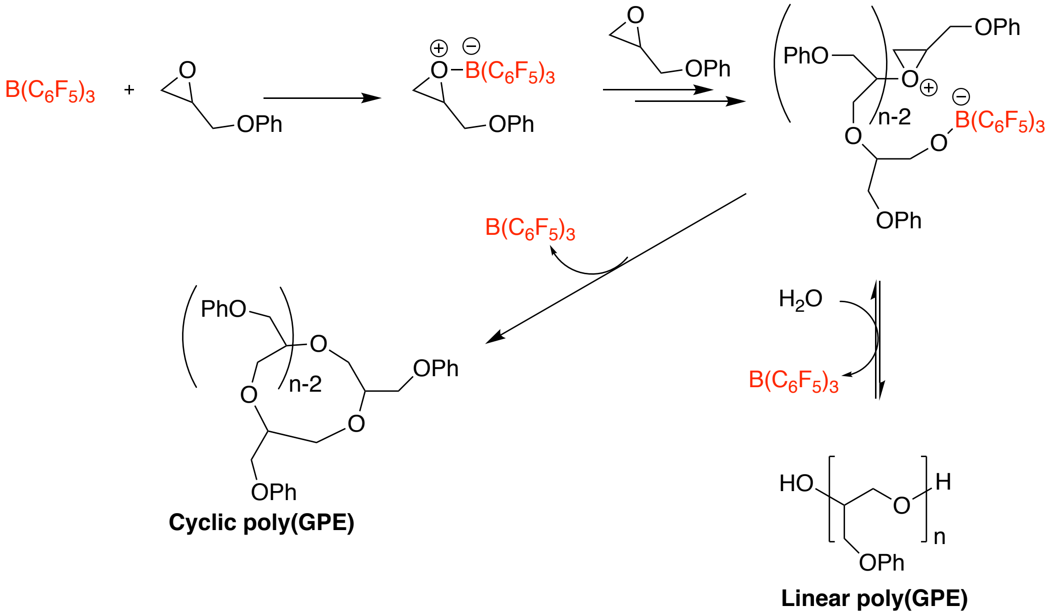

Scheme 1.6. Proposed reaction mechanism by Barroso-Bujans and co-workers for the zwitterionic ring-opening polymerization of glycidol phenyl ether (GPE) with $B(C_6F_5)_3$.

More recently, there has been two reports of BEt_3 catalysed ROP of epoxides to form polyethers. Zhao and co-workers reported the living ROP of epoxides by BEt_3 in combination with an alcohol or water initiator and an organobase (e.g. phosphazenes).[84] Their system proved very active, with TOFs exceeding 6000 h^{-1} and low catalyst loadings.

It was active for the ROP of both EO and PO yielding polyethers with high molecular weights and narrow dispersities. When the strength of organobase was increased ROP occurred much faster. However, the use of BEt_3 or organobase alone showed no conversion, demonstrating the synergistic role they play in the mechanism. Detailed kinetic and mechanistic studies gave insight into key reaction intermediates that impact the overall reactivity of the catalytic system. It was found that activation of the epoxide by uncomplexed BEt_3 is dependent on the ratios of [hydroxyl]/[organobase]/[BEt_3] along with the basicity of the organobase, nature of solvent and steric factors. Further, the system was tested with various substituted epoxides and the system could be employed in a one-pot fashion to yield PPO-based polyurethanes via the sequential addition of hexamethylene diisocyanate.

Very shortly following this initial report, Zhang and co-workers reported a very similar study using the same catalytic system and hence included similar data to the previous report.[85] The key difference was the system was able to yield block copolymers incorporating carbonyl sulfide (COS) and hence products featured alternating poly(COS-alt-PO) and PPO linkages. Further, by changing the macroinitiator to either alpha-OH terminated polyethylene glycol (PEG) or hydroxy-terminated polystyrene (PS), blocks containing PEG and PS could be incorporated.

1.7.2 Boron catalyzed reactions of CO_2 and epoxides

In terms of the reaction of epoxides with CO_2 to yield polycarbonates, there have only been two reports for boron-centered catalysis prior to the research presented in this thesis. In related research, boronic acids have been used to activate the epoxides via hydrogen-bonding in order to form cyclic carbonates.[86] The first polymerization example focused on triethylborane, BEt_3, which could copolymerize PO or CHO with CO_2.[87] The catalytic system was composed of BEt_3 and a Lewis base or onium salt, such as ammonium and phosphonium halides or metal alkoxides, with reactions performed in a co-solvent instead (typically THF) instead of neat epoxide. These systems were able to catalyse the copolymerization of PO and CO_2 at a 4 mol% catalyst loading under moderate reaction conditions (10 bar CO_2, 60 °C, 10 h). Screening a variety of co-catalysts, they found tetrabutyl ammonium chloride (Bu_4NCl) gave the highest activity with TOF values close to 50 h^{-1} and >90% carbonate content. In the absence of BEt_3 or co-catalyst no copolymerization was observed between PO and CO_2. In addition, the same systems were tested for the copolymerization of CHO and CO_2 at the same CO_2 pressure but at 80 °C for 6 h giving TOF values of up to 600 h^{-1}. The authors proposed that the BEt_3 served to activate the epoxide, while the ammonium cation activated CO_2 towards insertion into the resulting boron-alkoxide group but little experimental evidence was provided to support this step.

Following this study, Darensbourg et al. reported a similar catalytic system based on BEt_3 but for the copolymerization of carbonyl sulfide (COS) instead of CO_2 in combination with epoxides.[88] While the scope of this thesis focuses on the use of CO_2 in polymerization reactions we thought this report on COS polymerization reactions is relevant as it builds on the previously discussed BEt_3 system described above. The copolymerization of COS has been studied extensively by the Darensbourg group and it is well-established that metal-based systems follow a coordination-insertion mechanism similar to CO_2/epoxides as discussed in previous sections. COS, similar to CO_2 is a C-1 building block produced from the burning of fossil fuels and when released into the atmosphere is a contributor to acid rain and sulfur aerosols leading to damage of the ozone layer. Hence the utilization of COS in an atom economical fashion is desirable. It was reported that BEt_3 combined with various Lewis bases (i.e. amidine, quinidine) and quaternary onium salts in the presence of COS and several epoxides could yield perfectly regioselective copolymers. Initially the copolymerization of COS and PO was studied. A strong temperature dependence was observed. These systems gave the highest polymer yields at 25 °C with greater than 99% copolymer selectivity. However, as the temperature was increased, they saw a larger amount of cyclic carbonate formation as a result of the competing back-biting mechanism. For example, when 1,8-diazobicyclo[5.4.0]undec-7-ene (DBU) was added in addition to BEt_3 at 80 °C, 100% conversion to the cyclic product was observed. Additionally, they were able to optimize reaction conditions for the copolymerization of COS with CHO and phenyl glycidol ether at 25 °C. Further, the group aimed to give mechanistic insight into several catalytic steps and reaction intermediates. Using ^1H NMR spectroscopy, they studied the BEt_3/DBU catalytic system. They were able to identify the formation of a BEt_3/DBU adduct, followed by PO activation by this pre-formed Lewis pair. Ring-opening of PO then occurred via attack by DBU serving as the external nucleophile generating a boron-alkoxide intermediate. This step was followed by formal COS insertion, similar to the metal-based CO_2/epoxide systems previously described (**Scheme 1.7**). It is likely that the CO_2/PO reactions catalysed by BEt_3 described in the previous paragraph also proceed through a similar mechanism.

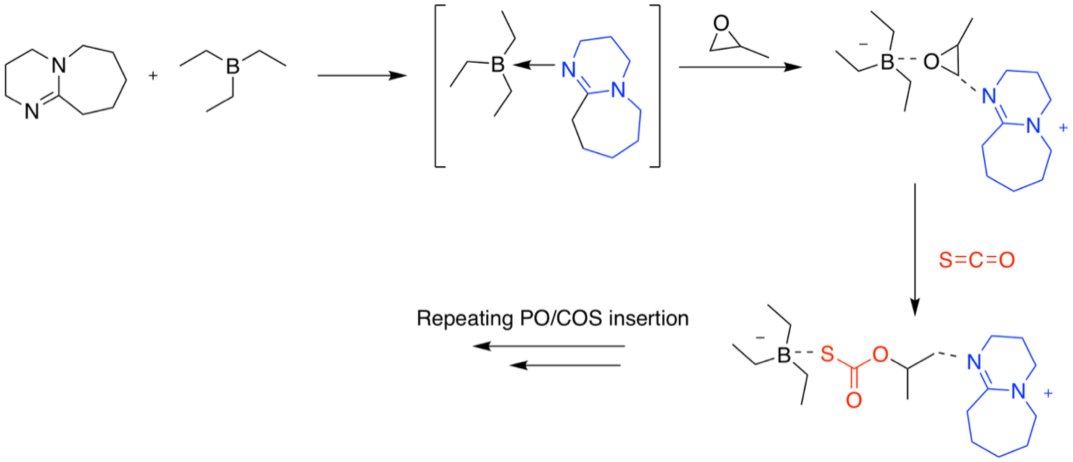

Scheme 1.7. Proposed reaction key intermediates by Darensbourg et al. for their BEt_3/DBU system with propylene oxide.

To the best of our knowledge the only other report of a borane catalysed CO_2/epoxide ROCOP system was reported by our group in 2019 (and reported in **Chapter 4** herein).[89] Based on the activity of the BEt_3 systems discussed above and the relation between Lewis acidic strength and reactivity control in other classes of reactions we chose to evaluate triarylboranes as catalysts. We envisioned that triarylboranes are more readily modified than trialkylboranes. This approach introduces the potential to tailor reactivity through modifying the Lewis acid strength and sterics of the central borane. As this was the first report of an aryl borane catalyst for these transformations, we chose to study it in more detail from a kinetic and mechanistic standpoint. This work will be discussed in detail in **Chapter 4**.

1.7.3 Boron catalyzed reactions of epoxides and anhydrides

The ring-opening alternating copolymerization of epoxides and cyclic anhydrides (ROAC) to produce a diverse class of polyesters is another promising route to the development of sustainable polymeric materials (**Scheme 1.8**).[9, 90] This atom economical reaction is a promising route to polyesters as many of the epoxide and anhydride monomers can be sourced from biomass and are commercially available.[90-92] In addition, the development of a metal-free catalytic route to these materials remains challenging with only a few reported examples, which is of relevance to boron-centered catalysis.

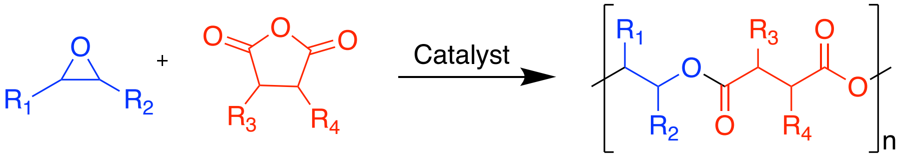

Scheme 1.8. General reaction scheme for the ring-opening alternating copolymerization of epoxides and cyclic anhydrides to produce polyesters

The use of boranes for these ROAC transformations are new and underexplored with only a few publications to date. First, Zhang and co-workers reported the use of boranes, BEt_3, BPh_3, and BCF for the copolymerization of PO and maleic anhydride (MA).[93] The binary catalytic system was comprised of a Lewis acid and a co-catalyst with the combination of BEt_3 and N,N,N-trimethyl-1-dodecana-minium bromide (DTMeAB) yielding the best results. Conversions of MA >99% could be obtained within 12 h (TOF = 102 h^{-1}), and obtained polymers had M_n 5.7 kDa and $Đ = 1.3$. In addition, the system was also able to catalyze the copolymerization of PO and phthalic anhydride (PAH) with a TOF of 303 h^{-1}. Interestingly, the authors could produce block polyesters. First, a mixture of PO and MA was copolymerized in the presence of phenylethylalcohol. Once, the MA was consumed a 1:1 mixture of PO and succinic anhydride (SA) was added allowing the growth of a second polyester block (**Scheme 1.9**). [93]

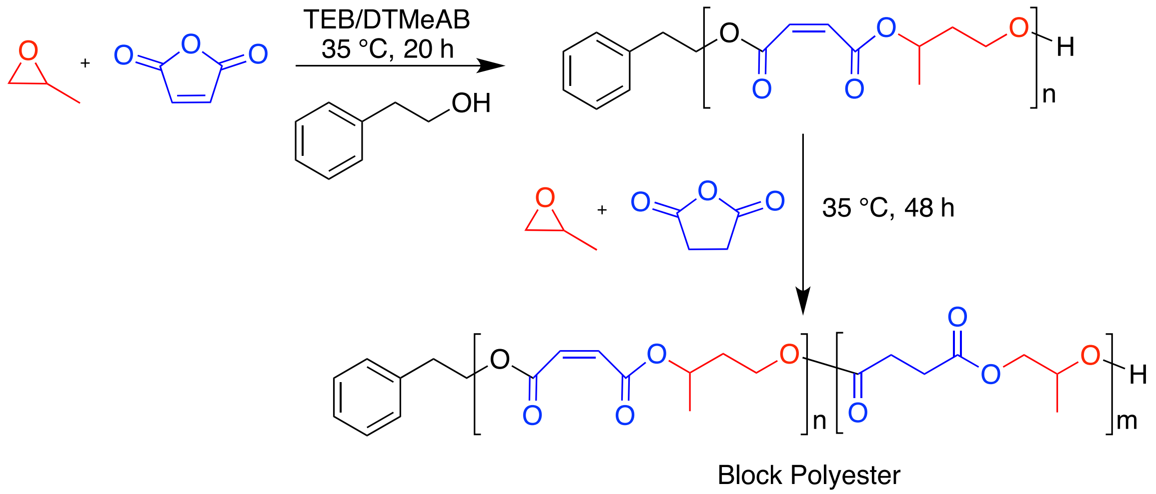

Scheme 1.9. Block polyester formation of [(PO-alt-MA)-b-(PO-alt-SA)] by Zhang and co-workers

Following this initial study, Chakraborty and co-workers expanded the substrate scope to include several other epoxides (i.e. CHO, *tert*-butyl glycidol ether (*t*BGE) and 2-benzyloxirane (BO)).[94] They first screened combinations of various Lewis bases (DMAP, DBU and 1,5,7-Triazabicyclo[4.4.0]dec-5-ene (TBD)) or PPNCl alongside Lewis acids (BEt_3, $Al(CH)_3$, $n$$Bu_2Mg$ and Et_2Zn) for the copolymerization of PAH and CHO. It was found that the reactivity of Lewis acids was in the following order: $BEt_3>>>nBu_2Mg>Al(CH)_3>Et_2Zn$, with the combination of BEt_3/PPNCl being the most promising of those screened. *In situ* NMR studies between the Lewis pairs and monomers demonstrated insight into rate determining steps within the catalytic cycle. The BEt_3/PPNCl adduct serves as an initiator for polymerization, while the excess BEt_3 aids in epoxide activation towards ring-opening. As such, they found that a molar ratio of 2:1 BEt_3:PPNCl was needed for high conversions. The ring-opened epoxide serves as an initiator to ring-open an anhydride unit in the polymerization. They showed that in terms of rates: i) the rate of anhydride ring-opening by alkoxide anions (from a ring-opened epoxide species) is faster than by carboxylate anions (from a ring-opened anhydride species). ii) the rate of anhydride addition to the growing polymeric chain is faster than the addition of a second epoxide unit, explaining the perfectly alternating nature of the obtain product (**Scheme 1.10**).[94] Finally, when *t*BGE was used in the copolymerizations, the *t*-butyl could be cleaved leading to the formation of polyester-co-glycerols.

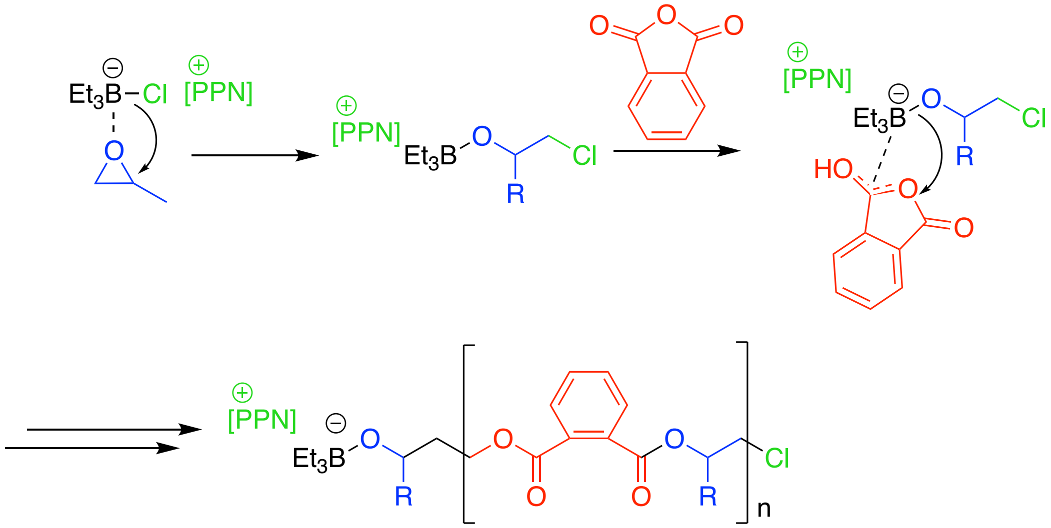

Scheme 1.10. Proposed mechanism for the copolymerization of PO and PAH catalyzed by BEt_3/PPNCl.

Very shortly following this, the same catalytic system, BEt_3/PPNCl, was used by another group for the ring-opening alternating copolymerization of epoxides and tricyclic anhydrides.[95] A collection of nine epoxides and four tricyclic anhydrides were screened, all reactions yielded well-defined polyesters with uniform molecular weights and dispersities. No epimerization or transesterification was observed in all cases. In addition, a one-pot quasi-block copolyester was synthesized by the terpolymerization of a mixture of ECH, AGE and *exo*-NB. The block nature of the polyester was possible in a one-pot fashion due to the difference in rates of consumption between ECH and AGE. ECH ring-opening was found to be much faster than that of AGE, such that once nearly all ECH had reacted (>91% after 45 min) AGE had only just begun to incorporate into the growing chain, leading to the production of a gradient co-polyester (**Scheme 1.11**).[95]

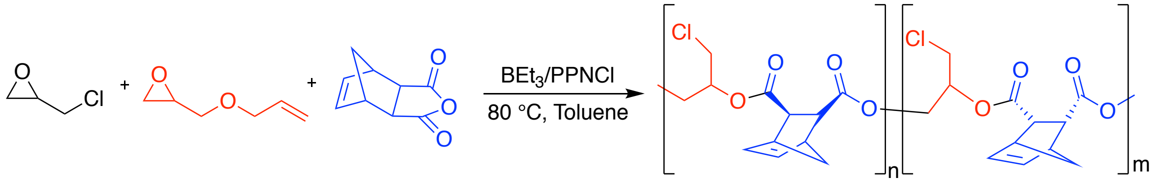

Scheme 1.11. One-pot terpolymerization of PO, AGE and *exo*-NB by BEt_3/PPNCl to yield quasi-block copolymers

1.8 Thesis Objectives

Previous work in the Kerton group had shown a series of iron amino-bis(phenolate) chloride complexes were active for the selective production of cyclic carbonates. During coupling reactions, a distinct color change of reaction mixtures from purple to brick red was observed. Motivated by this result, we were interested in studying these systems further to give insight into the active catalytic species present during reactions. This detailed study is presented in **Chapter 2**.

Building upon this work and other results from the Kozak group we synthesized a series of iron(III) amino-bis(phenolate) possessing different coordination geometries (both trigonal bipyramidal and square-based pyramidal) and studied their reactivity for both cyclic and polycarbonate formation. It was found that only those complexes in a trigonal bipyramidal geometry were active towards polycarbonate formation. In addition, the nature of the pendent donor on the ligand backbone along with the phenolate substituents of the ligand were critical for controlling product selectivity. This study is presented in **Chapter 3**.

Organocatalysts have gained attention in recent years in the area of CO_2/epoxide coupling and polymerization in a drive to move away from potentially more costly transition metals.[96] Furthermore, these classes of catalysts may be advantageous in terms of ease of product purification. Boranes are well-studied reagents in FLP chemistry but prior to our work there have only been two reports of using boranes in CO_2/epoxide chemistry (i.e. triethylborane). We envisioned, based on our knowledge of the importance of the Lewis acidic strength of the borane in FLP chemistry, that aryl boranes would be attractive catalysts as they are more easily modified that alkyl boranes. This led to the first report of an aryl borane as a catalyst for both cyclic and polycarbonate formation. This work is presented in **Chapter 4**.

A new emerging area within the field of polycarbonate synthesis is post-synthesis polymer functionalization. This can lead to the production of materials with fine-tuned properties specific to an area of application and broadens the potential use of these materials on an industrial scale. It has been well documented in the literature that the Lewis acidic borane, BCF, is an active catalyst for the hydrosilylation of alkenes. However, in comparison BPh_3 has not been reported to catalyze these transformations. Building on our previous work with BPh_3 catalyzed polymerizations in **Chapter 4**, we envisioned that BPh_3

could serve as a catalyst for both polymerizations followed by a post-polymerization hydrosilylation of the resulting material leading to the production of a functionalized material in a one-pot manner. This work was successful and is discussed in detail in **Chapter 5**.

Finally, another similar area of polymer research revolves around the copolymerization of epoxides and anhydrides to yield polyesters. Similar to CO_2/epoxide reactions, this field has been dominated by metal-based catalytic systems. There have been very few reports on borane catalysed systems and no reports to date of an aryl borane serving as a catalyst. Again, we envisioned the potential for aryl boranes to serve as an efficient catalyst for polyester synthesis. In addition, while the production of these materials is important, the controlled depolymerization is equally of crucial importance. We saw the potential for boranes to fill this gap and chose to explore it further. These results on both polymerization and depolymerization are presented in **Chapter 6**.

1.9 References

1. Anastas, P. T., *Chem. Rev.* **2007,** *107* (6), 2167-2168.

2. Anastas, P. T.; Warner, J. C., *Green Chemistry: Theory and Practice*. Oxford University Press: New York, 2000; p 152.

3. Aresta, M., Carbon Dioxide Reduction and Uses as a Chemical Feedstock. In *Activation of Small Molecules*, Wiley-VCH Verlag GmbH & Co. KGaA: 2006; pp 1-41.

4. Liu, Q.; Wu, L.; Jackstell, R.; Beller, M., *Nat. Commun.* **2015,** *6*, 5933.

5. Childers, M. I.; Longo, J. M.; Van Zee, N. J.; LaPointe, A. M.; Coates, G. W., *Chem. Rev.* **2014,** *114* (16), 8129-8152.

6. Herzberger, J.; Niederer, K.; Pohlit, H.; Seiwert, J.; Worm, M.; Wurm, F. R.; Frey, H., *Chem. Rev.* **2016,** *116* (4), 2170-2243.

7. Kozak, C. M.; Ambrose, K.; Anderson, T. S., *Coord. Chem. Rev.* **2018,** *376*, 565-587.

8. Wang, Y.; Darensbourg, D. J., *Coord. Chem. Rev.* **2018,** *372*, 85-100.

9. Longo, J. M.; Sanford, M. J.; Coates, G. W., *Chem. Rev.* **2016,** *116* (24), 15167-15197.

10. Lu, X.-B.; Darensbourg, D. J., *Chem. Soc. Rev.* **2012,** *41* (4), 1462-1484.

11. Sheng, X.; Wu, W.; Qin, Y.; Wang, X.; Wang, F., *Polym. Chem.* **2015,** *6* (26), 4719-4724.

12. Ni, K.; Kozak, C. M., *Inorg. Chem.* **2018,** *57* (6), 3097-3106.

13. Darensbourg, D. J.; Yarbrough, J. C.; Ortiz, C.; Fang, C. C., *J. Am. Chem. Soc.* **2003,** *125* (25), 7586-7591.

14. Liu, J.; Ren, W.-M.; Liu, Y.; Lu, X.-B., *Macromolecules* **2013,** *46* (4), 1343-1349.

15. Andrea, K. A.; Kerton, F. M., *ACS Catal.* **2019,** *9* (3), 1799-1809.

16. Kozak, C. M.; Ambrose, K.; Anderson, T. S., *Coord. Chem. Rev.* **2018,** *376*, 565-587.

17. Small, B. L.; Brookhart, M.; Bennett, A. M. A., *J. Am. Chem. Soc.* **1998,** *120* (16), 4049-4050.

18. Ittel, S. D.; Johnson, L. K.; Brookhart, M., *Chem. Rev.* **2000,** *100* (4), 1169-1204.

19. Britovsek, G. J. P.; Bruce, M.; Gibson, V. C.; Kimberley, B. S.; Maddox, P. J.; Mastroianni, S.; McTavish, S. J.; Redshaw, C.; Solan, G. A.; Strömberg, S.; White, A. J. P.; Williams, D. J., *J. Am. Chem. Soc.* **1999,** *121* (38), 8728-8740.

20. Qi, M.; Dong, Q.; Wang, D.; Byers, J. A., *J. Am. Chem. Soc.* **2018,** *140* (17), 5686-5690.

21. Delle Chiaie, K. R.; Biernesser, A. B.; Ortuño, M. A.; Dereli, B.; Iovan, D. A.; Wilding, M. J. T.; Li, B.; Cramer, C. J.; Byers, J. A., *Dalton Trans.* **2017,** *46* (38), 12971-12980.

22. Biernesser, A. B.; Delle Chiaie, K. R.; Curley, J. B.; Byers, J. A., *Angew. Chem. Int. Ed.* **2016,** *55* (17), 5251-5254.

23. Wei, J.; Riffel, M. N.; Diaconescu, P. L., *Macromolecules* **2017,** *50* (5), 1847-1861.

24. Wei, J.; Diaconescu, P. L., *Acc. Chem. Res.* **2019,** *52* (2), 415-424.

25. Wang, X.; Thevenon, A.; Brosmer, J. L.; Yu, I.; Khan, S. I.; Mehrkhodavandi, P.; Diaconescu, P. L., *J. Am. Chem. Soc.* **2014,** *136* (32), 11264-11267.

26. Quan, S. M.; Wang, X.; Zhang, R.; Diaconescu, P. L., *Macromolecules* **2016,** *49* (18), 6768-6778.

27. Lai, A.; Hern, Z. C.; Diaconescu, P. L., *ChemCatChem* **2019,** *11* (16), 4210-4218.

28. Swart;, W. J. K. D. J. 1985.

29. Kruper, W. J.; Dellar, D. V., *J. Org. Chem.* **1995,** *60* (3), 725-727.

30. Darensbourg, D. J.; Rainey, P.; Yarbrough, J., *Inorg. Chem.* **2001,** *40* (5), 986-993.

31. Darensbourg, D. J.; Adams, M. J.; Yarbrough, J. C.; Phelps, A. L., *Inorg. Chem.* **2003,** *42* (24), 7809-7818.

32. Shibasaki, Y.; Sanada, H.; Yokoi, M.; Sanda, F.; Endo, T., *Macromolecules* **2000,** *33* (12), 4316-4320.

33. Suriano, F.; Coulembier, O.; Hedrick, J. L.; Dubois, P., *Polym. Chem.* **2011,** *2* (3), 528-533.

34. Brignou, P.; Priebe, G. M.; Casagrande, O.; Carpentier, J.-F.; Guillaume, S. M., *Macromolecules* **2010,** *43*, 8007-8017.

35. Saito, T.; Takojima, K.; Oyama, T.; Hatanaka, S.; Konno, T.; Yamamoto, T.; Tajima, K.; Isono, T.; Satoh, T., *ACS Sus. Chem. Eng.* **2019,** *7* (9), 8868-8875.

36. Gao, L.; Dong, B.; Zhang, J.; Chen, Y.; Qiao, H.; Liu, Z.; Chen, E.; Dong, Y.; Cao, C.; Huang, D.; Chen, W., *ACS Macro Lett.* **2019,** *8* (12), 1552-1558.

37. Marquis, E. T. Sanderson, J. R. US Patent 5, 283, 356, 1994.

38. Ji, D. F.; Lu, X. B.; He, R., *Appl. Catal. A-Gen.* **2000,** *203* (2), 329-333.

39. Jin, L.; Jing, H.; Chang, T.; Bu, X.; Wang, L.; Liu, Z., *J. Mol. Catal. A-Chem.* **2007,** *261* (2), 262-266.

40. Buchard, A.; Kember, M. R.; Sandeman, K. G.; Williams, C. K., *Chem. Commun.* **2011,** *47* (1), 212-214.

41. Dengler, J. E.; Lehenmeier, M. W.; Klaus, S.; Anderson, C. E.; Herdtweck, E.; Rieger, B., *Eur. J. Inorg. Chem.* **2011,** *2011* (3), 336-343.

42. Sheng, X.; Qiao, L.; Qin, Y.; Wang, X.; Wang, F., *Polyhedron* **2014,** *74*, 129-133.

43. Adolph, M.; Zevaco, T. A.; Walter, O.; Dinjus, E.; Döring, M., *Polyhedron* **2012,** *48* (1), 92-98.

44. Adolph, M.; Zevaco, T. A.; Altesleben, C.; Walter, O.; Dinjus, E., *Dalton Trans.* **2014,** *43* (8), 3285-3296.

45. Fuchs, M. A.; Zevaco, T. A.; Ember, E.; Walter, O.; Held, I.; Dinjus, E.; Doring, M., *Dalton Trans.* **2013,** *42* (15), 5322-5329.

46. Whiteoak, C. J.; Martin, E.; Martinez Belmonte, M.; Benet-Buchholz, J.; Kleij, A. W., *Adv. Synth. Catal.* **2012,** *354* (2-3), 469-476.

47. Whiteoak, C. J.; Gjoka, B.; Martin, E.; Martinez Belmonte, M.; Escudero-Adan, E. C.; Zonta, C.; Licini, G.; Kleij, A. W., *Inorg. Chem.* **2012,** *51* (20), 10639-10649.

48. Whiteoak, C. J.; Martin, E.; Escudero-Adán, E.; Kleij, A. W., *Adv. Synth. Catal.* **2013,** *355* (11-12), 2233-2239.

49. Buonerba, A.; De Nisi, A.; Grassi, A.; Milione, S.; Capacchione, C.; Vagin, S.; Rieger, B., *Catal. Sci. Technol.* **2015,** *5* (1), 118-123.

50. Al-Qaisi, F. a. M.; Nieger, M.; Kemell, M. L.; Repo, T. J., *ChemistrySelect* **2016,** *1* (3), 545-548.

51. Alhashmialameer, D.; Collins, J.; Hattenhauer, K.; Kerton, F. M., *Catal. Sci. Technol.* **2016,** *6* (14), 5364-5373.

52. Andrea, K. A.; Brown, T. R.; Murphy, J. N.; Jagota, D.; McKearney, D.; Kozak, C. M.; Kerton, F. M., *Inorg. Chem.* **2018,** *57* (21), 13494-13504.

53. Andrea, K. A.; Butler, E. D.; Brown, T. R.; Anderson, T. S.; Jagota, D.; Rose, C.; Lee, E. M.; Goulding, S. D.; Murphy, J. N.; Kerton, F. M.; Kozak, C. M., *Inorg. Chem.* **2019,** *58* (16), 11231-11240.

54. Fazekas, E.; Nichol, G. S.; Shaver, M. P.; Garden, J. A., *Dalton Trans.* **2018,** *47* (37), 13106-13112.

55. Della Monica, F.; Maity, B.; Pehl, T.; Buonerba, A.; De Nisi, A.; Monari, M.; Grassi, A.; Rieger, B.; Cavallo, L.; Capacchione, C., *ACS Catal.* **2018,** *8* (8), 6882-6893.

56. Cozzolino, M.; Leo, V.; Tedesco, C.; Mazzeo, M.; Lamberti, M., *Dalton Trans.* **2018,** *47* (37), 13229-13238.

57. Kamphuis, A. J.; Milocco, F.; Koiter, L.; Pescarmona, P.; Otten, E., *ChemSusChem* **2019,** *0* (ja).

58. Driscoll, O. J.; Hafford-Tear, C. H.; McKeown, P.; Stewart, J. A.; Kociok-Köhn, G.; Mahon, M. F.; Jones, M. D., *Dalton Trans.* **2019,** *48* (40), 15049-15058.

59. Nakano, K.; Kobayashi, K.; Ohkawara, T.; Imoto, H.; Nozaki, K., *J. Am. Chem. Soc.* **2013,** *135* (23), 8456-8459.

60. Taherimehr, M.; Al-Amsyar, S. M.; Whiteoak, C. J.; Kleij, A. W.; Pescarmona, P. P., *Green Chem.* **2013,** *15* (11), 3083-3090.

61. Taherimehr, M.; Serta, J.; Kleij, A. W.; Whiteoak, C. J.; Pescarmona, P. P., *ChemSusChem* **2015,** *8* (6), 1034-1042.

62. Lawson, J. R.; Melen, R. L., *Inorg. Chem.* **2017,** *56* (15), 8627-8643.

63. Lawson, J. R.; Melen, R. L., Recent developments and applications of Lewis acidic boron reagents. In *Organometallic Chemistry: Volume 41*, The Royal Society of Chemistry: 2017; Vol. 41, pp 1-27.

64. Beckett, M. A.; Strickland, G. C.; Holland, J. R.; Sukumar Varma, K., *Polymer* **1996,** *37* (20), 4629-4631.

65. Sivaev, I. B.; Bregadze, V. I., *Coord. Chem. Rev.* **2014,** *270-271*, 75-88.

66. Slootweg, J. C.; Jupp, A. R., *Frustrated Lewis Pairs*. Springer: 2020.

67. Christe, K. O.; Dixon, D. A.; McLemore, D.; Wilson, W. W.; Sheehy, J. A.; Boatz, J. A., *J. Fluor. Chem.* **2000,** *101* (2), 151-153.

68. Mock, M. T.; Potter, R. G.; Camaioni, D. M.; Li, J.; Dougherty, W. G.; Kassel, W. S.; Twamley, B.; DuBois, D. L., *J. Am. Chem. Soc.* **2009,** *131* (40), 14454-14465.

69. Welch, G. C.; Juan, R. R. S.; Masuda, J. D.; Stephan, D. W., *Science* **2006,** *314* (5802), 1124.

70. Stephan, D. W., *Science* **2016,** *354* (6317).

71. Stephan, D. W., *Acc. Chem. Res.* **2015,** *48* (2), 306-316.

72. Stephan, D. W., *Angew. Chem., Int. Ed.* **2017,** *56* (22), 5984-5992.

73. Stephan, D. W.; Erker, G., *Angew. Chem. Int. Ed.* **2015,** *54* (22), 6400-6441.

74. Stephan, D. W., *J. Am. Chem. Soc.* **2015,** *137* (32), 10018-10032.

75. Stephan, D. W., *Org. Biomol. Chem.* **2012,** *10* (30), 5740-5746.

76. Stephan, D. W.; Erker, G., *Angew. Chem. Int. Ed.* **2010,** *49* (1), 46-76.

77. Morgan, M. M.; Marwitz, A. J. V.; Piers, W. E.; Parvez, M., *Organometallics* **2013,** *32* (1), 317-322.

78. Bergquist, C.; Bridgewater, B. M.; Harlan, C. J.; Norton, J. R.; Friesner, R. A.; Parkin, G., *J. Am. Chem. Soc.* **2000,** *122* (43), 10581-10590.

79. Chakraborty, D.; Rodriguez, A.; Chen, E. Y. X., *Macromolecules* **2003,** *36* (15), 5470-5481.

80. Asenjo-Sanz, I.; Veloso, A.; Miranda, J. I.; Pomposo, J. A.; Barroso-Bujans, F., *Polym. Chem.* **2014,** *5* (24), 6905-6908.

81. Laurent, B. A.; Grayson, S. M., *Chem. Soc. Rev.* **2009,** *38* (8), 2202-2213.

82. Hoskins, J. N.; Grayson, S. M., *Polym. Chem.* **2011,** *2* (2), 289-299.

83. Chang, Y. A.; Waymouth, R. M., *J. Polym. Sci. A: Polym. Chem.* **2017,** *55* (18), 2892-2902.

84. Chen, Y.; Shen, J.; Liu, S.; Zhao, J.; Wang, Y.; Zhang, G., *Macromolecules* **2018,** *51* (20), 8286-8297.

85. Zhang, C.-J.; Duan, H.-Y.; Hu, L.-F.; Zhang, C.-H.; Zhang, X.-H., *ChemSusChem* **2018,** *11* (24), 4209-4213.

86. Wang, J.; Zhang, Y., *ACS Catal.* **2016,** *6* (8), 4871-4876.

87. Zhang, D.; Boopathi, S. K.; Hadjichristidis, N.; Gnanou, Y.; Feng, X., *J. Am. Chem. Soc.* **2016,** *138* (35), 11117-11120.

88. Yang, J.-L.; Wu, H.-L.; Li, Y.; Zhang, X.-H.; Darensbourg, D. J., *Angew. Chem. Int. Ed.* **2017,** *56* (21), 5774-5779.

89. Andrea, K. A.; Kerton, F. M., *ACS Catal.* **2019,** *9* (3), 1799-1809.

90. Paul, S.; Zhu, Y.; Romain, C.; Brooks, R.; Saini, P. K.; Williams, C. K., *Chem. Commun.* **2015,** *51* (30), 6459-6479.

91. Tong, R., *Ind. Eng. Chem. Res.* **2017,** *56* (15), 4207-4219.

92. Rabnawaz, M.; Wyman, I.; Auras, R.; Cheng, S., *Green Chem.* **2017,** *19* (20), 4737-4753.

93. Hu, L.-F.; Zhang, C.-J.; Wu, H.-L.; Yang, J.-L.; Liu, B.; Duan, H.-Y.; Zhang, X.-H., *Macromolecules* **2018,** *51* (8), 3126-3134.

94. Kummari, A.; Pappuru, S.; Chakraborty, D., *Polym. Chem.* **2018,** *9* (29), 4052-4062.

95. Ji, H.-Y.; Chen, X.-L.; Wang, B.; Pan, L.; Li, Y.-S., *Green Chem.* **2018,** *20* (17), 3963-3973.

96. Fiorani, G.; Guo, W.; Kleij, A. W., *Green Chem.* **2015,** *17* (3), 1375-1389.

Co-authorship Statement

Chapter 2 : Characterization of Oxo-Bridged Iron Amino-bis(phenolate) Complexes Formed Intentionally or in Situ: Mechanistic Insight into Epoxide Deoxygenation during the Coupling of CO_2 and Epoxides

This chapter has been peer reviewed and published in:

Inorganic Chemistry, **2018**, 57 (21), 13494-13504

Authors: Kori A. Andrea[a], Tyler R. Brown[a], Jennifer N. Murphy[a], Dakshita Jagota[a], Declan McKearney[b], Christopher M. Kozak[a] and Francesca M. Kerton*[a]

[a] Department of Chemistry, Memorial University of Newfoundland, St. John’s, NL, A1B 3X7, Canada

[b] Department of Chemistry, Simon Fraser University, Burnaby, BC, V5A 1S6, Canada

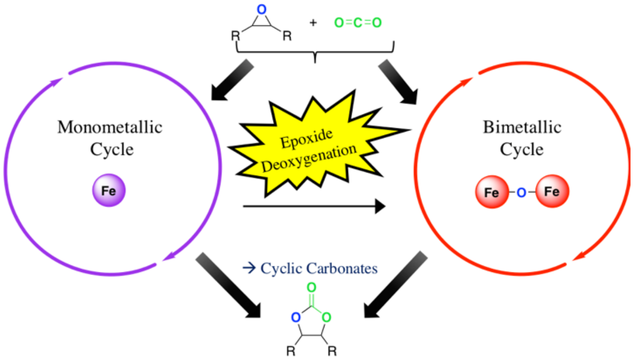

The first author (K. A. Andrea) contributed to 90% of the article, including manuscript writing, performing experiments and data analysis. T. R. Brown and D. Jagota were undergraduate students supervised by K. A. Andrea. Jennifer N. Murphy collected, analyzed and solved all crystallographic data. D. McKearney collected SQUID magnetometry data that were interpreted by C. M. Kozak. The corresponding author, F. M. Kerton, directed the project, assisted in experimental design and manuscript writing.

Chapter 2: Characterization of Oxo-Bridged Iron Amino-bis(phenolate) Complexes Formed Intentionally or in Situ: Mechanistic Insight into Epoxide Deoxygenation during the Coupling of CO_2 and Epoxides

See Appendix A for additional data

2.1 Introduction

The use of CO_2 as a renewable C-1 feedstock is driven by the potential to create a renewable carbon economy.[1-4] Its use in the preparation of commercially viable chemicals in a 'green' manner is attractive due to its low toxicity and cost. Due to the thermodynamic stability of CO_2, the use of highly reactive substrates such as epoxides allows the thermodynamic barrier of reactions to be overcome.[5-7] While the reaction between CO_2 and epoxides is generally well understood, producing either polycarbonates or cyclic carbonates, catalyst design is crucial in targeting selective formation of one product.[1, 8-10] For example, if the rate of epoxide ring-opening is greater than the rate of CO_2 insertion, homopolymerization of epoxides can occur to yield polyethers. Backbiting of the metal-carbonate group yields cyclic carbonate as the product, which is desirable when selective due to varied applications of cyclic carbonates as polar aprotic solvents (including their use in the preparation of electrolytes for lithium ion batteries), fillers in cosmetics, and as starting materials for polycarbonate formation.[11-13] The deoxygenation of epoxides is another potential reaction that can occur in these catalytic systems but to date has been overlooked in the literature surrounding reactions of CO_2 with epoxides.

To date, there have been several catalytic systems based upon iron reported that have shown excellent activity in the production of cyclic and polycarbonates.[14-22] The first report of an iron catalyst for either polycarbonate or cyclic carbonate formation was reported by Williams in 2011.[15] The system was based on an air-stable di-iron tetrachloride complex, in which the selective formation of either poly(cyclohexene) carbonate or *cis*-cyclohexene carbonate could be controlled by the amount of anionic co-catalyst present in the reaction. Although active at 1 atm CO_2, the resulting copolymer was not strictly alternating, and it contained only 66% carbonate linkages. In 2013, Nozaki and co-workers reported an oxo-bridged iron(IV) corrole complex capable of copolymerizing CO_2 and propylene oxide (PO), which was the first iron complex capable of copolymerizing CO_2 and PO. The polycarbonates obtained, however, contained a high percentage of ether-linkages. These complexes could also copolymerize glycidyl phenyl ether yielding highly crystalline materials.[23] In terms of other oxo-complexes capable of catalyzing reactions between epoxides and CO_2, Al-O-Al salen catalysts developed by North and co-workers are capable of catalyzing the production of cyclic carbonates.[24-28] Through both experimental and density functional theory studies, it has been demonstrated that such complexes form a carbonato-bridged Al intermediate that is a key species in the catalytic cycle.[29]

The ability of metal-oxo compounds to form via deoxygenation reactions of epoxides, while known, is not widely studied.[30-31] In comparison, the forward reaction upon which epoxides are formed from alkenes is well understood and practiced in organic synthesis on both small and industrial scales. Metal-oxo compounds are biologically important cofactors in enzymes and have shown the ability to control toxic epoxide levels within living cells.[32] Recently, a bacterial monooxygenase containing a catalytic di-iron center has been characterized and the metal site was shown to be involved in deoxygenation processes occurring within cells.[32] Computational studies on similar iron-based enzymes propose these types of deoxygenation reactions occur via a radical 2-step pathway.[33] Although synthetic (biomimetic) models for epoxidase enzymes have been developed,[34-37] we are not aware of any models that have potential to mimic the corresponding and more recently discovered deoxygenation-detoxification process.

We recently reported the synthesis of iron amino-bis(phenolate) chloride complexes and their ability to produce cyclic carbonates selectively.[38] While these proved to be highly active catalysts, we were interested in obtaining further insight into the active catalytic species and the possible in situ formation of oxo complexes formed by epoxide deoxygenation. Epoxide deoxygenation has been overlooked by researchers in the field of epoxide-CO_2 reactions. Here we present the synthesis and characterization of new bimetallic oxo-bridged iron amino-bis(phenolate) complexes, including variable temperature magnetic data. We report the activity of these compounds toward the coupling of CO_2 and epoxide substrates for cyclic carbonate formation and spectroscopic evidence for a radical-mediated epoxide deoxygenation step.

2.2 Synthesis and characterization of oxo-bridged iron complexes

A series of tetradentate amino-bis(phenol) compounds $H_2[N_2O_2]^{RR'Pip}$ (H_2**L2.1**-H_2**L2.5**) were synthesized as previously reported.[38] The monometallic iron(III) species (**2.1**-**2.5**) were prepared via the dropwise addition of anhydrous $FeCl_3$ in methanol to a slurry of the ligand in methanol, as previously reported for **2.1**, **2.3**-**2.5**. [38] The resulting purple solution was neutralized with triethylamine, extracted into acetone and dried under vacuum. The corresponding bimetallic oxo-bridged species were prepared by a modified literature procedure[39] through the dropwise addition of a solution of NaOH in methanol to a methanolic slurry of **2.1**-**2.5** (**Scheme 2.1**). A color change from dark purple to brick red and precipitate formation was observed indicative of the oxo-bridged species (**Figure A1**).[39] This reaction occurred after 24 h for **2.6**, **2.7** and **2.10** and within only 2 h for **2.8**. However, 72 h was needed for **2.9** to form. These relative reaction rates can be attributed to the increased Lewis acidity of the iron center in **2.3** due to the presence of electron withdrawing chlorine atoms on the phenolate rings, resulting in a more oxophillic metal center. The opposite reactivity is seen for complex **2.4**, which contains electron donating groups (R' = OMe) on the rings, resulting in a more electron rich iron center and hence longer reaction times are needed to form the oxo-bridged species. The red solid was isolated by vacuum filtration and washed several times with deionized water to remove the NaCl by-product. The synthesized complexes were characterized by elemental analysis, MALDI-TOF mass spectrometry and UV-vis spectroscopy. The structures of **2.6**, **2.8** and **2.10** were determined via single crystal X-ray diffraction analysis.

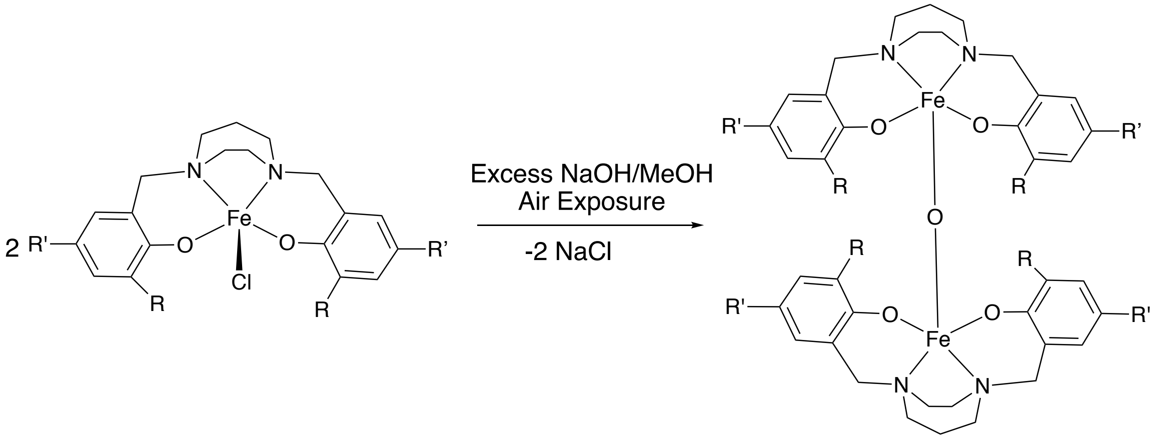

R = R' = *t*Bu (**2.1**)
R = R '= Me (**2.2**)
R = R' = Cl (**2.3**)
R = *t*Bu, R' = OMe (**2.4**)
R = *t*Bu, R' = Me (**2.5**)

R = R' = *t*Bu (**2.6**)
R = R '= Me (**2.7**)
R = R' = Cl (**2.8**)
R = *t*Bu, R' = OMe (**2.9**)
R = *t*Bu, R' = Me (**2.10**)

Scheme 2.1. Synthesis of oxo-bridged iron amino-bis(phenolate) complexes.

2.3 Crystal structure determination

Single crystals of **2.8** suitable for X-ray diffraction analysis were obtained by slow evaporation at room temperature of a saturated dichloromethane solution with the addition of 1 mL of 1 M NaCl in water. Crystals of **2.6**, **2.9** and **2.10** were grown by slow evaporation at room temperature from saturated solutions of the compounds in dichloromethane and methanol. The ORTEP diagrams of the structures are shown in **Figure 2.1** and **Figures A2-A4** and crystallographic data are reported in **Table A1**. Selected bond lengths (Å) and angles (°) for complexes **2.6**, **2.8**, **2.9** and **2.10** can be found in **Tables A2-A3**. All three complexes exhibit bimetallic structures through a bridging oxide ligand with five-coordinate iron centers bonded to the two phenolate oxygen atoms and the two amine nitrogen atoms of the ligand. The Fe-O-Fe bond angles for **2.6**, **2.8**, **2.9** and **2.10** were found to be 180.0°, 171.92(19)°, 180.0° and 171.75(19)°, respectively. The coordination geometry around each iron center is best described as distorted square pyramidal for all complexes with τ_5 values ranging from 0.22 to 0.31.[40] As all complexes are closely related except for substituents on the phenolate rings (i.e. chloride, methyl and *tert*-butyl groups) the bond lengths within the ligands and around the iron centers have little variation. The Fe-Ophen bond distances are similar to those observed for oxo-bridged iron(III) complexes containing salen, salan and bis(phenolate) ligands adopting distorted square pyramidal geometries.[41-45] In **2.8**, these distances are 1.915(3), 1.890(3), 1.895(3) and 1.912(3) Å for Fe(1)-O(1), Fe(1)-O(2), Fe(2)-O(3) and Fe(2)-O(4), respectively. The Fe(1)-O(5) distance relating to the bridging oxygen exhibits a slightly shorter bond length of 1.770(3) Å, which is also consistent with reported literature values of similar systems. The Fe-N bonds of the nitrogen donors in the amine backbone exhibit lengths of 2.151(4)-2.180(4) Å, again consistent with similar reported structures.[42-43, 46]

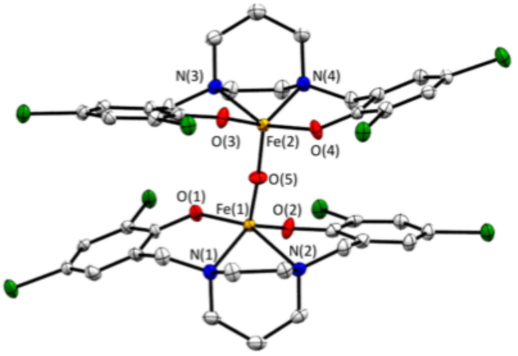

Figure 2.1. Molecular structure (ORTEP) and partial numbering scheme for **2.8**. Ellipsoids are shown at the 50% probability level (H-atoms omitted for clarity).

2.4 UV-visible spectroscopic and magnetic data

The formation of the Fe-O-Fe species was further supported by electronic absorption data in dichloromethane. During formation of the oxo-species a color change from deep purple to brick red is observed. Similar to our previous work with iron(III) compounds containing tetradentate amino-bis(phenolate) ligands, compounds **2.6** to **2.10** exhibit intense bands in the UV and visible regions.[47-49] The electronic absorption spectra of complexes **2.2** and **2.7** are shown in **Figure 2.2** and those for complexes **2.6** and **2.8** – **2.10** are shown in **Figures A5 – A8**. In **Figure 2.2**, the high energy bands below 300 nm result from $\pi \rightarrow \pi^*$ transitions arising from the phenolate rings of the ligand. Intense bands from the phenolate moieties are also observed in the range of 330-400 nm. These can be assigned to charge transfer transitions from the HOMO of the phenolate oxygen to the half-filled d_{x2-y2}/d_{z2} orbital of the high-spin iron(III). The bands in the visible region arise from the charge-transfer transitions from the in-plane p_{π} orbital of the phenolate ring to the half-filled d_{π^*} orbital of iron(III) accounting for the intense purple color in complexes **2.1** – **2.5**. Upon oxo-bridge formation to give complexes **2.6** – **2.10** these visible bands undergo a hypsochromic shift accounting for the color change from purple to red and resulting from a higher energy electronic transition compared to the Fe-Cl compounds.[50] Furthermore, in complexes **2.1** – **2.5** the halide ligands are anticipated to be labile in solution,[49, 51-52] and so interaction with the solvent may also influence the electronic spectra.

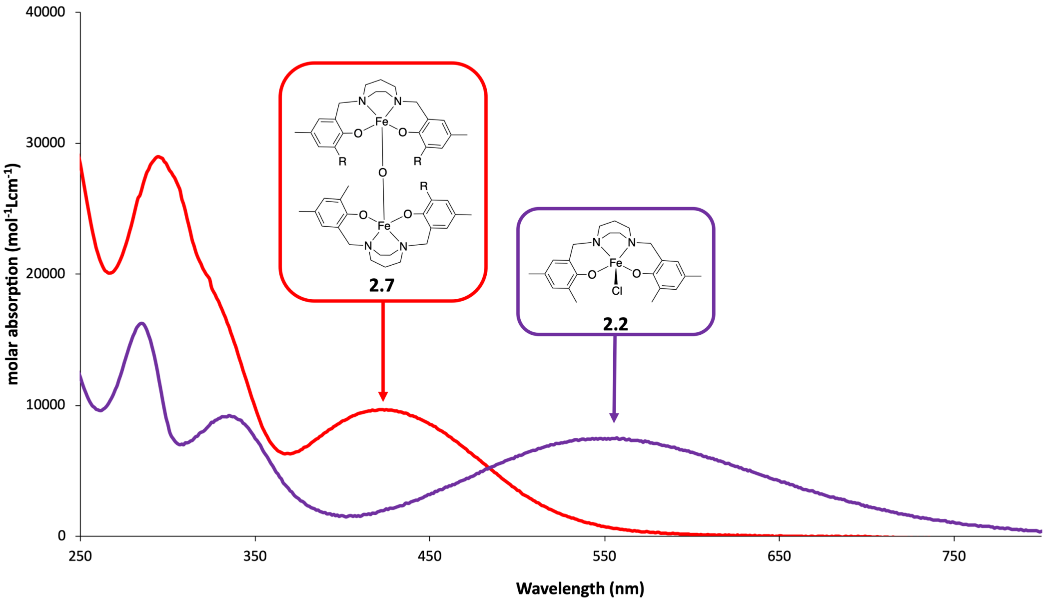

Figure 2.2. Electronic absorption spectra of **2.2** and **2.7** in dichloromethane.

The spin-only magnetic moment for complexes **2.6** – **2.10** in solution were determined using Evans' NMR method at room temperature in $CDCl_3$ with ferrocene as the internal reference. The oxo-bridged iron complexes displayed lower room temperature magnetic moments (2.41-3.20 μ_B) compared to the monometallic species we have previously reported.[38] This is expected as antiferromagnetic coupling may occur across the oxo bridge, which would lead to an overall lower magnetic moment.

The temperature dependence of the magnetic susceptibility (χ_m) and resulting magnetic moments (μ_{eff}) for **2.6** – **2.10** were measured from 2 – 300 K at a field strength of 1 T. The plots of $\chi_m T$ vs T for all compounds are given in **Figure 2.3**. The data were modelled using a Bleaney-Bowers expression for two magnetically coupled S = 5/2 Fe^{III} spins. This model has been applied successfully to related oxo-bridged Fe^{III} complexes.[44, 53] A Curie-Weiss term is added to the Bleaney-Bowers equation to account for the presence of a small amount of paramagnetic impurity $\chi_{para} = C/(T - \theta)$, according to $\chi_m = [1 - P]\,\chi + P\chi_{para} + TIP$ where P represents the fraction of paramagnetic $S = 5/2$ impurity, likely monomeric Fe^{III} compounds. A temperature independent paramagnetic contribution (TIP) was added. The *g*-value is assumed to be 2.00 consistent with a $^6A_{1g}$ ground state for the Fe^{III} sites.

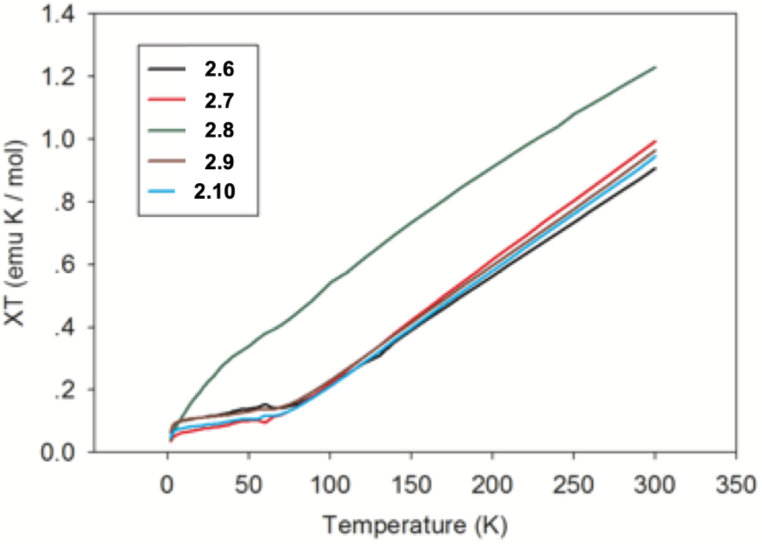

Figure 2.3. Plots of $\chi_m T$ vs temperature for compounds **2.6** – **2.10**.

The observed moments decrease with decreasing temperature typical for antiferromagnetic coupling of two high-spin Fe^{III} centers. A plateau of the moments of compounds **2.6**, **2.7**, **2.9** and **2.10** at ca. 50 K is attributed to the presence of a small degree of paramagnetic impurity whereas complex **2.8** was found to contain a larger degree of impurity. The magnetic data of these complexes could be modelled using the parameters given in **Table 2.1**. Plots of magnetic susceptibility and moments vs. temperature with best fits to the experimental data are given in **Figures A24 – A28**. These compounds exhibit strong antiferromagnetic coupling, which is consistent with that observed for other reported oxide bridged dinuclear Fe^{III} complexes.[44, 54-56] In the case of **2.8**, the data were modelled using a much higher percentage of paramagnetic impurity than compounds **2.6**, **2.7**, **2.9** and **2.10**. The experimentally determined elemental analysis for **2.8** can be acceptably modelled by including 10% of monomeric **2.3** and one molecule of H_2O. The shorter reaction times used for the preparation of **2.8** (due to the increased Lewis acidity of the metal center) based on the observed rates of color change likely results in incomplete reaction of the chloride starting material, **2.3**, compared to the analogous compounds containing electron-donating substituents on the phenolate donors.

Table 2.1. Magnetic properties of **2.6–2.10**

Entry	Complex	J (cm^{-1})	P	TIP	θ (K)	R^2
1	**2.6**	-185 ± 5	0.025	5.00×10^{-4}	-1.1	0.9931
2	**2.7**	-162 ± 3	0.016	5.00×10^{-4}	-1.6	0.9925
3	**2.8**	-148 ± 4	0.120	5.00×10^{-4}	-8.8	0.9703
4	**2.9**	-163 ± 3	0.025	2.69×10^{-4}	-1.1	0.9957
5	**2.10**	-166 ± 3	0.019	4.00×10^{-4}	-1.2	0.9955

2.5 Coupling of propylene oxide with carbon dioxide

The ability of complexes **2.6** – **2.10** to catalyze the coupling of propylene oxide and CO_2 to form cyclic carbonates was investigated and their activity compared to the corresponding monometallic iron chloride species under identical conditions (**Table 2.2**). Reactions were not optimized for complete conversion of epoxide, as greater mechanistic insight (i.e. structure-activity relationships) can be ascertained by performing reactions at a lower level of conversion. Oxo-bridged iron compounds of other ligands have afforded catalytically active systems.[23] With phenolate ligands, one of the most reactive systems for cyclic carbonate formation reported to date was based on an air-stable thioether-triphenolate iron(III) complex with TOFs up to 580 h^{-1}.[14] In comparing the monometallic species **2.1** – **2.5** against their oxo-bridged counterparts no significant differences in reactivity were observed, except when the R substituents on the phenyl groups were *tert*-butyl groups, **2.1** and **2.6**, or **2.5** and **2.10** (**Table 2.2**, entries 1, 6 and 5, 10 respectively). This decrease in conversion to the cyclic carbonate product is likely due to the increased steric bulk around the iron center where catalysis occurs. This steric congestion around the iron centers caused by the orientation of the *tert*-butyl groups can be seen in the molecular structure of **2.6**. No significant difference in catalytic activity was observed between the chlorido- and oxo-complexes, **2.2** – **2.4** and **2.7** – **2.9**, when functionalities on the phenyl rings were either electron withdrawing or donating groups of similar sizes, suggesting steric rather than electronic factors were the major contributors to catalytic efficiency of the systems.

Table 2.2. Coupling reactions of propylene oxide and carbon dioxide catalyzed by mono-metallic iron chloride complexes **2.1** – **2.5** and oxo-bridged iron complexes **2.6** – **2.10**.

Entry[a]	Complex	Conv[b].%	TON[c]	TOF[d](h^{-1})
1	**2.1**	40	1600	73
2	**2.2**	44	1760	80
3	**2.3**	53	2120	96
4	**2.4**	60	2400	109
5	**2.5**	41	1640	75
6	**2.6**	29	1160	53
7	**2.7**	39	1560	71
8	**2.8**	45	1800	82
9	**2.9**	40	1600	73
10	**2.10**	29	1160	53

[a] Reaction conditions (unless otherwise stated): Propylene oxide (4.3 x 10^{-2} mol), catalyst (1.08 x 10^{-5} mol, 0.025 mol%), PPNCl (4.30 x 10^{-5} mol, 0.1 mol%), 100 °C, 20 bar CO_2, 22 h. [b] Determined by ^1H NMR spectroscopy. [c] Overall turnover number ($mol_{PC}\cdot mol_{Cat}^{-1}$). [d] Overall turnover frequency (TON/reaction time) observed.

We have previously observed reaction mixtures changed from purple to red-brown over the course of the CO_2/epoxide coupling reactions.[38] Therefore, we speculated whether oxo-bridged compounds were the true catalytic species. For the oxo-bridged species, **2.6** was studied most extensively to give further insight into mechanistic details and for comparison against similar systems in the literature. In all cases, in situ IR spectroscopy (**Figures A31-A38**) and ^1H NMR analysis of unpurified products showed selective formation of cyclic carbonate. The influence of co-catalyst, P_{CO2}, t, T and mole ratio of iron to propylene oxide was investigated. The presence of a co-catalyst was necessary for the reaction to proceed (**Table 2.3**, entries 1 and 3), and some background conversion attributed to the co-catalyst alone was observed (**Table 2.3**, entry 2). The need for a co-catalyst was expected, as the oxo-bridged species lacks a suitable nucleophile (such as a labile halide ligand present in compounds **2.1** – **2.5**) to ring-open the coordinated epoxide. However, changing from 2 molar equiv of PPNCl per iron center to 4 molar equiv did not affect the conversion significantly (**Table 2.3**, entries 3 and 6) – this contrasts with the behaviour of **2.1** – **2.5** where an optimum Fe:ionic co-catalyst ratio of 1:4 was observed.[38] Investigating other anionic co-catalysts (**Table 2.3**, entries 3-5) there was no substantial difference in conversion, suggesting the increased atomic radius of the incoming nucleophile from Cl^- to I^- has no substantial effect on epoxide ring-opening, and that backbiting to yield the carbonate and regenerate the 'free' nucleophile as a leaving group is not the rate-determining step.

The CO_2 pressure did show some influence on conversion. At a CO_2 pressure of 10 bar, 44% cyclic carbonate was obtained whereas only 29% was produced at 20 bar (**Table 2.3**, entries 3 and 8). The activity further declined at 40 bar CO_2, where only a 26% conversion was observed (**Table 2.3**, entry 9). This decline in conversion is likely not attributed to competitive binding of CO_2 to the iron centers as we could not observe any CO_2/iron adduct formation via in situ React IR spectroscopy. However, it is possible that (i) an anti-solvent effect is taking place i.e. the catalyst and co-catalyst are precipitating from the propylene oxide rich phase, or (ii) the propylene oxide volume expands due to CO_2 absorption hence diluting the concentration of epoxide at the catalyst. Both of these phenomena would inhibit reaction kinetics.[11] North and co-workers have extensively studied bimetallic oxo-bridged Al-salen complexes as catalysts for cyclic carbonate formation, and some of these are active without the addition of an external halide co-catalyst.[29] The high activity of one such system has been attributed to the formation of an intermediate carbonato species in which CO_2 inserts into one of the Al-O_{oxo} bonds. We initially postulated a similar intermediate may be present in our systems. However, not only are our systems inactive without an external nucleophile, but we were unable to observe the formation of carbonato species via in situ infrared spectroscopy at temperatures from 25 – 100 °C and pressures up to 60 bar CO_2.

Coupling of CO_2 to propylene oxide is highly influenced by temperature. We found that elevated temperatures (100 °C) were needed for higher conversions, with the catalytic system remaining stable at these temperatures. Conducting the reaction at room temperature showed no conversion of propylene oxide (**Table 2.3**, entry 10). This is understandable especially since the coupling of propylene oxide and CO_2 to form the cyclic product is more kinetically accessible at elevated temperatures. These trends are consistent with our previous work as well as similar reported iron systems.[19, 38]

Table 2.3. Reaction parameter screening for the coupling of propylene oxide and carbon dioxide catalyzed by **2.6**.

Entry[a]	Co-catalyst	[Fe]:[PO]:[Cocat]	*t* (h)	*T* (°C)	P_{CO2} (bar)	Conv[b]. %	TON[c]	TOF[d] (h^{-1})
1		1:4000:0	22	100	20	0	-	-
2	PPNCl	0:4000:4	22	100	20	23	920	42
3	PPNCl	1:4000:4	22	100	20	29	1160 (240)	53
4	TBAB	1:4000:4	22	100	20	23	920	42
5	TBAI	1:4000:4	22	100	20	25	1000	45
6	PPNCl	1:4000:2	22	100	20	32	1280	58
7	PPNCl	1:1000:4	22	100	20	60	2400	109
8	PPNCl	1:4000:4	22	100	10	44	1760	80
9	PPNCl	1:4000:4	22	100	40	26	1360	62
10	PPNCl	1:4000:4	22	60	20	7	280	13
11	PPNCl	1:4000:4	22	25	20	0	-	-
12	PPNCl	1:4000:4	6	100	20	14	560	93

[a] Reaction conditions (unless otherwise stated): Propylene oxide (4.3×10^{-2} mol), catalyst (1.08×10^{-5} mol, 0.025 mol%), PPNCl (4.30×10^{-5} mol, 0.1 mol%). [b] Determined by ^1H NMR spectroscopy. [c] Overall turnover number ($mol_{PC}{\cdot}mol_{Cat}^{-1}$). The value in parentheses is corrected TON incorporating the background conversion due to the use of PPNCl alone. [d] Overall turnover frequency (TON/reaction time) observed.

Catalyst **2.6** was used to investigate the substrate scope of these oxo-bridged bimetallic iron catalytic systems with several commercially available epoxides having varied steric and electronic properties (**Table 2.4**). The presence of an electron withdrawing functionality on the epoxide in the case of epichlorohydrin resulted in nearly complete conversion to the cyclic product (**Table 2.4**, entry 2). This increased reactivity has been widely reported in the literature,[14, 19, 57] and a similarly high conversion was achieved using phenyl glycidyl ether (**Table 2.4**, entry 6). In the case of styrene oxide (**Table 2.4**, entry 4) only 31% conversion was obtained. This could be a result of steric effects but also due to the nature of the alkoxide intermediate formed. Kleij and co-workers showed via computational studies that the alkoxide intermediate formed during the ring-opening of styrene oxide is less nucleophilic and hence less reactive towards carbon dioxide insertion.[58] Cyclohexene oxide resulted in the lowest conversion to the cyclic product and no polycarbonate formed (**Table 2.4**, entry 5). These results are in agreement with those reported previously in our group and by the groups of Kleij, Wang, Capacchione and Rieger.[14, 16, 19] It is also worth noting that there was no homopolymer (polyether) formation observed at various temperatures in the presence of PPNCl at 25 – 80 °C. We also investigated phenyl glycidol ether as a substrate at 1 atm CO_2 and obtained a 74% conversion to the cyclic product in 22 h (**Table 2.4**, entry 6).

Table 2.4. Catalytic cyclic carbonate formation from epoxides and carbon dioxide using **2.6**.

Entry[a]	Substrate	Conv[b]. %	TON[c]	TOF[d] (h^{-1})
1	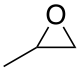	26	1040	47
2	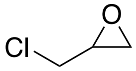	99	3960	180
3	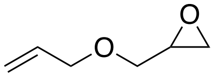	31	1240	56
4	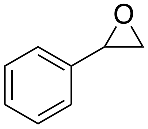	31	1240	56
5	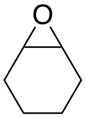	17	680	31
6[e]	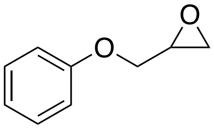	86 (74)	3440 (2960)	156 (135)

[a] Reaction conditions (unless otherwise stated): substrate (4.3×10^{-2} mol), catalyst (1.08×10^{-5} mol, 0.025 mol%), PPNCl (4.30×10^{-5} mol, 0.1 mol%), P_{CO2} (20 bar), 100 °C, 22 h. [b] Determined by ^{1}H NMR spectroscopy. [c] Overall turnover number ($mol_{PC} \cdot mol_{Cat}^{-1}$). [d] Overall turnover frequency (TON/reaction time) observed. [e] Values in parentheses correspond to reaction at P_{CO2} 1 atm.

2.6 Transformation of 2.1–2.5 to 2.6–2.10 via deoxygenation of epoxides

As previously mentioned, we observed that CO_2/epoxide coupling catalyzed by monometallic species **2.1** – **2.5** resulted in color changes from purple to red/orange over the course of the reactions. To determine whether the formation of the oxide bridge was due to air/water contamination or the presence of the epoxide we performed test reactions under air- and moisture-free conditions in a glovebox. Hence, the only oxygen source available for formation of the oxo species was the epoxide. When **2.1** was combined with propylene oxide with or without PPNCl, a color change from purple to red/orange was observed within hours (**Figure 2.4 A**). Analyzing aliquots via UV-vis spectroscopy in dichloromethane after the color change shows a shift to a higher energy electronic transition corresponding to formation of oxo complex **2.6** (**Figure 2.4 C**). This suggests formation of complexes **2.6** – **2.10** during coupling reactions results from the presence of epoxide as an oxygen source. We pursued the mechanism of this process by analyzing the resulting red/orange mixture via GC-MS, which detected organochloride by-products (**Figure 2.4 B**). In addition, 2-chloropropane was detected in crude ^{1}H NMR mixtures. Slow evaporation of the red/orange mixture of **2.1** in PO gave crystals suitable for single crystal X-ray diffraction, which upon analysis confirmed the formation of **2.6**, giving a structure identical to that obtained for the product of the reaction of **2.1** with NaOH as described above. When we included a molar equivalent of TEMPO, a commonly used radical scavenger, the conversion of **2.1-2.5** to **2.6-2.10** via the deoxygenation of the propylene oxide was not observed (**Figure A30**).

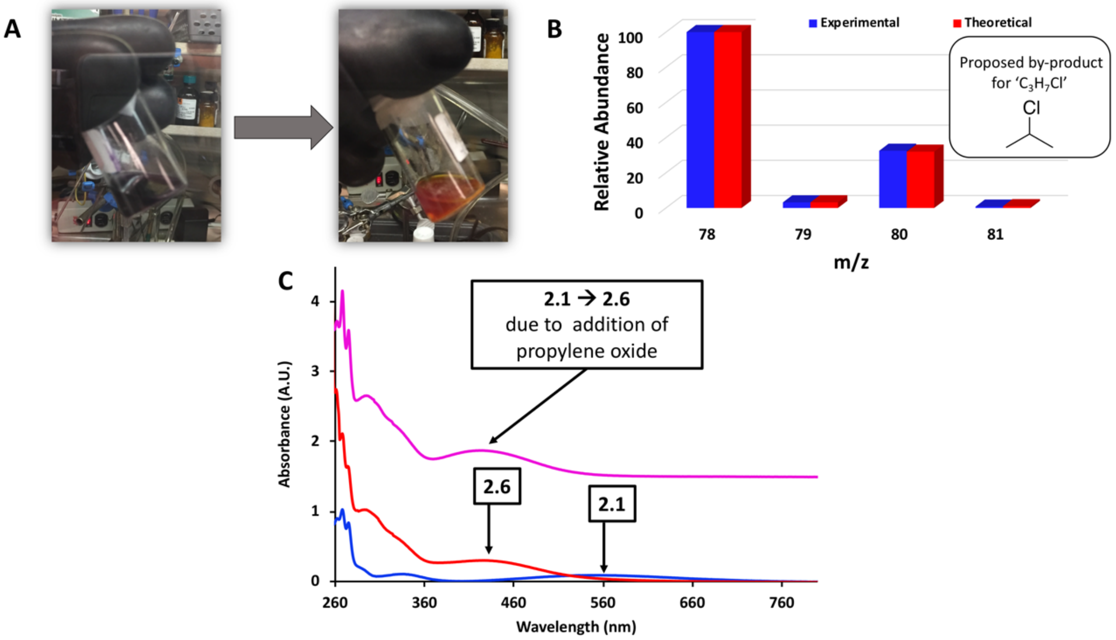

Figure 2.4. (A) Color change indicating transformation of **2.1** to **2.6** due to addition of PO (under nitrogen in an inert atmosphere workstation). (B) Experimentally observed mass and relative abundance data compared to theoretical isotopic distribution consistent for chloropropane obtained from reaction of **2.1** in PO (C) UV-vis spectra of **2.1** (blue) and **2.6** (red) in dichloromethane. Off-set UV-vis trace of orange product from reaction of **2.1** and PO dissolved in dichloromethane (pink).

Deoxygenation of epoxides is a relatively understudied field. Rhenium catalysts have recently been reported that were shown to provide both a stereo- and chemoselective reduction of aliphatic epoxides.[59] Indium, and molybdenum systems have been well studied for these transformations in either a catalytic or stoichiometric fashion.[30-31, 60-61] To the best of our knowledge, the only iron catalyzed example is based upon a bacterial monooxygenase PaaABCE.[32] The catalytic di-iron center of the enzyme is key in the deoxygenation step. These types of compounds are critical from a biological standpoint as they control toxic levels of epoxides within cells.[32]

In our catalytic cycle for cyclic carbonate formation, we propose that upon ring-opening of the coordinated epoxide (either from the labile Cl in complexes **2.1** – **2.5** or additional excess chloride from the co-catalyst) deoxygenation of the epoxide occurs via a single electron transfer radical process from the iron center to the σ^*-orbital of the C-O bond. Upon formation of this radical intermediate, it is reasonable that the more stable 2° radical is quenched by chloride ions present in solution accounting for the oxo-bridge formation in the iron complexes **2.6** – **2.10** and a chloride containing by-product. Such a deoxygenation reaction has literature precedent for indium, iron (within enzymes), titanium and molybdenum systems.[30-32, 60-62] When the oxo-species forms it is then able to enter its own catalytic cycle leading to the cyclic carbonate product in the presence of CO_2 (**Scheme 2.2**). Once the oxo-complex has formed, however, we did not observe any instances where it could convert back into its monometallic counterpart, further explaining the red/orange colored reaction mixture observed upon quenching reactions catalyzed by **2.1** – **2.5**. It is worth noting that this color change was observed when all epoxides in **Table 2.4** were used as substrates with **2.1**.

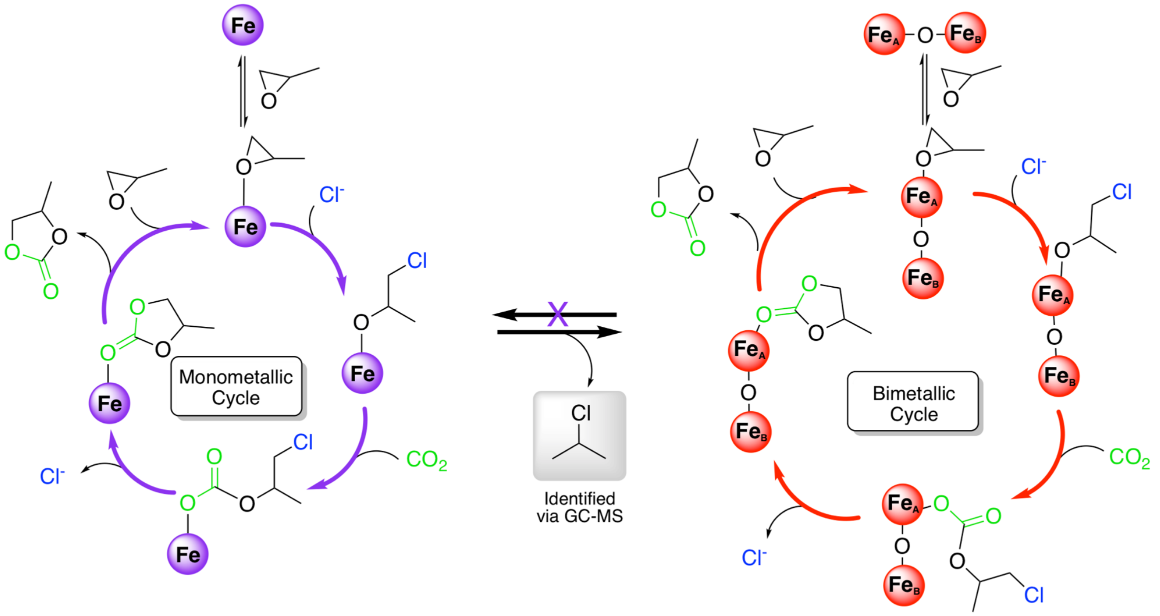

Scheme 2.2. Proposed catalytic cycle for the coupling of carbon dioxide and epoxides catalyzed by both monometallic iron(III) chloride and bimetallic iron(III) oxo-systems. In the bimetallic cycle the growing alkoxide chain is only shown on Fe_A for simplicity. It is possible for either Fe_A or Fe_B to be active at any instance separately or at the same time independently throughout the catalytic cycle

Finally, we investigated the initial reaction rate for cyclic carbonate formation using **2.1** and **2.6** under identical conditions. Due to the low solubility of PPNCl in PO, styrene oxide was used as a substrate. Initial reaction rates were monitored using in situ IR spectroscopy and showed a first order dependence in iron for both the monometallic and bimetallic complexes (**Figures A31-A38**). Data were only collected for the first 15 minutes of the reaction and upon opening the pressure vessel reaction mixtures were still purple for the monometallic catalysts. Allowing the reactions to proceed for longer periods resulted in the formation of the oxo-bridged species. For the bimetallic complex, a reaction order of 1.00 with respect to iron suggests that each iron center in the complex serves as an independent catalytic site. That is, epoxide coordination can occur at either iron center and there is no shuttling between iron centers of the growing alkoxide, nor CO_2 insertion into the oxo-bridge as previously observed by others for oxo-containing catalysts.[29] If both iron centers within the same complex were involved in a cooperative fashion, a reaction order of >1 with respect to iron would be expected. For example, Zn β-diiminate complexes reported by Coates and co-workers have shown reaction orders of 1.73 per Zn complex, proposing that both Zn centers are involved in the key transition state of epoxide ring-opening.[63] Our kinetic data therefore explains the similar activity observed amongst both the monometallic complexes (**2.1** – **2.5**) and bimetallic complexes (**2.6** – **2.10**). We observed the initial rates to be slightly faster for the monometallic catalysts (**Figures A31-A38**), suggesting that it is plausible for this cycle to be entered first before later transferring to the bimetallic cycle once the oxide bridge is formed.

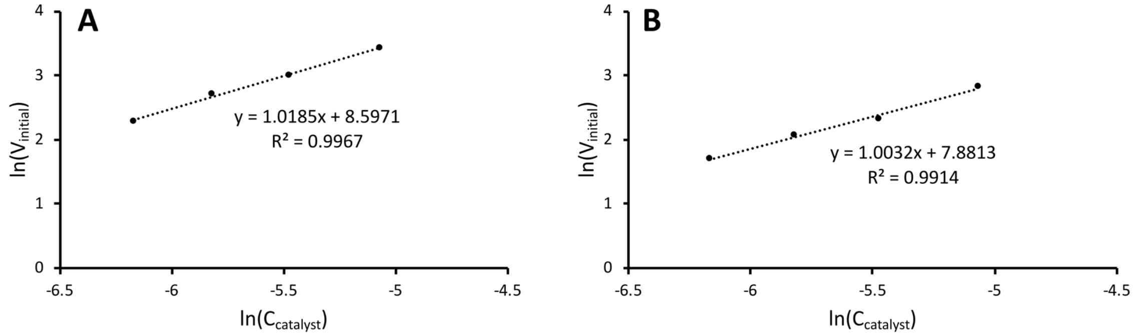

Figure 2.5. Determination of reaction order with respect to iron for (A) monometallic system **2.1** and (B) bimetallic system **2.6** via plots of initial rate ($v_{initial}$) and concentration on a double logarithmic scale, where the slope is equal to reaction order of reagent.

2.7 Conclusions

Five air-stable bimetallic iron(III) μ-oxo complexes supported by amino-bis(phenolate) ligands were prepared and characterized. The structure of **2.6** reveals a linear Fe-O-Fe bridge, whereas **2.8** and **2.10** contain Fe-O-Fe angles slightly less than 180°. The oxo bridges facilitate strong antiferromagnetic coupling between the two high-spin iron(III) ions present in each molecule. These compounds generally show reactivity similar to their monometallic iron(III) chloride analogs for conversion of epoxides and CO_2 into cyclic carbonates. The exception to this was **2.6**, which is significantly less reactive than **2.1** in these reactions. We propose that this is due to the steric congestion around the iron centers in **2.6** resulting from the presence of *tert*-butyl groups in both the 2- and 4-position of the phenolate donors. Formation of styrene carbonate using both families of catalyst were first order with respect to iron concentration, which implies that cooperative mechanisms (including μ-carbonato formation or alkoxide shuttling) do not occur in these bimetallic iron systems (**2.6** – **2.10**). Reaction mixtures post-catalysis employing **2.1** – **2.5** are typically red-brown in color. Therefore, we propose that the bimetallic iron(III) oxo complexes (**2.6** – **2.10**) form during the catalytic process when iron(III) chloride species are used in the reactions via a radical deoxygenation reaction of the epoxide substrate. Work on further optimizing reaction conditions and substrate screening for the deoxygenation of commonly used epoxides is currently under investigation in our group. The use of such compounds may be valuable synthetic models for biological systems.[32-33]

2.8 Experimental

2.8.1 General experimental conditions

All reagents used were purchased from Sigma Aldrich or Alfa Aesar and used without further purification. Commercially available solvents were used without further purification. All reactions were performed in air. Ligands H_2**L2.1**, H_2**L2.3**, H_2**L2.4**, H_2**L2.5** and iron complexes **2.1** and **2. 3** – **2.5** were prepared as previously reported in our group.[38,

[64] It is important to note that caution should be taken when operating high pressure equipment.

2.8.2 Instrumentation

^1H and ^{13}C NMR spectra were recorded on a Bruker Avance 300 MHz spectrometer at 25 °C and were referenced using the residual proton and ^{13}C resonances of the solvent. MALDI-TOF spectra were obtained on an Applied Biosystems 4800 MALDI-TOF/TOF Analyzer, equipped with a reflectron, delayed ion extraction and high-performance nitrogen laser (200 Hz operating at 355 nm). Samples were prepared at a concentration of 10.0 mg/mL in dichloromethane. Anthracene was used as the matrix and mixed with the sample at a concentration of 10 mg/mL to promote desorption and ionization. 100 μL of the sample and matrix solutions were combined and 1 μL of this solution was spotted on the MALDI plate and allowing to dry. Images of MALDI spectra were prepared using mMass^{TM} software (www.mmass.org). Magnetic moments in solution were determined at room temperature using Evans' NMR method with ferrocene serving as an internal reference in $CDCl_3$ and are reported per discrete metal complex.[65]. Magnetic susceptibility data in the solid state were acquired using a Quantum Design MPMS-XL7 SQUID magnetometer for variable temperature measurements. Data were corrected for the diamagnetism of all atoms. Samples were sealed in a polyethylene capsule from 1.8 – 300 K at an external DC field of 1 T. UV-vis data were collected on an Ocean Optics USB4000+ fiber optic spectrophotometer. All coupling reactions were carried out in a 100 mL stainless-steel autoclave reactor (Parr Instrument Company) equipped with a motorized mechanical stirrer and a heating mantle. For in situ FTIR-monitored reactions, the pressure vessel was additionally equipped with a silicon ATR sensor (SiComp Sentinel) connected to a ReactIR 15 base unit (Mettler-Toledo) via a DS silver-halide Fiber-to-Sentinel conduit. Similar reaction monitoring systems have been described previously.[66] Gas chromatography-mass spectrometry (GC-MS) was performed on an Agilent 7890A GC system coupled with an Agilent 5975C MS detector equipped with a 30 m HP5-MS column. Elemental analysis was performed at the Ocean Sciences Centre, Memorial University or by Guelph Chemical Laboratories Ltd., Canada.

2.8.3 Catalytic cyclic carbonate formation

The stainless-steel reaction vessel was cleaned and heated to 100 °C overnight under vacuum before use. Stock solutions of catalyst and co-catalyst in dichloromethane were prepared, required amounts were mixed in a vial and solvent removed under vacuum. The appropriate amount of propylene oxide (or epoxide being investigated) was then added to the vial resulting in a deep red solution. This was added to the pressure vessel via syringe, sealed, pressurized with CO_2 and heated to the desired temperature for the desired experiment run-time.

2.8.4 Single crystal X-ray determination

Crystallographic data were collected at Saint Mary's University (Halifax, Nova Scotia, Canada) on a Bruker APEX-II CCD diffractometer at 125 K. The structures were solved using Olex2[67] with the ShelXT[68] structure solution program using Intrinsic Phasing and refined with the ShelXL[68] refinement package using Least Squares minimization.

2.8.5 Synthesis and characterization of ligands and catalysts

2.8.5.1 Synthesis of H_2L2.1

A mixture of 2,4-dimethylphenol (24.4 g, 0.123 mol), 37% w/w formaldehyde (10.0 mL, 0.123 mol) and homopiperzine (6.25 g, 0.0624 mol) in water (50 mL) was stirred and heated to reflux for 24 h. Upon cooling to room temperature, water was decanted from the yellow oil that formed. This oil was triturated with methanol to yield a colorless powder, which was recrystallized from a mixture of methanol and chloroform to afford a colorless, crystalline solid (15.1 g, 66.1%). ^{1}H NMR (300 MHz, 298 K, $CDCl_3$) δ 10.87 (2H, s, O*H*), 6.86 (2H, d, Ar*H*), 6.61 (2H, d, Ar*H*), 3.73 (4H, s, ArC-CH_2-N), 2.82 (4H, t, N-CH_2CH_2-N), 2.77 (4H, s, N-CH_2CH$_2$CH_2-N), 2.2 (12H, s, ArC-CH_3), 1.94 (2H, quintet, N-CH$_2$CH_2CH$_2$-N). ^{13}C{^{1}H} NMR (75 MHz, 298 K, $CDCl_3$) δ 153.62 (ArC-O), 130.65 (ArC), 127.68 (ArC), 126.64 (ArCH), 124.63 (ArCH), 120.76 (ArC-CH$_2$-N), 61.88 (ArC-CH$_2$-N), 54.54 (N-CH$_2${CH$_2$}CH$_2$-N), 26.64 (N-CH$_2${CH$_2$}CH$_2$-N), 20.41 (ArC-CH$_3$), 15.63 (ArC-CH$_3$). Anal. calc'd for $C_{23}H_{32}N_2O_2$: C, 74.96; H, 8.75; N, 7.60. Found: C, 74.78; H, 8.59; N, 7.33.

2.8.5.2 Synthesis of 2.2

To a methanol solution (50 mL) of recrystallized H_2**L2** (2.52 g, 7.14 mmol), a solution of anhydrous $FeCl_3$ (1.11 g, 6.84 mmol) in methanol (10 mL) was added dropwise resulting in the formation of a dark purple solution. Triethylamine (1.39 g, 13.7 mmol) was added to this solution and stirred for 2 h. Solvent was removed under vacuum and the resulting purple solid was dissolved in acetone (80 mL) and filtered. Removal of acetone under vacuum yielded a dark purple powder (2.45 g, 78.3%). MS (MALDI-TOF) *m/z* (%, ion): 457.16 (99, FeCl[$N_2O_2^{MeMePip}$]$^+$), 422.18 (14, Fe[$N_2O_2^{MeMePip}$]$^+$). Anal. calc'd for $C_{23}H_{30}ClFeN_2O_2$: C, 60.34; H, 6.61; N, 6.12. Found: C, 59.92; H, 6.32; N, 5.87. μ_{eff} (solution, 25 °C) = 4.47 μ_B. λ_{max} in CH_2Cl_2, nm (ε/dm^3 mol^{-1} cm^{-1}): 237 (15492), 287 (16015), 333 (9124), 550 (7461).

2.8.5.3 Synthesis of 2.6

To a methanol solution (50 mL) of purified **1** (0.99 g, 1.59 mmol), a solution of NaOH (0.68 g, 17.0 mmol) in methanol (15 mL) was added dropwise and allowed to stir for 24 h resulting in the slow formation of a brick red precipitate. The red solid was filtered and washed with distilled water (50 mL) and dried under vacuum yielding a dark red powder (0.62 g, 65.1%). MS (MALDI-TOF) *m/z* (%, ion): 1197.0 (5, Fe_2(μ-O)[$N_2O_2^{tButBuPip}$]$^+$), 589.4 (55, Fe[$N_2O_2^{tButBuPip}$]$^+$), 536.5 (98, H_2[$N_2O_2^{tButBuPip}$]$^+$). Anal. calc'd for $C_{70}H_{108}Fe_2N_4O_5$: C, 70.22; H, 9.09; N, 4.68. Found: C, 70.08; H, 8.79; N, 4.67. μ_{eff} (solution, 25 °C) = 2.61 μ_B. λ_{max} in CH_2Cl_2, nm (ε/dm^3 mol^{-1} cm^{-1}): 243 (45046), 285 (31682), 423 (11405).

2.8.5.4 Synthesis of 2.7

This was prepared in a similar manner to **2.6** to yield a brick red powder (0.49 g, 52.1%). MS (MALDI-TOF) *m/z* (%, ion): 860.5 (20, Fe_2(μ-O)[$N_2O_2^{MeMePip}$]$^+$), 438.2 (99, FeO[$N_2O_2^{MeMePip}$]$^+$), 421.2 (29, Fe[$N_2O_2^{MeMePip}$]$^+$). Anal. calc'd for $C_{46}H_{60}Fe_2N_4O_5(H_2O)$: C, 62.88; H, 7.11; N, 6.38. Found: C, 62.89; H, 7.49; N, 6.37. μ_{eff} (solution, 25°C) = 3.13 μ_B. λ_{max} in CH_2Cl_2, nm (ε/dm^3 mol^{-1} cm^{-1}): 292 (28701), 426 (9633).

2.8.5.5 Synthesis of 2.8

This was prepared in a similar manner to **2.6**, except stirred for 2 h to yield a brick red powder (0.39 g, 38.3%). Anal. calc'd for $C_{38}H_{36}Cl_8Fe_2N_4O_5(H_2O)$: C, 43.80; H, 3.68; N, 5.38. Found: C, 43.88; H, 3.44; N, 5.21. Anal. calc'd for $(C_{38}H_{36}Cl_8Fe_2N_4O_5)_{0.90}(C_{19}H_{18}Cl_5FeN_2O_2)_{0.10}(H_2O)$: C, 43.64; H, 3.67; N, 5.36. Found: C, 43.88; H, 3.44; N, 5.21. MS (MALDI-TOF) *m/z* (%, ion): 1024.8 (6, $Fe_2(\mu\text{-}O)[N_2O_2{}^{ClClPip}]^+$), 520.0 (98, $FeO[N_2O_2{}^{ClClPip}]^+$), 503.9 (11, $Fe[N_2O_2{}^{ClClPip}]^+$). μ_{eff} (solution, 25°C) = 2.41 μ_B. λ_{max} in CH_2Cl_2, nm (ε/dm^3 mol^{-1} cm^{-1}): 248 (40426), 299 (35083), 414 (11932).

2.8.5.6 Synthesis of 2.9

This was prepared in a similar manner to **2.6**, except stirred for 72 h to yield a brick red powder (0.78 g, 81.5%). MS (MALDI-TOF) *m/z* (%, ion): 1092.5 (9, $Fe_2(\mu\text{-}O)[N_2O_2{}^{tBuOMePip}]^+$), 554.3 (98, $FeO[N_2O_2{}^{tBuOMePip}]^+$), 537.2 (55, $Fe[N_2O_2{}^{tBuOMePip}]^+$). Anal. calc'd for $C_{58}H_{84}Fe_2N_4O_9(H_2O)$: C, 62.70; H, 7.80; N, 5.04. Found: C, 62.74; H, 7.45; N, 4.07. μ_{eff} (solution, 25°C) = 2.49 μ_B. λ_{max} in CH_2Cl_2, nm (ε/dm^3 mol^{-1} cm^{-1}): 244 (30176), 308 (34739), 437 (9647).

2.8.5.7 Synthesis of 2.10

This was prepared in a similar manner to **2.6** to yield a brick red powder (0.66 g, 65.8%). MS (MALDI-TOF) *m/z* (%, ion): 1028.7 (11, $Fe_2(\mu\text{-}O)[N_2O_2{}^{tBuMePip}]^+$), 522.3 (96, $FeO[N_2O_2{}^{tBuMePip}]^+$), 505.3 (64, $Fe[N_2O_2{}^{tBuMePip}]^+$). Anal. calc'd for $C_{58}H_{84}Fe_2N_4O_5(H_2O)_2$: C, 65.41; H, 8.33; N, 5.26. Found: C, 65.74; H, 8.59; N, 5.27. μ_{eff} (solution, 25°C) = 2.42 μ_B. λ_{max} in CH_2Cl_2, nm (ε/dm^3 mol^{-1} cm^{-1}): 248 (39460), 296 (35210), 422 (12303).

2.8.6 Kinetic monitoring of styrene carbonate formation by in situ React IR spectroscopy

Aliquots of **2.1** or **2.6** and PPNCl stock solutions in dichloromethane were combined and the solvent was removed under vacuum. The solids were dissolved in 4 g of styrene oxide and the solution was added into the pressure vessel. The vessel was then pressurized to 20 bar CO_2 and heated to 100 °C with mechanical stirring. Profiles of the absorbance at 1820 cm^{-1} were measured every 5 s (254 scans per spectrum) for 15 minutes. Similar methods for in situ reaction monitoring by FTIR spectroscopy have been reported by others, demonstrating the linear response of absorbance vs. concentration.[66, 69-71]

2.9 References

1. Liu, Q.; Wu, L.; Jackstell, R.; Beller, M., *Nat. Commun.* **2015,** *6*, 5933.

2. Aresta, M.; Dibenedetto, A.; Angelini, A., *Chem. Rev.* **2014,** *114* (3), 1709-1742.

3. Song, Q.-W.; Zhou, Z.-H.; He, L.-N., *Green Chem.* **2017,** *19* (16), 3707-3728.

4. Aresta, M., Carbon Dioxide Reduction and Uses as a Chemical Feedstock. In *Activation of Small Molecules*, Wiley-VCH Verlag GmbH & Co. KGaA: 2006; pp 1-41.

5. Pescarmona, P. P.; Taherimehr, M., *Catal. Sci. Tech.* **2012,** *2* (11), 2169-2187.

6. Klaus, S.; Lehenmeier, M. W.; Anderson, C. E.; Rieger, B., *Coord. Chem. Rev.* **2011,** *255* (13), 1460-1479.

7. Darensbourg, D. J.; Holtcamp, M. W., *Coord. Chem. Rev.* **1996,** *153*, 155-174.

8. Allen, S. D.; Byrne, C. M.; Coates, G. W., Carbon Dioxide as a Renewable C1 Feedstock: Synthesis and Characterization of Polycarbonates from the Alternating Copolymerization of Epoxides and CO_2. In *Feedstocks for the Future*, American Chemical Society: 2006; Vol. 921, pp 116-129.

9. Coates, G. W.; Jeske, R. C., Homogeneous Catalyst Design for the Synthesis of Aliphatic Polycarbonates and Polyesters. In *Handbook of Green Chemistry*, Wiley-VCH Verlag GmbH & Co. KGaA: 2010.

10. Crabtree, R. H.; Mingos, D. M. P., Comprehensive Organometallic Chemistry III, Volumes 1 - 13. Elsevier.

11. North, M.; Pasquale, R.; Young, C., *Green Chem.* **2010,** *12* (9), 1514-1539.

12. Zevenhoven, R.; Eloneva, S.; Teir, S., *Catal. Today* **2006,** *115* (1), 73-79.

13. Shaikh, A.-A. G.; Sivaram, S., *Chem. Rev.* **1996,** *96* (3), 951-976.

14. Buonerba, A.; De Nisi, A.; Grassi, A.; Milione, S.; Capacchione, C.; Vagin, S.; Rieger, B., *Catal. Sci. Tech.* **2015,** *5* (1), 118-123.

15. Buchard, A.; Kember, M. R.; Sandeman, K. G.; Williams, C. K., *Chem. Commun.* **2011,** *47* (1), 212-4.

16. Whiteoak, C. J.; Gjoka, B.; Martin, E.; Martinez Belmonte, M.; Escudero-Adan, E. C.; Zonta, C.; Licini, G.; Kleij, A. W., *Inorg. Chem.* **2012,** *51* (20), 10639-10649.

17. Taherimehr, M.; Al-Amsyar, S. M.; Whiteoak, C. J.; Kleij, A. W.; Pescarmona, P. P., *Green Chem.* **2013,** *15* (11), 3083-3090.

18. Fuchs, M. A.; Zevaco, T. A.; Ember, E.; Walter, O.; Held, I.; Dinjus, E.; Doring, M., *Dalton Trans.* **2013,** *42* (15), 5322-5329.

19. Sheng, X.; Qiao, L.; Qin, Y.; Wang, X.; Wang, F., *Polyhedron* **2014,** *74*, 129-133.

20. Taherimehr, M.; Serta, J. P. C. C.; Kleij, A. W.; Whiteoak, C. J.; Pescarmona, P. P., *ChemSusChem* **2015,** *8* (6), 1034-1042.

21. Chen, F.; Liu, N.; Dai, B., *ACS Sus. Chem. Eng.* **2017,** *5* (10), 9065-9075.

22. Whiteoak, C. J.; Martin, E.; Martinez Belmonte, M.; Benet-Buchholz, J.; Kleij, A. W., *Adv. Synth. Catal.* **2012,** *354* (2-3), 469-476.

23. Nakano, K.; Kobayashi, K.; Ohkawara, T.; Imoto, H.; Nozaki, K., *J. Am. Chem. Soc.* **2013,** *135* (23), 8456-8459.

24. North, M.; Pasquale, R., *Angew. Chem., Int. Ed.* **2009,** *48* (16), 2946-2948.

25. Clegg, W.; Harrington, R. W.; North, M.; Pasquale, R., *Chem. Eur. J.* **2010,** *16* (23), 6828-6843.

26. North, M.; Wang, B.; Young, C., *Energy Environ. Sci.* **2011,** *4* (10), 4163-4170.

27. North, M.; Young, C., *ChemSusChem* **2011,** *4* (11), 1685-1693.

28. North, M.; Quek, S. C. Z.; Pridmore, N. E.; Whitwood, A. C.; Wu, X., *ACS Catal.* **2015,** *5* (6), 3398-3402.

29. Castro-Osma José, A.; North, M.; Offermans Willem, K.; Leitner, W.; Müller Thomas, E., *ChemSusChem* **2016,** *9* (8), 791-794.

30. Mahesh, M.; Murphy, J. A.; Wessel, H. P., *J. Org. Chem.* **2005,** *70* (10), 4118-4123.

31. Moloy, K. G., *Inorg. Chem.* **1988,** *27* (4), 677-681.

32. Teufel, R.; Friedrich, T.; Fuchs, G., *Nature* **2012,** *483*, 359.

33. Liao, R.-Z.; Siegbahn, P. E. M., *Chem. Sci.* **2015,** *6* (5), 2754-2764.

34. Costas, M.; Mehn, M. P.; Jensen, M. P.; Que, L., *Chem. Rev.* **2004,** *104* (2), 939-986.

35. Cussó, O.; Ribas, X.; Costas, M., *Chem. Commun.* **2015,** *51* (76), 14285-14298.

36. Fingerhut, A.; Serdyuk, O. V.; Tsogoeva, S. B., *Green Chem.* **2015,** *17* (4), 2042-2058.

37. Vicens, L.; Costas, M., *Dalton Trans.* **2018,** *47* (6), 1755-1763.

38. Alhashmialameer, D.; Collins, J.; Hattenhauer, K.; Kerton, F. M., *Catal. Sci. Technol.* **2016,** *6* (14), 5364-5373.

39. Grapperhaus, C. A.; Li, M.; Patra, A. K.; Poturovic, S.; Kozlowski, P. M.; Zgierski, M. Z.; Mashuta, M. S., *Inorg. Chem.* **2003,** *42* (14), 4382-4388.

40. Addison, A. W.; Rao, T. N.; Reedijk, J.; van Rijn, J.; Verschoor, G. C., *J. Chem. Soc., Dalton Trans.* **1984**, 1349.

41. Wu, T.; Zhang, X.-P.; You, X.-Z.; Li, Y.-Z.; Bouř, P., *ChemPlusChem* **2014,** *79* (5), 698-707.

42. Eguchi, H.; Umemura, M.; Kurotani, R.; Fukumura, H.; Sato, I.; Kim, J.-H.; Hoshino, Y.; Lee, J.; Amemiya, N.; Sato, M.; Hirata, K.; Singh, D. J.; Masuda, T.; Yamamoto, M.; Urano, T.; Yoshida, K.; Tanigaki, K.; Yamamoto, M.; Sato, M.; Inoue, S.; Aoki, I.; Ishikawa, Y., *Sci. Rep.* **2015,** *5*, 9194.

43. Mayilmurugan, R.; Stoeckli-Evans, H.; Suresh, E.; Palaniandavar, M., *Dalton Trans.* **2009**, 5101-5114.

44. Strautmann, J. B. H.; Freiherr von Richthofen, C.-G.; Heinze-Brückner, G.; DeBeer, S.; Bothe, E.; Bill, E.; Weyhermüller, T.; Stammler, A.; Bögge, H.; Glaser, T., *Inorg. Chem.* **2011,** *50* (1), 155-171.

45. Whiteoak, C. J.; Martin de Rosales, R. T.; White, A. J. P.; Britovsek, G. J. P., *Inorg. Chem.* **2010,** *49* (23), 11106-11117.

46. Rusere, L. N.; Shalumova, T.; Tanski, J. M.; Tyler, L. A., *Polyhedron* **2009,** *28* (17), 3804-3810.

47. Qian, X.; Dawe, L. N.; Kozak, C. M., *Dalton Trans.* **2011,** *40*, 933-943.

48. Hasan, K.; Fowler, C.; Kwong, P.; Crane, A. K.; Collins, J. L.; Kozak, C. M., *Dalton Trans.* **2008**, 2991-2998.

49. Reckling, A. M.; Martin, D.; Dawe, L. N.; Decken, A.; Kozak, C. M., *J. Organomet.Chem.* **2011,** *696*, 787-794.

50. Solomon, E. I.; Lever, A. B. P., *Inorganic electronic structure and spectroscopy*. Wiley: Toronto, 1999.

51. Velusamy, M.; Palaniandavar, M.; Gopalan, R. S.; Kulkarni, G. U., *Inorg. Chem.* **2003,** *42*, 8283-8293.

52. Schugar, H. J.; Rossman, G. R.; Barraclough, C. G.; Gray, H. B., *J. Am. Chem. Soc.* **1972,** *94* (8), 2683-2690.

53. Moon, D.; Lah, M. S.; Del Sesto, R. E.; Miller, J. S., *Inorg. Chem.* **2002,** *41* (18), 4708-4714.

54. Gorun, S. M.; Lippard, S. J., *Inorg. Chem.* **1991,** *30* (7), 1625-1630.

55. Weihe, H.; Güdel, H. U., *J. Am. Chem. Soc.* **1997,** *119* (28), 6539-6543.

56. Norman, R. E.; Holz, R. C.; Menage, S.; Que, L.; Zhang, J. H.; O'Connor, C. J., *Inorg. Chemi.* **1990,** *29* (23), 4629-4637.

57. Whiteoak, C. J.; Martin, E.; Martinez Belmonte, M.; Benet-Buchholz, J.; Kleij, A. W., *Adv. Synth. Catal.* **2012,** *354* (2-3), 469-476.

58. Castro-Gómez, F.; Salassa, G.; Kleij, A. W.; Bo, C., *Chem. Eur. J.* **2013,** *19* (20), 6289-6298.

59. Nakagiri, T.; Murai, M.; Takai, K., *Org. Lett.* **2015,** *17* (13), 3346-3349.

60. Asako, S.; Sakae, T.; Murai, M.; Takai, K., *Adv. Synth. Catal.* **2016,** *358* (24), 3966-3970.

61. Robertson, J.; Srivastava, R. S., *Mol. Catal.* **2017,** *443*, 175-178.

62. Shiraishi, Y.; Hirakawa, H.; Togawa, Y.; Hirai, T., *ACS Catal.* **2014,** *4* (6), 1642-1649.

63. Moore, D. R.; Cheng, M.; Lobkovsky, E. B.; Coates, G. W., *J. Am. Chem. Soc.* **2003,** *125* (39), 11911-11924.

64. Alhashmialameer, D.; Ikpo, N.; Collins, J.; Dawe, L. N.; Hattenhauer, K.; Kerton, F. M., *Dalton Trans.* **2015,** *44* (46), 20216-20231.

65. Schubert, E. M., *J. Chem. Edu.* **1992,** *69* (1), 62.

66. Darensbourg, D. J.; Yarbrough, J. C.; Ortiz, C.; Fang, C. C., *J. Am. Chem. Soc.* **2003,** *125* (25), 7586-7591.

67. Dolomanov, O. V. B., L. J., Gildea, R. J., Howard, J. A. K., Puschmann, H., *J. Appl. Cryst.* **2009,** *42*, 339-341.

68. Sheldrick, G. M., *Acta. Cryst. C71* **2015**, 3-8.

69. Lehenmeier, M. W.; Kissling, S.; Altenbuchner, P. T.; Bruckmeier, C.; Deglmann, P.; Brym, A.-K.; Rieger, B., *Angew. Chem., Int. Ed.* **2013,** *52* (37), 9821-9826.

70. Liu, J.; Ren, W.-M.; Liu, Y.; Lu, X.-B., *Macromolecules* **2013,** *46* (4), 1343-1349.

71. Ni, K.; Kozak, C. M., *Inorg. Chem.* **2018,** *57* (6), 3097-3106.

Co-authorship Statement

Chapter 3 : Iron Complexes for Cyclic Carbonate and Polycarbonate Formation: Selectivity Control from Ligand Design and Metal-Centre Geometry

This chapter has been peer reviewed and published in:

Inorganic Chemistry, **2019**, 58 (16), 11231-11240

Authors: Kori A. Andrea[a], Erika D. Butler[a], Tyler R. Brown[a], Timothy S. Anderson[a], Dakshita Jagota[a], Cassidy Rose[a], Emily M. Lee[b], Sarah D. Goulding[c], Jennifer N. Murphy[a], Francesca M. Kerton[a]* and Christopher M. Kozak*[a]

[a] Department of Chemistry, Memorial University of Newfoundland, St. John’s, NL, A1B 3X7, Canada

[b] St. Kevin’s High School, 435 Blackline Rd, Goulds, NL, A1S 1G6

[c] Holy Heart High School, 55 Bonaventure Ave, St. John's, NL A1C 6N8

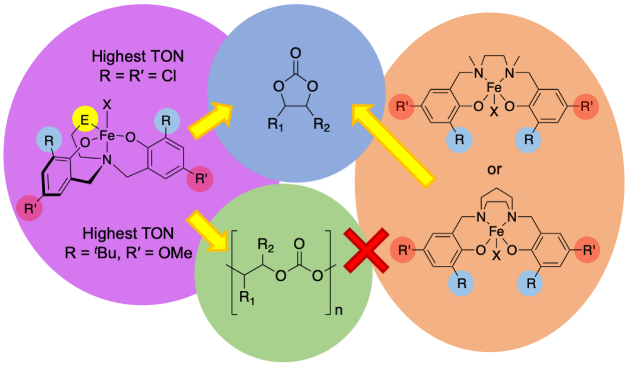

The first author (K. A. Andrea) contributed to 90% of the article, including manuscript writing, performing experiments and data analysis. Erika D. Butler performed the experimental work on catalytic screening for cyclic carbonate formation, which appears in the original publication but is not included herein. T. R. Brown, D. Jagota and C. Rose were undergraduate students, while E. M. Lee and S. D. Goulding were high school students supervised by K. A. Andrea. J. N. Murphy and T. S. Anderson collected, analyzed and solved all crystallographic data (J. N. Murphy was responsible for complexes **3.1a**, **3.3**, **3.11** and **3.14b** and T. S. Anderson for complexes **3.8** and **3.10**). The corresponding authors, F. M. Kerton and C. M. Kozak, directed the project, assisting in experimental design and manuscript writing.

Chapter 3: Iron Complexes for Cyclic Carbonate and Polycarbonate Formation: Selectivity Control from Ligand Design and Metal-Centre Geometry

See Appendix B for additional data

3.1 Introduction

The conversion of carbon dioxide (CO_2) into value-added materials has gained interest over the past decade, with an overall vision of creating a renewable carbon economy.[1-3] CO_2 remains an attractive C-1 feedstock due to its abundance, low cost and low toxicity. Among the many possible transformations of CO_2 into useful materials, the coupling or ring-opening copolymerization (ROCOP) of CO_2 with epoxides to selectively produce either cyclic or polycarbonate is attractive (**Figure 3.1**). The activation of CO_2, however, presents challenges due to its high thermodynamic stability;[4-5] therefore, along with the use of a catalyst, reaction conditions involving high temperatures and pressures must often be employed.[4, 6-7] The latter however has become less problematic with the design of catalytic systems that can operate at ambient temperatures and pressures.[8-12]

In terms of metal-based catalysts, systems based on zinc, chromium, cobalt and aluminum have dominated the field,[13-19] while more recently work has been done using non-metal and organocatalytic systems.[9, 20] Iron-based catalyst systems have recently been gaining attention for these reactions.[21-28] From both an environmental and economical stand-point, iron is attractive due to its low cost, abundance and reduced toxicity in comparison to the heavy-metal based catalytic systems.[26]

The nature of the ligand framework around the Lewis acidic iron center is crucial in not only controlling reactivity but also product selectivity. In 2013, Nozaki and co-workers reported an iron(IV) complex supported by a macrocyclic corrole ligand framework.[22] This system could copolymerize cyclohexene oxide (CHO), propylene oxide (PO) and glycidyl phenyl ether (GPE) with CO_2. For PO, the polymers obtained displayed higher molecular weights (up to 51 000 g mol^{-1}) with narrow molecular weight dispersity, but modest carbonate incorporation (up to 29%). Aside from this system, phenoxy-based ligands have dominated the field for iron and similarly for zinc, chromium, aluminum and cobalt systems.[13] An important example was reported by Williams and co-workers of a dinuclear iron(III) complex,[21] which was active at 1 bar CO_2 and catalyzed the copolymerization of CHO and CO_2 giving 29% epoxide conversion to polycyclohexene carbonate (PCHC) after 48 h with 66% carbonate linkages. At 10 bar, 70% conversion of epoxide to perfectly alternating PCHC was obtained after 24 h. However, in the presence of excess nucleophile, selectivity changed from PCHC to *cis*-cyclohexene carbonate (*cis*-CHC) due to increased backbiting of the growing alkoxide chain. More recently, [OSSO]-type iron(III) complexes have been reported to catalyze the cycloaddition of CO_2 and epoxides at ambient conditions;[27-28] while iron(II) formazanate and pincer complexes have also shown promise in this area.[29-30]

Two studies of iron aminophenolate complexes as catalysts for ROCOP reactions of CO_2 and epoxides employed supercritical CO_2 ($scCO_2$) conditions (P = 80 bar, T = 85 °C).[23-24] The first system focused on a series of iron(III) amino-tris(phenolate) compounds with varying steric factors on the *ortho*-positions of the phenolate groups.[23] The polycarbonates obtained showed low molecular weights, which were attributed to the presence of trace amounts of water in the reaction vessels. However, when performed under strictly anhydrous conditions, molecular weights could be improved substantially. An iron(III) pyridylamino-bis(phenolate) catalyst active for both cyclic and polycarbonate formation in $scCO_2$ (P = 80 bar, T = 60 °C) was also reported, however, all the polycarbonates obtained were oligomeric with molecular weights typically below 1500 g mol^{-1} (>90 % carbonate linkages).[24] Along with these reports there have been several other iron-based systems evaluated in the recent years with high activity for cyclic and polycarbonates.[30-31] We recently reported a family of tetradentate amino-bis(phenolate) iron(III) complexes that formed oxo-bridged iron(III) species during catalysis as a result of in situ epoxide deoxygenation.[25, 32] These complexes were found to be only active for cyclic carbonate formation and catalysis performed by the oxo-bridged counterpart demonstrated slower initial reaction kinetics.

Due to the wide range of reactivities reported to date for iron amino-phenolate complexes for reactions of CO_2 with epoxides, we decided to perform a comprehensive study toward determining a structure-activity relationship across such catalysts for CO_2/epoxide coupling and ROCOP. Relationships such as this have previously been established for group 3 metal catalysts toward ethylene and α-olefin polymerization,[33-35] and group 3/lanthanide complexes for ring opening polymerization of cyclic esters.[36-40] Our study probes the effects of (i) the steric and electronic influence of the phenolate donors, (ii) the nature of the neutral donor arm of the ligand, and (iii) the geometry of the central iron atom on both activity and product selectivity. We found that a careful combination of the above factors could result in the selective production of perfectly alternating PCHC at pressures as low as 7 bar. Addition of excess nucleophile causes the selectivity to switch, exclusively producing the corresponding cyclic carbonate (**Figure 3.1**).

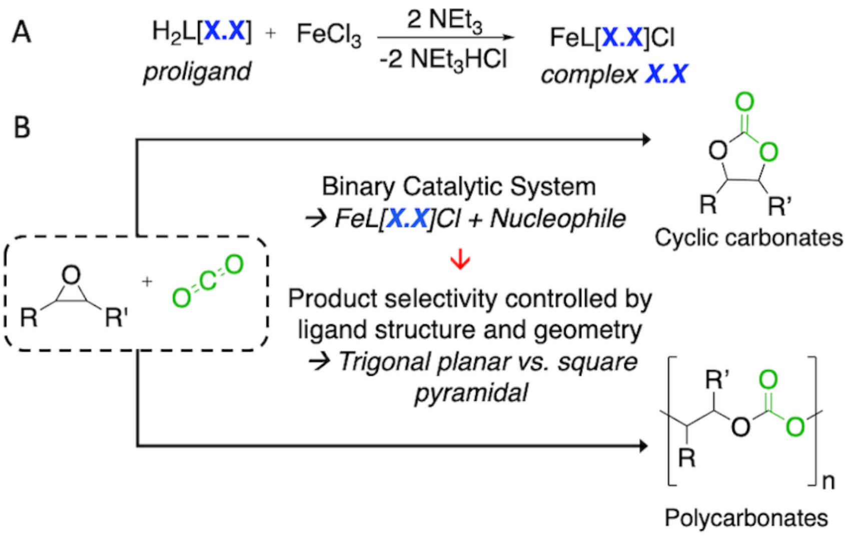

Figure 3.1. (A) General reaction scheme for the synthesis of iron complexes used in this report. [**X.X**] refers to numbering scheme of ligands used in **Figure 3.2**. (B) Products obtained through the catalytic coupling or copolymerization of CO_2 and epoxides.

3.2 Synthesis and characterization of iron complexes

A series of amino-phenolate ligands H_2L[**3.1**]–H_2L[**3.7**],[41-47] H_2L[**3.11**][48] and H_2L[**3.12**]–H_2L[**3.15**][25, 49] and iron(III) complexes **3.1a** and **3.7**,[41, 50] **3.4**,[24] **3.6** and **3.7**,[41, 51] **3.11** – **3.14b**[25, 52] and **3.15**[53] were prepared as previously reported. Proligands H_2L[**3.8**]–H_2L[**3.10**] and complexes **3.1b**, **3.3**, **3.5**, and **3.8–3.10** are new, and their synthesis and characterization are described herein. The solid-state molecular structures for six compounds are reported (**3.1b**, **3.8** and **3.10**, which are new compounds, and **3.2**, **3.11** and **3.14b**, which have not been structurally characterized via X-ray diffraction to date). The 17 complexes evaluated in this study are shown in **Figure 3.2**.

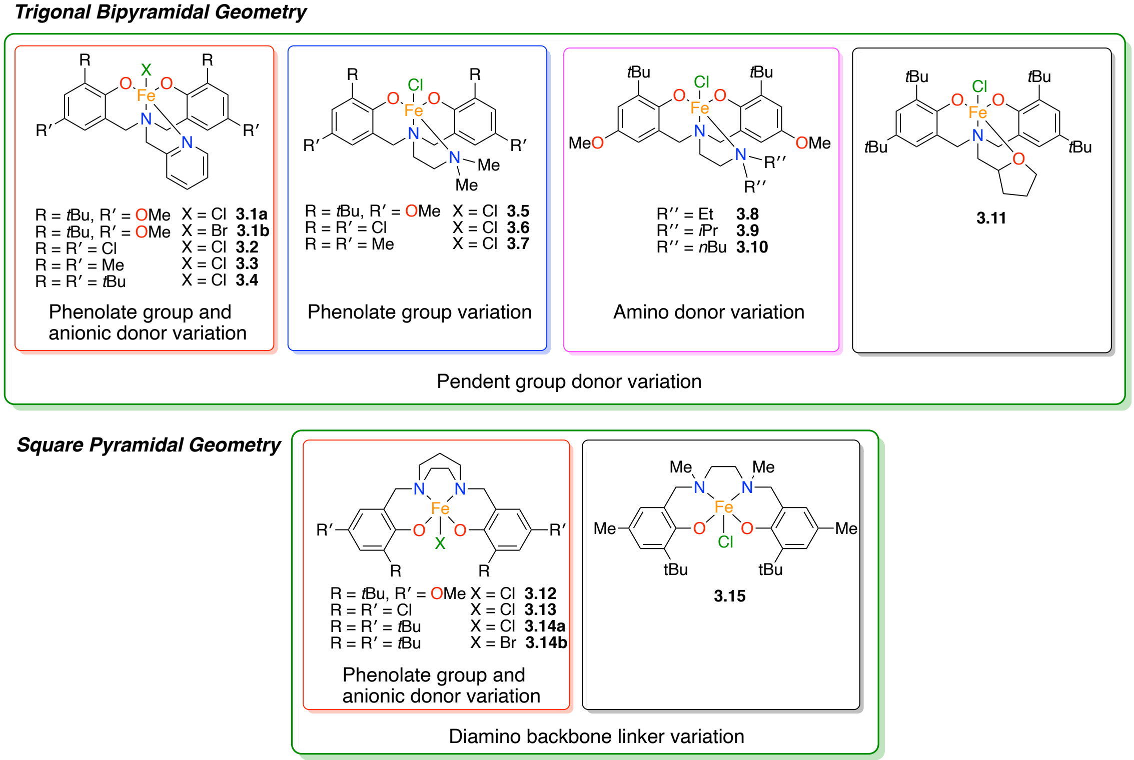

Figure 3.2. Complexes used for the catalytic coupling and co-polymerization of CO_2 and epoxides.

Single crystals of **3.1b, 3.2** and **3.14b** suitable for X-ray diffraction were grown by slow evaporation of saturated solutions in dichloromethane at –20 °C, whereas single crystals of **3.8**, **3.10** and **3.11** were grown in a similar manner from saturated methanol solutions. All recrystallizations were performed in air. The molecular diagrams (ORTEP) of the structures are shown in **Figure 3.3**, and crystallographic data and selected bond lengths and angles are reported in Appendix B.

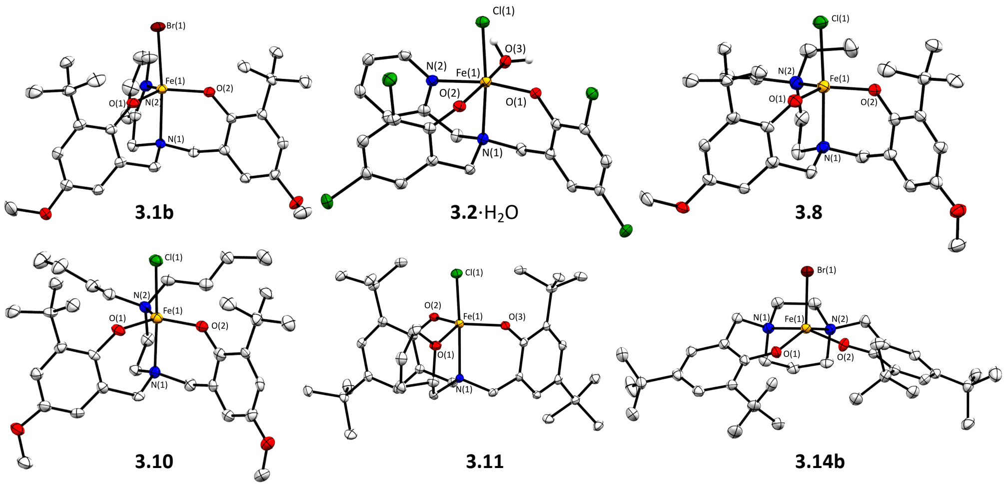

3.1b **3.2**·H$_2$O **3.8**

3.10 **3.11** **3.14b**

Figure 3.3. Molecular structures (ORTEP) and partial numbering schemes for **3.1b**, **3.2·H$_2$O**, **3.8**, **3.10**, **3.11** and **3.14b**. Ellipsoids are shown at the 50% probability level. Only the H-atoms of the aqua ligand on **3.2·H$_2$O** are shown for clarity.

Complex **3.2** was found to exist as a 6-coordinate aqua complex in the solid-state unlike the other structurally similar complexes reported here; therefore, when discussing its solid-state structure, it is referred to as **3.2**·H$_2$O. We have previously reported a related aqua adduct of an iron(III) bromide complex of ligand L[**3.2**].[41] The coordination of adventitious water in **3.2**·H$_2$O attests to the increased Lewis acidity of Fe(III) in this electron-withdrawing group-containing ligand environment. The metric parameters of **3.2**·H$_2$O and the previously reported Fe-Br complex are very similar except of course for the metal-halide bond distance. The structure displays intramolecular π-π stacking between the pyridine ring and a phenolate ring, showing a distance between centroids of 3.519 Å with an angle of 26.55° between the planes of the two aromatic rings. Between adjacent molecules in the unit cell, intermolecular hydrogen bonding is observed between the O-H of the aqua ligand and a phenolate O-atom, as well as π-π stacking between two dichlorophenolate groups (see **Figure B1**).[54]

Complexes **3.1b**, **3.8**, **3.10** and **3.11** exhibit distorted trigonal bipyramidal geometries around the iron centers (τ parameters ranging from 0.77-0.74, where τ = 1 describes a perfect trigonal bipyramidal structure and τ = 0 a perfect square pyramidal geometry) while complex **3.14b** is best described as having a distorted square pyramidal geometry (τ = 0.14).[55] The structures of the trigonal bipyramidal compounds are very similar, differing only by the nature of their neutral donor or substituents on the phenolate rings. The bond lengths between the chelating ligands and central iron atom are similar in these complexes. The Fe-Cl bonds ranged from 2.2712(8)-2.2748(10) Å, while the Fe-Br bonds varied from 2.4037(9)-2.4550(4) Å, in agreement with similar reported structures.[25, 52] For complexes **3.8** and **3.10** the increased steric bulk of the terminal nitrogen donor does not appear to significantly impact the Fe-N bond distance. The structure of **3.5** (the dimethylethyl amino-group containing analog of **3.8** and **3.10**) has been previously reported and the bond lengths and angles reported are experimentally similar to those given here.[56] The 5-coordinate complexes of the electron-donating (R = *t*Bu, R' = OMe, and R = tBu, R' = Me) analogs of **3.2** have been previously reported[24, 53] and used as hydrogen evolution catalysts.[50] The corresponding bond lengths and angles of these amino-bis(phenolate) iron complexes determined via single crystal X-ray diffraction are comparable. Compound **3.14b** displays a square pyramidal geometry similar to Fe(III) compounds of the related salen[57] and salan[58-59] ligand systems.

3.3 Copolymerization of cyclohexene oxide and CO_2

All iron complexes in **Figure 3.2** were assessed as catalysts for the copolymerization of CO_2 and cyclohexene oxide (CHO). In general, all trigonal bipyramidal complexes, except complexes **3.8**, **3.9** and **3.10**, were active exclusively for polycarbonate formation giving polymers with >99% carbonate linkages (**Table 3.1**, entries 1–12). For **3.8**, **3.9** and **3.10**, modest yields of *cis*-cyclohexene carbonate were produced instead, whereas catalysts giving polycarbonate showed no cyclic carbonate formation. Square pyramidal complexes **3.12** – **3.14b** bearing a homopiperzine backbone showed no conversion of CHO (**Table 3.1**, entries 13 – 16), while complex **3.15** with a salan backbone gave a conversion of 34% to *cis*-cyclohexene carbonate (**Table 3.1**, entry 17). As mentioned above, complexes **3.12** – **3.14b** can undergo epoxide deoxygenation with the substrate and it is possible that complex **3.15** behaves similarly. When **3.15** was combined with CHO the immediate formation of a brick red precipitate suggestive of μ-oxo complex formation, which we and others have previously observed.[32, 58] Characterization of this red complex by UV-vis and MALDI-TOF MS was consistent with these earlier reports of μ-oxo complex formation. Therefore, we propose that the μ-oxo complex formation by iron chloride complexes may be indicative of no activity toward ROCOP (i.e. it shuts down this reaction manifold).

In terms of complexes that are active for the copolymerization of CHO and CO_2, the overall reactivity was highly dependent on the nature of the pendent donor, the electronics and sterics of the phenolate donor, and the halide ligand at the iron center. The iron chloride complexes gave a higher overall conversion than the corresponding iron bromides (**Table 3.1**, entries 2–3). For complexes possessing pyridyl pendent groups, electron-rich phenolate rings resulted in slightly improved conversions over those with electron withdrawing groups (**Table 3.1**, entries 1–2). The sterics of the phenolate groups were inconsequential on the reactivity (**Table 3.1**, entries 4–5).

When the hybridization of the pendent donor is changed from an sp^2 nitrogen of a pyridyl group (complex **3.1a**) to an sp^3 amine (complex **3.5**), the influence of the electronic nature of the phenolate groups was reversed. That is, instead of electron donating groups giving the highest reactivity, electron withdrawing substituents paired with the sp^3 nitrogen-containing pendent donor were most active (**Table 3.1**, entries 2 and 7). As the steric bulk of the sp^3-*N* pendent donor increased, selectivity of the product switched from perfectly alternating polycarbonate to *cis*-cyclohexene carbonate (**Table 3.1**, entries 6 and 9-11). Compound **3.11**, bearing an oxygen pendent donor, gave modest conversions to cyclohexene carbonate (**Table 3.1**, entry 12), and square pyramidal complexes were inactive for polycarbonate formation (**Table 3.1**, entries 13-17). These results show that not only the geometry of the metal center, but also a careful pairing of the pendent donor and the electronics of the phenolate rings is crucial for product selectivity and activity. Our study demonstrates that the highly modifiable amino-phenolate ligands can be tailored to yield iron complexes for ROCOP activity in a similar way to titanium and zirconium systems for ethylene and α-olefin polymerization.[33-35] Reactivity control using these ligands has also been shown for cyclic ester ROP using group 3 and lanthanide centers.[36-40]

Compound **3.1a** showed the best activity for polycarbonate formation and so its reactions were studied in more detail. At 0.5 mol% Fe, 99% conversion to perfectly alternating polycyclohexene carbonate was observed with narrow dispersity (**Table 3.1**, entry 2). However, when the catalyst loading was decreased to 0.2 mol% conversions decreased (**Table 3**, entry 18). Lowering the temperature from 60 °C to 40 °C showed only a small decrease in conversion but decreasing the temperature further to 25 °C resulted in no conversion (**Table 3**, entries 2 and 19-20). Lower conversions were observed with decreasing CO_2 pressure. We were pleased to observe a conversion of 56% CHO to PCHC at 7 bar CO_2 but decreasing pressure to 1 bar afforded only 5% conversion to PCHC (**Table 3.1**, entries 2 and 21-25). It was also found that as CO_2 pressure decreased, the polymer molecular weights and dispersities remained constant. While overall conversions declined with decreasing CO_2 pressure, strictly alternating copolymers were always produced. An [OSSO]-iron(III) system has also been shown to provide completely alternating polycarbonate at CO_2 pressures as low as 1 bar, but also with decreased conversions.[28] Related catalysts, however, typically give a lower carbonate content in the polymer product when CO_2 pressure is decreased.[21-22]

Varying reaction time showed copolymerization occurred with 41% conversion obtained in 1 h (**Table 3.1**, entry 26), corresponding to a TOF of 82 h^{-1}, which was not further optimized. Allowing reactions to continue for 8 h gave 66% conversion while after 22 h 99% conversion to polycarbonates was obtained (**Table 3.1**, entries 2 and 27). The influence of the co-catalysts was explored and anionic co-catalysts (PPNCl and TBAB) gave the best results, with PPNCl slightly out-performing TBAB which we attributed to the enhanced ability of Cl^- to ring-open the coordinated epoxide because of its smaller size in comparison to Br$^-$. No reactivity was observed when the neutral co-catalyst DMAP was used. We believe the stronger binding of DMAP to the iron center hinders coordination of the incoming epoxide for activation (as mentioned above, Fe-DMAP adduct formation was observed via MALDI-TOF MS). This potentially leads to less active systems for propylene carbonate formation and inhibits polycarbonate formation. When PPNCl was used in excess relative to iron, product selectivity switched from perfectly alternating polycarbonate to *cis*-CHC (**Table 3.1**, entries 2 and 30). This switching of selectivity for polymeric vs cyclic carbonate formation has been previously reported for iron catalysts by Williams,[21] and by Kleij and Pescarmona.[23-24] End-group analysis of the polycarbonates obtained was performed using MALDI-TOF MS and showed both chloride and hydroxide end-groups (see Appendix B). These are expected as the nucleophilic chloride initiates ring-opening of the coordinated epoxide, while termination of the growing chain occurs when reactions are quenched with acidified methanol.

Table 3.1. Copolymerization of CHO and CO_2 catalyzed by **3.1** – **3.15**.

Entry[a]	Complex	[CHO]:[Cocat]:[Fe]	Co-cat	PCO_2 (bar)	Conv. (%)[b,c]	M_n (g mol^{-1})[d]	Đ[d]
1	**3.2**	200:1:1	PPNCl	60	89	8100	1.09
2	**3.1a**	200:1:1	PPNCl	60	99	9200	1.14
3	**3.1b**	200:1:1	PPNCl	60	76	4300	1.07
4	**3.3**	200:1:1	PPNCl	60	89	5800	1.07
5	**3.4**	200:1:1	PPNCl	60	88	7500	1.10
6	**3.5**	200:1:1	PPNCl	60	48	3600	1.02
7	**3.6**	200:1:1	PPNCl	60	90	7500	1.09
8	**3.7**	200:1:1	PPNCl	60	78	4500	1.07
9	**3.8**	200:1:1	PPNCl	60	20 (*cis*)	-	-
10	**3.9**	200:1:1	PPNCl	60	12 (*cis*)	-	-
11	**3.10**	200:1:1	PPNCl	60	7 (*cis*)	-	-
12	**3.11**	200:1:1	PPNCl	60	48	3500	1.04
13	**3.12**	200:1:1	PPNCl	60	0	-	-
14	**3.13**	200:1:1	PPNCl	60	0	-	-
15	**3.14a**	200:1:1	PPNCl	60	0	-	-
16	**3.14b**	200:1:1	PPNCl	60	0	-	-
17	**3.15**	200:1:1	PPNCl	60	34 (*cis*)	-	-
18	**3.1a**	500:1:1	PPNCl	60	39	4700	1.02
19[e]	**3.1a**	200:1:1	PPNCl	60	0	-	-
20[f]	**3.1a**	200:1:1	PPNCl	60	89	5700	1.06
21	**3.1a**	200:1:1	PPNCl	40	88	5400	1.05
22	**3.1a**	200:1:1	PPNCl	20	77	6400	1.13
23	**3.1a**	200:1:1	PPNCl	10	63	5000	1.04
24	**3.1a**	200:1:1	PPNCl	7	56	5200	1.09
25	**3.1a**	200:1:1	PPNCl	1	5	-	-

26[g]	**3.1a**	200:1:1	PPNCl	60	41	3600	1.03
27[h]	**3.1a**	200:1:1	PPNCl	60	66	4900	1.01
28	**3.1a**	200:1:1	TBAB	60	81	5700	1.09
29	**3.1a**	200:1:1	DMAP	60	0	-	-
30	**3.1a**	200:4:1	PPNCl	60	99 (*cis*)	-	-

[a] Reaction conditions unless otherwise stated: Neat cyclohexene oxide (3.06×10^{-2} mol), Fe catalyst (1.52×10^{-4} mol), PPNCl (1.52×10^{-4} mol), 60 °C, 22 h. [b] Conversion determined using ^{1}H NMR spectroscopy by comparing the integral resonances for PCHC (4.60 – 4.65 ppm), CHC (3.90 – 4.07 ppm (*trans*) or 4.63 – 4.70 ppm (*cis*)) and resonances for residual epoxide. No mixtures of polycarbonate and cyclic carbonate were observed by NMR. [c] Values describe conversion to polycarbonate unless followed by (*cis*), which denotes *cis*-cyclic cyclohexene carbonate formation. No *trans*-cyclic carbonate was observed. [d] Determined in THF by GPC equipped with a multi-angle light scattering detector. [e] Reaction temperature: 25 °C [f] Reaction temperature: 40 °C [g] Reaction time: 1 h. [h] Reaction time: 8 h.

3.4 Conclusions

Seventeen air-stable iron(III) complexes bearing amino-bis(phenolate) ligands were synthesized and evaluated as catalysts for the reaction of CO_2 with epoxides to selectively yield either cyclic or polycarbonates. For polycarbonate formation from CHO and CO_2, it was found that only those complexes in a trigonal bipyramidal geometry were active for ROCOP and their reactivity was highly dependent on the pendent donor and electronic properties of the phenolates. Indeed, both variables need to be tailored to give optimum reactivity and complex **3.1a**, possessing electron donating groups on the phenolate groups, was most effective at polycarbonate formation. The catalysts presented here are active at CO_2 pressures as low as 7 bar and the resulting monodisperse, low molecular weight polycarbonates contained >99% carbonate linkages. In addition, selectivity could be completely switched from polycarbonate to cyclic carbonate via addition of excess chloride cocatalyst. This work demonstrates, as others have shown, the tailorable properties of amino-phenolate ligands that are highly desirable for optimum catalyst design.

3.5 Experimental

3.5.1 General experimental conditions

Bis(triphenylphosphine)iminium chloride, tetra-*n*-butylammonium bromide and 4-dimethylaminopyridine were purchased from Alfa Aesar or Sigma Aldrich and used without further purification. Commercially available solvents (ACS Grade) were used without purification. All epoxides were dried over CaH_2 and distilled under nitrogen before use. Synthesis of all ligands and iron complexes was performed in air. The proligands H_2L[**3.1**]–H_2L[**3.7**],[41-44, 46-47, 60] H_2L[**3.11**][48] and H_2L[**3.12**]–H_2L[**3.15**],[25, 61] and iron(III) complexes **3.1**–**3.2**,[41, 50] **3.4**[24], **3.6**, **3.7**,[41, 51] **3.11**–**3.14**[25, 52] and **3.15**[25, 52-53] were prepared as previously reported. *Caution should be taken when operating high pressure equipment.*

3.5.2 Instrumentation

^1H and ^{13}C NMR spectra were recorded on a Bruker Avance III 300 MHz spectrometer at 25 °C and were referenced using the residual proton and ^{13}C resonances of the solvent or to TMS internal standards. UV-vis data were collected on an Ocean Optics USB4000+ fiber optic spectrophotometer. MALDI-TOF mass spectra were obtained on an Applied Biosystems 4800 MALDI-TOF/TOF Analyzer, equipped with a reflectron, delayed ion extraction and high-performance nitrogen laser (200 Hz, operating at 355 nm). Anthracene was used as the matrix and samples were prepared at a concentration of 10.0 mg/mL in dichloromethane. Images of MALDI spectra were prepared using mMass software (www.mmass.org). Electrospray ionization mass spectrometry was performed on an

Agilent 6200 series LC/MSD (TOF) mass spectrometer. Mass spectra were obtained in positive mode with dual ESI on acetonitrile/methanol solutions. Elemental analysis was performed at Saint Mary's University, Centre for Environmental Analysis and Remediation or Guelph Chemical Laboratories Ltd., Canada. All high-pressure reactions were performed in a 100 mL stainless steel autoclave reactor (Parr Instrument Company) equipped with a heating mantle and mechanical stirrer. For in situ IR-monitored reactions, the vessel was equipped with a silicon ATR sensor (SiComp Sentinel) connected to a ReactIR 15 base unit (Mettler-Toledo) via a DS silver-halide Fiber-to-Sentinel conduit.

3.5.3 Iron catalyzed cyclic and polycarbonate formation

Prior to each reaction, the stainless-steel reaction vessel was heated to 100 °C under vacuum overnight. Stock solutions of catalyst and co-catalyst in dichloromethane were prepared. Appropriate amounts of each were combined in a vial and solvent removed under vacuum. The appropriate amount of desired epoxide was then added to the catalyst mixture and the resulting solution injected into the pressure vessel. The vessel was sealed, pressurized and heated to the desired temperature for the appropriate reaction time. In the case of kinetic studies, similar protocols were followed as per in situ reaction monitoring by IR spectroscopy reported by our group and others, demonstrating the linear response of the absorbance vs. concentration.[62-65]

3.5.4 Single crystal X-ray determination

Crystallographic data were collected on a Rigaku Saturn70 diffractometer at 125 K. The structures were solved using Olex2[66] with the ShelXT[67] structure solution program using

Intrinsic Phasing and refined with the ShelXL[67] refinement package using Least Squares minimization. CCDC reference numbers are given in Tables B1 and B2.

3.5.5 Synthesis and characterization of ligands and catalysts

Synthesis of H_2L[3.8]: A mixture of 3-*tert*-butyl-4-hydroxyanisole (11.88 g, 65.91 mmol), 37% w/w formaldehyde (5.5 mL, 73.39 mmol) and *N,N*-diethylethylenediamine (3.83 g, 32.96 mmol) in water (50 mL) was stirred and heated to reflux for 24 h. Upon cooling to room temperature, water was decanted from the remaining orange oil. This oil was triturated with methanol to yield a colorless powder, which was recrystallized from a mixture of methanol and chloroform to afford a colorless, crystalline solid (13.51 g, 81.9%). ^{1}H NMR (300 MHz, $CDCl_3$, δ): 9.27 (s, OH, 2H); 6.81 (d, J = 3.0 Hz, ArH, 2H); 6.48 (d, J = 3.0 Hz, ArH, 2H); 3.75 (s, OCH_3, 6H); 3.57 (s, NCH_2Ar, 4H); 2.67 (s, NCH_2CH_2N, 4H); 2.61 (q, J = 7.3 Hz, NCH_2CH_3, 4H); 1.39 (s, $C(CH_3)_3$, 18H); 1.09 (t, J = 7.1 Hz, NCH_2CH_3, 6H). $^{13}C\{^1H\}$ NMR (75 MHz, 298 K, $CDCl_3$): δ 151.39 (Ar); 149.66 (Ar); 138.26 (Ar); 122.64 (Ar); 113.15 (Ar); 112.50 (Ar); 56.33 (OCH_3); 55.68 (CH_2); 49.58 (CH_2); 48.82 (CH_2); 45.14 (CH_2); 34.97 ($C(CH_3)_3$); 29.40 ($C(CH_3)_3$); 9.57 (NCH_2CH_3). Anal. calc'd for $C_{30}H_{48}N_2O_4$: C, 71.96; H, 9.66; N, 5.59. Found: C, 71.52; H, 9.12; N, 5.31.

Synthesis of H_2L[3.9]: A mixture of 3-*tert*-butyl-4-hydroxyanisole (12.53 g, 69.52 mmol), 37% w/w formaldehyde (5.5 mL, 73.39 mol) and *N,N*-diisopropylethylenediamine (5.01 g, 34.75 mmol) in water (70 mL) was stirred and heated to reflux for 24 h. Upon cooling to room temperature, water was decanted from the remaining brown solid. This solid was triturated with methanol to yield a colorless powder, which was recrystallized from a mixture of methanol and chloroform to afford a colorless, crystalline solid (8.81 g, 47.9%). ^{1}H NMR (300 MHz, $CDCl_3$, δ): 8.52 (s, OH, 2H); 6.79 (d, J = 3.1 Hz, ArH, 2H); 6.46 (d, J = 3.1 Hz, ArH, 2H); 3.73 (s, OCH_3, 6H); 3.55 (s, NCH_2Ar, 4H); 3.22 (septet, J = 6.6 Hz,

$CH(CH_3)_2$, 2H); 2.78 (t, J = 6.2 Hz, NCH_2CH_2N, 2H); 2.55 (t, J = 6.2 Hz, NCH_2CH_2N, 2H); 1.37 (s, $C(CH_3)_3$, 18H); 1.06 (d, J = 6.6 Hz, $CH(CH_3)_2$, 12H). $^{13}C\{^1H\}$ NMR (75 MHz, 298 K, $CDCl_3$): δ 151.56 (Ar); 149.15 (Ar); 138.22 (Ar); 122.56 (Ar); 113.14 (Ar); 112.48 (Ar); 56.44 (OCH_3); 55.66 (CH_2); 49.37 (CH_2); 46.27 (CH_2); 39.58 (CH); 34.93 ($C(CH_3)_3$); 29.41 ($C(CH_3)_3$); 19.77 ($CH(CH_3)_2$). Anal. calc'd for $C_{32}H_{52}N_2O_4$: C, 72.69; H, 9.91; N, 5.30. Found: C, 72.44; H, 9.67; N, 5.32.

Synthesis of H_2L[3.10]: A mixture of 3-*tert*-butyl-4-hydroxyanisole (8.43 g, 46.67 mmol), 37% w/w formaldehyde (4.0 mL, 53.37 mmol) and *N,N*-di-*n*-butylethylenediamine (4.03 g, 23.39 mmol) in water (50 mL) was stirred and heated to reflux for 24 h. Upon cooling to room temperature, water was decanted from the remaining brown solid. This solid was triturated with methanol to yield a colorless powder, which was recrystallized from a mixture of methanol and chloroform to afford a colorless, crystalline solid (12.43 g, 95.5%). ^1H NMR (300 MHz, $CDCl_3$, δ): 9.24 (s, OH, 2H); 6.81 (d, J = 3.0 Hz, ArH, 2H); 6.48 (d, J = 3.0 Hz, ArH, 2H); 3.75 (s, OCH_3, 6H); 3.59 (s, NCH_2Ar, 4H); 2.62 (s, NCH_2CH_2N, 4H); 2.54 (m, $NCH_2CH_2CH_2CH_3$, 4H); 1.51 (m, $NCH_2CH_2CH_2CH_3$, 4H); 1.40 (s, $C(CH_3)_3$, 18H); 1.24 (dq, J = 14.5, 7.3 Hz, $NCH_2CH_2CH_2CH_3$, 4H); 0.89 (t, J = 7.3 Hz, $NCH_2CH_2CH_2CH_3$, 6H). $^{13}C\{^1H\}$ NMR (75 MHz, 298 K, $CDCl_3$): δ 151.40 (Ar); 149.74 (Ar); 138.30 (Ar); 122.77 (Ar); 113.16 (Ar); 112.49 (Ar); 56.82 (OCH_3); 55.70 (CH_2); 52.10 (CH_2); 50.87 (CH_2); 49.20 (CH_2); 34.97 ($C(CH_3)_3$); 29.44 ($C(CH_3)_3$); 26.24 ($NCH_2CH_2CH_2CH_3$); 20.92 ($NCH_2CH_2CH_2CH_3$); 14.10 ($NCH_2CH_2CH_2CH_3$). Anal. calc'd for $C_{34}H_{56}N_2O_4$: C, 73.64; H, 10.24; N, 4.91. Found: C, 72.96; H, 9.88; N, 5.06.

Synthesis of 3.3: To a suspension of recrystallized H_2L[**3.3**] (2.00 g, 4.10 mmol) in methanol (50 mL), a solution of anhydrous $FeBr_3$ (1.20 g, 4.10 mmol) in methanol was added dropwise resulting in the formation of a dark purple solution. To this triethylamine (0.822 g, 0.0081 mol) was added dropwise and the resulting mixture was stirred for 2 h, followed by solvent removal under vacuum. The resulting product was extracted into acetone, filtered and removal of solvent under vacuum yielded a dark purple powder (2.01 g, 79.1 %). UV-Vis (CH_2Cl_2) λ_{max}, nm (ε): 570 (5520). Anal. calc'd for $C_{30}H_{38}BrFeN_2O_4$ + 0.5 CH_2Cl_2: C, 54.49; H, 6.43; N, 4.61. Found: C, 54.77; H, 5.88; N, 4.19. X-ray quality crystals of **1.3** were obtained by slow evaporation of saturated solutions in dichloromethane at –20 °C.

Synthesis of 3.4: This was prepared in a similar manner to **3.3** to yield a dark purple powder (3.05 g, 85.7%). UV-Vis (CH_2Cl_2) λ_{max}, nm (ε): 580 (4980). MS (ESI in MeOH), *m/z* 431.19, $[M–Cl]^+$, 466.10, $[M+H]^+$ (very weak abundance).

Synthesis of 3.5: This was prepared in a similar manner to **3.3** to yield a dark purple powder (2.95 g, 49.5%). UV-Vis (CH_2Cl_2) λ_{max}, nm (ε): 580 (4190). Anal. calc'd for $C_{28}H_{42}FeClN_2O_4$: C, 59.85; H, 7.53; N, 4.99. Found: C, 59.69; H, 7.28; N, 5.29. MS (ESI in MeOH), *m/z* 562.28, $[M+H]^+$.

Synthesis of 3.8: This was prepared in a similar manner to **3.3** to yield a dark purple powder (5.87 g, 78.1%). UV-Vis (CH_2Cl_2) λ_{max}, nm (ε): 514 (6670). Anal. calc'd for $C_{30}H_{46}FeClN_2O_4$: C, 61.07; H, 7.86; N, 4.75. Found: C, 60.80; H, 7.59; N, 4.97. X-ray quality crystals of **3.1** were obtained by slow evaporation of saturated solutions in methanol at –20 °C.

Synthesis of 3.9: This was prepared in a similar manner to **3.3** to yield a dark purple powder (2.49 g, 61.1%). UV-Vis (CH_2Cl_2) λ_{max}, nm (ε): 530 (3120). Anal. calc'd for $C_{32}H_{50}FeClN_2O_4$: C, 62.19; H, 8.15; N, 4.53. Found: C, 62.40; H, 7.94; N, 4.52.

Synthesis of 3.10: This was prepared in a similar manner to **3.3** to yield a dark purple powder (5.14 g, 80.4%). UV-Vis (CH_2Cl_2) λ_{max}, nm (ε): 514 (5930). Anal. calc'd for $C_{34}H_{54}FeClN_2O_4$: C, 63.20; H, 8.42; N, 4.34. Found: C, 63.34; H, 8.18; N, 4.60. X-ray quality crystals of **3.10** were obtained by slow evaporation of saturated solutions in methanol at –20 °C.

Synthesis of 3.14: This was prepared in a similar manner to **3.3** to yield a dark purple powder (2.63 g, 89.3%). UV-Vis (CH_2Cl_2) λ_{max}, nm (ε): 573 (5670). Anal. calc'd for $C_{35}H_{54}FeBrN_2O_2 + 0.5\ H_2O$: C, 61.51; H, 8.43; N, 4.72. Found: C, 61.86; H, 8.16; N, 4.12. X-ray quality crystals of **3.14** were obtained by slow evaporation of saturated solutions in methanol at –20 °C.

3.5 References

1. Artz, J.; Müller, T. E.; Thenert, K.; Kleinekorte, J.; Meys, R.; Sternberg, A.; Bardow, A.; Leitner, W., *Chem. Rev.* **2018,** *118* (2), 434-504.

2. Aresta, M.; Dibenedetto, A.; Angelini, A., *Chem. Rev.* **2014,** *114* (3), 1709-1742.

3. Aresta, M., Carbon Dioxide Reduction and Uses as a Chemical Feedstock. In *Activation of Small Molecules*, Wiley-VCH Verlag GmbH & Co. KGaA: 2006; pp 1-41.

4. Liu, Q.; Wu, L.; Jackstell, R.; Beller, M., *Nat. Commun.* **2015,** *6*, 5933.

5. Song, Q.-W.; Zhou, Z.-H.; He, L.-N., *Green Chem.* **2017,** *19* (16), 3707-3728.

6. Pescarmona, P. P.; Taherimehr, M., *Catal. Sci. Technol.* **2012,** *2* (11), 2169-2187.

7. Klaus, S.; Lehenmeier, M. W.; Anderson, C. E.; Rieger, B., *Coord. Chem. Rev.* **2011,** *255* (13), 1460-1479.

8. Lu, X. B.; Wang, Y., *Angew. Chem. Int. Ed.* **2004,** *43* (27), 3574-3577.

9. Shaikh, R. R.; Pornpraprom, S.; D'Elia, V., *ACS Catal.* **2018,** *8* (1), 419-450.

10. Xiao, Y. L.; Wang, Z.; Ding, K. L., *Macromolecules* **2006,** *39* (1), 128-137.

11. Kember, M. R.; White, A. J. P.; Williams, C. K., *Macromolecules* **2010,** *43* (5), 2291-2298.

12. Andrea, K. A.; Kerton, F. M., *ACS Catal.* **2019,** *9* (3), 1799-1809.

13. Kozak, C. M.; Ambrose, K.; Anderson, T. S., *Coord. Chem. Rev.* **2018,** *376*, 565-587.

14. Trott, G.; Saini, P. K.; Williams, C. K., *Philos. Trans. Royal Soc. A* **2016,** *374* (2061), 20150085.

15. Darensbourg, D. J., *Chem. Rev.* **2007,** *107* (6), 2388-2410.

16. Coates, G. W.; Moore, D. R., *Angew. Chem. Int. Ed.* **2004,** *43* (48), 6618-6639.

17. Plommer, H.; Reim, I.; Kerton, F. M., *Dalton Trans.* **2015,** *44* (27), 12098-12102.

18. Wang, Y.; Darensbourg, D. J., *Coord. Chem. Rev.* **2018,** *372*, 85-100.

19. Lehenmeier, M. W.; Bruckmeier, C.; Klaus, S.; Dengler, J. E.; Deglmann, P.; Ott, A.-K.; Rieger, B., *Chem. Eur. J.* **2011,** *17* (32), 8858-8869.

20. Fiorani, G.; Guo, W.; Kleij, A. W., *Green Chem.* **2015,** *17* (3), 1375-1389.

21. Buchard, A.; Kember, M. R.; Sandeman, K. G.; Williams, C. K., *Chem. Commun.* **2011,** *47* (1), 212-214.

22. Nakano, K.; Kobayashi, K.; Ohkawara, T.; Imoto, H.; Nozaki, K., *J. Am. Chem. Soc.* **2013,** *135* (23), 8456-8459.

23. Taherimehr, M.; Al-Amsyar, S. M.; Whiteoak, C. J.; Kleij, A. W.; Pescarmona, P. P., *Green Chem.* **2013,** *15* (11), 3083-3090.

24. Taherimehr, M.; Serta, J.; Kleij, A. W.; Whiteoak, C. J.; Pescarmona, P. P., *ChemSusChem* **2015,** *8* (6), 1034-1042.

25. Alhashmialameer, D.; Collins, J.; Hattenhauer, K.; Kerton, F. M., *Catal. Sci. Technol.* **2016,** *6* (14), 5364-5373.

26. Della Monica, F.; Buonerba, A.; Capacchione, C., *Adv. Synth. Catal.* **2019,** *361* (2), 265-282.

27. Della Monica, F.; Buonerba, A.; Paradiso, V.; Milione, S.; Grassi, A.; Capacchione, C., *Adv. Synth. Catal.* **2019,** *361* (2), 283-288.

28. Della Monica, F.; Maity, B.; Pehl, T.; Buonerba, A.; De Nisi, A.; Monari, M.; Grassi, A.; Rieger, B.; Cavallo, L.; Capacchione, C., *ACS Catal.* **2018,** *8* (8), 6882-6893.

29. Kamphuis, A. J.; Milocco, F.; Koiter, L.; Pescarmona, P.; Otten, E., *ChemSusChem* **2019,** (ja), DOI: 10.1002/cssc.201900740.

30. Chen, F.; Liu, N.; Dai, B., *ACS Sustain. Chem. Eng.* **2017,** *5* (10), 9065-9075.

31. Della Monica, F.; Vummaleti, S. V. C.; Buonerba, A.; Nisi, A. D.; Monari, M.; Milione, S.; Grassi, A.; Cavallo, L.; Capacchione, C., *Adv. Synth. Catal.* **2016,** *358* (20), 3231-3243.

32. Andrea, K. A.; Brown, T. R.; Murphy, J. N.; Jagota, D.; McKearney, D.; Kozak, C. M.; Kerton, F. M., *Inorg. Chem.* **2018,** *57* (21), 13494-13504.

33. Segal, S.; Goldberg, I.; Kol, M., *Organometallics* **2005,** *24* (2), 200-202.

34. Tshuva, E. Y.; Goldberg, I.; Kol, M.; Goldschmidt, Z., *Chem. Commun.* **2001**, 2120-2121.

35. Groysman, S.; Tshuva, E. Y.; Goldberg, I.; Kol, M.; Goldschmidt, Z.; Shuster, M., *Organometallics* **2004,** *23* (22), 5291-5299.

36. Kerton, F. M.; Whitwood, A. C.; Willans, C. E., *Dalton Trans.* **2004,** 2237-2244.

37. Clark, L.; Cushion, M. G.; Dyer, H. E.; Schwarz, A. D.; Duchateau, R.; Mountford, P., *Chem. Commun.* **2010,** *46* (2), 273-275.

38. Liu, B.; Roisnel, T.; Guégan, J.-P.; Carpentier, J.-F.; Sarazin, Y., *Chem. Eur. J.* **2012,** *18* (20), 6289-6301.

39. Dyer, H. E.; Huijser, S.; Susperregui, N.; Bonnet, F.; Schwarz, A. D.; Duchateau, R.; Maron, L.; Mountford, P., *Organometallics* **2010,** *29* (16), 3602-3621.

40. Ajellal, N.; Carpentier, J.-F.; Guillaume, C.; Guillaume, S. M.; Helou, M.; Poirier, V.; Sarazin, Y.; Trifonov, A., *Dalton Trans.* **2010,** *39* (36), 8363-8376.

41. Reckling, A. M.; Martin, D.; Dawe, L. N.; Decken, A.; Kozak, C. M., *J. Organomet. Chem.* **2011,** *696*, 787-794.

42. Toupance, T.; Dubberley, S. R.; Rees, N. H.; Tyrrell, B. R.; Mountford, P., *Organometallics* **2002,** *21*, 1367-1382.

43. Shimazaki, Y.; Huth, S.; Odani, A.; Yamauchi, O., *Angew. Chem. Int. Ed.* **2000,** *39* (9), 1666-1669.

44. Devaine-Pressing, K.; Lehr, J. H.; Pratt, M. E.; Dawe, L. N.; Sarjeant, A. A.; Kozak, C. M., *Dalton Trans.* **2015,** *44* (27), 12365-12375.

45. Groysman, S.; Goldberg, I.; Kol, M.; Genizi, E.; Goldschmidt, Z., *Organometallics* **2004,** *23* (8), 1880-1890.

46. Devaine-Pressing, K.; Dawe, L. N.; Kozak, C. M., *Polym. Chem.* **2015,** *6*, 6305-6315.

47. Tshuva, E. Y.; Goldberg, I.; Kol, M.; Goldschmidt, Z., *Organometallics* **2001,** *20* (14), 3017-3028.

48. Groysman, S.; Goldberg, I.; Kol, M.; Genizi, E.; Goldschmidt, Z., *Inorg. Chim. Acta* **2003,** *345*, 137-144.

49. Mialane, P.; Anxolabéhère-Mallart, E.; Blondin, G.; Nivorojkine, A.; Guilhem, J.; Tchertanova, L.; Cesario, M.; Ravi, N.; Bominaar, E.; Girerd, J.-J.; Münck, E., *Inorg. Chim. Acta* **1997,** *263* (1), 367-378.

50. Tang, L.-Z.; Lin, C.-N.; Zhan, S.-Z., *Polyhedron* **2016,** *110*, 247-253.

51. Velusamy, M.; Palaniandavar, M.; Gopalan, R. S.; Kulkarni, G. U., *Inorg. Chem.* **2003,** *42*, 8283-8293.

52. Dean, R. K.; Fowler, C. I.; Hasan, K.; Kerman, K.; Kwong, P.; Trudel, S.; Leznoff, D. B.; Kraatz, H. B.; Dawe, L. N.; Kozak, C. M., *Dalton Trans.* **2012,** *41* (16), 4806-4816.

53. Hasan, K.; Fowler, C.; Kwong, P.; Crane, A. K.; Collins, J. L.; Kozak, C. M., *Dalton Trans.* **2008**, 2991-2998.

54. Janiak, C., *Dalton Trans.* **2000,** (21), 3885-3896.

55. Addison, A. W.; Rao, T. N.; Reedijk, J.; van Rijn, J.; Verschoor, G. C., *J. Chem. Soc., Dalton Trans.* **1984**, 1349.

56. Wang, Z.-Q.; Tang, L.-Z.; Zhang, Y.-X.; Zhan, S.-Z.; Ye, J.-S., *Transit. Met. Chem.* **2015,** *40* (5), 525-529.

57. Darensbourg, D. J.; Ortiz, C. G.; Billodeaux, D. R., *Inorg. Chim. Acta* **2004,** *357*, 2143-2149.

58. Whiteoak, C. J.; Torres Martin de Rosales, R.; White, A. J. P.; Britovsek, G. J. P., *Inorg. Chem.* **2010,** *49* (23), 11106-11117.

59. Gu, X.; Zhang, Y.; Xu, Z.-J.; Che, C.-M., *Chem. Commun.* **2014,** *50* (58), 7870-7873.

60. Groysman, S.; Goldberg, I.; Kol, M.; Genizi, E.; Goldschmidt, Z., *Organometallics* **2004,** *23* (8), 1880-1890.

61. Mialane, P.; Anxolabéhère-Mallart, E.; Blondin, G.; Nivorojkine, A.; Guilhem, J.; Tchertanova, L.; Cesario, M.; Ravi, N.; Bominaar, E.; Girerd, J.-J.; Münck, E., *Inorg. Chim. Acta* **1997,** *263* (1), 367-378.

62. Lehenmeier, M. W.; Kissling, S.; Altenbuchner, P. T.; Bruckmeier, C.; Deglmann, P.; Brym, A. K.; Rieger, B., *Angew. Chem. Int. Ed.* **2013,** *52* (37), 9821-9826.

63. Darensbourg, D. J.; Yarbrough, J. C.; Ortiz, C.; Fang, C. C., *J. Am. Chem. Soc.* **2003,** *125* (25), 7586-7591.

64. Liu, J.; Ren, W. M.; Liu, Y.; Lu, X. B., *Macromolecules* **2013,** *46* (4), 1343-1349.

65. Ni, K.; Kozak, C. M., *Inorg. Chem.* **2018,** *57* (6), 3097-3106.

66. Dolomanov, O. V. B., L. J., Gildea, R. J., Howard, J. A. K., Puschmann, H., *J. Appl. Cryst.* **2009,** *42*, 339-341.

67. Sheldrick, G. M., *Acta. Cryst. C71* **2015**, 3-8.

Co-authorship Statement

Chapter 4 : Triarylborane Catalyzed Formation of Cyclic Organic Carbonates and Polycarbonates

This chapter has been peer reviewed and published in:

ACS Catalysis, **2019**, 9 (3), 1799-1809

Authors: Kori A. Andrea[a] and Francesca M. Kerton[a]*

[a] Department of Chemistry, Memorial University of Newfoundland, St. John's, NL, A1B 3X7, Canada

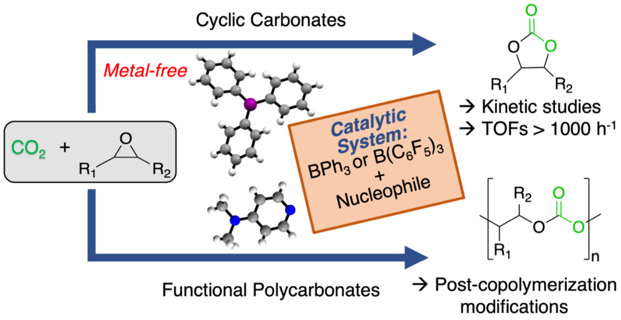

The first author (K. A. Andrea) contributed to 100% of the article, including manuscript writing, performing experiments and data analysis. The corresponding author, F. M. Kerton, directed the project, assisting in experimental design and manuscript writing.

Chapter 4: Triarylborane Catalyzed Formation of Cyclic Organic Carbonates and Polycarbonates

See Appendix C for additional data

4.1 Introduction

Use of carbon dioxide (CO_2) as a renewable feedstock is highly desirable but still poses a significant challenge for chemists.[1-5] Due to the thermodynamic stability of CO_2, its transformations are challenging, but ways to achieve this include combining it with reactive substrates such as epoxides or hydrogen. The former yields either cyclic carbonates or polycarbonates depending on the substrate, reaction conditions and catalyst used. Inroads have been made using other substrates, such as butadiene,[6-7] to yield CO_2-containing polymers but reactions with epoxides remain the cornerstone of research in this area.

In the past 50 years, since the discovery of Zn-based catalysts for copolymerization of epoxides with CO_2 in the 1960s, an in-depth understanding of how such catalysts work on a molecular level and design of more active species has been achieved. It was discovered that for zinc β-diiminate catalysts, the key active species were loosely bound zinc dimers that were significantly more reactive than monometallic analogs for the copolymerization of CO_2 and cyclohexene oxide (CHO).[8] This led to the development of di-zinc catalysts based on macrocyclic ligands, which were active at one atmosphere of CO_2 and could achieve exceptionally high turnover frequencies in the copolymerization reactions.[9-11] Similarly, for the production of cyclic carbonates, outstanding Al-catalysts have been developed,[12] including aluminum salen,[13-16] and triphenolate complexes.[17-18] Reactions that can be performed under near-ambient conditions, especially low pressures, are particularly important in terms of advances towards sustainability in this field.[19-20]

In the past decade, the use of metal-free catalysis in this area has grown.[19, 21] However, our mechanistic understanding of such systems is still in its infancy compared with the more mature field of metal-mediated reactions of CO_2 and epoxides. There have been two recent reports on using a trialkyl borane, triethyl borane, as a catalyst for copolymerizing propylene oxide with CO_2 or carbonyl sulfide (COS) (**Scheme 4.1**).[22-23] The catalyst systems comprised of the triethyl borane and a Lewis base including amidine, guanidine, metal alkoxides, ammonium and phosphonium halides. We thought that trialkyl boranes are less readily modified than triaryl boranes to tailor reactivity and so we decided to investigate the use of arylboranes in these reactions with commercially available triphenyl borane (BPh_3) and tris(perfluorophenyl) borane (BCF) as our initial catalysts. It is well understood that the reactivity of such boron compounds is strongly dependent on their Lewis acidity, which can be varied by modifying the aromatic backbone (i.e. addition of fluorine groups). Their Lewis acidity can then be measured using NMR methods such as Gutmann-Beckett and is described by an acceptor number. For example, BPh_3 has an acceptor number of 55 while the more Lewis acidic BCF is 76.[24]

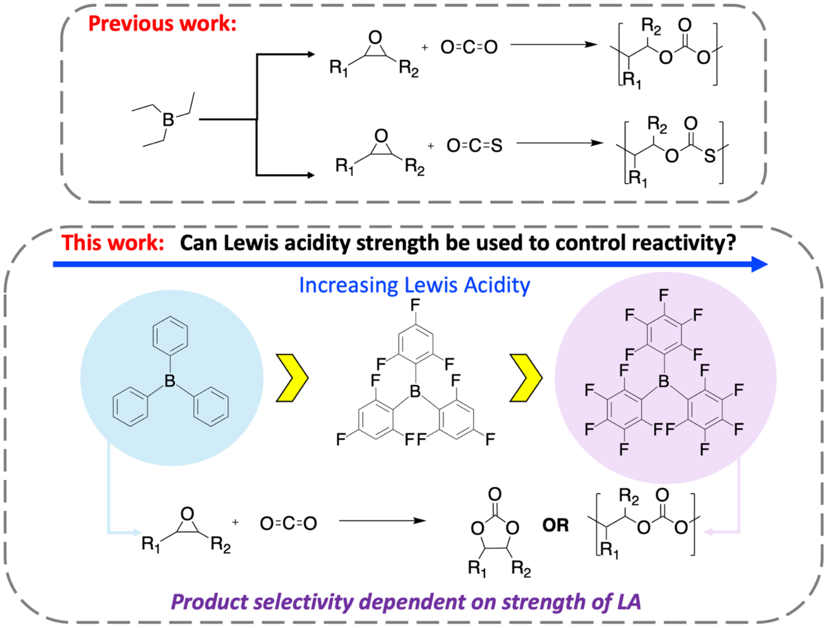

Scheme 4.1. Comparison of borane systems for reactions of epoxides with carbon dioxide [22] or carbonyl sulfide.[23]

Frustrated Lewis Pair (FLP) catalysts have made an impact in catalytic transformations of CO_2,[25-27] and a range of other substrates.[28-32] These are typically based on a range of combinations of Lewis acids, including boranes, and Lewis bases, including phosphines and amines, which are prevented from forming an adduct through incorporation of tethers or steric congestion. Boron-centered Lewis acids, especially BPh_3 and BCF, have been used to catalyze a wide range of reactions including diyne cyclizations, carboborations and hydroborations.[33] These recent examples show the versatility of arylboranes in a range of transformations.

As we have discovered and report herein, arylboranes (BPh_3 and BCF) can catalyze the reaction of epoxides and CO_2 to yield either cyclic carbonate or polycarbonate products depending on the substrate used. Low catalyst loadings (as low as 0.025% boron) can be used and some preliminary studies show that the reactions can be performed under 1 atm CO_2 pressure. One-pot bicatalytic reactions can be performed to yield functional and cross-linked polycarbonates using Grubbs 2nd generation olefin metathesis catalyst alongside BPh_3.

4.2 Catalytic screening of Lewis acidic boranes for cyclic and polycarbonate formation

At the outset, we investigated the activity of BPh_3 and BCF as catalysts for the reaction of propylene oxide (PO) and CO_2 in the absence of solvent. Both were active catalysts but BPh_3 outperformed BCF slightly under identical conditions **(Table 4.1**, entries 2 and 19), while the use of PPNCl alone led to low conversions (**Table 4.1**, entry 1). In terms of co-catalyst, the anionic nucleophile Cl^- (from bis(triphenylphosphine)iminium chloride, PPNCl) afforded significantly higher conversions compared with the neutral nucleophile 4-dimethylaminopyridine (DMAP) under identical conditions (**Table 4.1**, entries 2 and 3). From in situ reaction monitoring by IR spectroscopy, we observed selective formation of propylene carbonate ($\nu_{c=o}$ 1809 cm^{-1}) using either borane in the presence of an anionic co-catalyst under relatively mild conditions. This contrasts with previous work using triethyl borane as the catalyst, which produced poly(propylene carbonate).[22] We were excited to discover that even under our unoptimized reaction conditions, turnover number (TON) and turnover frequency (TOF) values were comparable with those reported for triethylborane in polymerization studies.[22-23]

Since this is the first observation of an arylborane serving as a catalyst in this type of reaction we decided to study it in more detail, specifically the reaction kinetics for the BPh_3 catalyzed transformation of PO to propylene carbonate. IR spectroscopy showed no cyclic or polymer product formation in the temperature range of 25-60 °C. Near the beginning of reactions, high concentrations of PO are present and therefore, an initial rates approach can be employed to ascertain the reaction rate law (See Appendx C). Data points were generally used from the first 3 min of the reaction. Furthermore, we noted that signal saturation occurs within the first few hours of reaction, therefore spectra were only collected during the first 3 h.

By varying the catalyst loading from 0.025 mol% to 0.1 mol% we observed a first order rate in boron concentration (**Figure 4.1A**). It is worth noting that when BCF was used as the catalyst under identical conditions the reaction rate was significantly lower (**Figure C4**). This is likely due to the more Lewis acidic nature of BCF,[33] which means that it forms a more stable adduct with the Cl^- anions of PPNCl at lower temperatures. It is understood in FLP-CO_2 chemistry that insertion of CO_2 into the Lewis acid/base adduct, results in an increased stabilization of the transition state, which has been well studied both experimentally and computationally by Erker and Stephan.[34] This has also been proposed to occur in BPh_3 catalyzed hydrosilylation of CO_2,[35] and the formation of $[PPN]^+[ClBPh_3]^-$ has been reported previously.[36] In the case of the neutral co-catalyst DMAP, we were able to isolate and characterize the Lewis pair BPh_3-DMAP (**Figure C14**). As shown below, one of the key steps in the proposed catalytic cycle (**Figure 4.1 D**) is coordination of the Lewis basic epoxide to the borane, which activates it towards ring-opening. This is inhibited if the borane is coordinated to another Lewis base.

Table 4.1. Catalytic data for arylborane catalyzed reactions of CO_2 with epoxides.

Cyclic Carbonates

Entry[a]	Cat.	[Epoxide]:[Cocat]:[B]	P_{CO_2} (bar)	Time (h)	Conv. (%)[b]	TON[c]	TOF[d] (h^{-1})
1	-	4000:4:0	20	22	23	920	42
2	BPh_3	4000:4:1	20	22	74	2960	135
3[e]	BPh_3	4000:4:1	20	22	34	1360	62
4	BPh_3	4000:4:1	20	3	33	1320	440
5	BPh_3	4000:4:2	20	3	48	960	320
6	BPh_3	4000:4:4	20	3	92	920	307
7[f]	BPh_3	4000:1:1	20	3	15	600	200
8[f]	BPh_3	4000:2:1	20	3	27	1080	360
9[f]	BPh_3	4000:3:1	20	3	30	1200	400
10[f]	BPh_3	4000:4:1	20	3	33	1320	440
11[f]	BPh_3	4000:8:1	20	3	41	1640	547
12[f]	BPh_3	4000:4:1	40	3	33	1320	440
13[f]	BPh_3	4000:4:1	20	3	33	1320	440
14[f]	BPh_3	4000:4:1	10	3	40	1600	533
15[f]	BPh_3	4000:4:1	5	3	60	2400	800
16[g]	BPh_3	4000:4:1	1	24	31	1240	52
17[h]	BPh_3	4000:4:1	20	3	76	3040	1013
18[h]	BPh_3	4000:4:1	1	24	>99	3960	165
19	BCF	4000:4:1	20	22	68	2720	124

Polycarbonates

Entry[i]	Cat.	[Epoxide]:[Cocat]:[B]	Substrate	% Conv.[j] (% yield)	% CO_3 linkages[k]	M_n (g mol^{-1})[l]	Đ[l]
20	BPh_3	200:1:1	CHO	65 (58)	>99	7 200	1.07
21	BPh_3	500:1:1	CHO	30 (25)	>99	6 700	1.08
22[e]	BPh_3	200:1:1	CHO	65 (5)	>99	13 650	1.16
23	BPh_3	200:1:1	VCHO	52 (45)	>99	6 270	1.03
24	BCF	200:1:1	CHO	<1	-	-	-
25[m]	BPh_3	200:0.5:1	PO	<1	-	-	-
26[m]	BCF	200:0.5:1	PO	>99	<1	168 600	2.45

---

[a] General reaction conditions unless otherwise indicated: PO (57 mmol), PPNCl co-catalyst, 100 °C. [b] Determined by ^1H NMR spectroscopy using the normalized integrals of the methylene resonances. [c] Overall turnover number ($mol_{epoxide\ consumed} \times mol_{Cat}^{-1}$). [d] Overall turnover frequency (TON/reaction time) observed. [e] DMAP was used as the co-catalyst. [f] Reactions completed in 3 mL of dichloromethane in addition to epoxide.

[g] PO (14.3 mmol), BPh_3 (0.0034 mmol), PPNCl (0.014 mmol), 750 mL ampoule sealed under 1 atm CO_2, 100 °C. [h]Glycidyl chloride used as substrate. [i] Reaction conditions: Epoxide (2.5 g; 21 mmol), PPNCl or DMAP co-catalyst, 60 °C, 24 h, 40 bar CO_2. [j] Conversion determined using ^1H NMR spectroscopy by comparing the integral resonances at 4.65 ppm (PCHC) or 4.75-4.90 ppm (PVCHC) carbonate and resonances for residual epoxide. Yield determined using isolated mass after polymer precipitation, filtration and drying in vacuum oven. [k] % Carbonate= (copolymer carbonate linkages)/(copolymer carbonate + ether linkages). [l] Determined in THF by GPC equipped with a multi-angle light scattering detector. [m] Reactions performed at 25 °C.

We also studied the effect of PPNCl on reaction rate in a similar manner. However, due to the low solubility of PPNCl in PO, the reactions were performed in dichloromethane to ensure the correct ratios of co-catalyst. As has been shown by others, the presence of solvent generally slows reaction rates,[37-40] this can be seen by comparing a neat reaction (**Figure C1**) with a reaction in dichloromethane (**Figure C8**). However, a first order rate dependence in PPNCl concentration is demonstrated for lower concentrations of the co-catalyst (**Figure 4.1 B**) when the reaction is performed in dichloromethane. If the amount of PPNCl is greater than 4 equivalents relative to BPh_3, we observe no further increase in reaction rate and rates obtained for 4 and 8 equivalents of PPNCl were similar (**Figures C8-C9** and **Table C2**). We postulate that this plateau in observed rate was due to competitive binding of Cl^- anions versus epoxide to the empty p orbital of the borane. This is further supported by the ^{11}B NMR spectrum of the BPh_3/PPNCl adduct.

Lastly, we investigated the role of CO_2 pressure on the reaction rate. Remarkably, we observed that lower CO_2 pressures not only led to faster reaction rates, but higher overall conversions of substrate (**Table C3**). By varying CO_2 pressure, we observed an inverse relationship leading to an overall reaction order of −1 for CO_2 (**Figure 4.1 C**). The lower reaction rates at higher pressures of CO_2 suggest that high concentrations of CO_2 somehow decelerate the initial epoxide ring-opening of borane-activated PO. Transformations of CO_2 by Lewis acids, particularly boranes, is quite well-established chemistry, particularly in light of their role in reduction of CO_2 by FLPs.[41-42] During catalytic hydrosilylation reactions of CO_2 catalyzed by BPh_3 performed in propylene carbonate as the solvent, only ^{11}B NMR resonances for BPh_3 were observed and none for BPh_3-CO_2 nor BPh_3-propylene carbonate adducts.[35] Therefore, it is unlikely that we would observe product inhibition in our reactions and reaction profiles herein show no evidence for this.

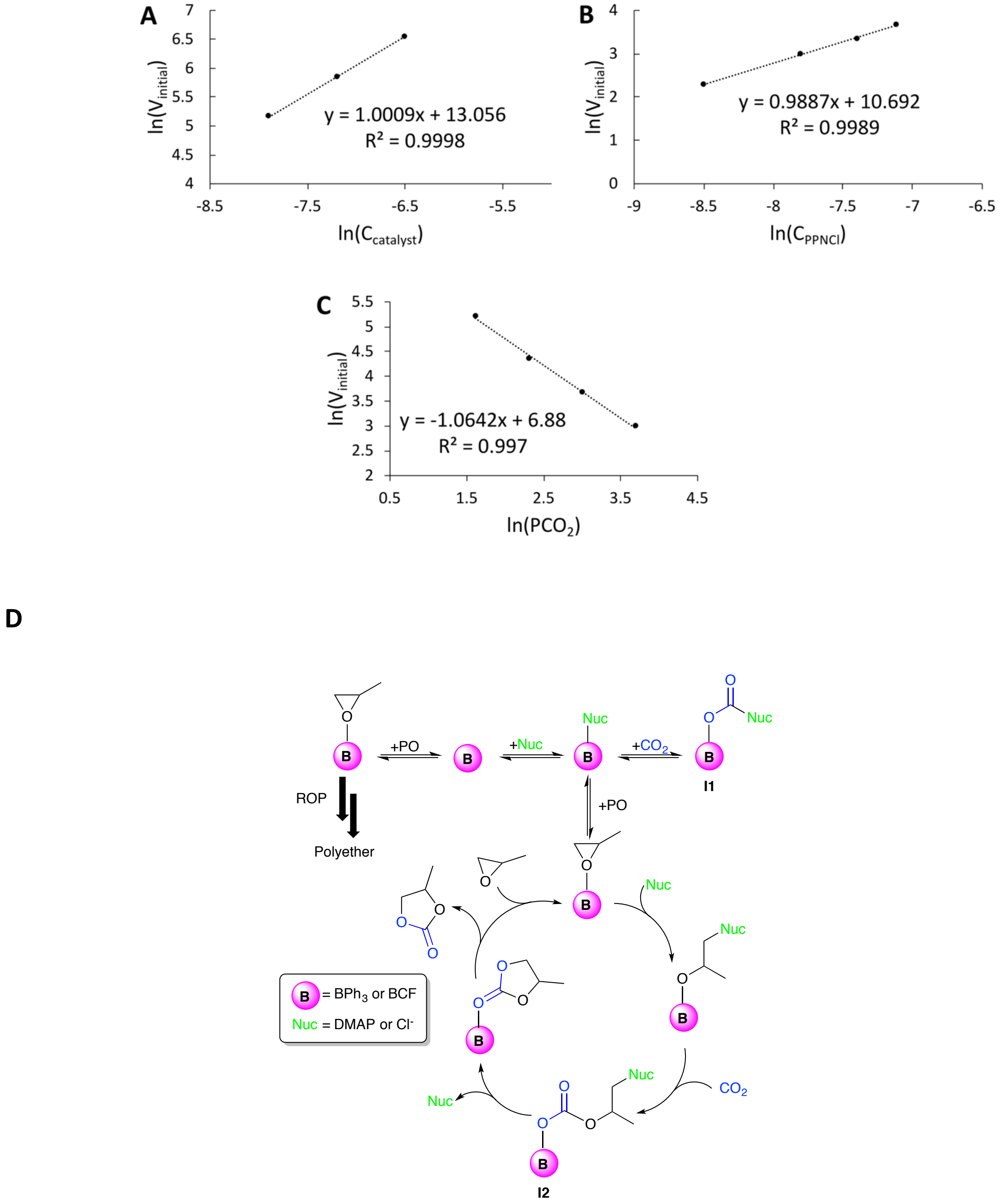

Figure 4.1. BPh_3 catalyzed propylene carbonate formation from PO and CO_2: Determination of reaction order with respect to: (A) catalyst, (B) co-catalyst (PPNCl), and (C) CO_2 pressure, via plots of initial rate ($v_{initial}$) and concentrations/pressure on a double logarithmic scale, where the slope is equal to reaction order of reagent. (D) Proposed catalytic pathway and reaction intermediates (I1, $\nu_{C=O}$ 1680 cm^{-1}, ^{11}B δ 9.3; I2, $\nu_{C=O}$ 1748 cm^{-1}).

Taking the results of these kinetic studies into account we can devise the following simple rate law, shown in Eq. (1).

$$rate = k[epoxide]^1[CO_2]^{-1}[BPh_3]^1[PPNCl]^1 \qquad \text{[Eq. (1)]}$$

The rate determining step in our proposed catalytic cycle is nucleophilic attack and ring-opening of the coordinated epoxide. The other steps within the cycle are fast, especially release of the product from the borane. Evidence of nucleophile-borane adducts is provided by ^{11}B NMR of mixtures (**Figure C14**), and the isolation of BPh_3-DMAP. For the more Lewis acidic borane, BCF, a larger proportion of adduct is evident from ^{11}B NMR data under the same conditions compared with BPh_3 (**Figure C15**) and this goes some way to explain the lower reaction rates when using this borane for carbonate synthesis and correlates with its greater Lewis acidity. We were also able to identify several other borane adducts and reaction intermediates (**Figure 4.1 D** and **Figure C16)**. In ^{11}B NMR spectra of a 1:1 mixture of PPNCl and BPh_3 exposed to 1 atm of CO_2, a new signal grew in, which we assign to the CO_2 insertion product, PPN[Ph_3B-CO_2-Cl], **I1**. This is an unproductive intermediate (i.e. does not appear within the catalytic cycle). However, we could use this reaction mixture directly in a coupling reaction with PO and CO_2 (conditions from **Table 4.1**, entry 2) and observed similar conversions, suggesting that formation of PPN[Ph_3B-CO_2-Cl] is reversible. Coordination and activation of epoxides is critical in these reactions and therefore, the formation of **I1**, which prevents coordination of the epoxide, leads to inhibition of the reaction and the inverse reaction rate order with respect to [CO_2]. Data from in situ IR spectroscopy experiments conducted at 40 bar CO_2 pressure provided valuable mechanistic insights and bands were assigned based on literature precedent.[43] From a reaction of 200:1:1 PO:PPNCl:BPh_3, in addition to the dominant band from the cyclic carbonate product $\nu_{C=O}$ 1809 cm^{-1}, a prominent band was observed at 1748 cm^{-1} assigned to **I2**, PPN[Ph_3B-CO_2-ring-opened PO-Cl] and a much less intense band at 1680 cm^{-1} was observed and assigned to **I1**, PPN[Ph_3B-CO_2-Cl]. For reactions of 200:1:1 CHO:DMAP:BPh_3, bands were observed at 1647 cm^{-1} and 1652 cm^{-1} assigned to $\nu_{C=C}$ of DMAP in various intermediates, and at 1675 cm^{-1} assigned to $\nu_{C=O}$ in **I2**, [Ph_3B-CO_2-ring-opened CHO-DMAP]. However, further experiments including computational studies would be needed to provide additional evidence to support this. Several catalysts have been described where related reactions are zero order in CO_2 for its coupling with epoxides i.e. independent of CO_2 pressure,[8-9, 11, 43-44-45] but these are typically for the formation of polycarbonate and not for the formation of the cyclic product. In examples where reaction order has been determined, it is normally first order in CO_2 pressure for cyclic carbonate formation.[13, 45-49] Therefore, an inverse order is extraordinary so we explored the reactivity of BPh_3 under atmospheric pressure CO_2 (1.00 atm = 1.01 bar). Due to the low boiling point of propylene oxide (b.p. = 34 °C) we switched substrate and performed a reaction under 1 atm CO_2 at 100 °C using glycidyl chloride (epichlorohydrin, b.p. = 118 °C) overnight and >99% conversion was achieved for this reaction (TON >3960, **Table 4.1**, entry 18).

Compared with organocatalysts, whose maximum TONs are typically ~100 and are normally used at catalyst loadings of 2-10 mol%,[19-21] the TONs achieved using BPh_3 are outstanding (**Table 4.1**). Maximum TOFs of 800 h^{-1} and 1013 h^{-1} were determined for PO and glycidyl chloride conversion respectively (**Table 4.1**, entries 15 and 17). Boronic acids, functioning through hydrogen-bonding rather than Lewis acidity, have been used at 10 mol% loadings achieving TON up 10 and TOF up to 3 h^{-1}.[50] To allow an easier comparison with organocatalyst systems reported to date that operate under ambient conditions, a selection of literature examples are presented in **Table 4.2**. We investigated our optimized conditions (**Table 4.1,** entry 2) at ambient temperature and pressure for comparison but saw no conversion of starting material utilizing propylene oxide and >5% conversion with glycidyl chloride. Therefore, although ambient pressures can be used with aryl borane catalysts, elevated temperatures are essential in order to achieve meaningful TOFs using our systems. When we increased our catalyst and co-catalyst loadings to values similar to those used for the organocatalysts presented in **Table 4.2**, we observed a mixture of both cyclic carbonate and polypropylene carbonate, demonstrating the loss of selectivity of our system at higher catalyst concentrations. For conversion of cis-2,3-epoxybutane, a yield of 53% was recently reported for a squareamide organocatalyst ,[51] which functions through hydrogen-bonding, at 80 °C using 30 bar CO_2. At lower pressures (1 atm, balloon of CO_2), a bifunctional pincer organocatalyst afforded a yield of 83% for this substrate.[53] However, we observed no conversion of this substrate under their conditions with our BPh_3/PPNCl system and this is not unusual for this challenging substrate. TOF of metal-free catalysts are typically much lower than the more established metal-containing ones that can often achieve TOFs >5000 h^{-1} per metal centre for the conversion of PO to propylene carbonate.[39] As the Lewis acidic borane catalysts function in a similar fashion to the metal coordination complexes i.e. the epoxides are activated via formation of a Lewis acid epoxide adduct, it is not surprising that BPh_3 can achieve TON and TOF values approaching a level similar to many of the established catalysts in this field and can be used at low catalyst concentrations (0.025 mol% catalyst loading).

Table 4.2. Selected examples of catalytic coupling of CO_2 and epoxides using organocatalysts in the scientific literature[a]

Catalyst	Substrate	Co-catalyst	Conditions	% Yield
2-pyridinemethanol, Hirose, 2016[52]	propylene oxide	*n*Bu_4NI	20 h, 8 mol% catalyst, 8 mol% co-cat	86
Ascorbic acid, D'Elia, 2017[53]	propylene oxide	TBAI	23 h, 4 mol% catalyst, 8 mol% co-cat	64
Phosphorous ylide, Lu, 2015[38]	propylene oxide	None	4 h, 5 mol% catalyst	71
Organic Pincer, Liu and Wei, 2018[53]	propylene oxide	None	24 h, 4 mol% catalyst	96
Phenol, D'Elia, 2018[54]	epichlorohydrin	TBAI	23 h, 2 mol% catalyst, 4 mol% co-cat	87[b]
Oragnic Pincer[c], Liu and Wei, 2018[53]	cis-2,3-epoxybutane	None	24 h, 4 mol% catalyst	83
Squareamide[d], Kleij, 2017[51]	cis-2,3-epoxybutane	TEAB	18 h, 3 mol% catalyst, 6 mol% co-cat	53

[a]Conditions and data as reported in original papers, 1 atm CO_2 (balloon), 25 °C. [b]Reported as % conversion rather than yield. [c]1 atm CO_2 (balloon), 80 °C. [d]30 bar CO_2, 80 °C.

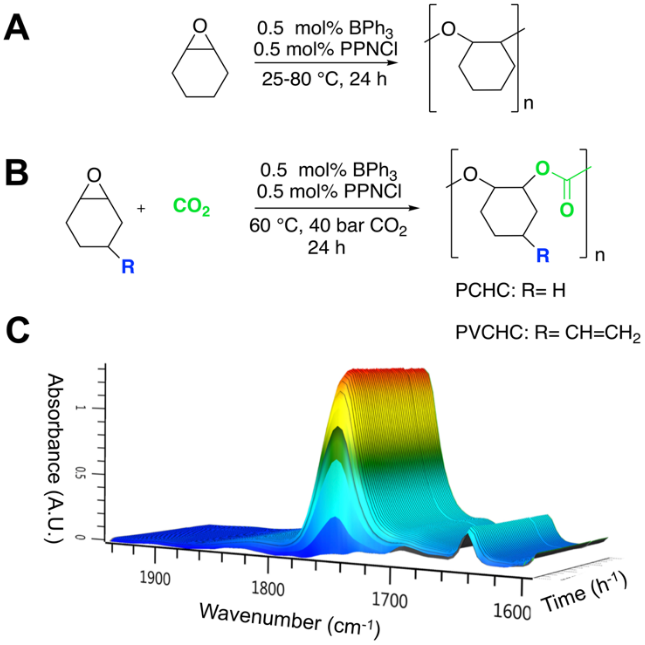

Figure 4.2. Polymerization and copolymerization of bicyclic epoxides catalyzed by BPh_3. (A) Formation of polyether using BPh_3. (B) Formation of polycarbonates using BPh_3. (C) IR absorbance vs. time graph showing growth of carbonate band in PVCHC at 1747 cm^{-1}.

We also investigated the ability of BPh_3 to catalyse the copolymerization of cyclohexene oxide (CHO) and CO_2 to yield polycarbonates (**Figure 4.2**). We obtained polycarbonate with a molecular weight of 7 200 g mol^{-1} and excellent dispersity (**Table 4.1**, entry 20). In the presence of BPh_3 and absence of CO_2, CHO was ring-opened to form homopolymer (**Figure 4.2** and **Table C4**). However, unusually the conversion of epoxide to homopolymer decreased as temperature increased and in the presence of CO_2, no ether linkages were observed in the resulting copolymer. When BCF was used as a catalyst under similar conditions no polymer was obtained, neither polyether nor polycarbonate (**Table 4.1**, entry 24). With the aim to further functionalize the copolymers obtained, we turned to the copolymerization of vinyl cyclohexene oxide (VCHO). We could obtain poly(vinyl-cyclohexenecarbonate) (PVCHC) in moderate yields with excellent dispersity and no evidence of ether linkages (**Table 4.1**, entry 23). This epoxide is less-readily ring-opened and therefore, this led to strictly alternating copolymerization and we saw no evidence for ether linkages in the PVCHC copolymer. As the only previous reports of borane catalysts (i.e. triethyl borane) had a strong focus on the copolymerization of PO and CO_2, we sought to investigate our systems for its reactivity towards the formation of polypropylene carbonate (PPC) for comparison. To allow a direct comparison, we used identical reaction conditions to those reported by Zhang et al.[22] We observed only a 3% conversion to propylene carbonate with no formation of PPC. However, during reaction preparation, we observed that when the BPh_3/PPNCl binary catalyst system was combined with THF, ring-opening of THF occurred leading to the formation of polytetrahydrofuran (**Figure C17**). This is not surprising, as there is precedent for ring-opening polymerization of THF using borane catalysts.[57] However, in the presence of PO and CO_2 this was not observed. In a further attempt to optimize reaction conditions towards the formation of PPC, we investigated the copolymerization at 25 °C, as we had previously noticed at higher temperatures (i.e. 60 °C) the cyclic carbonate was the dominant product. As can be seen in **Table 4.1**, entries 24 and 25, neither BPh_3 nor BCF lead to the formation of PPC at these conditions; however, BCF was active towards catalyzing the ring-opening of PO leading to the formation of polypropylene oxide with high molecular weights. These results strongly suggest that a careful pairing of both the Lewis acidity of the borane along with the nature of the epoxide substrate is crucial in controlling reactivity. Thus, further supporting the potential advantage of using aryl over alkyl boranes, as aryl boranes provide the opportunity to add further functionality and the ability to modify electronic properties of the central boron atom.[58]

4.3 Modification of obtained co-polymers using Grubbs Generation II catalyst

The vinyl groups of PVCHC provide several potential routes to modification of the polymer, which allows the potential to add further functionality leading to polycarbonates with various different physical and chemical properties. Others have performed catalytic transformations, in particular olefin metathesis,[59-60] on the isolated vinyl-substituted polycarbonate i.e. post-polymerization modification.[59-61] We have also been able to produce modified polymers in this way using Grubbs' 2nd generation catalyst and could produce either cross-linked or amine functionalized polycarbonates (**Figure 4.3**). We note that the molecular weight of the dimethylaminoethyl methacrylate (DMAEMA) modified copolymer correlated with 100% cross-metathesis of the vinyl groups, and this was also confirmed via elemental analysis where the nitrogen level had increased to 4.24%. Recently, a one-pot sequential catalytic-radical process has been developed to yield self-healing polycarbonate materials.[62] This built upon prior two-pot work using radical or photo-initiated thiol-ene crosslinking reactions.[63-64] As Grubbs' 2nd generation catalyst is known to be robust and able to maintain activity under a range of conditions,[55-58] we decided to attempt a one-pot sequential bicatalytic reaction. Copolymerization of CO_2 and VCHO was catalyzed by BPh_3/PPNCl, followed by depressurization and addition of Grubbs' 2nd generation catalyst in toluene. This led to the formation of a high molecular weight cross-linked polycarbonate with a bimodal weight distribution but as unreacted VCHO was also present in the mixture, the product would contain both intermolecularly cross-linked polymer and cross-metathesis products. When cross-metathesis was performed on the isolated polymer in a more dilute solution, intramolecular crosslinking occurred as indicated by the similar molecular weight of the product polymer (M_n 7,710 g mol^{-1}) and the starting PVCHC (M_n 7,200 g mol^{-1}). The results reported herein provides proof of principle that copolymerization/olefin metathesis can be performed in a one-pot manner using BPh_3/PPNCl for the initial polymerization step. Through the use of olefin metathesis in a one-pot or two-pot process, the T_g of the polymers could be increased from 99 °C up to 184 °C (**Figure 4.3 A**), which shows there is potential to tune the polymer properties in this way.

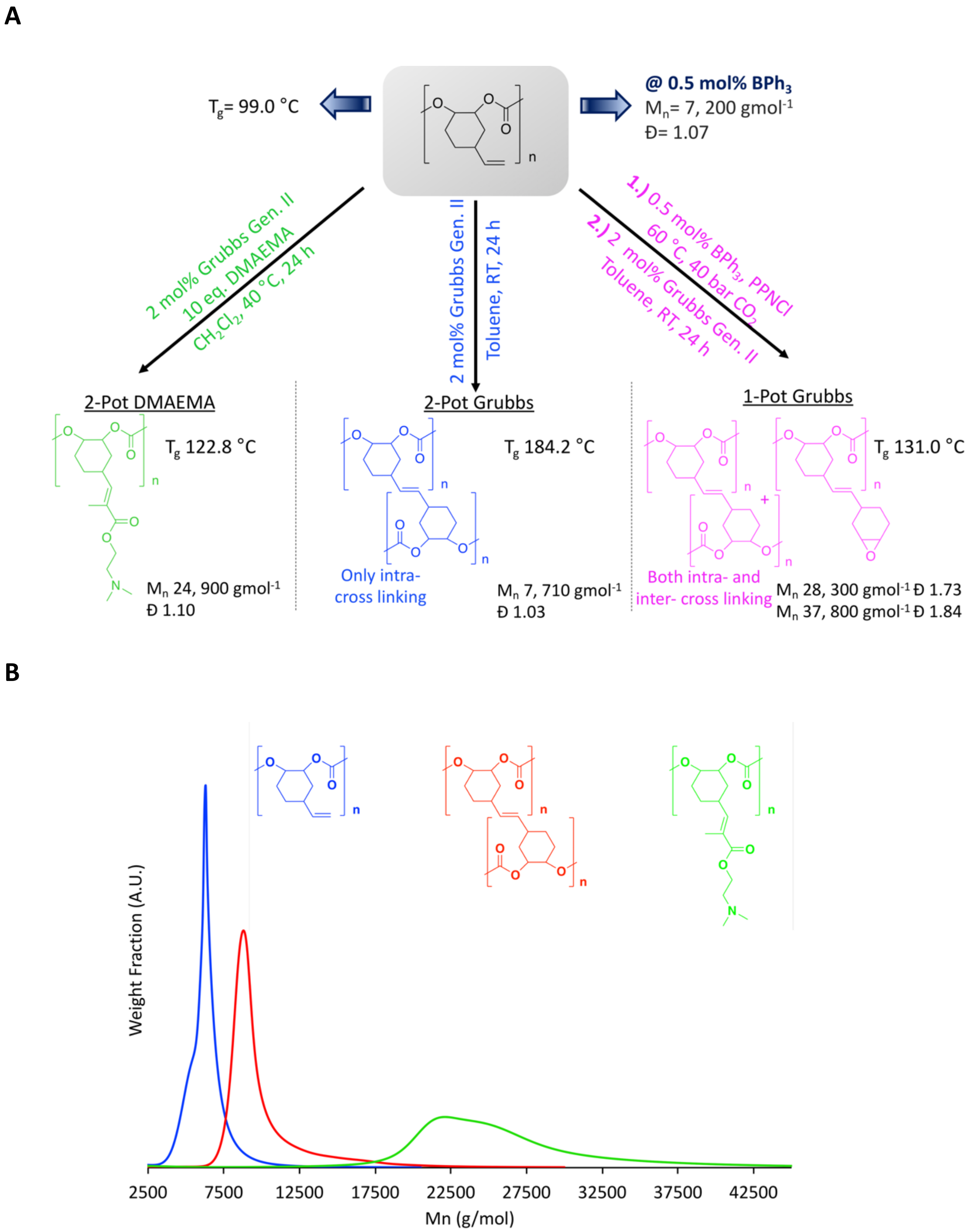

Figure 4.3. One- and two-pot catalytic modification of PVCHC. (A) Functionalization of polycarbonates via cross-metathesis with dimethyaminoethylmethacrylate (DMAEMA), and intra- and intermolecular crosslinking using Grubbs' second generation catalyst. (B) Molecular weight distributions for functionalized polycarbonates.

4.4 Conclusions

In summary, we demonstrate herein that arylboranes can catalyze both the formation of cyclic carbonates and polycarbonates from epoxides and CO_2. Their catalytic activity is superior in terms of catalyst loading compared to most metal-free systems to date but moderate temperatures are needed to achieve high TOF and this means such systems have more in common with established metal-containing catalysts. These data suggests that new metal-free synthetic approaches to CO_2-incorporation including more complex products via substrate controlled mechanistic divergence previously demonstrated by Al-centered catalysts[67] should be accessible using a borane-containing catalyst system. ^{11}B NMR studies provide evidence for insertion of CO_2 into the nucleophile-borane bond, in a similar way to FLP catalyst systems, and the CO_2 insertion product can be used directly as a catalyst for these reactions. Our systems were found to be inactive under the conditions explored using triethyl borane,[22,23] which strongly suggests the importance of both the Lewis acidity of the borane and the nature of the starting epoxide in both selectivity and reactivity. Methods for preparing a wide range of aryl boranes with different electronic, steric and stereochemical properties are known, and we look forward to using these compounds in future catalytic reactions and bridging the gap in reactivity between non-metal and metal-catalyzed processes. In addition there are several systems capable of utilizing waste CO_2 (e.g. flue gas), which is an aspect we wish to explore in the near future.[20]

4.5 Experimental

4.5.1 General experimental conditions

Unless otherwise stated, all experimental procedures were performed using an MBraun Labmaster glove box or under dry oxygen-free nitrogen using Schlenk techniques. Propylene oxide (PO), bis(triphenyphosphine)iminium chloride (PPNCl) and 4-dimethylaminopyridine (DMAP) was purchased from Alfa Aesar, cyclohexene oxide, vinyl cyclohexene oxide and Grubbs' Generation II catalyst were purchased from Sigma Aldrich. The epoxides were distilled from CaH_2 under N_2. All solvents were dried and degassed using an MBraun Manual Solvent Purification system. Triphenylborane (BPh_3) and tris(perfluorophenyl)borane (BCF) were purchased from Strem Chemicals and used without further purification.

4.5.2 Instrumentation

^{1}H and $^{13}C\{^{1}H\}$, ^{11}B, ^{29}Si NMR spectra were recorded on a Bruker Avance III 300 MHz spectrometer at 25 °C (frequencies were ^{13}C, 75.43 MHz; ^{11}B, 96.25 MHz; ^{29}Si, 59.60 MHz). All NMR spectra were obtained in $CDCl_3$ purchased from Cambridge Isotope Laboratories, Inc. ^{1}H and ^{13}C NMR spectra were referenced using the residual proton and ^{13}C resonances of the solvent. ^{29}Si was referenced to external tetramethylsilane (TMS, $\delta = 0$ ppm). Boron trifluoride diethyl etherate ($BF_3.OEt_2$, $\delta = 0$ ppm) was used as the external reference for ^{11}B NMR spectroscopy and all ^{11}B NMR experiments were performed in quartz NMR tubes to eliminate interference from the boron in glass. All cyclization and copolymerization reactions were carried out in a 100 mL stainless steel reactor vessel (Parr Instrument Company) equipped with a silicon sensor (SiComp), mechanical stirrer and a heating mantel. For kinetic measurements, the Si sensor was connected to a ReactIR 15 base unit (Mettler-Toledo) through a DS silver-halide Fiber-to-Sentinel conduit. The vessel was baked at 100 °C under vacuum overnight prior to any experiment. Gel permeation chromatography (GPC) analysis was performed on a set-up consisting of a miniDawn TREOS light scattering detector, a Viscostar-II viscometer, and an Optilab T-rEX differential refractive index detector (Wyatt Technology) connected to an Agilent Infinity 1260 HPLC system equipped with two Phenogel 10^3 Å 300 × 4.60 mm columns with THF as eluent. Samples were prepared in THF at a concentration of 4 mg mL^{-1}, filtered through a 0.2 μm syringe filter, and analyzed at a flow rate of 0.3 mL min^{-1} at 25 °C. The values of dn/dc were calculated online (columns detached) assuming 100% mass recovery using the Astra 6 software package (Wyatt Technologies) giving dn/dc of poly(cyclohexene carbonate) = 0.0701 $mL\cdot g^{-1}$, poly(cyclohexene oxide) = 0.1058 $mL\cdot g^{-1}$, poly(vinylcyclohexene carbonate), PVCHC = 0.0698 $mL\cdot g^{-1}$, silylated PVCHC = 0.0856 $mL\cdot g^{-1}$, intra-molecularly cross-linked PVCHC = 0.0830 $mL\cdot g^{-1}$, DMAEMA functionalized PVCHC = 0.0251 $mL\cdot g^{-1}$ and for the bimodal inter-molecularly cross-linked PVCHC (prepared in one-pot fashion) = 0.0934 $mL\cdot g^{-1}$ and 0.0870 $mL\cdot g^{-1}$. Glass transition temperatures (T_g) were obtained on a Mettler Toledo DSC Star^e system equipped with a Julabo FT 100 immersion cooling system for low temperatures (-100 °C +20 °C). Samples were weighed into 40 μL aluminum pans and exposed to 3 heating cycles from 0 to 200 °C at a rate of 10 °C min^{-1}, with a hold time of 2 min at both 0 °C and 200 °C in each cycle. The reported T_g values were determined using data from the third heating cycle. A MALDI-TOF mass spectrum of BPh_3-DMAP (anthracene matrix, high resolution, positive mode) was obtained using a Waters SYNAPT G2-Si HDMS system by technical personnel at Waters Corporation, Beverly, MA. Elemental analytical data were obtained by Guelph Chemical Laboratories, Canada.

4.5.3 Kinetic monitoring of propylene carbonate formation by in situ React IR spectroscopy.

Aliquots of BPh_3 (24.4 mg mL^{-1}) and PPNCl stock solutions in toluene were combined and the solvent was removed under vacuum. The solids were dissolved in 3 mL of dichloromethane and the solution was injected into the pressure vessel via syringe. An appropriate amount of PO was then injected into the vessel, which was pressurized with CO_2, heated to the desired temperature and mechanically stirred. Profiles of the absorbance at 1809 cm^{-1} were measured every 5 s (254 scans per spectrum) for 3 h. Similar methods for in situ reaction monitoring by FTIR spectroscopy have been reported by others, demonstrating the linear response of absorbance vs. concentration.[11, 59-61]

4.5.4 Formation of glycidyl carbonate from glycidyl chloride using 1 atm CO_2.

In a glovebox BPh_3 (1.95 mg, 0.008 mmol) and PPNCl (18.6 mg, 0.032 mmol) were combined in a 250 mL round bottom flask in dichloromethane (3 mL). Solvent was removed under vacuum leaving a white residue. The flask was removed from the glovebox, backfilled with CO_2 (× 3) and dry glycidyl chloride (3.00 g, 32.4 mmol) was added. CO_2 was bubbled through the glycidyl chloride for 5 min to ensure saturation of the epoxide with CO_2. The flask was then attached to a condenser, connected to a gas inlet under constant atmospheric flow of CO_2. The mixture was heated to 100 °C with stirring for 24 h, cooled and the mixture analyzed by ^1H NMR spectroscopy.

4.5.5 NMR experiments on the formation of Lewis Acid/Base Adducts.

In a glove box, triphenylborane (BPh_3) or tris(perfluorophenyl)borane (BCF) were combined in a 1:1 molar ratio with PPNCl in $CDCl_3$, and transferred to a quartz NMR tube. ^{11}B NMR spectra shown below.

Characterization of isolated BPh_3-DMAP Adduct. ^1H NMR (300 MHz, 298 K, $CDCl_3$-d_1) δ 8.18 (2H, d, ArH), 7.98 (6H, d, ArH), 7.45 (2H, d, ArH), 7.19 (9H, multiplet, ArH), 2.34 (6H, s, N-CH_3). $^{13}C\{^1H\}$ NMR (75 MHz, $CDCl_3$-d_1, 298 K) δ 154.98 (ArCH), 146.95 (ArCH), 134.86 (ArCH), 129.11 (ArCH) 126.85 (ArCH), 124.73 (ArCH), 105.88 (N=CH), 39.43 (N-CH_3). ^{11}B NMR (96 MHz, $CDCl_3$-d_1, 298 K) 2.45 ppm. MALDI-TOF MS, $[C_{25}H_{25}BN_2]^{+\bullet}$ *m/z* 364.2117 experimental, 364.2115 theoretical.

4.5.6 Polycyclohexene/vinylcyclohexene carbonate formation catalysed by triphenylborane.

Stock solutions of BPh_3 (24.4 mg mL^{-1}) and PPNCl in toluene were combined and solvent was removed under vacuum. The solids were dissolved in 3 mL of dichloromethane and the solution was injected into the pressure vessel. The dichloromethane removed under vacuum, before the desired amount of the cyclohexene oxide monomer was injected into the pressure vessel. The vessel was pressurized with CO_2, heated to the desired temperature and mechanically stirred for 24 h. The vessel was cooled and the CO_2 slowly vented into a fume hood. The crude product was dissolved in minimal dichloromethane and precipitated in cold acidified methanol.

4.5.7 Intramolecular cross-linking of polyvinylcyclohexene carbonate

Purified PVCHC (0.25 g, 1.26 mmol vinyl units) was dissolved in 250 mL of toluene. To this solution was added a solution of Grubbs' Generation II catalyst (11.0 mg, 13.0×10^{-3} mmol) in 5 mL of toluene. The reaction was stirred at room temperature under dynamic vacuum for 24 h. Solvent was removed under vacuum affording a thick yellow oil. This was dissolved in minimal dichloromethane and the resulting intramolecular cross-linked copolymer was precipitated with cold acidified methanol.

4.5.8 Polyvinylcyclohexene carbonate cross-metathesis with dimethylaminoethyl methacrylate (DMAEMA)

Purified PVCHC (0.446 g, 2.35 mmol vinyl units) was dissolved in 80 mL of dichloromethane. To this solution was added DMAEMA (3.83 mL, 22.7 mmol) along with a solution of Grubbs' Generation II catalyst (38.2 mg, 4.50×10^{-2} mmol) in 5 mL of dichloromethane. The reaction was heated to 35 °C under dynamic vacuum for 24 h. The solvent and excess DMAEMA was removed under vacuum, the residue re-dissolved in minimal dichloromethane and the resulting modified copolymer was precipitated with cold acidified methanol.

4.5.9 One-pot polymerization/cross-linking of polyvinylcyclohexene carbonate with Grubbs Generation II catalyst

Stock solutions of BPh_3 (21 mg, 0.089 mmol) and PPNCl (0.051 g, 0.089 mmol) in toluene were combined and the solvent removed under vacuum. The resulting white residue was dissolved in dichloromethane (3 mL), injected into a 100 mL Parr reactor, and the solvent removed under vacuum. Vinyl cyclohexene oxide (2.20 g, 17.7 mmol) was injected into the vessel which was then pressurized to 40 bar CO_2 and heated to 60 °C for 24 h. After 24 h, the vessel was cooled to room temperature and slowly depressurized. Next, a solution of Grubbs' Generation II catalyst (0.30 g, 0.35 mmol) in 55 mL of toluene was injected into the vessel. This was stirred at room temperature under a dynamic vacuum for 24 h. Solvent was removed under vacuum affording a thick brown oil. This was dissolved in minimal dichloromethane and the resulting intermolecular cross-linked copolymer was precipitated with cold acidified methanol.

4.6 References

1. Cokoja, M.; Bruckmeier, C.; Rieger, B.; Herrmann, W. A.; Kuehn, F. E., *Angew. Chem., Int. Ed.* **2011,** *50* (37), 8510-8537.

2. Liu, Q.; Wu, L.; Jackstell, R.; Beller, M., *Nat. Commun.* **2015,** *6*, 5933.

3. North, M.; Styring, P., *Faraday Discuss.* **2015,** *183* (Carbon Dioxide Utilisation), 489-502.

4. Aresta, M.; Dibenedetto, A.; Quaranta, E., *J. Catal.* **2016,** *343*, 2-45.

5. Artz, J.; Muller, T. E.; Thenert, K.; Kleinekorte, J.; Meys, R.; Sternberg, A.; Bardow, A.; Leitner, W., *Chem. Rev.* **2018,** *118* (2), 434-504.

6. Dove, A. P., *Nat. Chem.* **2014,** *6* (4), 276-7.

7. Nakano, R.; Ito, S.; Nozaki, K., *Nat. Chem.* **2014,** *6* (4), 325-31.

8. Moore, D. R.; Cheng, M.; Lobkovsky, E. B.; Coates, G. W., *J. Am. Chem. Soc.* **2003,** *125* (39), 11911-11924.

9. Kember, M. R.; Knight, P. D.; Reung, P. T. R.; Williams, C. K., *Angew. Chem., Int. Ed.* **2009,** *48* (5), 931-933.

10. Kissling, S.; Lehenmeier, M. W.; Altenbuchner, P. T.; Kronast, A.; Reiter, M.; Deglmann, P.; Seemann, U. B.; Rieger, B., *Chem. Commun.* **2015,** *51* (22), 4579-4582.

11. Lehenmeier, M. W.; Kissling, S.; Altenbuchner, P. T.; Bruckmeier, C.; Deglmann, P.; Brym, A.-K.; Rieger, B., *Angew. Chem., Int. Ed.* **2013,** *52* (37), 9821-9826.

12. Comerford, J. W.; Ingram, I. D. V.; North, M.; Wu, X., *Green Chem.* **2015,** *17* (4), 1966-1987.

13. North, M.; Pasquale, R., *Angew. Chem., Int. Ed.* **2009,** *48* (16), 2946-2948.

14. North, M.; Quek, S. C. Z.; Pridmore, N. E.; Whitwood, A. C.; Wu, X., *ACS Catal.* **2015,** *5* (6), 3398-3402.

15. North, M.; Wang, B.; Young, C., *Energy Environ. Sci.* **2011,** *4* (10), 4163-4170.

16. North, M.; Young, C., *ChemSusChem* **2011,** *4* (11), 1685-1693.

17. Whiteoak, C. J.; Kielland, N.; Laserna, V.; Escudero-Adan, E. C.; Martin, E.; Kleij, A. W., *J. Am. Chem. Soc.* **2013,** *135* (4), 1228-1231.

18. Whiteoak, C. J.; Kielland, N.; Laserna, V.; Castro-Gomez, F.; Martin, E.; Escudero-Adan, E. C.; Bo, C.; Kleij, A. W., *Chem. - Eur. J.* **2014,** *20* (8), 2264-2275.

19. Büttner, H.; Longwitz, L.; Steinbauer, J.; Wulf, C.; Werner, T., *Top. Curr. Chem.* **2017,** *375* (3), 1-56.

20. Shaikh, R. R.; Pornpraprom, S.; D'Elia, V., *ACS Catal.* **2018,** *8* (1), 419-450.

21. Fiorani, G.; Guo, W.; Kleij, A. W., *Green Chem.* **2015,** *17* (3), 1375-1389.

22. Yang, J.-L.; Wu, H.-L.; Li, Y.; Zhang, X.-H.; Darensbourg, D. J., *Angew. Chem., Int. Ed.* **2017,** *56* (21), 5774-5779.

23. Zhang, D.; Boopathi, S. K.; Hadjichristidis, N.; Gnanou, Y.; Feng, X., *J. Am. Chem. Soc.* **2016,** *138* (35), 11117-20.

24. Sivaev, I. B.; Bregadze, V. I., *Coord. Chem. Rev.* **2014,** *270-271*, 75-88.

25. Courtemanche, M. A.; Legare, M. A.; Maron, L.; Fontaine, F. G., *J. Am. Chem. Soc.* **2013,** *135* (25), 9326-9.

26. Courtemanche, M. A.; Legare, M. A.; Maron, L.; Fontaine, F. G., *J. Am. Chem. Soc.* **2014,** *136* (30), 10708-17.

27. Courtemanche, M. A.; Pulis, A. P.; Rochette, E.; Legare, M. A.; Stephan, D. W.; Fontaine, F. G., *Chem. Commun.* **2015,** *51* (48), 9797-800.

28. Stephan, D. W., *J. Am. Chem. Soc.* **2015,** *137* (32), 10018-10032.

29. Stephan, D. W., *Acc. Chem. Res.* **2015,** *48* (2), 306-316.

30. Stephan, D. W., *Science* **2016,** *354* (6317), 1248.

31. Stephan, D. W., *Angew. Chem., Int. Ed.* **2017,** *56* (22), 5984-5992.

32. Stephan, D. W.; Erker, G., *Angew. Chem., Int. Ed.* **2015,** *54* (22), 6400-6441.

33. Lawson, J. R.; Melen, R. L., *Inorg. Chem.* **2017,** *56* (15), 8627-8643.

34. Mömming, C. M.; Otten, E.; Kehr, G.; Fröhlich, R.; Grimme, S.; Stephan, D. W.; Erker, G., *Angew. Chem. Int. Ed.* **2009,** *48* (36), 6643-6646.

35. Mukherjee, D.; Sauer, D. F.; Zanardi, A.; Okuda, J., *Chem. Eur. J.* **2016,** *22* (23), 7730-3.

36. Kelsen, V.; Vallée, C.; Jeanneau, E.; Bibal, C.; Santini, C. C.; Chauvin, Y.; Olivier-Bourbigou, H. l. n., *Organometallics* **2011,** *30* (16), 4284-4291.

37. Pena Carrodeguas, L.; Cristofol, A.; Fraile, J. M.; Mayoral, J. A.; Dorado, V.; Herrerias, C. I.; Kleij, A. W., *Green Chem.* **2017,** *19* (15), 3535-3541.

38. Zhou, H.; Wang, G.-X.; Zhang, W.-Z.; Lu, X.-B., *ACS Catal.* **2015,** *5* (11), 6773-6779.

39. Martín, C.; Fiorani, G.; Kleij, A. W., *ACS Catal.* **2015,** *5* (2), 1353-1370.

40. North, M.; Pasquale, R.; Young, C., *Green Chem.* **2010,** *12* (9), 1514-1539.

41. Lim, C. H.; Holder, A. M.; Hynes, J. T.; Musgrave, C. B., *Inorg Chem* **2013,** *52* (17), 10062-6.

42. Fontaine, F.-G.; Stephan, D. W., *Curr. Opin. Green Sustain. Chem.* **2017,** *3*, 28-32.

43. Xiao, Y.; Wang, Z.; Ding, K., *Macromolecules* **2006,** *39* (1), 128-137.

44. Kember, M. R.; Williams, C. K., *J. Am. Chem. Soc.* **2012,** *134* (38), 15676-15679.

45. Castro-Osma, J. A.; North, M.; Wu, X., *Chem. Eur. J.* **2014,** *20* (46), 15005-15008.

46. Martínez, J.; Castro-Osma José, A.; Earlam, A.; Alonso-Moreno, C.; Otero, A.; Lara-Sánchez, A.; North, M.; Rodríguez-Diéguez, A., *Chem. Eur. J.* **2015,** *21* (27), 9850-9862.

47. Cuesta-Aluja, L.; Castilla, J.; Masdeu-Bulto, A. M., *Dalton Trans.* **2016,** *45* (37), 14658-14667.

48. Castro-Osma, J. A.; Lamb, K. J.; North, M., *ACS Catal.* **2016,** *6* (8), 5012-5025.

49. Rintjema, J.; Kleij, A. W., *ChemSusChem* **2017,** *10* (6), 1274-1282.

50. Wang, J.; Zhang, Y., *ACS Catal.* **2016,** *6* (8), 4871-4876.

51. Sopeña, S.; Martin, E.; Escudero-Adán, E. C.; Kleij, A. W., *ACS Catal.* **2017,** *7* (5), 3532-3539.

52. Wang, L.; Zhang, G.; Kodama, K.; Hirose, T., *Green Chem.* **2016,** *18* (5), 1229-1233.

53. Arayachukiat, S.; Kongtes, C.; Barthel, A.; Vummaleti, S. V. C.; Poater, A.; Wannakao, S.; Cavallo, L.; D'Elia, V., *ACS Sus. Chem. Eng.* **2017,** *5* (8), 6392-6397.

54. Yingcharoen, P.; Kongtes, C.; Arayachukiat, S.; Suvarnapunya, K.; Vummaleti, S. V. C.; Wannakao, S.; Cavallo, L.; Poater, A.; D' Elia, V., *Adv. Synth. Catal.* **2018,** *0* (0).

55. Watanabe, K.; Tanaka, R.; Takada, K.; Kim, M.-J.; Lee, J.-S.; Tajima, K.; Isono, T.; Satoh, T., *Polym. Chem.* **2016,** *7* (29), 4782-4792.

56. Descour, C.; Macko, T.; Schreur-Piet, I.; Pepels, M. P. F.; Duchateau, R., *RSC Adv.* **2015,** *5* (13), 9658-9666.

57. Cherian, A. E.; Sun, F. C.; Sheiko, S. S.; Coates, G. W., *J. Am. Chem. Soc.* **2007,** *129* (37), 11350-11351.

58. Liu, S.; Zhao, X.; Guo, H.; Qin, Y.; Wang, X.; Wang, F., *Macromol. Rapid Commun.* **2017,** *38* (9).

59. Darensbourg, D. J.; Yarbrough, J. C.; Ortiz, C.; Fang, C. C., *J. Am. Chem. Soc.* **2003,** *125* (25), 7586-7591.

60. Liu, J.; Ren, W.-M.; Liu, Y.; Lu, X.-B., *Macromolecules* **2013,** *46* (4), 1343-1349.

61. Ni, K.; Kozak, C. M., *Inorg. Chem.* **2018,** *57* (6), 3097-3106.

Co-authorship Statement

Chapter 5: Functionalized Polycarbonates via Triphenylborane Catalyzed Polymerization-Hydrosilylation

This chapter has been peer reviewed and published in:

RSC Advances, **2019**, 9, 26542-26546

Authors: Kori A. Andrea[a] and Francesca M. Kerton[a]*

[a] Department of Chemistry, Memorial University of Newfoundland, St. John's, NL, A1B 3X7, Canada

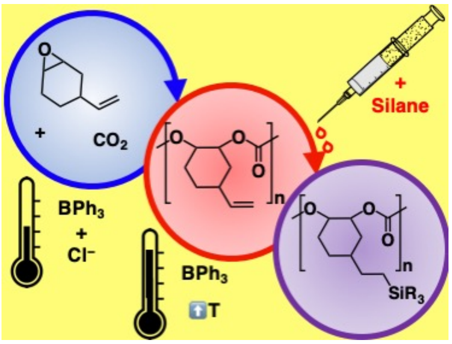

The first author (K. A. Andrea) contributed to 100% of the article, including manuscript writing, performing experiments and data analysis. The corresponding author, F. M. Kerton, directed the project, assisting in experimental design and manuscript writing.

Chapter 5 : Functionalized Polycarbonates via Triphenylborane Catalyzed Polymerization-Hydrosilylation

See Appendix D for additional data.

5.1 Introduction

Transformation of carbon dioxide (CO_2) into useful organic materials is important from an economic and environmental viewpoint.[1-2] Specifically, the reaction of CO_2 and epoxides can yield either cyclic carbonates or polycarbonates, with product selectivity relying on several factors such as temperature, pressure, substrate and catalyst design. The polycarbonate product is attractive as it paves a new road towards the development new sustainable polymeric materials that may serve as alternatives to the traditional petroleum-based products that dominate society today.[3-5] The use of catalysts that can incorporate a mixture of epoxide monomers into the final product has evolved in recent years, which can allow renewable functional epoxides to be incorporated into a bio-renewable end product.[6-7] Furthermore, such functional epoxides including unsaturated building blocks allow for subsequent modification and tailoring of the polymer and its properties. This has been achieved previously, for example, via olefin metathesis, and thiol-ene crosslinking reactions.[8-14]

Copolymerization of epoxides and CO_2 is usually facilitated by metal-based catalytic systems,[6, 15] but recently the use of organo- and non-metal catalysts has emerged,[16] including two examples making use of organoboranes. The first used triethylborane to yield polycarbonates with high carbonate content when either propylene oxide (PO) or cyclohexene oxide (CHO) were used as the substrate.[17] We recently reported the use of arylboranes, both triphenylborane (BPh_3) and the more Lewis acidic tris(pentafluorophenyl)borane (BCF), as catalysts for the production of either cyclic carbonate or polycarbonate products with substrate dependent selectivity.[18]

Triarylboranes, particularly BCF alone or as a Frustrated Lewis Pair (FLP) are known to catalyze a broad range of reactions,[19-24] including hydroelementations that possess enormous potential for production of chemicals in a sustainable manner.[25-26] Specifically, hydrosilylation involves the addition of Si-H groups across C-C, C-O and C-N multiple bonds.[27] As hydrosilylation of alkenes by BCF had been reported,[21] along with our recent report of BPh_3 catalyzed copolymerization of CO_2 and vinylcyclohexene oxide (VCHO), we were motivated to combine these two reactions in a one-pot manner to yield silylated-functional polycarbonates. Herein, we report the first example of an alkene hydrosilylation catalyzed by the less Lewis acidic BPh_3. Building upon our previous findings on the ability of BPh_3 to produce perfectly alternating polycarbonates, we report sequential copolymerization-hydrosilylation in a one-pot manner via assisted tandem catalysis (**Scheme 5.1**). We anticipate that such processes can lead to CO_2-derived polymers with tailorable physical properties including glass transition temperatures. Also, these polymers may show enhanced solubility in organic solvents, which will facilitate film-casting, and if some Si-H bonds remain, it may allow polymers to be attached to surfaces via covalent bonding or grafted to other macromolecular species to form more complex architectures.

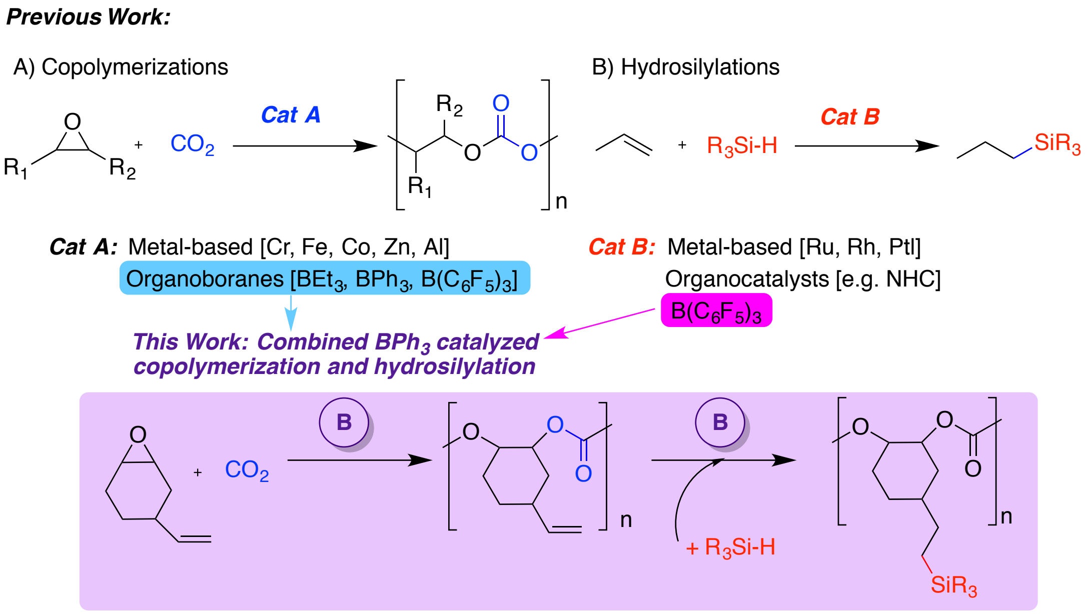

Scheme 5.1. Catalytic copolymerization and hydrosilylation

5.2 One-pot hydrosilylation of polyvinylcyclohexene carbonate

The vinyl groups of the polyvinylcyclohexene carbonate (PVCHC) provide several potential routes to polymer modification, which could result in tuning of its physical and chemical properties. This has been done previously using methods such as thiol-ene click chemistry[28] and metathesis.[10, 18] BCF is known to activate Si-H bonds and facilitate their addition across unsaturated substrates,[21, 29-30] whereas BPh_3 has been studied to a lesser extent. We envisioned that BPh_3 would be able to catalyze the addition of Si-H groups onto a vinyl-substituted polycarbonate. Therefore, we performed the following 'one-pot' sequence: BPh_3 was used to catalyze the copolymerization of VCHO and CO_2, the CO_2 was vented and phenyldimethylsilane added to the reaction mixture so the BPh_3 present could then catalyze the hydrosilylation of the alkene within the polycarbonate. We did not attempt to perform the hydrosilylation reaction in the presence of CO_2, or prior to or during the copolymerization, as BPh_3 is able to hydrosilylate CO_2 but does not react with propylene carbonate,[31] and we presume other carbonates. We monitored the one-pot process via in situ IR spectroscopy. The formation of PVCHC was monitored via growth of the carbonate stretch at 1747 cm^{-1}. We observed no induction period and signal saturation occurred within approximately 1 h. After 24 h, we cooled and depressurized the vessel before injecting a mixture of phenyldimethylsilane in dichloromethane and heating to 40 °C. A trial hydrosilylation reaction (NMR scale) on isolated PVCHC was successful at this temperature. However, for the one pot process after 4 days, no new bands were observed in the IR spectrum. Upon increasing the temperature to 60 °C, within hours we saw a decrease in intensity of bands at 2122 and 882 cm^{-1} ($PhMe_2SiH$), and an increase in intensity of bands at 834 and 791 cm^{-1} demonstrating the successful addition of the silane across the alkene of the polycarbonate. The higher temperature for the one-pot process is likely needed to displace the Cl^- anion from the boron centre and allow activation of the Si-H bond by the borane. Cl^- is used as a co-catalyst in the CO_2 epoxide copolymerization process and the NMR scale trial reaction was performed in the absence of PPNCl. The successful one-pot reaction was confirmed with ^1H, ^{13}C, HSQC and ^{29}Si NMR spectroscopy (**Figure D1-D6**), and integration of ^1H NMR signals for the residual vinyl protons and the silyl protons ($Si-(CH_3)_2$, Si-ArH) showed 10% of the vinyl groups had been modified. In the refocused INEPT ^{29}Si NMR spectrum of the product, a new signal appeared at $\delta = -1.26$ ppm characteristic of a Si-C saturated bond cf. $PhMe_2SiH$ $\delta = -17.27$ ppm. Gel permeation chromatography (GPC) traces show an increase in M_n for the product, while calculated Mark-Houwink Sakurada (MHS) confirmation plots show an increased degree of branching in the product (a = 0.697 in PVCHC vs. silyl-PVCHC a = 0.479), further confirming successful functionalization (**Figures D7-D8**).[32] As anticipated the silyl-modified polymer exhibited a lower glass transition temperature (T_g) 71.5 °C compared with PVCHC, 99.0 °C. This T_g may possibly be further decreased if a larger proportion of vinyl groups are converted or a different silane employed. Polycarbonates with relatively low T_g includes to yield modified commercially available polypropylene carbonate that finds applications in films and coatings. This one-pot copolymerization-silylation process is an example of assisted tandem catalysis,[33] as the silane reagent triggers the mode of catalysis to change, and represents a new approach to functionalized polycarbonate.

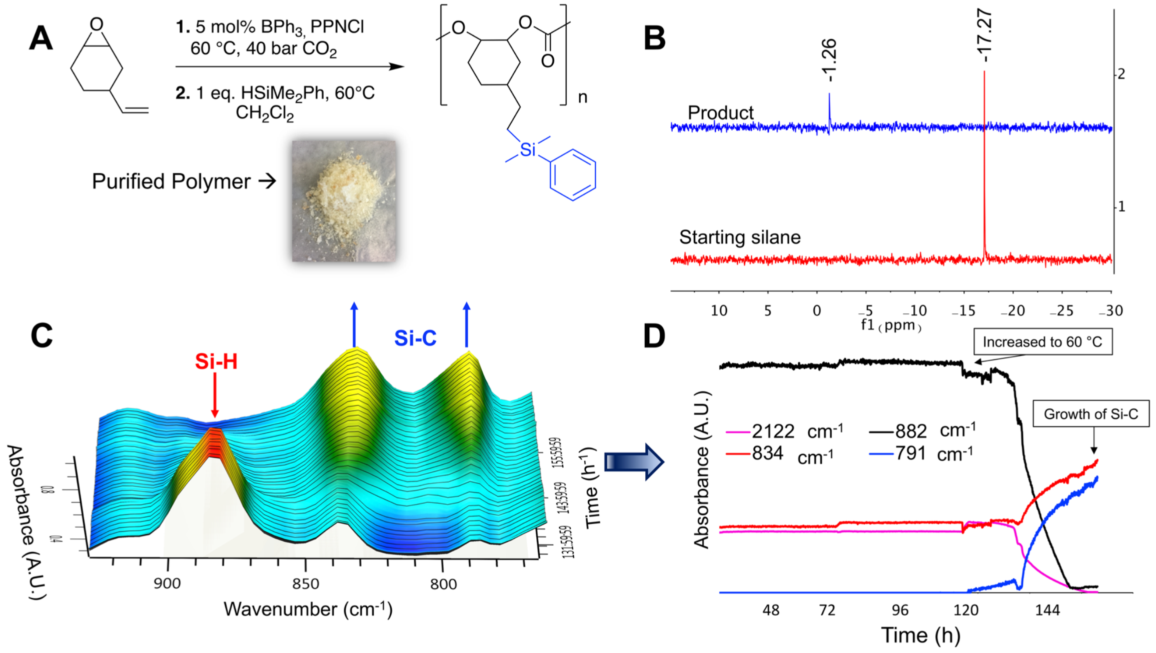

Figure 5.1. One-pot assisted tandem catalysis to yield silane modified polycarbonate. (A) One-pot catalytic formation of silylated-PVCHC. (B) ^{29}Si NMR spectra of $PhMe_2SiH$ and product. (C) In situ IR spectra of reaction mixture over time. (D) Reaction profile obtained from in situ IR data.

5.3 Mixed terpolymerizations of epoxides and CO_2

To obtain more examples of functional polycarbonates, while building upon past examples of mixed epoxide/CO_2 terpolymerizations,[34-38] we sought to investigate our BPh_3/PPNCl catalytic system for similar activity. In our previous research, when propylene oxide (PO) was used as the substrate neither polypropylene oxide nor polypropylene carbonate (PPC) was formed.[18] However, when an initial monomer mixture of 50:50 CHO:PO was used, we saw an incorporation ratio of 4:1 CHO:PO in the resulting polycarbonate i.e. 20% PPC linkages (**Table 5.1**, entry 1). Moving to a 10:90 CHO:PO monomer mixture, a terpolymer with 50% PPC linkages and a lower T_g, 37.3 °C, was obtained (**Table 5.1**, entry 2). From in situ IR monitoring, in addition to terpolymer, a notable amount of cyclic propylene carbonate formed. However, traces showed from a kinetic standpoint while the cyclic product formed quickly, once polymerization began there was no further cyclic formation (**Figure D13**). Instead, the starting PO monomer continued to insert into the growing polymeric chain. When these ratios were reversed 90:10 CHO:PO (**Table 5.1**, entry 3), the polymer contained mostly PCHC linkages with a T_g similar to polycyclohexene carbonate. When CHO was replaced with VCHO in combination with PO (**Table 5.1**, entries 1 and 4), a larger proportion of PO was incorporated into the terpolymer. The BPh_3/PPNCl system did not give cyclic or polymer product when glycidol was used (**Table 5.1**, entry 6). Allyl glycidyl ether (AGE) in the presence of CHO or VCHO (**Table 5.1**, entries 7 and 9) could be incorporated into terpolymers but only modest amounts of AGE were found in the resulting polymer. All obtained terpolymers were characterized by ^1H and ^{13}C NMR spectroscopy, GPC and DSC

(**Figures D9-26**). DOSY NMR spectroscopy confirmed the incorporation of both epoxides within the same polymeric chain. The terpolymers with alkene functionality (i.e. those containing VCHO and AGE) are attractive as they introduce the potential to further modify the polymers.

Table 5.1. Terpolymerizations of epoxides and CO_2 catalyzed by BPh_3[a]

Entry	Epoxide A equiv. (%)	Epoxide B equiv. (%)	Monomer incorporation[b] (A:B)	M_n (gmol^{-1})[c]	Đ[c]	T_g (°C)[d]
1	CHO (50)	PO (50)	4:1	7 989	1.03	79.9
2	CHO (10)	PO (90)	1:2	7 306	1.06	37.3
3	CHO (90)	PO (10)	25:1	3 760	1.03	110.2
4	VCHO (50)	PO (50)	1.5:1	9 663	1.08	78.4
5	CHO (50)	Glycidol (50)	No reaction	-	-	-
6	CHO (50)	AGE (50)	1:0.1	6083	1.07	72.5
7	CHO (50)	VCHO (50)	1:0.5	5120	1.10	109.1
8	VCHO (50)	AGE (50)	2.2:1	7541	1.09	76.6

[a] General reaction conditions unless otherwise indicated: total epoxide (A+B) (0.025 mol), PPNCl (0.124 mmol), BPh_3 (0.124 mmol), 60 °C, 40 bar CO_2. All obtained terpolymers contained >99% CO_3 linkages, no evidence of polyether formation. [b] Determined by ^1H NMR spectroscopy. [c] Đ, dispersity = M_w/M_n. Determined in THF by GPC equipped with a multiangle light-scattering detector. [d] Determined from DSC.

Building upon our initial polycarbonate hydrosilylation results, we then performed 'one-pot' hydrosilylation using the CHO/VCHO terpolymer (**Table 5.1**, entry 8) following similar procedures to those discussed above (**Figure 5.2**). For the copolymerization step, a catalyst loading of 2.5 mol% BPh_3 was used, which corresponds to 5 mol% BPh_3 for the hydrosilylation step (as only 50% VCHO was present). After 24 h the vessel was cooled, depressurized and a mixture of diphenylsilane in dichloromethane was injected into the vessel. The mixture was then heated to 60 °C for 24 h. Via in situ IR spectroscopy, we observed a decreased in intensity of the silane bands (2144 and 845 cm^{-1}), which plateaued after approximately 12 h and growth of a band at 830 cm^{-1} corresponding to the hydrosilylated product. The hydrosilylated polymer was further characterized by ^1H, ^{13}C, HSQC and refocused INEPT ^{29}Si NMR spectroscopy (**Figures D27-D32**). From ^1H NMR integration of signals for the residual vinyl protons and the aromatic protons (-$SiPh_2$), 36% of vinyl groups had been modified. The ^{29}Si INEPT NMR spectrum of the product had a resonance at $\delta = -19.32$ ppm, *cf.* $\delta = -33.18$ ppm (Ph_2SiH_2). From both ^1H and ^{29}Si NMR it is evident that only one Si-H bond added across the alkene of the terpolymer and hence no cross-linking occurred. From DSC data, a decline in T_g from 111.6 °C to 47.8 °C was observed for the silylated product (**Figure D33**). From GPC, an increase in molecular weight from 4.31×10^3 $gmol^{-1}$ (Đ = 1.07) to 6.20×10^3 $gmol^{-1}$ (Đ = 1.12) was observed as well as increased branching in MHS confirmation plots (**Figure D34**).

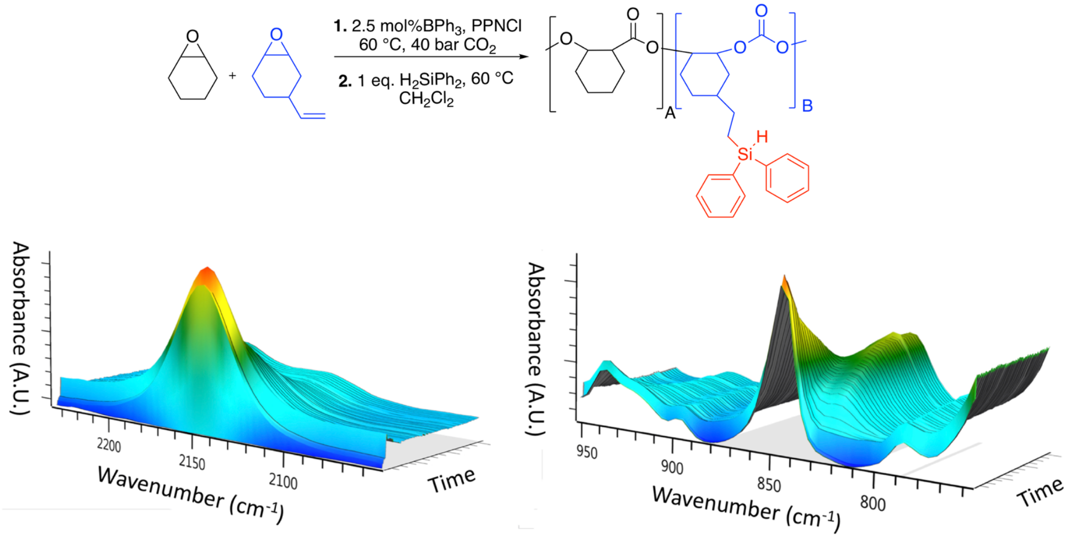

Figure 5.2. One-pot assisted tandem catalysis to yield silylated-terpolymers. General reaction scheme (top) and three-dimensional plots obtained via in situ IR spectroscopy showing a decreased for silane bands and growth of product bands (bottom).

Finally, we set out to evaluate the substrate scope of these transformations by evaluating the reactivity of a hydride terminated polydimethylsiloxane. For the hydride terminated polydimethylsiloxane (DMS-HO3) and PVCHC, the resulting polymer was characterized by ^{1}H, ^{13}C, refocused INEPT ^{29}Si, and H-Si HMQC NMR spectroscopy (**Figures D35-D37**). Via integration of the ^{1}H NMR spectrum, hydrosilylation has occurred to a similar extent to other hydrosilylations reported herein. We note that only one Si-H group per DMS-HO3 has undergone reaction and no cross-linking between polycarbonate chains was indicated by NMR and DSC data. FTIR spectra of the hydrosilylated-polycarbonate showed new bands at ν = 1013, 907 and 788 cm^{-1} corresponding to O-Si-O, Si-H and Si-CH_3 groups respectively (**Figure D38**). From GPC, there was a moderate increase in molecular weight and no significant change in *Đ*. There was a decline in the slope of the MHS plot indicating a higher degree of branching in the final product (**Figure D39**). DSC analysis demonstrated a slight increase in T_g from 99.0 °C to 104.6 °C. The residual unreacted Si-H bonds in the functionalized polymer introduces further functionality potential. For example, BCF has been reported to catalyze the addition of Si-H bonds onto silica derived materials.[39]

5.4 Conclusions

In summary, we report the first example of BPh_3 catalyzed hydrosilylation of perfectly alternating PVCHC in a tandem catalytic manner. These reactions were monitored by in situ IR spectroscopy, which demonstrated the addition of the Si-H bond across the pendent alkenes in the polymer. In an attempt to build new classes of polymeric materials, we showed the ability of BPh_3 to catalyze the terpolymerization of CO_2 and several epoxide combinations, yielding products with T_g values from 37.3 °C to 110.2 °C, which we could then functionalize in a similar one-pot manner as above. Finally, we evaluated the reactivity of a polymeric hydride terminated siloxane which can serve as a precursor for silica surface modification. Using the results in-hand, we will work towards developing sustainable surface functionalized materials in the future.

5.5 Experimental

5.5.1 General experimental conditions

Unless otherwise stated, all experimental procedures were performed using an MBraun Labmaster glove box or under dry oxygen-free nitrogen using Schlenk techniques. Propylene oxide and bis(triphenyphosphine)iminium chloride (PPNCl) were purchased from Alfa Aesar. Cyclohexene oxide, vinyl cyclohexene oxide, allyl glycidol ether, epichlorohydrin and glycidol were purchased from Sigma Aldrich. All epoxides were dried over CaH_2 and distilled under vacuum. Phenyldimethylsilane, diphenylsilane and hydride terminated polydimethylsiloxane (DMS-H03) were purchased from Gelest and used without further purification. All solvents were dried and degassed using an MBraun Manual Solvent Purification system. Triphenylborane (BPh_3) was purchased from Strem Chemicals and used without further purification. Caution should be taken when operating high pressure equipment.

5.5.2 Instrumentation

^1H and $^{13}C\{^1H\}$, ^{29}Si NMR spectra were recorded on a Bruker Avance III 300 MHz spectrometer at 25 °C (frequencies were ^{13}C, 75.43 MHz; ^{29}Si, 59.60 MHz). All NMR spectra were obtained in $CDCl_3$ or $(CD_3)_2CO$ purchased from Cambridge Isotope Laboratories, Inc. ^1H and ^{13}C NMR spectra were referenced using the residual proton and ^{13}C resonances of the solvent. Refocused INEPT ^{29}Si was referenced to external tetramethylsilane (TMS, $\delta = 0$ ppm). All cyclization and copolymerization reactions were carried out in a 100 mL stainless steel reactor vessel (Parr Instrument Company) equipped with a silicon sensor (SiComp), mechanical stirrer and a heating mantel. For kinetic measurements, the Si sensor was connected to a ReactIR 15 base unit (Mettler-Toledo) through a DS silver-halide Fiber-to-Sentinel conduit. The vessel was baked at 100 °C under vacuum overnight prior to any experiment. Gel permeation chromatography (GPC) analysis was performed on a set-up consisting of a miniDawn TREOS light scattering detector, a Viscostar-II viscometer, and an Optilab T-rEX differential refractive index detector (Wyatt Technology) connected to an Agilent Infinity 1260 HPLC system equipped with two Phenogel 10^3 Å 300 × 4.60 mm columns with THF as eluent. Samples were prepared in THF at a concentration of 4 mg mL^{-1}, filtered through a 0.2 μm syringe filter, and analyzed at a flow rate of 0.3 mL min^{-1} at 25 °C. The values of dn/dc were calculated online (columns detached) assuming 100% mass recovery using the Astra 6 software package (Wyatt Technologies). Glass transition temperatures (T_g) were obtained on a Mettler Toledo DSC Star^e system equipped with a Julabo FT 100 immersion cooling system for low temperatures (-100 °C +20 °C). Samples were weighed into 40 μL aluminum pans and exposed to 3 heating cycles from 0 to 200 °C at a rate of 10 °C min^{-1}, with a hold time of 2 min at both 0 °C and 200 °C in each cycle. The reported T_g values were determined using data from the third heating cycle.

5.5.3 One-pot formation of silyl-modified polycarbonate

Stock solutions of BPh_3 (24.4 mg mL^{-1}) and PPNCl in toluene were combined and solvent was removed under vacuum. The solids were dissolved in 3 mL of dichloromethane and the solution was injected into the pressure vessel. The dichloromethane removed under vacuum, before the desired amount of the vinylcyclohexene oxide monomer was injected into the pressure vessel. The vessel was pressurized with CO_2, heated to the desired temperature and mechanically stirred for 24 h. After 24 h, the vessel was cooled to room temperature and slowly depressurized into a fume hood. A solution of phenyldimethylsilane (2.74 g, 20.1 mmol) in 20 mL of dichloromethane was injected into the vessel. The reaction mixture was heated to 40 °C for 4 days. However, after observing no change in signal intensity for phenyldimethylsilane, the temperature was increased to

60 °C for 24 h and IR bands corresponding to the silylated polymer grew in intensity (**Figure 5.1**). After 24 h, the vessel was cooled, the solution was taken out of the pressure vessel, concentrated and the polymer precipitated using cold, acidified methanol.

5.5.4 General procedure for terpolymerizations

Stock solutions of BPh_3 (24.4 mg mL^{-1}) and PPNCl in toluene were combined and the solvent was removed under vacuum. The solids were dissolved in 3 mL of dichloromethane and the solution was injected into the pressure vessel. The dichloromethane removed under vacuum, before the desired epoxide mixture was injected into the vessel. The vessel was pressurized with CO_2, heated to the desired temperature and mechanically stirred for 24 h. After 24 h, the vessel was cooled to room temperature and slowly depressurized into a fume hood. The crude product was dissolved in minimal dichloromethane and precipitated in cold acidified methanol.

5.5.5 Polydimethylsiloxane-functionalized polyvinylcyclohexene carbonate

In a glovebox, purified PVCHC (0.20 g, 1.01 mmol vinyl units) and BPh_3 (0.012 g, 0.050 mmol) was dissolved in 10 mL of dichloromethane. To this, hydride terminated polydimethylsiloxane (2.52 g, 5.04 mmol) was added dropwise with stirring. The vial was sealed and allowed to stir overnight at room temperature. The crude produced was exposed to air and precipitated in cold acidified methanol.

5.6 References

1. Artz, J.; Müller, T. E.; Thenert, K.; Kleinekorte, J.; Meys, R.; Sternberg, A.; Bardow, A.; Leitner, W., *Chem. Rev.* **2018,** *118* (2), 434-504.

2. Aresta, M.; Dibenedetto, A.; Angelini, A., *Chem. Rev.* **2014,** *114* (3), 1709-1742.

3. Cokoja, M.; Bruckmeier, C.; Rieger, B.; Herrmann, W. A.; Kühn, F. E., *Angew. Chem. Int. Ed.* **2011,** *50* (37), 8510-8537.

4. Liu, Q.; Wu, L.; Jackstell, R.; Beller, M., *Nat. Commun.* **2015,** *6*, 5933.

5. North, M.; Styring, P., *Faraday Discuss.* **2015,** *183* (0), 489-502.

6. Trott, G.; Saini, P. K.; Williams, C. K., *Philos. Trans. A Math Phys. Eng. Sci.,* **2016,** *374* (2061), 20150085.

7. Hauenstein, O.; Agarwal, S.; Greiner, A., *Nat. Commun.* **2016,** *7*, 11862.

8. Wang, Y.; Darensbourg, D. J., *Coord. Chem. Rev.* **2018,** *372*, 85-100.

9. Liu, S.; Zhao, X.; Guo, H.; Qin, Y.; Wang, X.; Wang, F., *Macromol. Rapid Commun.* **2017,** *38* (9), 1600754.

10. Cherian, A. E.; Sun, F. C.; Sheiko, S. S.; Coates, G. W., *J. Am. Chem. Soc.* **2007,** *129* (37), 11350-11351.

11. Darensbourg, D. J.; Chung, W.-C.; Arp, C. J.; Tsai, F.-T.; Kyran, S. J., *Macromolecules* **2014,** *47* (21), 7347-7353.

12. Yang, G.-W.; Zhang, Y.-Y.; Wang, Y.; Wu, G.-P.; Xu, Z.-K.; Darensbourg, D. J., *Macromolecules* **2018,** *51* (4), 1308-1313.

13. Martín, C.; Kleij, A. W., *Macromolecules* **2016,** *49* (17), 6285-6295.

14. Stößer, T.; Li, C.; Unruangsri, J.; Saini, P. K.; Sablong, R. J.; Meier, M. A. R.; Williams, C. K.; Koning, C., *Polym. Chem.* **2017,** *8* (39), 6099-6105.

15. Kozak, C. M.; Ambrose, K.; Anderson, T. S., *Coord. Chem. Rev.* **2018,** *376*, 565-587.

16. Shaikh, R. R.; Pornpraprom, S.; D'Elia, V., *ACS Catal.* **2018,** *8* (1), 419-450.

17. Zhang, D.; Boopathi, S. K.; Hadjichristidis, N.; Gnanou, Y.; Feng, X., *J. Am. Chem. Soc.* **2016,** *138* (35), 11117-11120.

18. Andrea, K. A.; Kerton, F. M., *ACS Catal.* **2019,** *9* (3), 1799-1809.

19. Stephan, D. W., *Science* **2016,** *354* (6317).

20. Lawson, J. R.; Melen, R. L., *Inorg. Chem.* **2017,** *56* (15), 8627-8643.

21. Rubin, M.; Schwier, T.; Gevorgyan, V., *J. Org. Chem.* **2002,** *67*, 1936-1940.

22. Pérez, M.; Hounjet, L. J.; Caputo, C. B.; Dobrovetsky, R.; Stephan, D. W., *J. Am. Chem. Soc.* **2013,** *135* (49), 18308-18310.

23. Holthausen, M. H.; Mehta, M.; Stephan, D. W., *Angew. Chem. Int. Ed.* **2014,** *53* (25), 6538-6541.

24. Simonneau, A.; Oestreich, M., *Angew. Chem. Int. Ed.* **2013,** *52* (45), 11905-11907.

25. Oestreich, M., *Angew. Chem. Int. Ed.* **2016,** *55* (2), 494-499.

26. Zeng, X., *Chem. Rev.* **2013,** *113* (8), 6864-6900.

27. Nakajima, Y.; Shimada, S., *RSC Adv.* **2015,** *5* (26), 20603-20616.

28. Darensbourg, D. J.; Wang, Y., *Polym. Chem.* **2015,** *6* (10), 1768-1776.

29. Berkefeld, A.; Piers, W. E.; Parvez, M., *J. Am. Chem. Soc.* **2010,** *132*, 10660–10661.

30. Wilkins, L. C.; Howard, J. L.; Burger, S.; Frentzel-Beyme, L.; Browne, D. L.; Melen, R. L., *Adv. Synth. Catal.* **2017,** *359* (15), 2580-2584.

31. Mukherjee, D.; Sauer, D. F.; Zanardi, A.; Okuda, J., *Chem. Eur. J.* **2016,** *22* (23), 7730-3.

32. Mori, S. B., H. G., *Size Exclusion Chromatography*. Springer Labratory Verlag Berlin Heidelberg New York, 1999.

33. Fogg, D. E.; dos Santos, E. N., *Coord. Chem. Rev.* **2004,** *248* (21-24), 2365-2379.

34. Li, H.; Niu, Y., *Polymer Journal* **2010,** *43*, 121.

35. Seong, J. E.; Na, S. J.; Cyriac, A.; Kim, B. W.; Lee, B. Y., *Macromolecules* **2010,** *43* (2), 903-908.

36. Wu, G. P.; Xu, P. X.; Zu, Y. P.; Ren, W. M.; Lu, X. B., *J. Polym. Sci., Part A-1: Polym. Chem.* **2013,** *51* (4), 874-879.

37. Darensbourg, D. J.; Poland, R. R.; Strickland, A. L., *J. Polym. Sci., Part A-1: Polym. Chem.* **2012,** *50* (1), 127-133.

38. Deng, K.; Wang, S.; Ren, S.; Han, D.; Xiao, M.; Meng, Y., *ACS Appl. Mater. Interfaces* **2016,** *8* (49), 33642-33648.

39. Moitra, N.; Ichii, S.; Kamei, T.; Kanamori, K.; Zhu, Y.; Takeda, K.; Nakanishi, K.; Shimada, T., *J. Am. Chem. Soc.* **2014,** *136* (33), 11570-11573.

Co-authorship Statement

Chapter 6 Borane Catalyzed Polymerization and Depolymerization Reactions Controlled by Lewis Acidic Strength

This chapter has been peer reviewed and published in:

Chemical Communications, **2021**, DOI: 10.1039/D1CC02218K

Authors: Kori A. Andrea[a], Mikhailey D. Wheeler[a] and Francesca M. Kerton[a]*

[a] Department of Chemistry, Memorial University of Newfoundland, St. John’s, NL, A1B 3X7, Canada

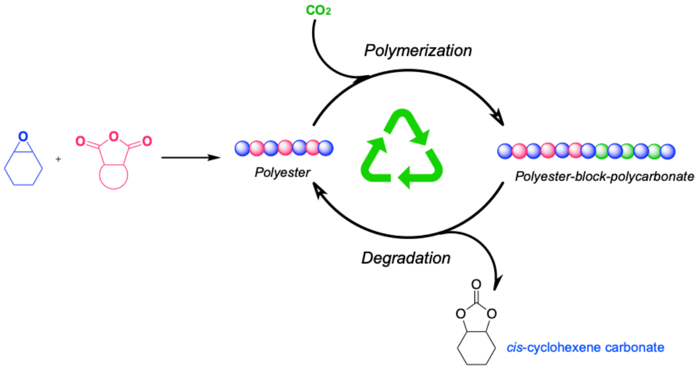

The first author (K. A. Andrea) contributed to >90% of the article, including manuscript writing, performing experiments and data analysis. M. D. Wheeler, assisted K. A. Andrea in the preliminary degradation studies. The corresponding author, F. M. Kerton, directed the project, assisting in experimental design and manuscript writing.

Chapter 6 : Borane Catalyzed Polymerization and Depolymerization Reactions Controlled by Lewis Acidic Strength

See Appendix E for additional data.

6.1 Introduction

Catalyst design remains crucial to ensure the selective production of a product under moderate reaction conditions. While transition metal catalysts have dominated the field of homogeneous catalysis, including copolymerizations of CO_2 and epoxides,[1] the move towards organocatalysts has become prevalent in recent years.[2-6] In particular, boron-based catalysts have demonstrated high reactivity in a broad range of reactions with frustrated Lewis pairs showing exceptional diversity and selectivity.[7-10] In our recent report, we showed that reaction selectivity originated in the Lewis acidity of the central borane and could be fine-tuned to selectively give a specific product, polycarbonate or cyclic carbonate.[11-12] Herein, we will demonstrate that the tuneability of Lewis acid strength afforded by boranes allows selective depolymerization of carbonate linkages in polyester-carbonate copolymers.

The ring-opening copolymerization (ROCOP) of epoxides and anhydrides to form polyesters has the potential to lead to the generation of sustainable materials as the epoxide and anhydride can be sourced renewably. These thermoplastic polyesters find a range of applications due to their good chemical resistance and durability, and their properties vary with the monomers and their relative proportions within the copolymer.[13] Combination of a second copolymer block in the material can have substantial effects on the physical properties of the material.[13-14] In addition, the development of these more exotic di-, triand tetra-block polymers can lead to a new class of materials that may find other unique applications.

The concept of combining polyesters and polycarbonates into one uniform polymeric chain is still in its infancy but some well-defined catalytic systems have been reported and focus on transition metal complexes.[15-26] Successful polymerization and polymer systems should take into account degradability, which is frequently ignored. Herein, we report the first example of an aryl borane-based catalytic system that can polymerize epoxides, anhydrides and CO_2 leading to perfectly alternating block copolymers and can also lead to their controlled catalytic degradation via a switch in Lewis acidity. When cyclohexene oxide is used, selective breakdown of the carbonate block to *cis*-cyclohexene carbonate leaves the polyester fragment entirely intact. Previous to this work there have been two other reports on borane catalyzed polyester and polyester-block-polycarbonate systems.[27-28] However, both of these reports have used triethylborane. Aryl boranes, on the other hand, have not been examined outside of he reports in this thesis. They are more easily modified and thus their Lewis acidity can be more easily fine-tuned to allow more controlled and potentially switchable catalytic routes. Additionally, to the best of our knowledge this is the first example of a selective borane catalyst for polycarbonate degradation.

6.2 Borane catalyzed epoxide, anhydride and CO_2 block copolymerization

The aryl borane-catalyzed copolymerization of both vinylcyclohexene oxide (VCHO) and limonene oxide (LO) with phthalic anhydride (PAH) and *cis*-4-cyclohexene-1,2-dicarboxylic anhydride (CDA) was investigated. These results are summarized in

Table 6.1. Polymerizations were carried out in neat epoxide at elevated temperatures and the kinetics monitored by NMR spectroscopy over time with >90% conversion of the anhydride being observed within 1-2 h (**Figures E1-E6**). After anhydride consumption, there was no evidence of additional incorporation of ring-opened epoxide units within the growing chain, and thus perfectly alternating copolymers were obtained. The absence of ring-opening polymerization (ROP) of excess epoxide is consistent with our previous studies using BPh_3.[11] Comparing anhydride reactivity, polymerization reaction rates were much faster with CDA compared to PAH (**Table 6.1**, entries 1-2). In comparing epoxides, CHO and VCHO showed faster reaction rates compared to LO (**Table 6.1**, entries 1-6) as expected.

In these reactions using LO, complete conversion of CDA was obtained within 1 h whereas PAH consumption was much slower (i.e. <50 % conversion within 1 h, **Figures E2 and E4**). Based on these results, we envisioned if both anhydrides were initially combined in the epoxide, which is both a monomer and solvent, incorporation of CDA into the growing chain would occur first, followed by PAH, leading to an alternating block copolymer product (**Scheme 6.1**). However, in a one-pot reaction, competition between both substrates occurred leading to the production of a random copolymer (**Table 6.1**, entry 7; **Figures E7-E8**, and **Scheme 6.1**). Hence, the above experiment was repeated but allowing CDA to react in excess epoxide first. Once full conversion of CDA was achieved, the second anhydride was added and allowed to react to completion. This led to the formation of a block polyester (**Table 6.1**, entry 8). However, it is worth noting that prolonged heating (i.e. after full conversion of both anhydrides is obtained) results in severe transesterification as observed by the large increase in polymer molar mass dispersities

(**Table E4**) and thus is it crucial that reactions be quenched immediately once the anhydride has reached full conversion.

Table 6.1. Copolymerization of epoxides and anhydrides catalyzed by BPh_3[a]

Entry	Epoxide	Anhydride	Time (min)	% Anhydride Conversion[b]	M_n[c]	$Đ$[c]	T_g[d]
1	LO	PAH	120	90	6100	1.16	113
2	LO	CDA	60	>99	2400	1.09	82
3	VCHO	PAH	60	>99	20300	1.17	113
4	VCHO	CDA	5	>99	4800	1.26	87
5	CHO	PAH	30	>99	5400	1.08	95
6	CHO	CDA	5	>99	3300	1.18	70
7	LO	PAH/CDA	120	>99	1700	1.75	78
8	LO	PAH/CDA	180	>99	2100	1.16	93

[a] General reaction conditions unless otherwise indicated: Epoxide (1.05 mmol), anhydride (0.21 mmol), PPNCl (2.1×10^{-3} mmol), BPh_3 (2.1×10^{-3} mmol), 130 °C. [b] Determined from ^{1}H NMR [c] $Đ$, dispersity = M_w/M_n. Determined in THF by GPC equipped with a multiangle light-scattering detector. [d] Determined from DSC. [e] Random block polyester. 500:100:100:1:1 Epoxide: PAH: CDA: PPNCl: BPh_3 130 °C, 2 h. [f] Controlled block polyester. Step 1: 500:100:1:1 Epoxide: PAH: PPNCl: BPh_3 130 °C, 1 h; Step 2: addition of 100 equiv. CDA, 130 °C, 1 h.

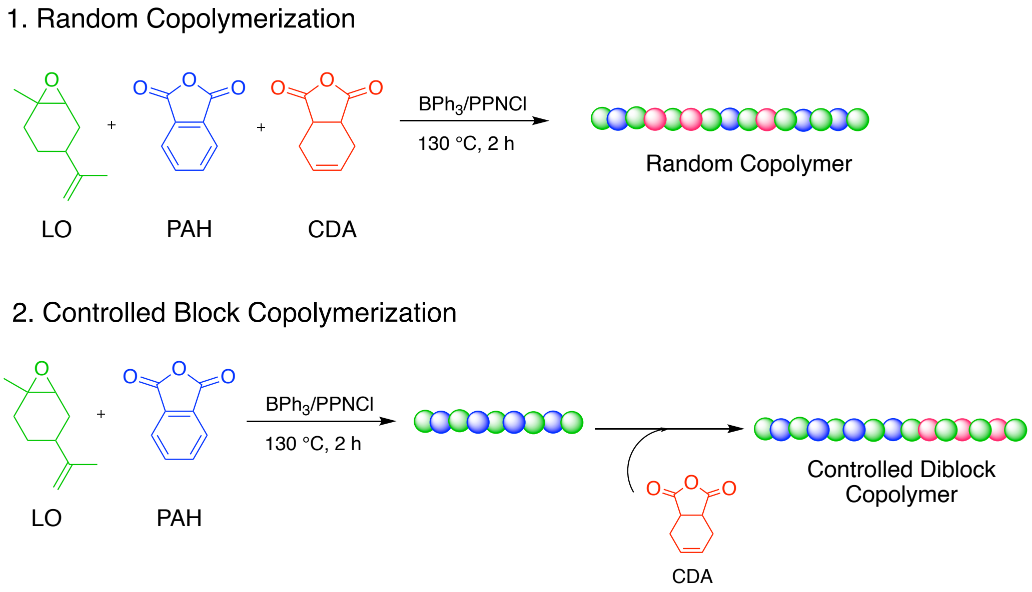

Scheme 6.1. Random and controlled polymerization of limonene oxide (LO), phthalic anhydride (PAH) and cis-4-cyclohexene-1,2-dicarboxylic anhydride (CDA).

Following these initial results and building on our previous work with BPh_3 catalyzed copolymerization of epoxides and CO_2, [11-12] we decided to pursue the formation of block co-polycarbonates-polyesters. For all polymerization reactions herein, including for both epoxide/anhydride and epoxide/anhydride/CO_2 copolymerizations, the more Lewis acidic tris(pentafluorophenyl)borane (BCF) was inactive as a catalyst. In a typical experiment, a mixture of epoxide and anhydride (5:1) was combined with BPh_3/PPNCl for 30 min at 100 °C in a stainless-steel reactor. The vessel was then cooled to room temperature, pressurized to 40 bar CO_2 and heated to 60 °C for 24 h (**Scheme 6.2**). The formation of block copolymers, incorporating all monomer units into the same polymer chain, was confirmed by diffusion NMR spectroscopy. In the case of both anhydrides employed (PAH and CDA), the incorporation of carbonate linkages into the copolymer led to an increase in glass transition temperatures by ~ 25 °C. To the best of our knowledge, this is the first example of a boron catalyzed di-block copolymer synthesis.

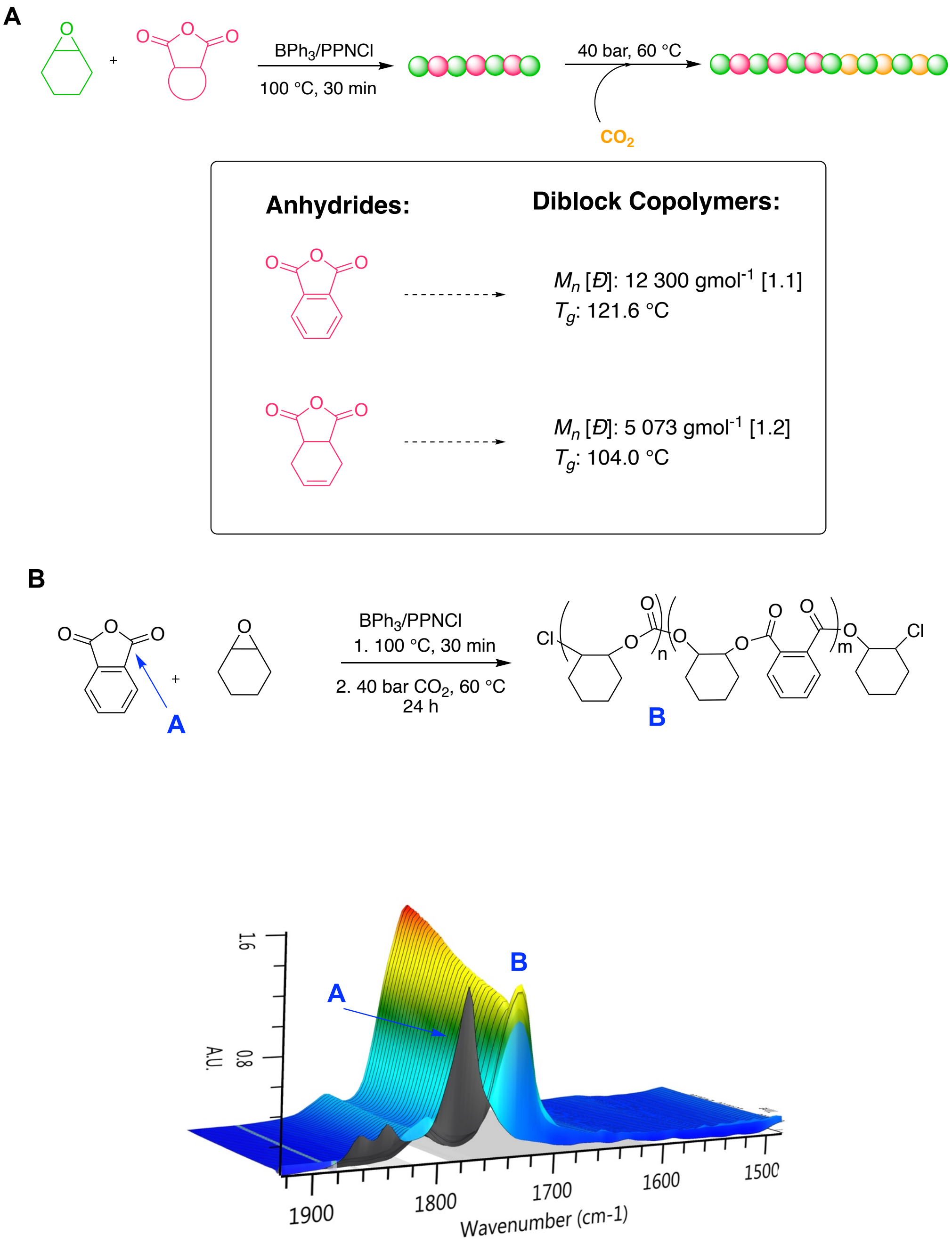

Scheme 6.2. (A) Formation of diblock copolymers catalyzed by BPh_3. (B) In situ IR spectrum showing the consumption of anhydride monomer (1782 cm^{-1}) and incorporation of carbonate linkages into the growing polymeric chain (1742 cm^{-1}). Note: the ester stretch in the resulting polymer could not be observed in the IR spectrum as it likely overlaps with the stretch resulting from the anhydride.

6.3. Borane catalyzed depolymerization of polycarbonates

While the ability to produce these materials in an efficient catalytic manner is important, their recycling and degradation properties are also critical for future use. Thermal depolymerization of similar materials has been reported in the literature but often under harsh conditions.[29-30] The ability of BPh_3 as a potential catalyst in the degradation of these materials was first studied. However, when combining any of these polymers in CH_2Cl_2 with 5 mol% BPh_3 at 130 °C, no degradation products were observed. When we switched to the more Lewis acidic BCF, degradation was observed. Poly(cyclohexene carbonate) selectively degraded to its corresponding cyclic carbonate product, *cis*-cyclohexene carbonate (*cis*-CHC). When a diblock copolymer, for example poly(CHO/PAH-alt-CHO/CO_2), was exposed to BCF under the same conditions, the carbonate block selectively degrades to *cis*-CHC while the polyester block remains fully intact (**Scheme 6.3**). In the absence of BCF, we see no evidence of depolymerization is observed. Commercially available poly(propylene carbonate) (M_n ~50,000 g mol^{-1}) could be fully degraded to the corresponding cyclic propylene carbonate under identical conditions. These preliminary results are promising as this degradation method could show value in repurposing of waste poly(propylene carbonate) and allow access to a circular economy.[31] Additionally, some preliminary studies were undertaken on the degradation kinetics of PCHC to provide some insight into the mechanism of depolymerization. It was found that by taking several aliquots throughout the course of the degradation experiments molecular weights declining trends were relatively linear, while maintaining low dispersities. These initial results suggest degradation likely occurs at the chain-end rather that via chain scission (**Figure E18**).

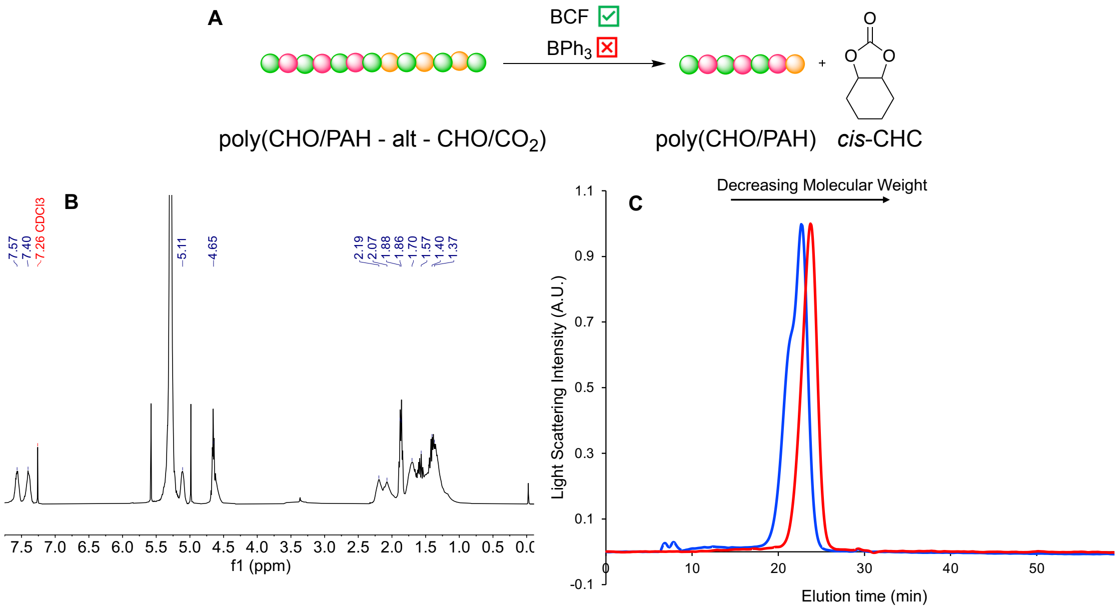

Scheme 6.3. (A) Selective degradation of block(CHO/PAH-alt-CHO/CO_2) to *cis*-CHC and poly(CHO/PAH). (B) ^1H NMR spectrum of the crude reaction mixture showing the selective degradation to *cis*-CHC (4.65 ppm) and remaining poly(CHO/PAH) (7.40-7.57 ppm). (C) GPC light scattering trace of block(CHO/PAH-alt-CHO/CO_2) (blue) and after degradation of carbonate block (i.e. poly(CHO/PAH) (red).

6.4 Conclusions

In summary, the first example of a boron catalyst (BPh_3) for the block copolymerization of epoxide/CO_2 and epoxide/anhydride is described. The introduction of CO_2 led to a catalytic switch from polyester synthesis to polycarbonate synthesis leading to block copolymer chain formation. Switching to the more Lewis acidic BCF, which was not an active catalyst for polymerization reactions, led to the selective degradation of the carbonate block to its corresponding cyclic product while leaving the polyester fragment perfectly intact. Future work will involve studying the kinetics and mechanistic details of the depolymerization process in further detail.

6.5 Experimental

6.5.1 General experimental conditions

Unless otherwise stated, all experimental procedures were completed using an MBraun Labmaster glove box or standard Schlenk techniques under a nitrogen atmosphere. Cyclohexene oxide, vinyl cyclohexene oxide, limonene oxide and poly(propylene carbonate) were purchased from Sigma Aldrich. All epoxides were dried over CaH_2 and distilled under vacuum prior to use. Bis(triphenylphosphine)iminium chloride (PPNCl), phthalic anhydride and *cis*-4-cyclohexene-1,2-dicarboxylic anhydride was purchased from Alfa Aesar. Anhydrides were recrystallized from chloroform prior to use. All solvents were dried and degassed using an MBraun Manual Solvent Purification system. Triphenylborane was purchased from Strem Chemicals and used as received. Caution should be taken when operating high pressure equipment.

6.5.2 Instrumentation

^{1}H and $^{13}C\{^{1}H\}$ NMR spectra were recorded on a Bruker Avance III 300 MHz spectrometer at 25 °C. All NMR spectra were obtained in $CDCl_3$ purchased from Cambridge Isotope Laboratories, Inc. ^{1}H and ^{13}C NMR spectra were referenced using the residual proton and ^{13}C resonances of the solvent. All cyclization and copolymerization reactions were carried out in a 100 mL stainless steel reactor vessel (Parr Instrument Company) equipped with a silicon sensor (SiComp), mechanical stirrer and a heating mantel. For kinetic measurements, the Si sensor was connected to a ReactIR 15 base unit (Mettler-Toledo) through a DS silver-halide Fiber-to-Sentinel conduit. The vessel was baked at 100 °C under vacuum overnight prior to any experiment. Gel permeation chromatography (GPC) analysis was performed on a set-up consisting of a miniDawn TREOS light scattering detector, a Viscostar-II viscometer, and an Optilab T-rEX differential refractive index detector (Wyatt Technology) connected to an Agilent Infinity 1260 HPLC system equipped with a Phenogel 10^3 Å 300 × 4.60 mm columns with THF as eluent. Samples were prepared in THF at a concentration of 4 mg mL^{-1}, filtered through a 0.2 μm syringe filter, and analyzed at a flow rate of 0.3 mL min^{-1} at 25 °C. The values of dn/dc were calculated online (columns detached) assuming 100% mass recovery using the Astra 6 software package (Wyatt Technologies). Glass transition temperatures (T_g) were obtained on a Mettler Toledo DSC Stare system equipped with a Julabo FT 100 immersion cooling system for low temperatures (-100 °C to +20 °C). Samples were weighed into 40 μL aluminum pans and exposed to 3 heating cycles from 0 to 200 °C at a rate of 10 °C min^{-1}, with a hold time of 2 min at both 0 °C and 200 °C in each cycle. The reported T_g values were determined using data from the third heating cycle. Polymer end-group analysis was determined using a Bruker ultrafleXtreme MALDI TOF-TOF mass spectrometer in positive-ion mode. Samples were prepared in a 1:3:20 sodium trifluoroacetate (NaTFA): 2,5-dihydroxybenzoic acid (DHB): sample ratio in a mixture of methanol and THF. 0.5 μL was spotted on the plate for analysis. Data were processed using Polymerix software.

6.5.3 Ring-opening alternating copolymerization of epoxides and anhydrides

BPh_3 (5 mg, 2.1×10^{-3} mmol), PPNCl (11.6 mg, 2.0×10^{-2} mmol) and the appropriate anhydride (100 equivalents to BPh_3) were combined in neat epoxide (1.00 g, 500 equivalents) and stirred under N_2 with heating for the desired time. NMR aliquots were taken and the bulk sample was exposed to air, dissolved in dichloromethane and precipitated in cold acidified methanol. The solvent was decanted and product dried at 60 °C in a vacuum oven overnight.

6.5.4 Controlled block polyester synthesis

BPh_3 (5 mg, 2.1×10^{-3} mmol), PPNCl (11.6 mg, 2.0×10^{-2} mmol) and the appropriate anhydride (100 equivalents to BPh_3) were combined in neat epoxide (1.00 g, 500 equivalents) and stirred under N_2 with heating for the desired time. Once full consumption of anhydride was reached, the second anhydride was added and allowed to react. NMR aliquots were taken and the bulk sample was exposed to air, dissolved in dichloromethane and precipitated in cold acidified methanol. The solvent was decanted and product dried at 60 °C in a vacuum oven overnight.

6.5.5 One-pot block copolymerization of epoxides, anhydrides and CO_2

Appropriate amounts of BPh_3 (31 mg, 0.13 mmol) and PPNCl (73 mg, 0.13 mmol) and anhydride (5.2 mmol, 40 equivalents) were combined in 3 mL of dichloromethane and the solution was injected into the pressure vessel. The dichloromethane was removed under vacuum and cyclohexene oxide (2.5 g, 26 mmol) was injected into the pressure vessel. The vessel was then heated to 100 °C for 30 min allowing the alternating copolymerization of anhydride and epoxide to occur. The vessel was then cooled back to room temperature, pressurized to 40 bar CO_2 and heated to 60 °C for 24 hours. The vessel was then cooled, the mixture was dissolved in dichloromethane and polymer precipitated in cold acidified methanol.

6.5.6 Penta(fluorophenyl)borane catalyzed degradation experiments

100 mg of polymer and BCF (5.1 mg, 1.0 x 10^{-2} mmol, 5 mol%) was combined in 3 mL of dichloromethane and sealed in a microwave vial inside a glovebox. The vial was taken out of the box and heated to 130 °C for 3 hours. The vial was then cooled, opened, a crude sample was taken for ^{1}H NMR analysis and the resulting mixture was concentrated to 1 mL and added to cold acidified methanol to precipitate the resulting polymer.

6.6 References

1. Kozak, C. M.; Ambrose, K.; Anderson, T. S., *Coord. Chem. Rev.* **2018,** *376*, 565-587.

2. Shaikh, R. R.; Pornpraprom, S.; D'Elia, V., *ACS Catal.* **2018,** *8* (1), 419-450.

3. Fiorani, G.; Guo, W.; Kleij, A. W., *Green Chem.* **2015,** *17* (3), 1375-1389.

4. Zhang, D.; Boopathi, S. K.; Hadjichristidis, N.; Gnanou, Y.; Feng, X., *J. Am. Chem. Soc.* **2016,** *138* (35), 11117-11120.

5. Zhang, Y.-Y.; Yang, G.-W.; Xie, R.; Yang, L.; Li, B.; Wu, G.-P., *Angew. Chem. Int. Ed.* **2020,** *59* (51), 23291-23298.

6. Yang, G.-W.; Zhang, Y.-Y.; Xie, R.; Wu, G.-P., *J. Am. Chem. Soc.* **2020,** *142* (28), 12245-12255.

7. Lawson, J. R.; Melen, R. L., *Inorg. Chem.* **2017,** *56* (15), 8627-8643.

8. Stephan, D. W., *Science* **2016,** *354* (6317).

9. Stephan, D. W., *Acc. Chem. Res.* **2015,** *48* (2), 306-316.

10. Melen, R. L., *Science* **2019,** *363* (6426), 479.

11. Andrea, K. A.; Kerton, F. M., *ACS Catal.* **2019,** *9* (3), 1799-1809.

12. Andrea, K. A.; Kerton, F. M., *RSC Adv.* **2019,** *9* (46), 26542-26546.

13. Longo, J. M.; Sanford, M. J.; Coates, G. W., *Chem. Rev.* **2016,** *116* (24), 15167-15197.

14. Zhou, Y.; Hu, C.; Zhang, T.; Xu, X.; Duan, R.; Luo, Y.; Sun, Z.; Pang, X.; Chen, X., *Macromolecules* **2019,** *52* (9), 3462-3470.

15. Carrodeguas, L. P.; Chen, T. T. D.; Gregory, G. L.; Sulley, G. S.; Williams, C. K., *Green Chem.* **2020**.

16. Sulley, G. S.; Gregory, G. L.; Chen, T. T. D.; Peña Carrodeguas, L.; Trott, G.; Santmarti, A.; Lee, K.-Y.; Terrill, N. J.; Williams, C. K., *J. Am. Chem. Soc.* **2020,** *142* (9), 4367-4378.

17. Kernbichl, S.; Reiter, M.; Adams, F.; Vagin, S.; Rieger, B., *J. Am. Chem. Soc.* **2017,** *139* (20), 6787-6790.

18. Winkler, M.; Romain, C.; Meier, M. A. R.; Williams, C. K., *Green Chem.* **2015,** *17* (1), 300-306.

19. Stößer, T.; Mulryan, D.; Williams, C. K., *Angew. Chem. Int. Ed.* **2018,** *57* (51), 16893-16897.

20. Stößer, T.; Williams, C. K., *Angew. Chem. Int. Ed.* **2018,** *57* (21), 6337-6341.

21. Jeske, R. C.; Rowley, J. M.; Coates, G. W., *Angew. Chem., Int. Ed.* **2008,** *47* (32), 6041-6044.

22. Jeon, J. Y.; Eo, S. C.; Varghese, J. K.; Lee, B. Y., *Beilstein J. Org. Chem.* **2014,** *10*, 1787-1795.

23. Saini, P. K.; Fiorani, G.; Mathers, R. T.; Williams, C. K., *Chem. Eur. J.* **2017,** *23* (18), 4260-4265.

24. Liu, Y.; Deng, K.; Wang, S.; Xiao, M.; Han, D.; Meng, Y., *Polym. Chem.* **2015,** *6* (11), 2076-2083.

25. Han, B.; Liu, B.; Ding, H.; Duan, Z.; Wang, X.; Theato, P., *Macromolecules* **2017,** *50* (23), 9207-9215.

26. Chen, T. T. D.; Zhu, Y.; Williams, C. K., *Macromolecules* **2018,** *51* (14), 5346-5351.

27. Ye, S.; Wang, W.; Liang, J.; Wang, S.; Xiao, M.; Meng, Y., *ACS Sus. Chem. Eng.* **2020,** *8* (48), 17860-17867.

28. Liu, S.; Bai, T.; Ni, K.; Chen, Y.; Zhao, J.; Ling, J.; Ye, X.; Zhang, G., *Angew. Chem. Int. Ed.* **2019,** *58* (43), 15478-15487.

29. Chen, S.; Xiao, M.; Sun, L.; Meng, Y., *Int. J. Mol. Sci.* **2018,** *19* (12).

30. Darensbourg, D. J.; Wei, S.-H., *Macromolecules* **2012,** *45* (15), 5916-5922.

31. Schäffner, B.; Schäffner, F.; Verevkin, S. P.; Börner, A., *Chem. Rev.* **2010,** *110* (8), 4554-4581.

Chapter 7 : Conclusions and Future Directions

7.1 Conclusions

The development and production of sustainable materials in a renewable fashion is a growing area of research in the past decade. While production of these materials from a non-petroleum feedstocks is attractive, effective catalyst design remains crucial to allow the controlled and selective production of materials with minimal side products.

At the beginning of **Chapter 1**, an introduction to Green Chemistry and its' 12 Principles is presented. This is followed by a discussion on the promising utilization of carbon dioxide as a C-1 feedstock and challenges that must be overcome allowing the utilization of CO_2 as a starting material. Following this a general section on the reactions of CO_2 and epoxides is presented and gives fundamental background material on the main theme of research upon which this thesis is based. This is followed by a thorough literature review on both iron and boron-based catalysts for these transformations. Both of these sections have been published in review articles of which I am the principal author or co-author.

In **Chapter 2** a series of iron(III) and iron(III) μ-oxo compounds supported by tetradentate amino-bis(phenolate) ligands were synthesized and screened as catalysts for the coupling of CO_2 and epoxides to give exclusively cyclic carbonates. While it was found that these complexes were active catalysts for coupling reactions, the monometallic iron(III) species could undergo an epoxide deoxygenation of the substrate leading to the formation of the corresponding μ-oxo-bridged species. Deoxygenation of epoxides during catalytic reactions with epoxides and CO_2 is often overlooked in the literature and should be considered as an alternative pathway that could occur in these reactions. This work has been published in *Inorg. Chem*. **2018**, 57 (21), 13494-13504.[1]

Chapter 3 builds upon the work reported in **Chapter 2**. At the time while I was working on the deoxygenation studies, a MSc student in Dr. Kozak's group, Erika Butler, was also studying a series of iron complexes based on a trigonal bipyramidal ligand framework for CO_2/epoxide reactions. Together, we noticed several differences in the reactivity of our catalytic systems, specifically in terms of their reactivity towards CO_2/CHO activation to form polycarbonates. Intrigued by these trends, I chose to study these complexes in further detail by synthesizing a series of complexes with varying electronic, steric and structural geometries. It was found that only those complexes in a trigonal bipyramidal structural geometry were active catalysts for polycarbonate formation. This work has been published in *Inorg. Chem.* **2019**, 58 (16), 11231-11240.[2]

Organocatalysts have found footholds in the literature within this field in recent years as there continues to be motivation to move away from using transition metal-based catalysts. Boranes, while extensively studied in the field of Frustrated Lewis Pair chemistry, show promise as catalysts for a variety of reactions due to their varying Lewis acidity. I found that boranes, specifically aryl boranes, were active catalysts for both the production of cyclic and polycarbonates when combined with CO_2 and epoxides. This initial work is presented in **Chapter 4**, has been published in *ACS Catal*. **2019**, 9 (3), 1799-1809.[3]

The BPh_3/PPNCl catalytic system (reported in **Chapter 4**) was successful at copolymerizing CO_2 and vinyl cyclohexene oxide leading to a polymer with an alkene functional group opening the door to potential post-polymerization functionalization of the material. Additionally, in terms of small molecule activation, the more Lewis acidic BCF is well known to catalyze hydrosilylations of unsaturated substrates. Thus, I chose to combine these two research avenues: 1. BPh_3 catalyzed copolymerizations and 2. borane catalyzed hydrosilylations. This led to the successful one pot tandem catalysis of hydrosilylated polymeric materials. This work is discussed in detail in **Chapter 5**, has been published in *RSC Adv.* **2019**, 9, 26542-26546.[4]

Finally, **Chapter 6** focuses on a borane catalyzed system for the block copolymerizations of epoxides, anhydrides and CO_2. This work has been published in Chem. Commun., 2021, DOI: 10.1039/D1CC02218K. Not only was the same borane catalytic system reported in **Chapters 3 and 4** active towards both polyester (epoxide/anhydride) and polycarbonate (epoxide/CO_2) containing materials, but by using a more Lewis acidic borane (i.e. BCF rather than BPh_3) I could selectively degrade the carbonate block into the corresponding cyclic carbonate.

7.2 Future work and directions

With respect to the research on iron containing catalysts discussed in **Chapters 2 and 3** there is certainly room for further exploration of these systems in polymerization reactions. Specifically, since my time working on these systems a doctoral student in the Kozak group has been studying their activity for the ROP of *rac*-lactide to produce well-defined polylactide under mild reaction conditions. Of particular interest would be the study of those complexes in **Chapter 3** active towards CHO/CO_2 polymerization to yield PCHC. If these complexes were active towards the polymerization of VCHO and CO_2, this would allow production of a polymeric material that could be further functionalized (similar to the work discussed in **Chapters 4 and 5**). Additionally, these complexes have been reported by Shaver et al. to catalyze controlled radical polymerizations between styrene and methyl methacrylate.[5] It would be worth exploring if VCHO/CO_2 could be polymerized, post polymerization functionalization via a second radical mediated process yielding a new branched polymeric material.

As I was the first student in the Kerton group to work with aryl boranes, along with my work on aryl boranes being the first in the literature for CO_2/epoxide-based reactions there is still many unanswered questions and avenues this research can be further explored. Building upon the results in **Chapters 4-6**, that only BPh_3 was an active polymerization catalyst while the more Lewis acidic BCF was inactive towards polymerization alludes to the strong importance of Lewis acidity on reactivity. Additionally, as reported in **Chapter 6** only BCF was active towards the depolymerization of produced polymers. As only preliminary studies were carried out on the depolymerization work there are still many avenues to explore. In particular it would be interesting to study the degradation kinetics and mechanistic steps in further detail. These results, along with the concept of redox-switchable catalysis (RSC) opens the door to a new avenue of controlled/switchable polymerizations. RSCs are based on the concept of manipulating the catalytic activity of the metal centre through oxidation/reduction of the coordinated ligand.[6-7] In homogeneous metal catalyzed processes, ferrocene is often included in the ligand backbone as it is easily functionalized and can be reversibly oxidized and reduced.[8-10] Another option is directly changing the oxidation state of the metal at the centre of the catalyst and this has been shown to ‘switch-on’ reactivity within the catalytic system.[11] During my doctoral studies, particularity as a component of my Vanier proposal, I proposed the development of a redox-switchable borane catalyst. Through introduction of redox active groups around the boron centre, I proposed I would create a more active catalyst, while introducing the option of switching catalysis on/off leading to increased control of the copolymer microstructures.[12-16] For example, a neutral ferrocene-tagged, Fe^{II}, Fc-BAr_3 should behave in a similar way to BAr_3. However, upon oxidation to a ferrocenium-tagged, Fe^{III}, $[Fc\text{-}BAr_3]^+$, the boron centre should become more Lewis acidic and therefore possess greater potential towards activating epoxides towards ring-opening (**Figure 7.1**). If the boron centre is more Lewis acidic, it may be possible to first polymerize epoxides/CO_2, then through a redox switch, the Lewis acidity could be altered and change to depolymerization. As well, by fine-tuning the Lewis acidity I may be able to incorporate a wider range of epoxides that initially were not reactive when using BPh_3 in our initial studies. Due to time constraints, in particular decreased lab access during the COVID-19 pandemic initial studies on this proposed project were not completed. However, a current doctoral student in the Kerton group will be investigating this work in further detail.

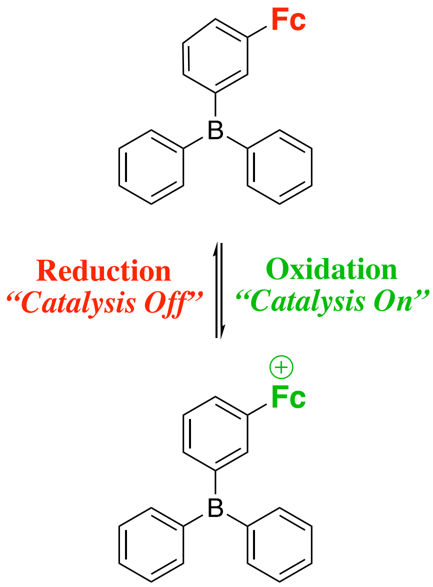

Figure 7.1. Proposed redox-active ferrocenium-tagged triphenylborane

7.3 References

1. Andrea, K. A.; Brown, T. R.; Murphy, J. N.; Jagota, D.; McKearney, D.; Kozak, C. M.; Kerton, F. M., *Inorg. Chem.* **2018,** *57* (21), 13494-13504.

2. Andrea, K. A.; Butler, E. D.; Brown, T. R.; Anderson, T. S.; Jagota, D.; Rose, C.; Lee, E. M.; Goulding, S. D.; Murphy, J. N.; Kerton, F. M.; Kozak, C. M., *Inorg. Chem.* **2019,** *58* (16), 11231-11240.

3. Andrea, K. A.; Kerton, F. M., *ACS Catal.* **2019,** *9* (3), 1799-1809.

4. Andrea, K. A.; Kerton, F. M., *RSC Adv.* **2019,** *9* (46), 26542-26546.

5. Allan, L. E. N.; MacDonald, J. P.; Reckling, A. M.; Kozak, C. M.; Shaver, M. P., *Macromol. Rapid Commun.* **2012,** *33* (5), 414-418.

6. Luca, O. R.; Crabtree, R. H., *Chem. Soc. Rev.* **2013,** *42* (4), 1440-1459.

7. Allgeier, A. M.; Mirkin, C. A., *Angew. Chem. Int. Ed.* **1998,** *37* (7), 894-908.

8. Savka, R.; Foro, S.; Gallei, M.; Rehahn, M.; Plenio, H., *Chem. Eur. J.,* **2013,** *19* (32), 10655-10662.

9. Klenk, S.; Rupf, S.; Suntrup, L.; van der Meer, M.; Sarkar, B., *Organometallics* **2017,** *36* (10), 2026-2035.

10. Broderick, E. M.; Guo, N.; Vogel, C. S.; Xu, C.; Sutter, J.; Miller, J. T.; Meyer, K.; Mehrkhodavandi, P.; Diaconescu, P. L., *J. Am. Chem. Soc.* **2011,** *133* (24), 9278-9281.

11. Biernesser, A. B.; Li, B.; Byers, J. A., *J. Am. Chem. Soc.* **2013,** *135* (44), 16553-16560.

12. Beller, M., *Adv. Synth. Catal.* **2004,** *346* (2-3), 107-108.

13. Huang, W.; Diaconescu, P. L., *Inorg. Chem.* **2016,** *55* (20), 10013-10023.

14. Quan, S. M.; Wang, X.; Zhang, R.; Diaconescu, P. L., *Macromolecules* **2016,** *49* (18), 6768-6778.

15. Shepard, S. M.; Diaconescu, P. L., *Organometallics* **2016,** *35* (15), 2446-2453.

16. Wang, X.; Thevenon, A.; Brosmer, J. L.; Yu, I.; Khan, S. I.; Mehrkhodavandi, P.; Diaconescu, P. L., *J. Am. Chem. Soc.* **2014,** *136* (32), 11264-11267.

Appendix A

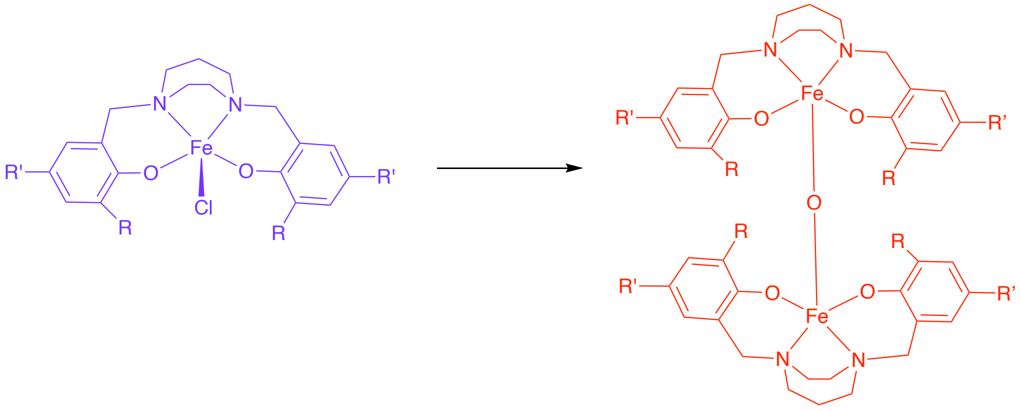

R = R' = *t*-Bu (**2.1**)
R = R '= Me (**2.2**)
R = R' = Cl (**2.3**)
R = tBu, R' = OMe (**2.4**)
R = tBu, R' = Me (**2.5**)

R = R' = *t*-Bu (**2.6**)
R = R '= Me (**2.7**)
R = R' = Cl (**2.8**)
R = tBu, R' = OMe (**2.9**)
R = tBu, R' = Me (**2.10**)

Figure A. 1. Color change upon oxo-bridged complex formation from chloride complex. In situ color change within modified pressure vessel (bottom).

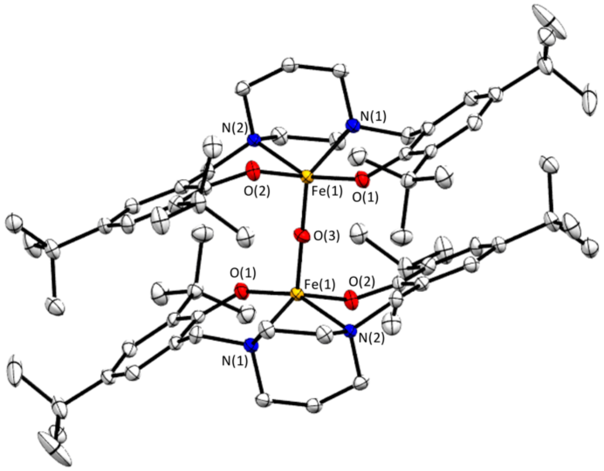

Figure A. 2. Molecular structure (ORTEP) and partial numbering scheme for **2.6**. Ellipsoids are shown at the 50% probability levels (H-atoms and solvent omitted for clarity).

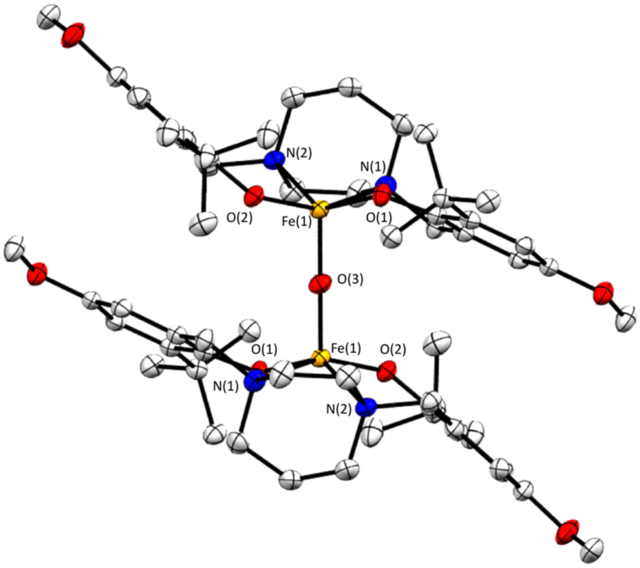

Figure A. 3. Molecular structure (ORTEP) and partial numbering scheme for **2.9**. Ellipsoids are shown at the 50% probability levels (H-atoms and solvent omitted for clarity).

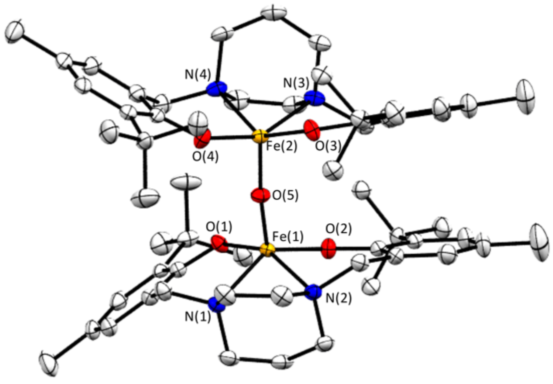

Figure A. 4. Molecular structure (ORTEP) and partial numbering scheme for **2.10**. Ellipsoids are shown at the 50% probability levels (H-atoms and solvent omitted for clarity).

Table A. 1. Crystallographic data and structure refinement for **2.6**, **2.8** and **2.10**.

Compound	**2.6**	**2.8**	**2.9**	**2.10**
Empirical Formula	$C_{70}H_{108}Fe_2N_4O_5$	$C_{40}H_{42}Cl_{12}Fe_2N_4O_6$	$C_{58}H_{84}Fe_2N_4O_9$	$C_{59}H_{86}Cl_2Fe_2N_4O_5$
CCDC no.	1585843	1585844	1864898	1585845
Formula Weight	1197.30	1211.87	1092.99	1113.91
Temperature/K	100	100	100	100
Crystal Color	Red	Red	Red	Red
Crystal System	Monoclinic	Triclinic	Monoclinic	Monoclinic
Crystal Dimensions/mm^3	0.28 x 0.22 x 0.09	0.19 x 0.13 x 0.12	0.3 x 0.25 x 0.1	0.23 x 0.2 x 0.15
Lattice Parameters	a = 10.6584(18) Å	a = 9.4993(3) Å	a = 14.8416(3) Å	a = 18.528(3) Å
	b = 27.833(5) Å	b = 13.5246(5) Å	b = 13.2846(2) Å	b = 14.6589(19) Å
	c = 10.9821(18) Å	c = 20.0226(7) Å	c = 15.8226(4) Å	c = 21.693(3) Å
	α = 90°	α = 97.193(2)°	α = 90°	α = 90°
	β = 91.339(2)°	β = 90.687(2)°	β = 116.307(3)°	β = 93.795(2)°
	γ = 90°	γ = 109.295(2)°	γ = 90°	γ = 90°
Space Group	$P2_1/c$	P-1	$P2_1/n$	$P2_1/n$
Z value	2	2	2	4
D_{calc}	1.221	1.674	1.298	1.259
F_{000}	1296.0	1228.0	1168.0	2376.0
μ (MoKα)	0.497	1.320	0.577	0.633
Reflections collected	33850	31940	36197	61075
Independent reflections	6171	9130	5304	11157
R_{int}	0.0733	0.0654	0.0419	0.0709
R, wR_2 (all)^a	0.0857, 0.1639	0.0878, 0.1498	0.0511, 0.1212	0.0936, 0.1892
R, wR_2 {I>=2σ (I)]^a	0.0596, 0.1504	0.0547, 0.1322	0.0485, 0.1190	0.0653, 0.1693
GOF-fit on F^2	1.079	1.032	1.118	1.037

Table A. 2. Selected Bond lengths (Å) and angles (°) for **2.6** and **2.9**.

	2.6	**2.9**
Fe(1)-O(1)	1.887(2)	1.7722(3)
Fe(1)-O(2)	1.912(2)	1.8966(15)
Fe(1)-O(3)	1.7729(6)	1.9070(15)
Fe(1)-N(1)	2.213(3)	2.1791(18)
Fe(1)-N(2)	2.196(3)	2.2004(18)
O(1)-Fe(1)-O(2)	98.90(11)	110.17(5)
O(1)-Fe(1)-N(1)	84.66(11)	107.29(5)
O(1)-Fe(1)-N(2)	137.16(11)	91.53(5)
O(2)-Fe(1)-N(1)	155.74(11)	136.27(7)
O(3)-Fe(1)-O(1)	109.42(8)	108.85(5)
O(3)-Fe(1)-O(2)	109.71(8)	100.59(6)
O(3)-Fe(1)-N(1)	91.34(8)	87.73(6)
O(3)-Fe(1)-N(2)	107.51(8)	155.69(7)
N(2)-Fe(1)-N(1)	73.47(11)	73.27(7)
Fe(1)-O(3)-Fe(1)	180.0	180.0

Table A. 3. Selected Bond lengths (Å) and angles (°) for **2.8** and **2.10**.

	2.8	**2.10**
Fe(1)-O(1)	1.907(3)	1.915(3)
Fe(1)-O(2)	1.896(3)	1.890(3)
Fe(1)-O(5)	1.770(3)	1.779(3)
Fe(1)-N(1)	2.151(4)	2.185(3)
Fe(1)-N(2)	2.180(4)	2.211(3)
Fe(2)-O(3)	1.913(3)	1.895(3)
Fe(2)-O(4)	1.918(3)	1.912(3)
Fe(2)-O(5)	1.769(3)	1.775(3)
Fe(2)-N(3)	2.168(4)	2.199(4)
Fe(2)-N(4)	2.156(4)	2.177(3)
O(1)-Fe(1)-N(1)	88.95(13)	88.71(13)
O(1)-Fe(1)-N(2)	154.29(14)	154.33(13)
O(2)-Fe(1)-O(1)	93.95(13)	99.42(12)
O(2)-Fe(1)-N(1)	137.12(15)	139.55(13)
O(2)-Fe(1)-N(2)	86.27(14)	84.32(13)
O(5)-Fe(1)-O(1)	107.20(14)	107.58(13)
O(5)-Fe(1)-O(2)	115.07(15)	112.42(13)
O(5)-Fe(1)-N(1)	104.68(14)	102.37(13)
O(5)-Fe(1)-N(2)	95.84(14)	94.07(13)
N(1)-Fe(1)-N(2)	73.97(14)	72.95(13)
O(3)-Fe(2)-O(4)	93.27(13)	98.84(13)
O(3)-Fe(2)-N(3)	86.56(14)	84.85(13)
O(3)-Fe(2)-N(4)	139.10(15)	139.48(13)
O(4)-Fe(2)-N(3)	152.53(14)	153.58(13)
O(4)-Fe(2)-N(4)	88.61(13)	88.62(13)
O(5)-Fe(2)-O(3)	114.81(15)	114.50(13)
O(5)-Fe(2)-O(4)	107.64(14)	106.57(14)
O(5)-Fe(2)-N(3)	97.22(14)	95.35(13)
O(5)-Fe(2)-N(4)	103.33(15)	101.00(13)
N(4)-Fe(2)-N(3)	74.16(14)	72.55(14)
Fe(2)-O(5)-Fe(1)	171.92(19)	171.75(19)

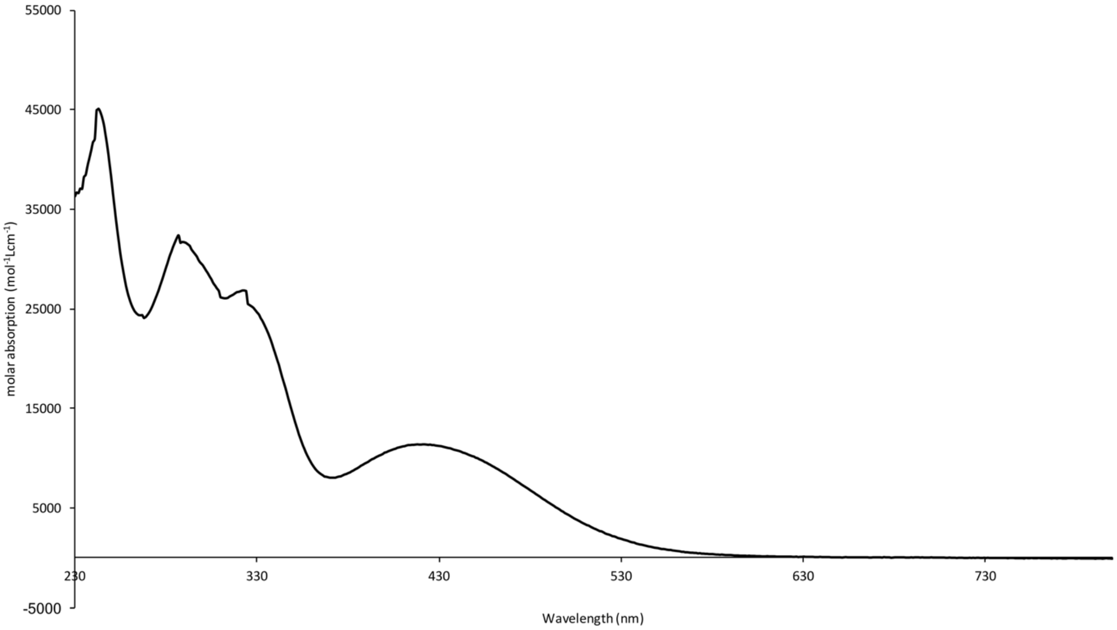

Figure A. 5. Electronic absorption spectrum of **2.6** in dichloromethane.

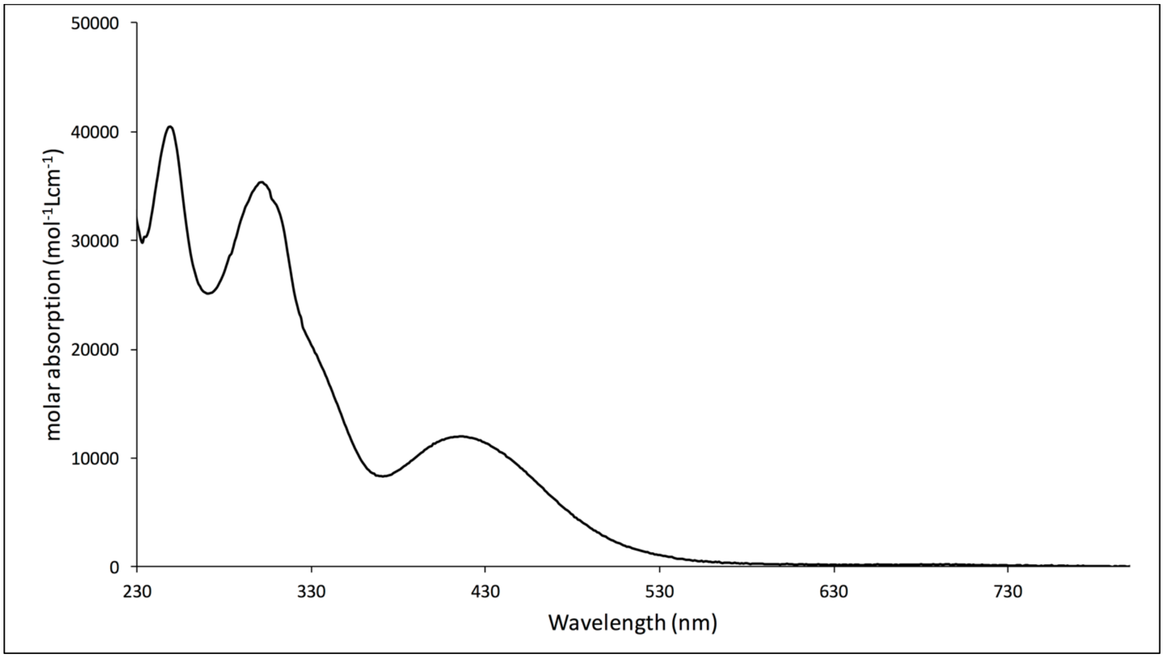

Figure A. 6. Electronic absorption spectrum of **2.8** in dichloromethane.

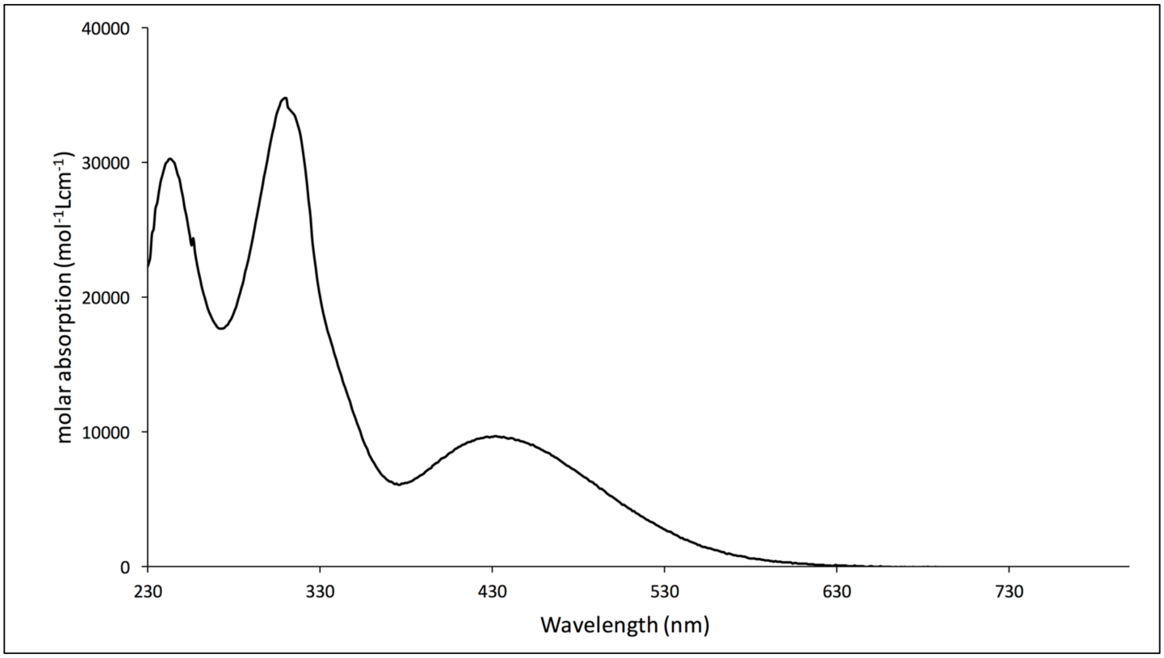

Figure A. 7. Electronic absorption spectrum of **2.9** in dichloromethane.

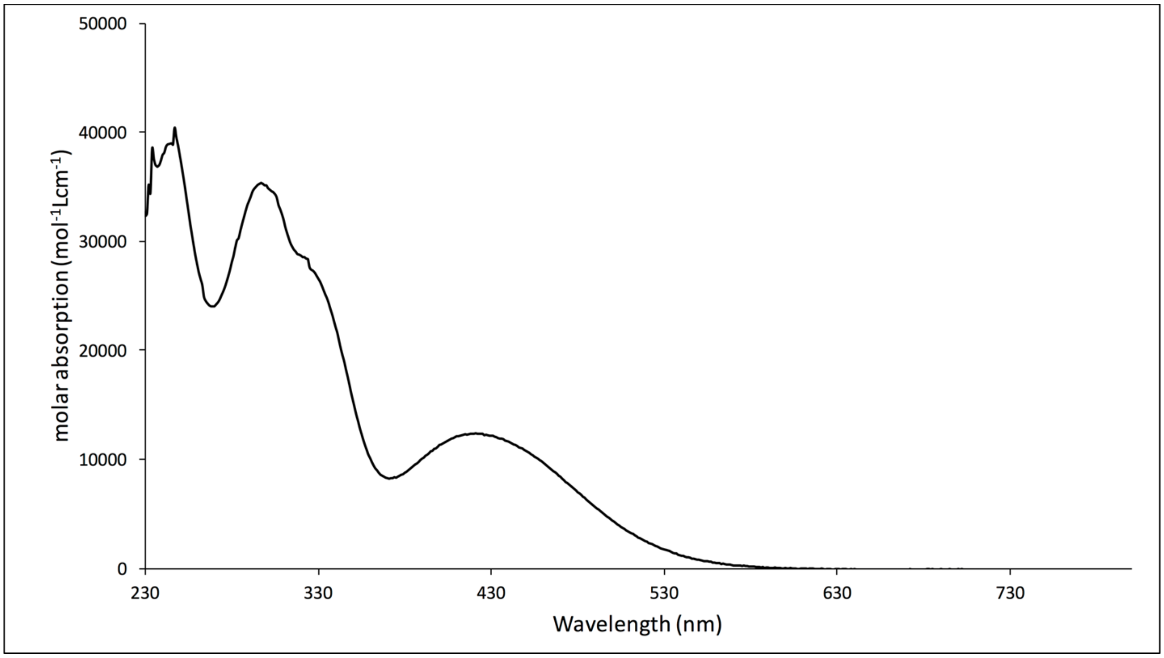

Figure A. 8. Electronic absorption spectrum of **2.10** in dichloromethane.

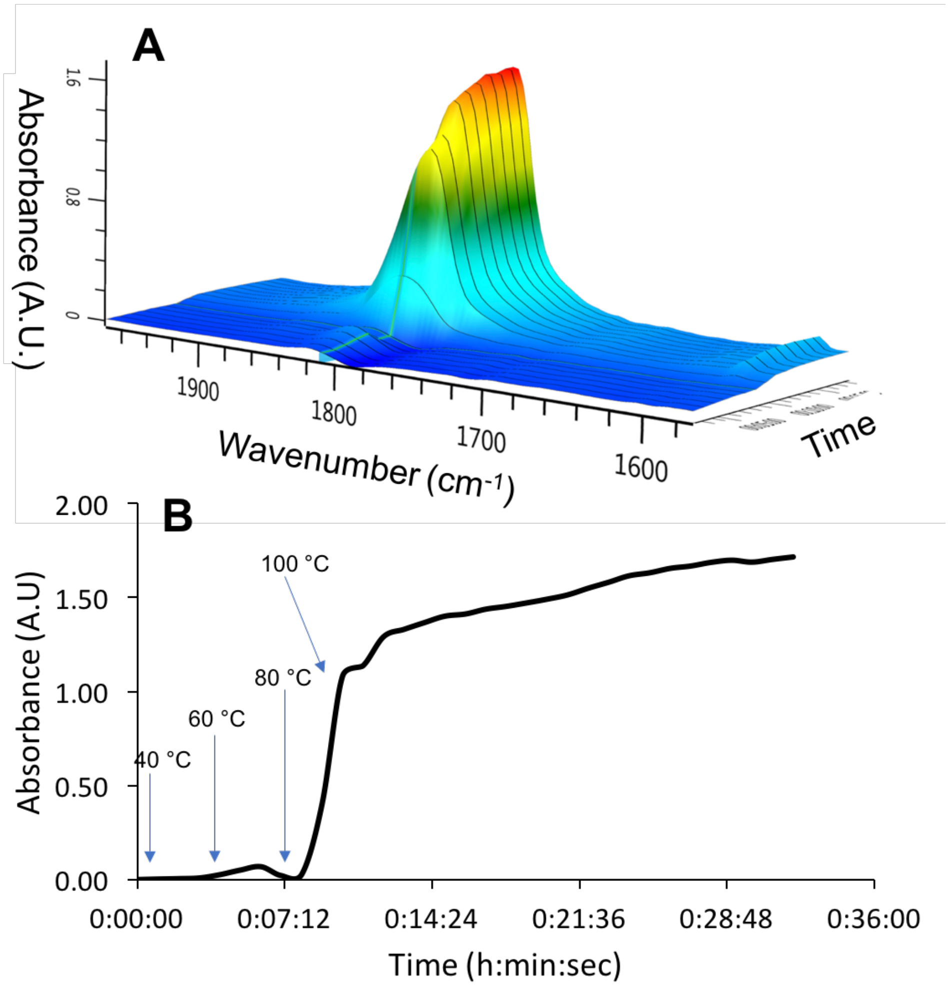

Figure A. 9. In situ React-IR monitoring showing selective formation of cyclic carbonate by **2.6**. (A) 3-D surface diagram of region between 1580 and 1960 cm^{-1} showing presence of one carbonate-containing product. (B) Time profile of band at 1809 cm^{-1} corresponding to carbonyl of propylene carbonate and temperature effect on reaction initiation.

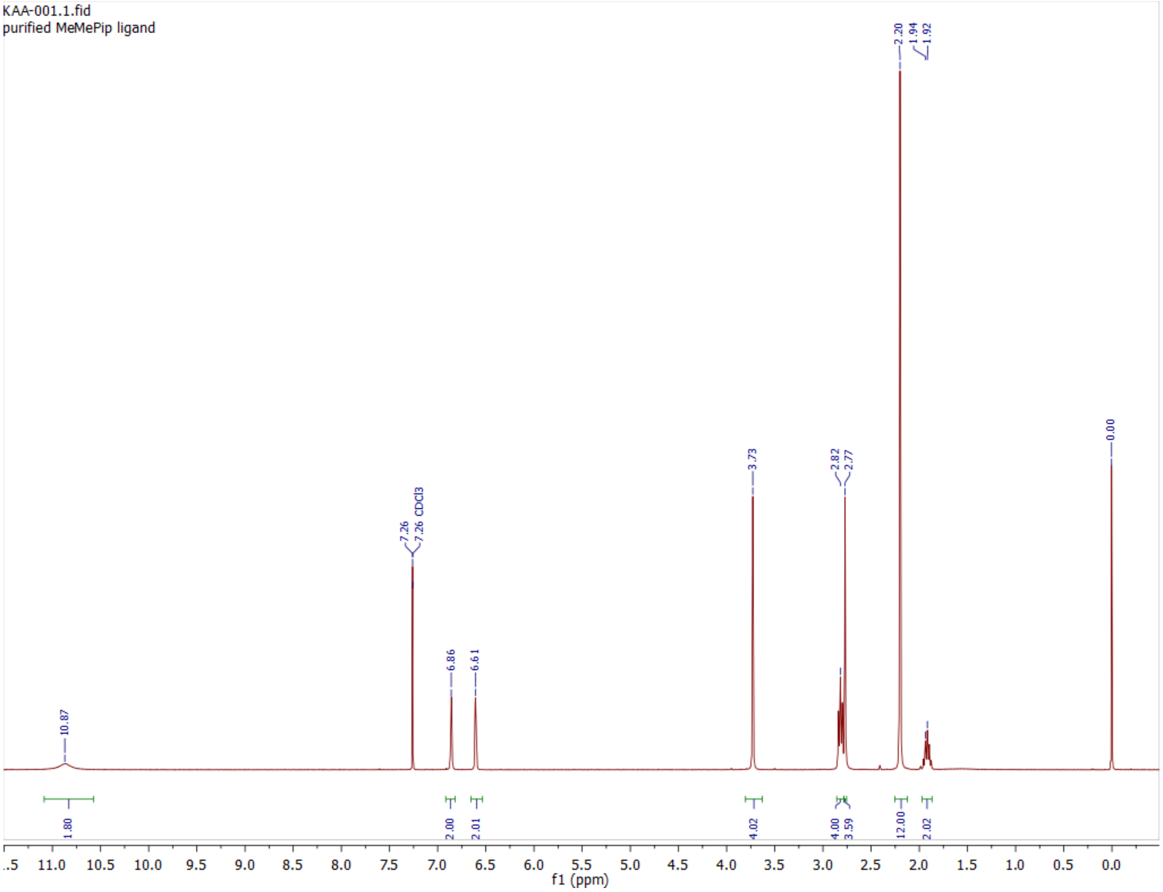

Figure A. 10. ^{1}H NMR spectrum (300 MHz, 298 K, $CDCl_3$) of H_2L**2.2**.

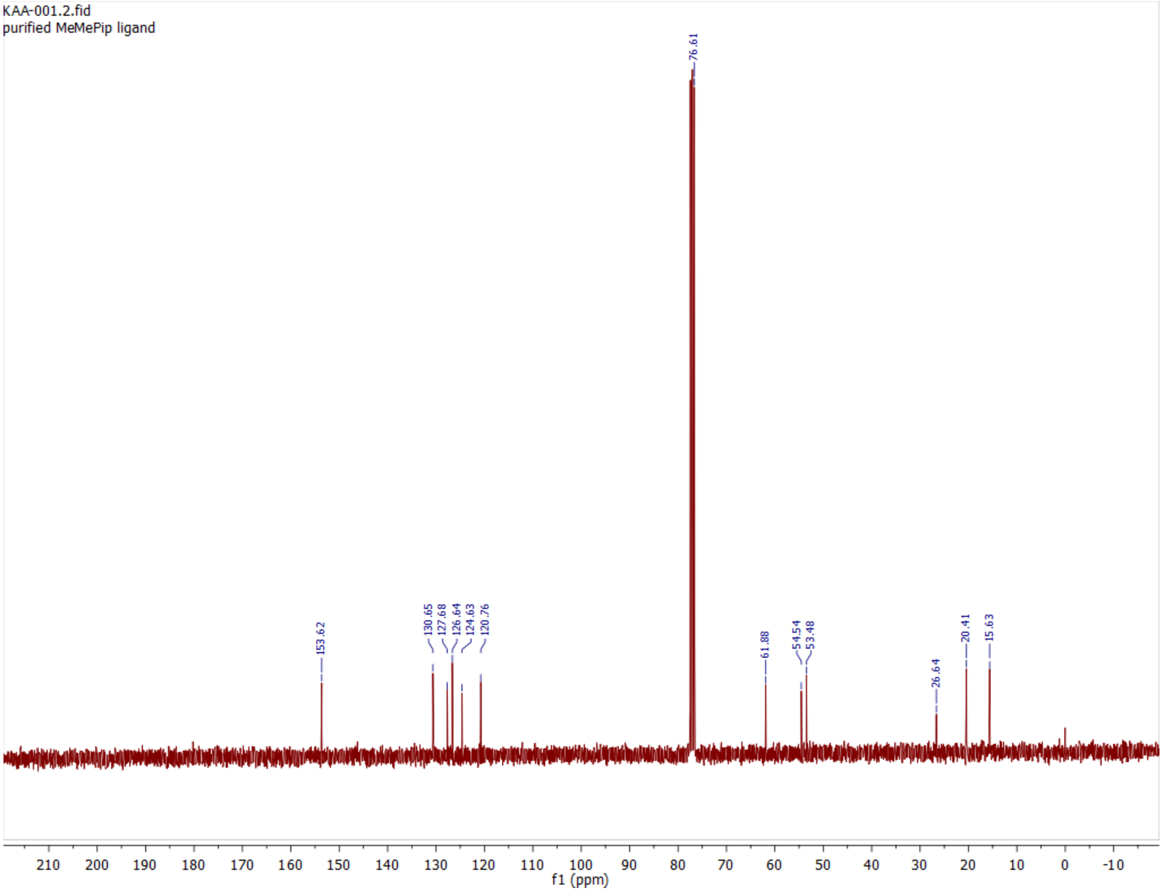

Figure A. 11. ^{13}C NMR spectrum (75 MHz, 298 K, $CDCl_3$) of H_2L**2.2**.

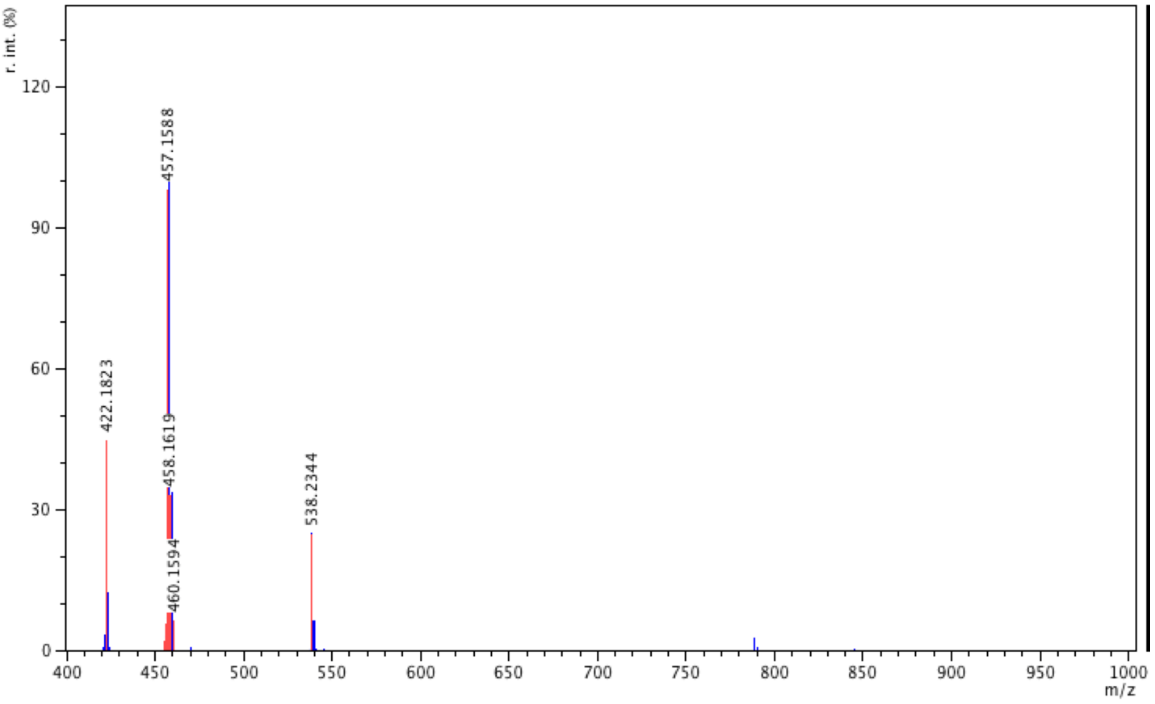

Figure A. 12. MALDI-TOF mass spectrum of **2.2**.

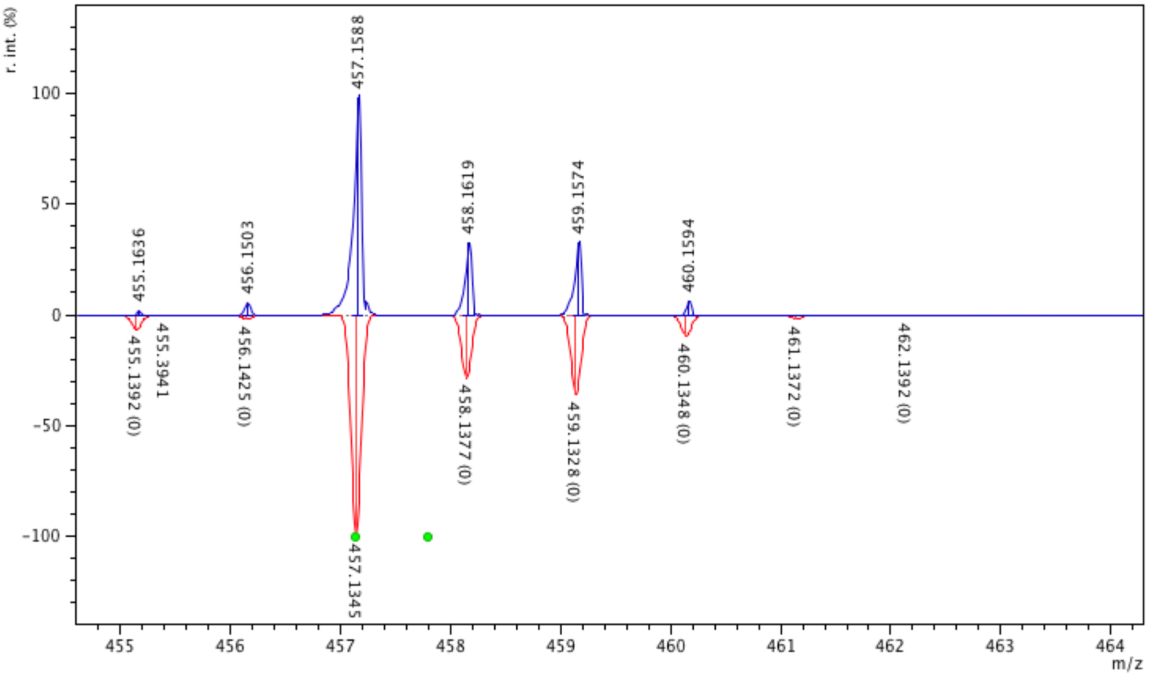

Figure A. 13. Theoretical and experimental isotopic distribution pattern of **2.2**.

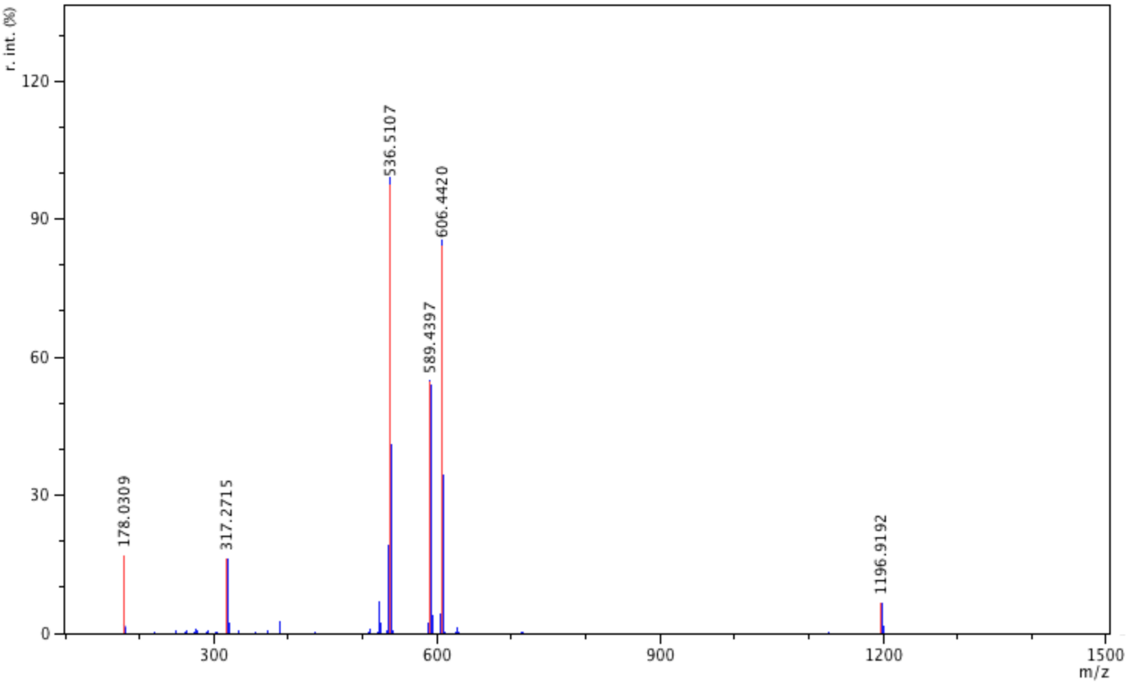

Figure A. 14. MALDI-TOF mass spectrum of **2.6**.

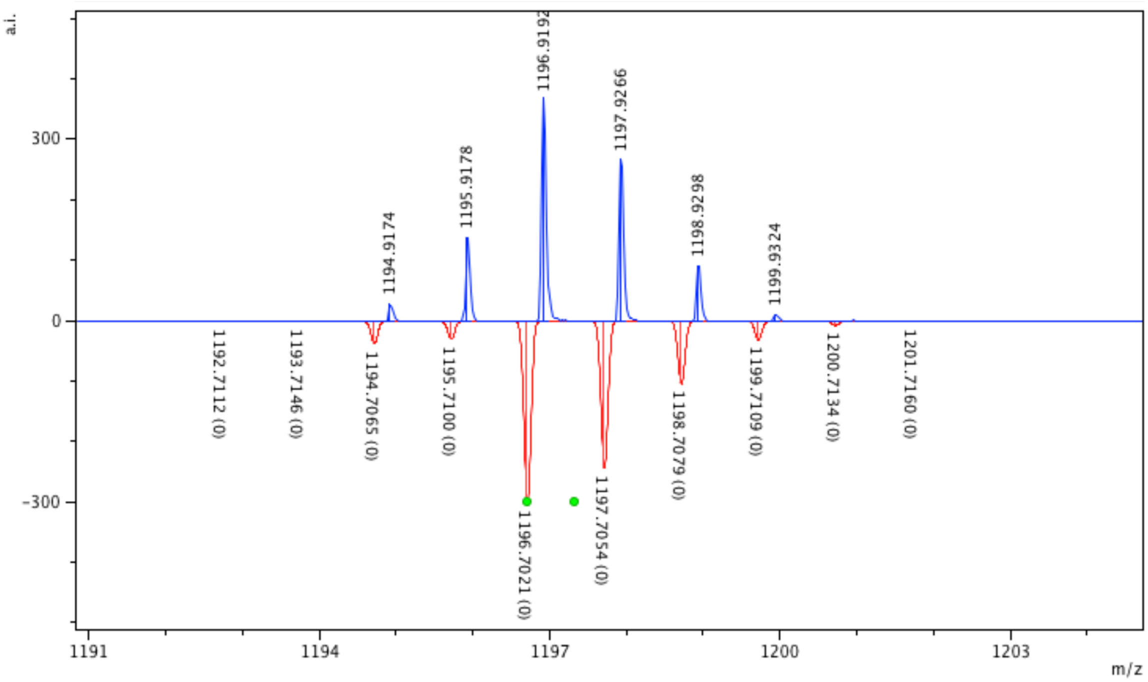

Figure A. 15. Theoretical and experimental isotopic distribution pattern of **2.6**.

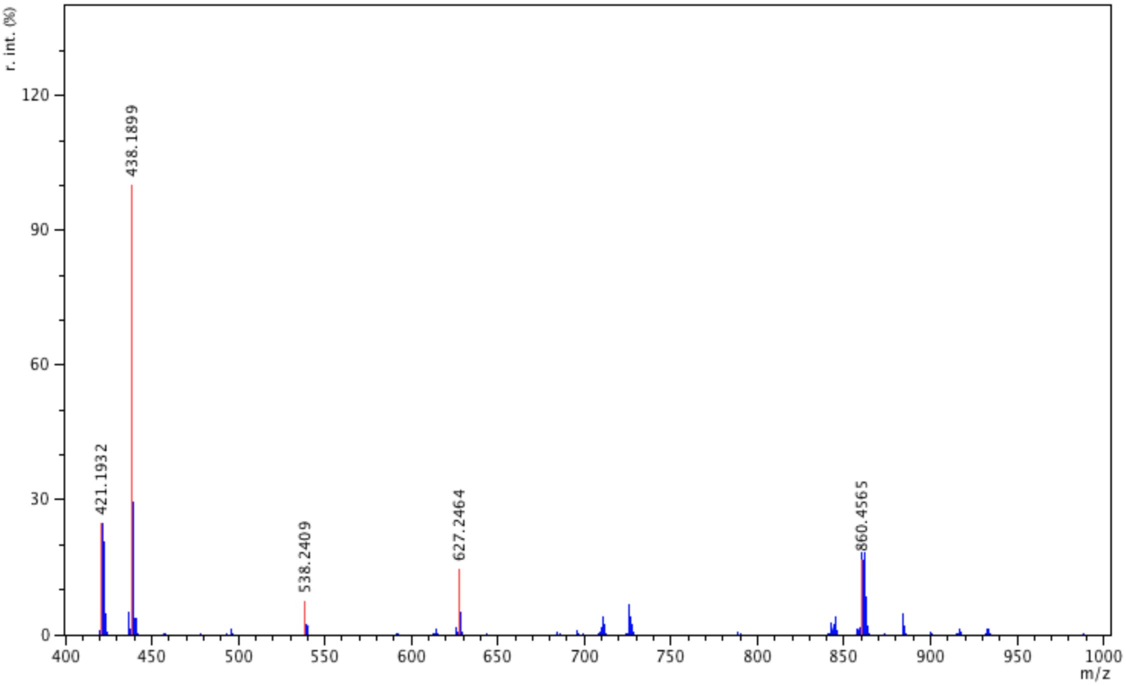

Figure A. 16. MALDI-TOF mass spectrum of **2.7**.

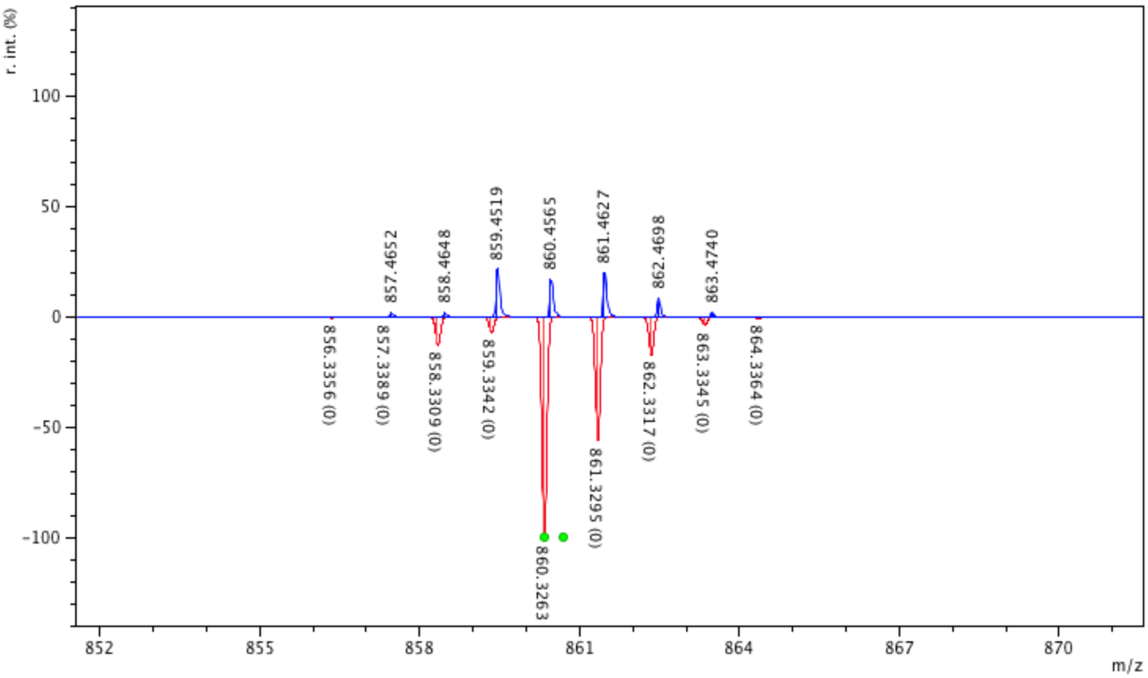

Figure A. 17. Theoretical and experimental isotopic distribution pattern of **2.7**.

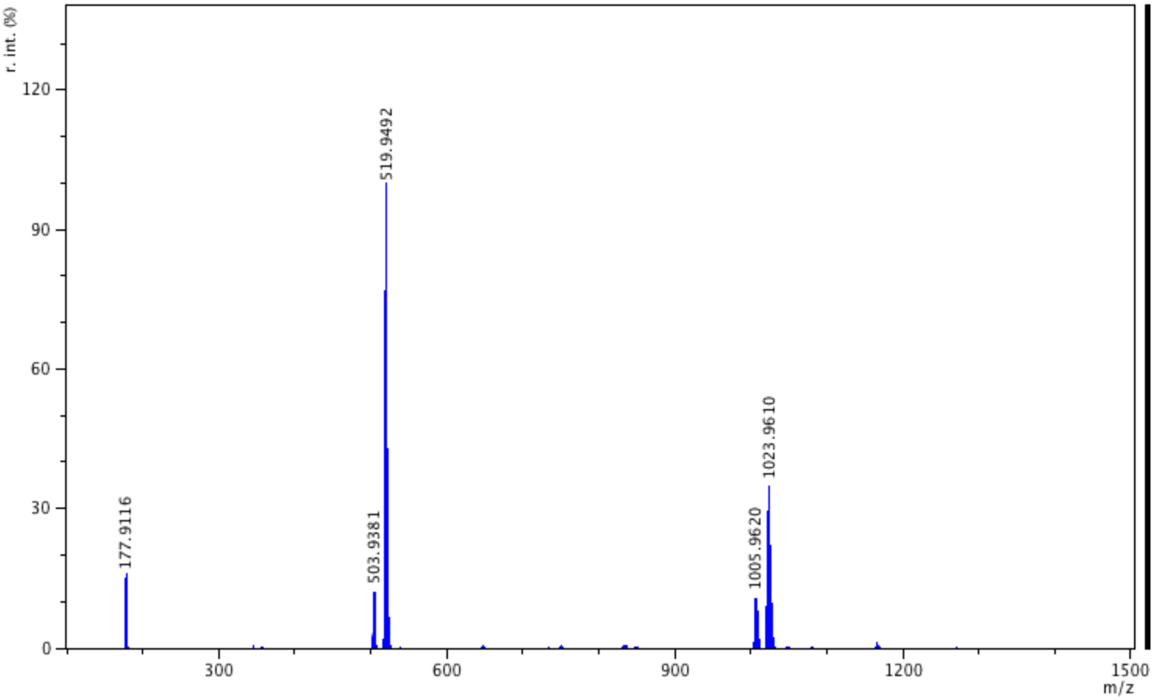

Figure A. 18. MALDI-TOF mass spectrum of **2.8**.

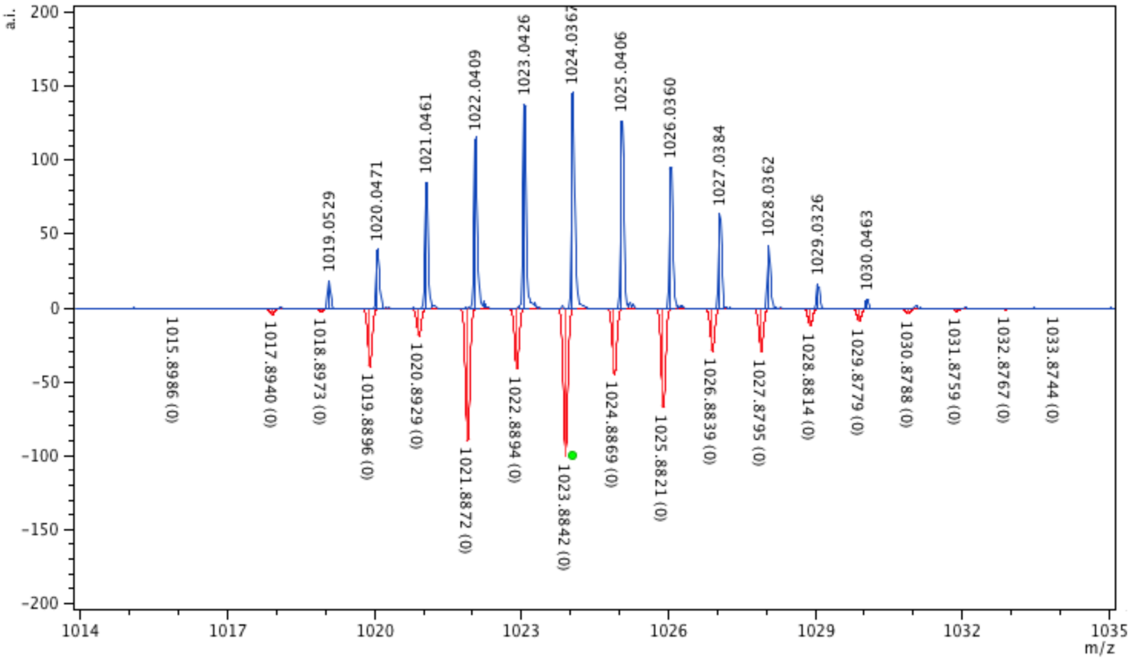

Figure A. 19. Theoretical and experimental isotopic distribution pattern of **2.8**.

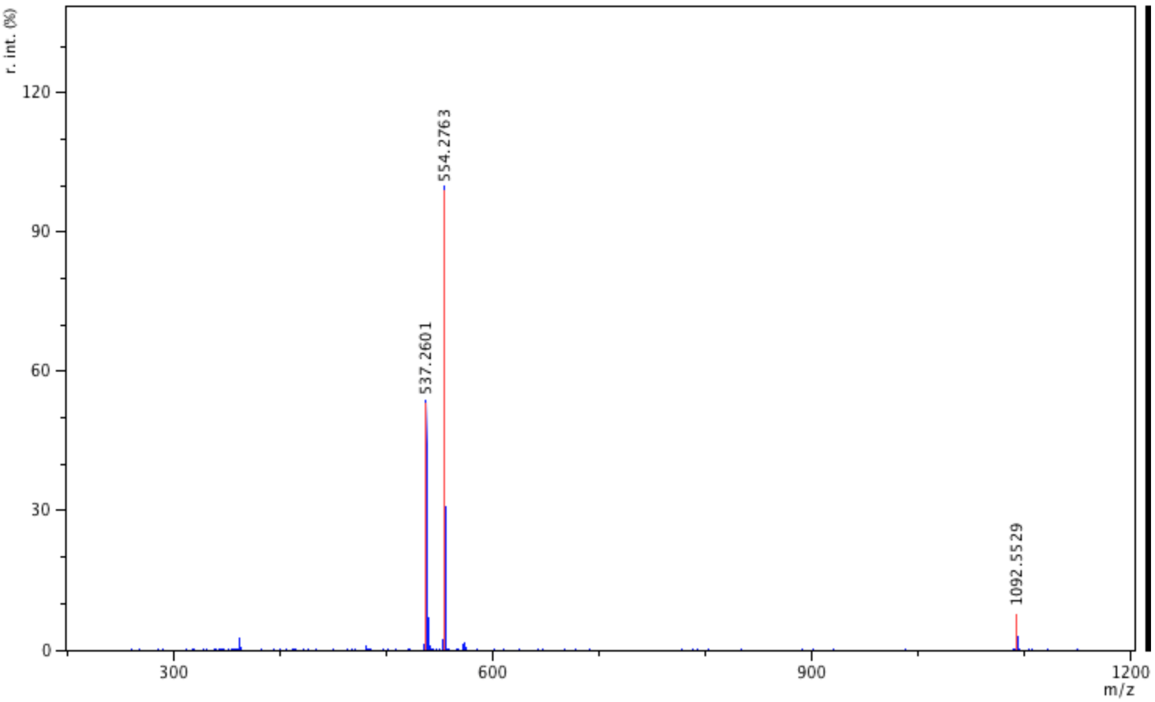

Figure A. 20. MALDI-TOF mass spectrum of **2.9**.

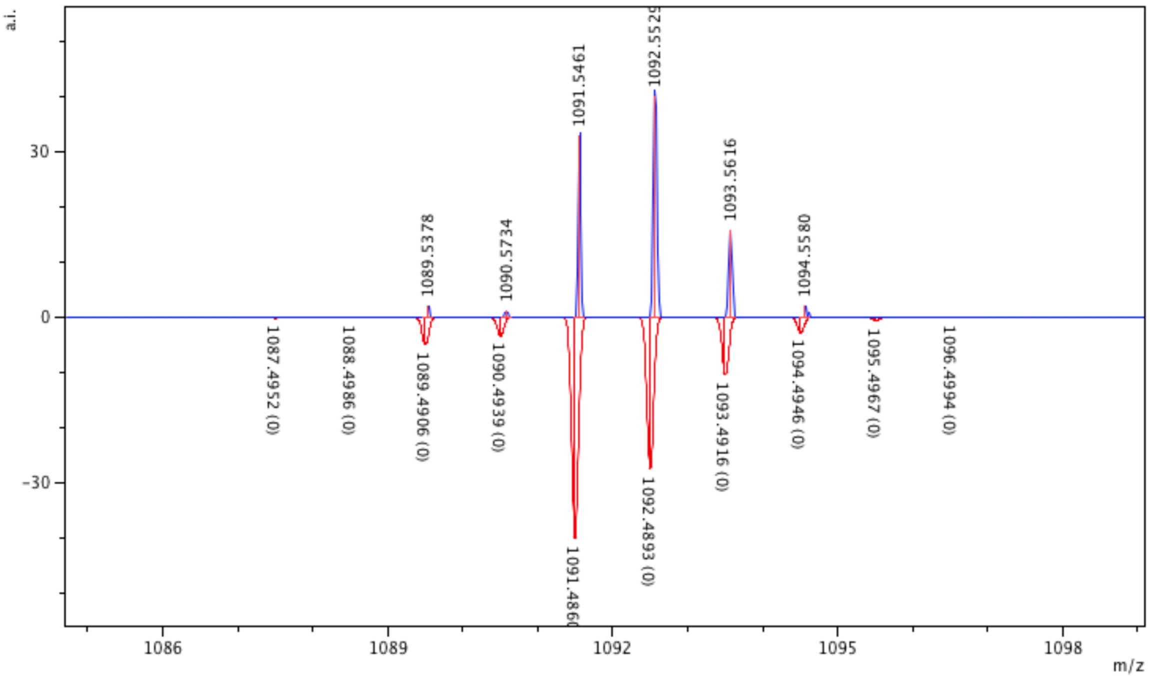

Figure A. 21. Theoretical and experimental isotopic distribution pattern of **2.9**.

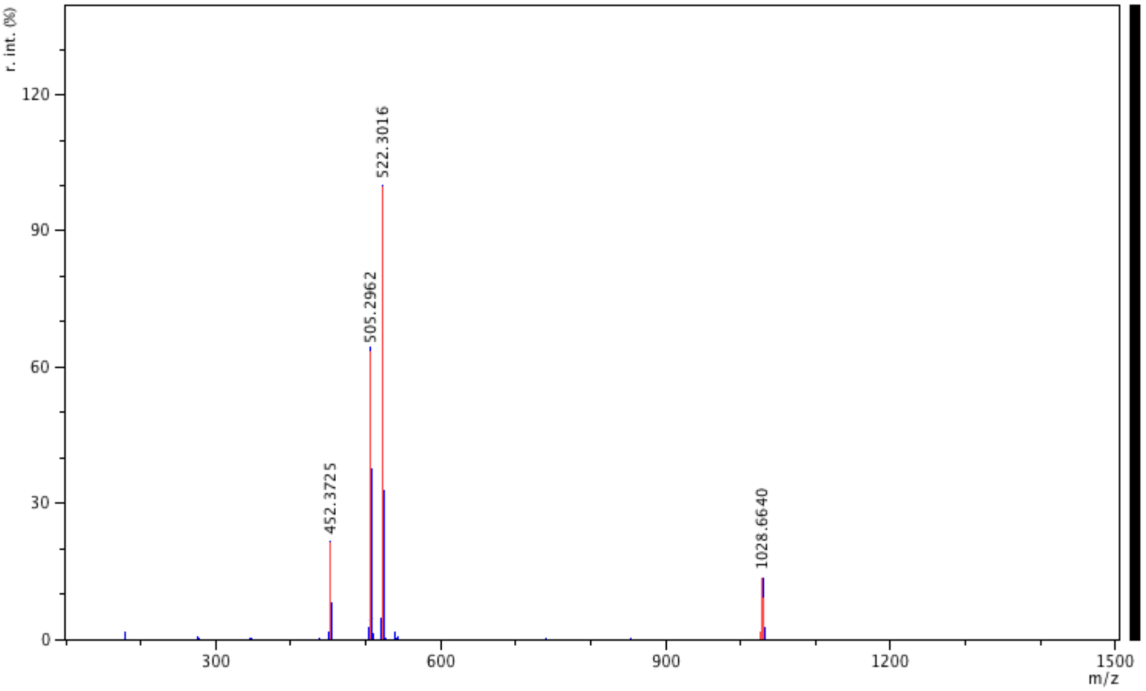

Figure A. 22. MALDI-TOF mass spectrum of **2.10**.

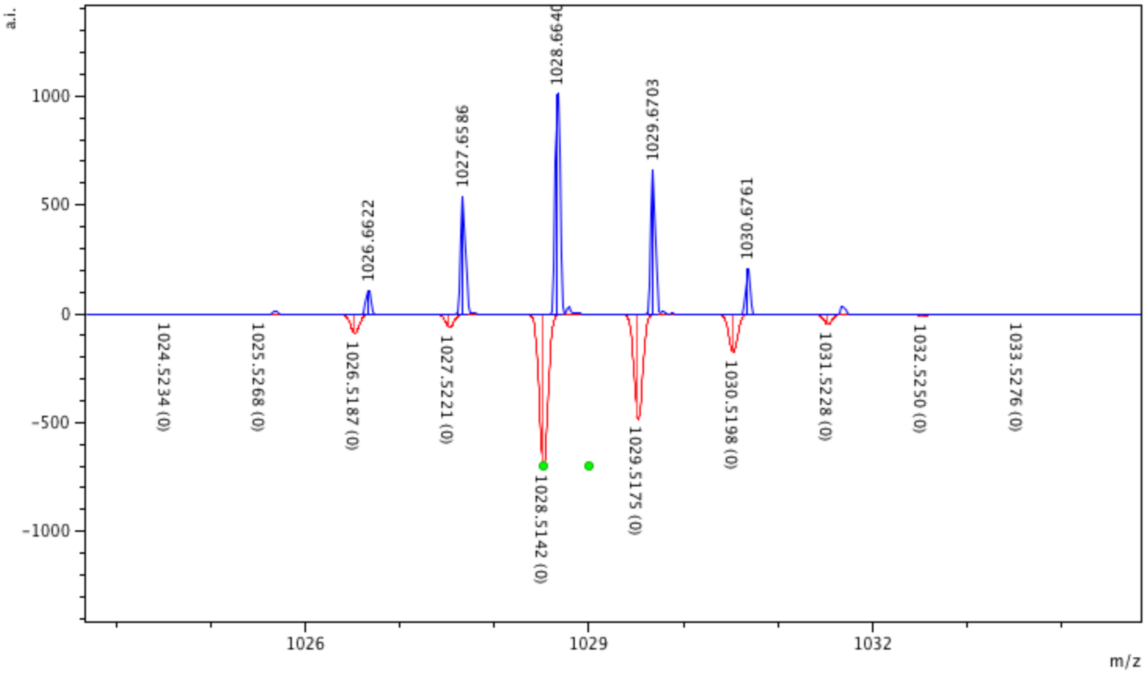

Figure A. 23. Theoretical and experimental isotopic distribution pattern of **2.10**.

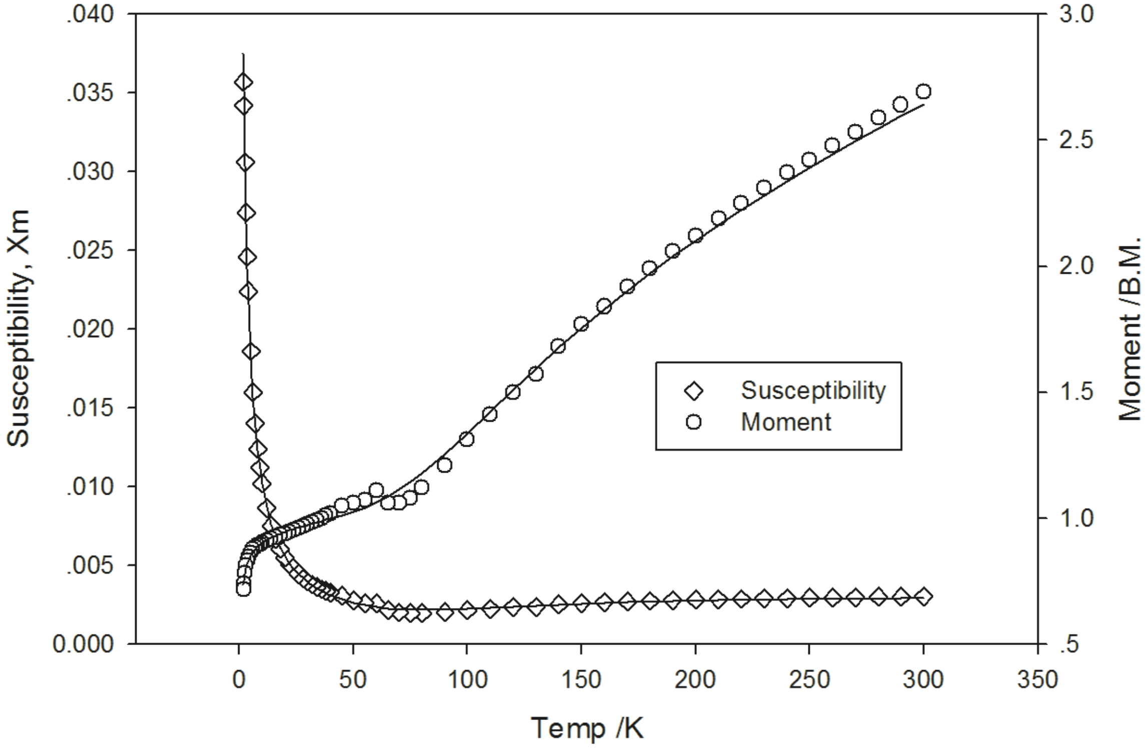

Figure A. 24. Magnetic susceptibility and moment vs temperature plots for solid **2.6** at 1 T. The solid lines are the fits to the experimental data with fitting parameters as described in Table 1.

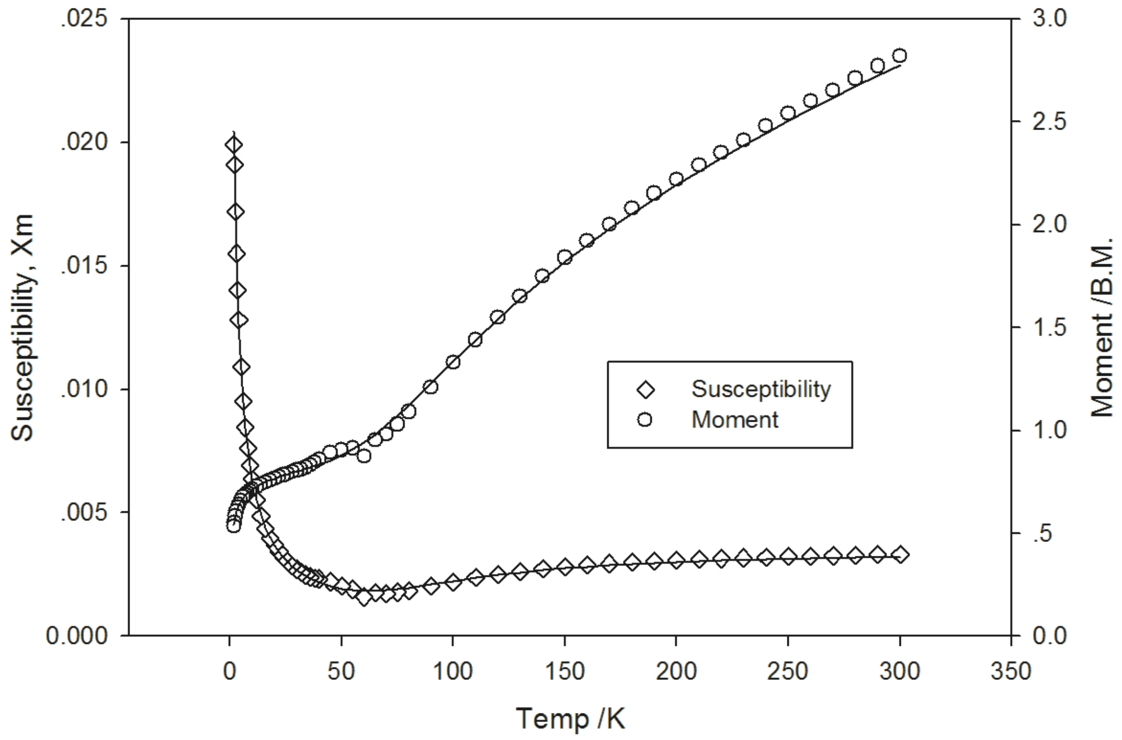

Figure A. 25. Magnetic susceptibility and moment vs temperature plots for solid **2.7** at 1 T. The solid lines are the fits to the experimental data with fitting parameters as described in Table 1.

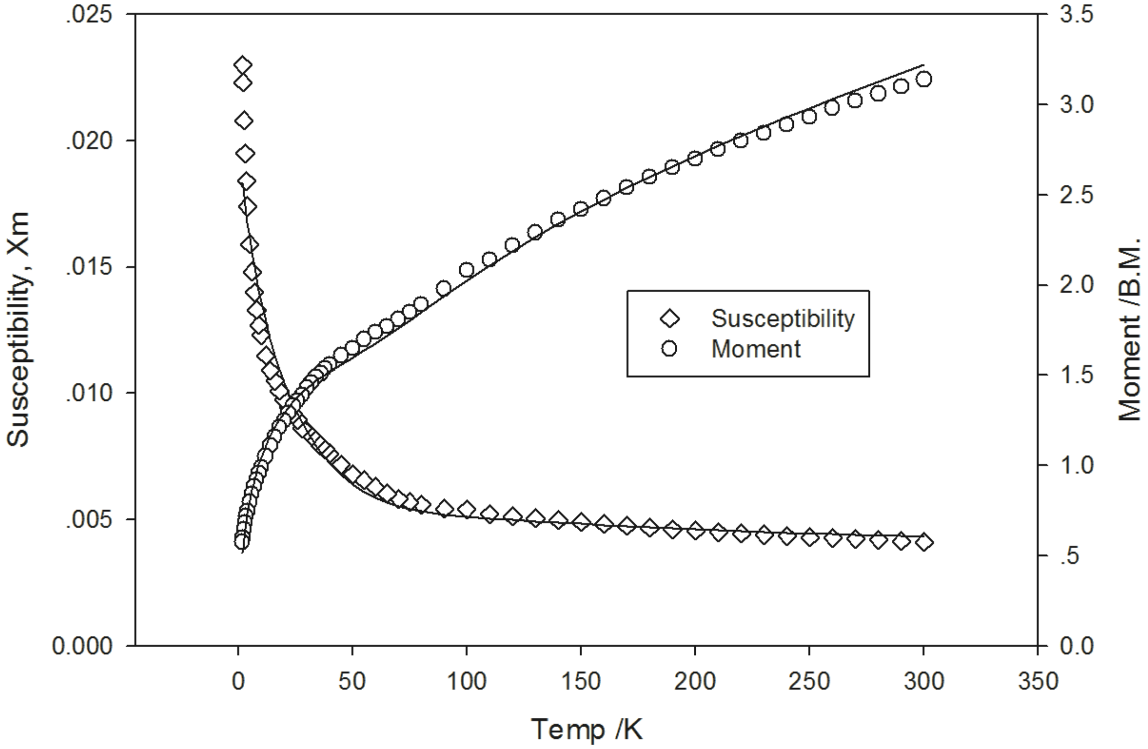

Figure A. 26. Magnetic susceptibility and moment vs temperature plots for solid **2.8** at 1 T. The solid lines are the fits to the experimental data with fitting parameters as described in Table 1.

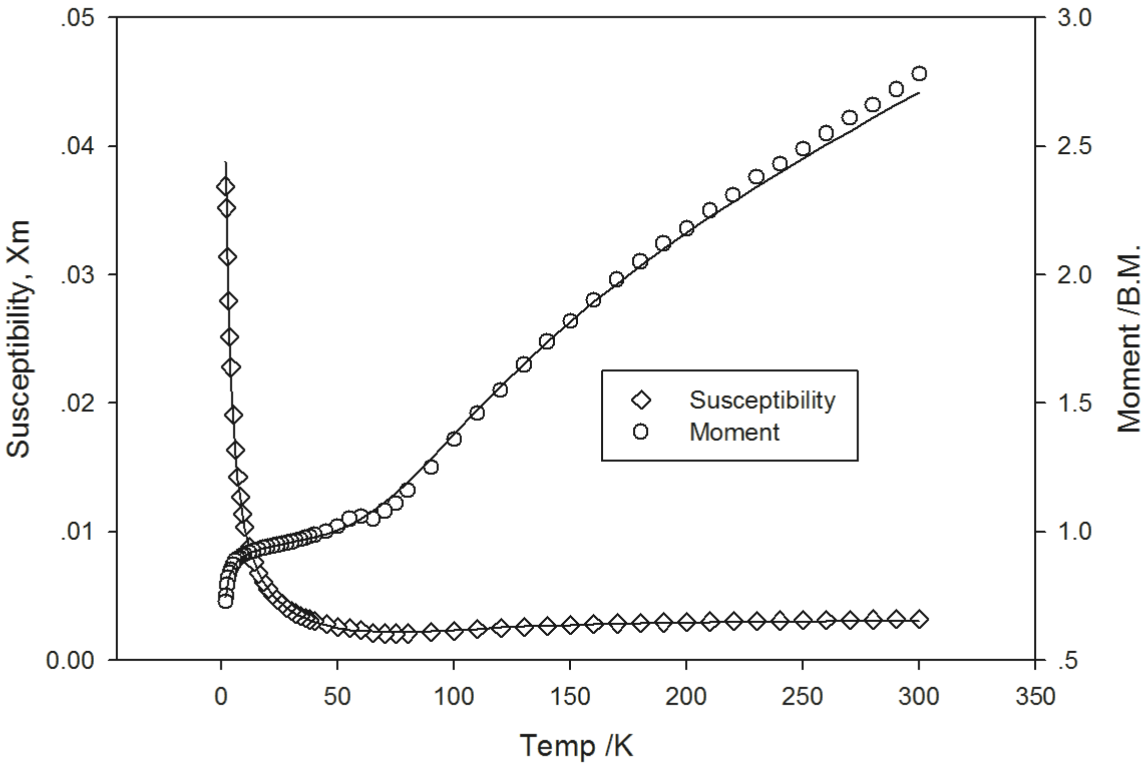

Figure A. 27. Magnetic susceptibility and moment vs temperature plots for solid **2.9** at 1 T. The solid lines are the fits to the experimental data with fitting parameters as described in Table 1.

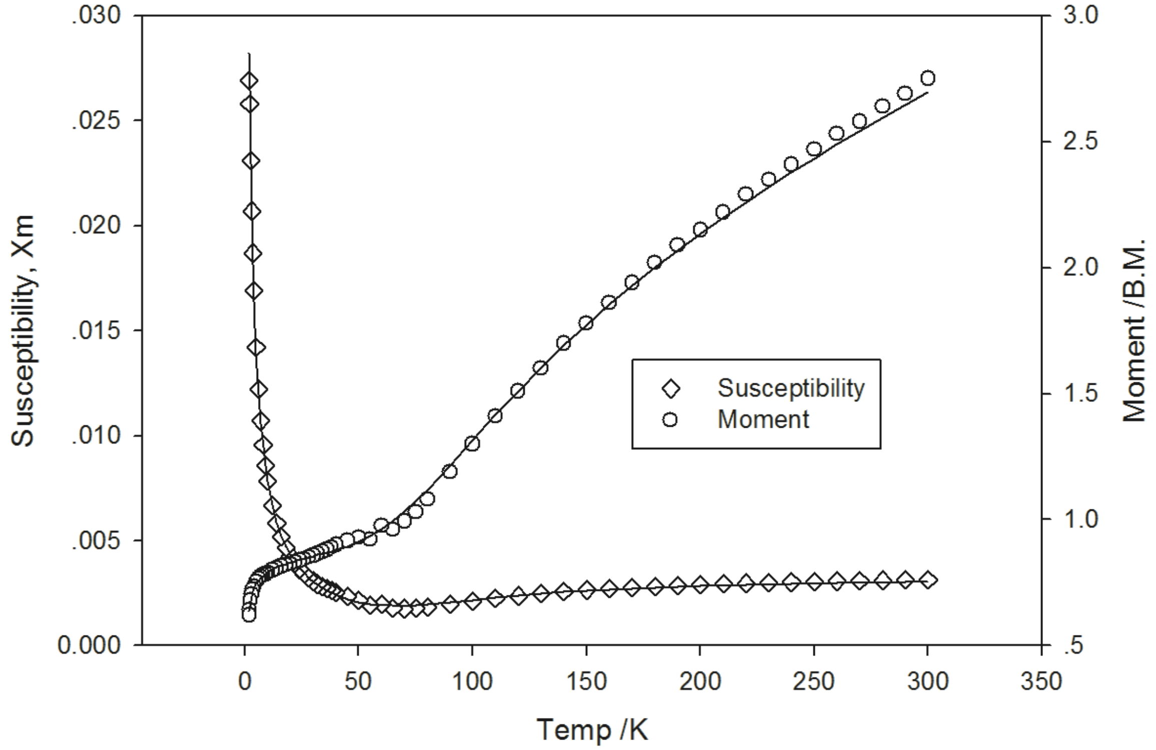

Figure A. 28. Magnetic susceptibility and moment vs temperature plots for solid **2.10** at 1 T. The solid lines are the fits to the experimental data with fitting parameters as described in Table 1.

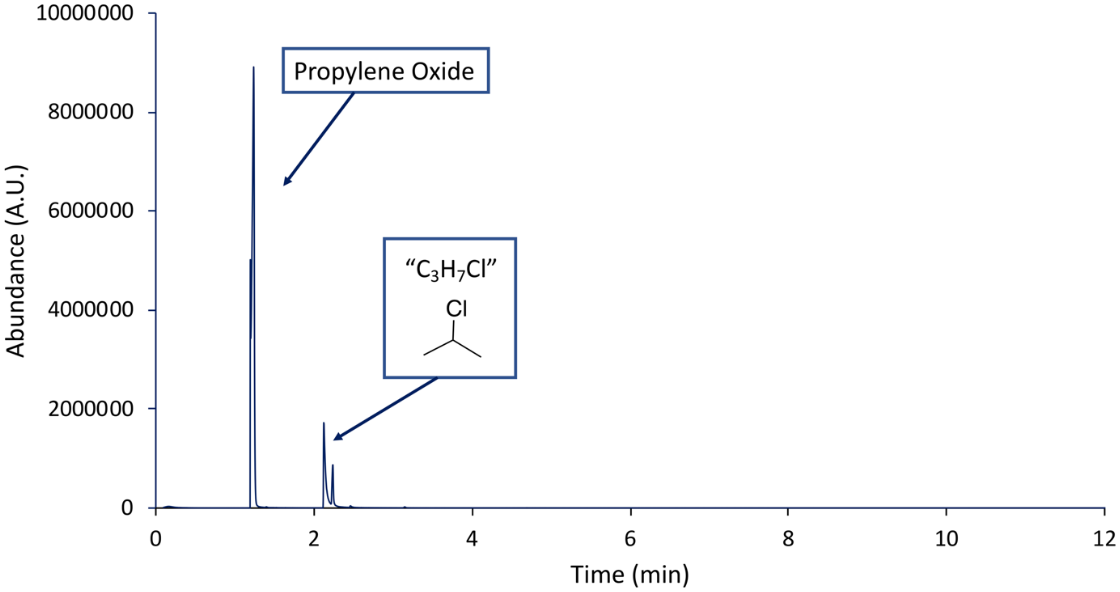

Figure A. 29. Gas Chromatography of post-reaction mixture of **2.1** and propylene oxide.

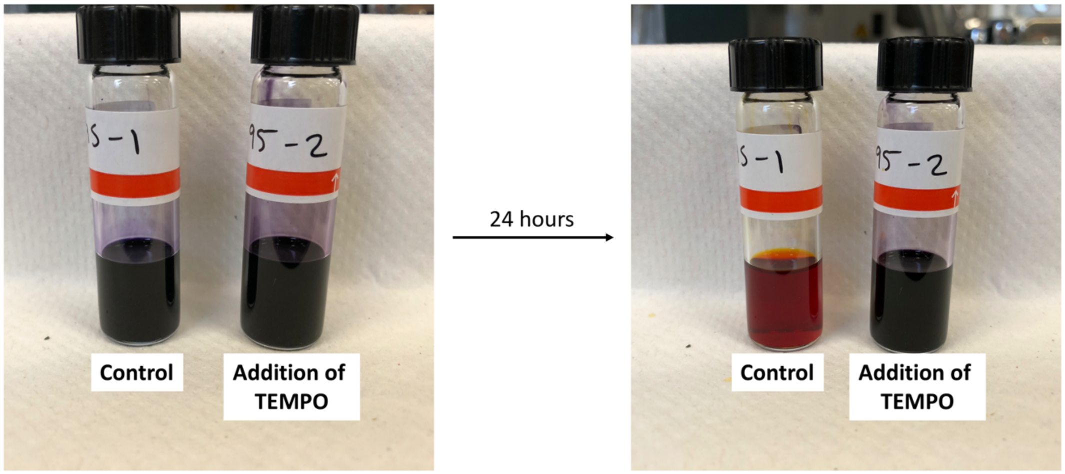

Figure A. 30. Radical scavenging mediated by TEMPO. The addition of one molar equivalent of TEMPO with respect to PO prevents the formation of the oxo-bridged species.

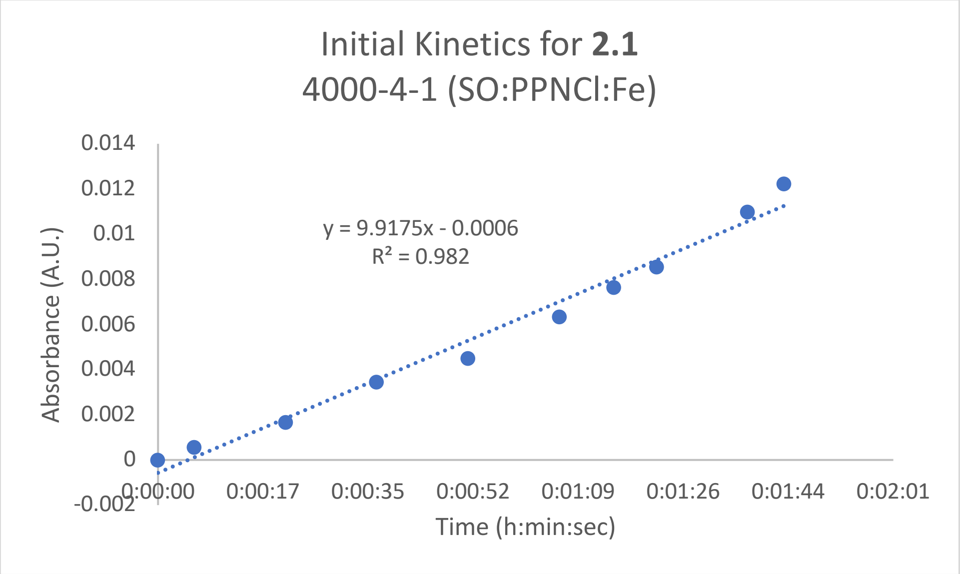

Figure A. 31. Absorbance vs. time plot for a reactant ratio of 4000:4:1 SO:PPNCl:Fe for **2.1**.

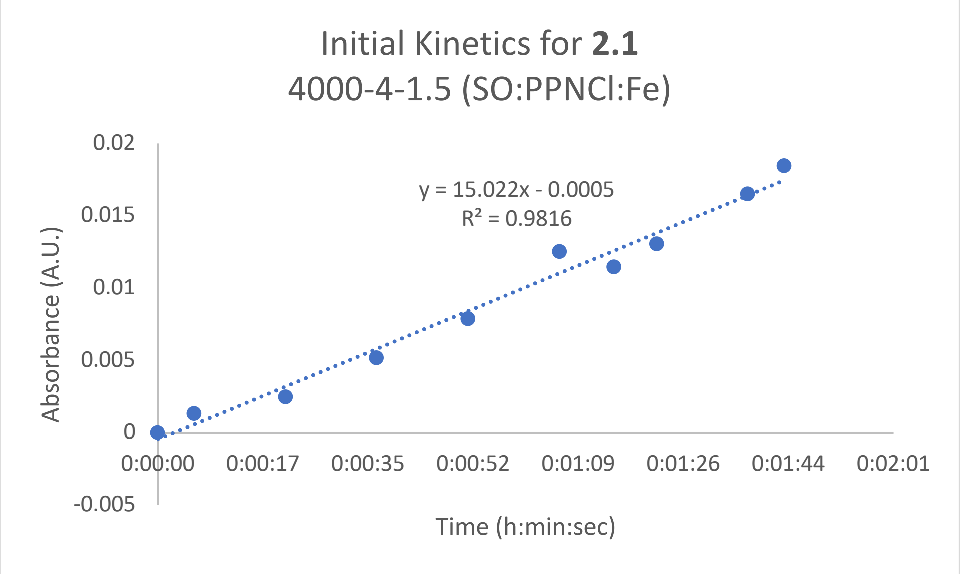

Figure A. 32. Absorbance vs. time plot for a reactant ratio of 4000:4:2 SO:PPNCl:Fe for **2.1**.

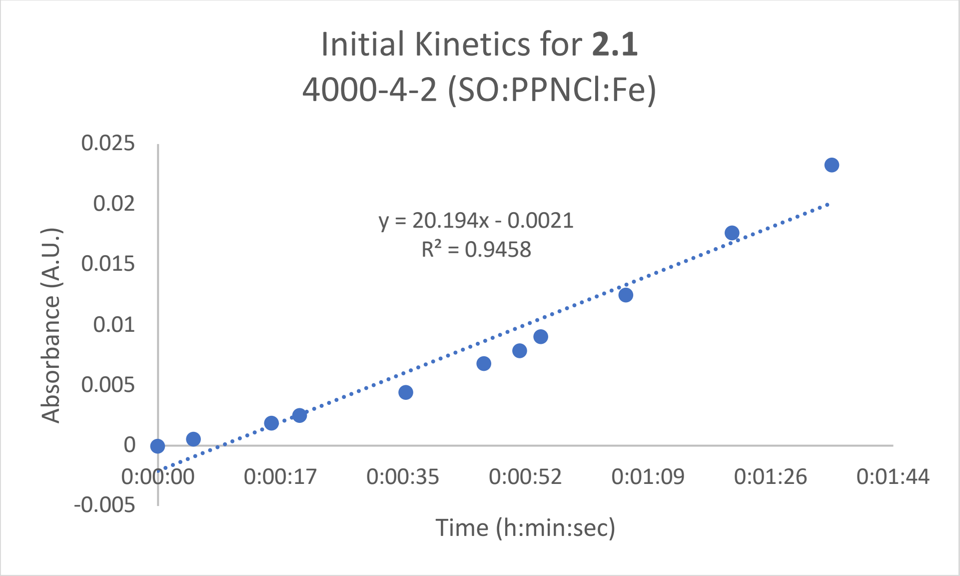

Figure A. 33. Absorbance vs. time plot for a reactant ratio of 4000:4:2 SO:PPNCl:Fe for **2.1**.

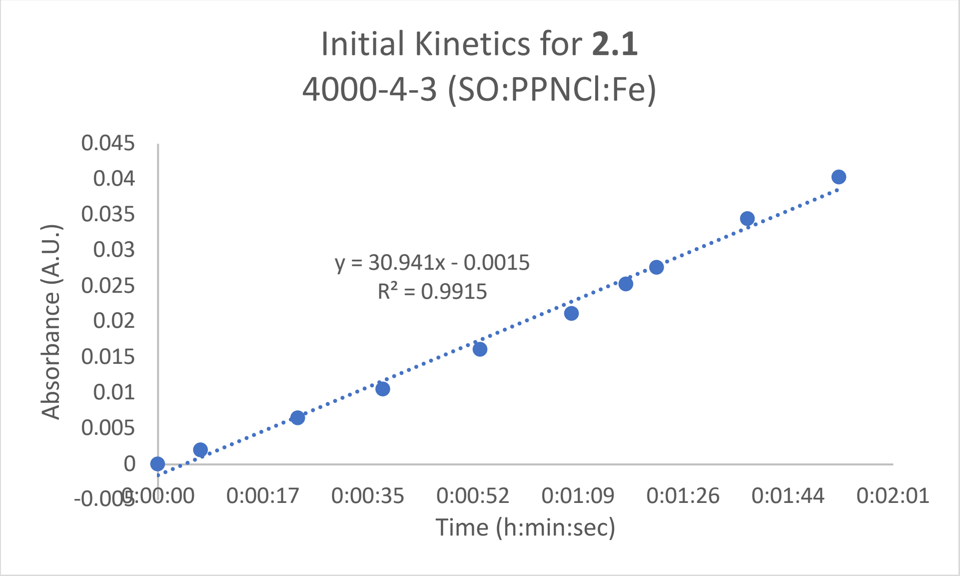

Figure A. 34. Absorbance vs. time plot for a reactant ratio of 4000:4:3 SO:PPNCl:Fe for **2.1**.

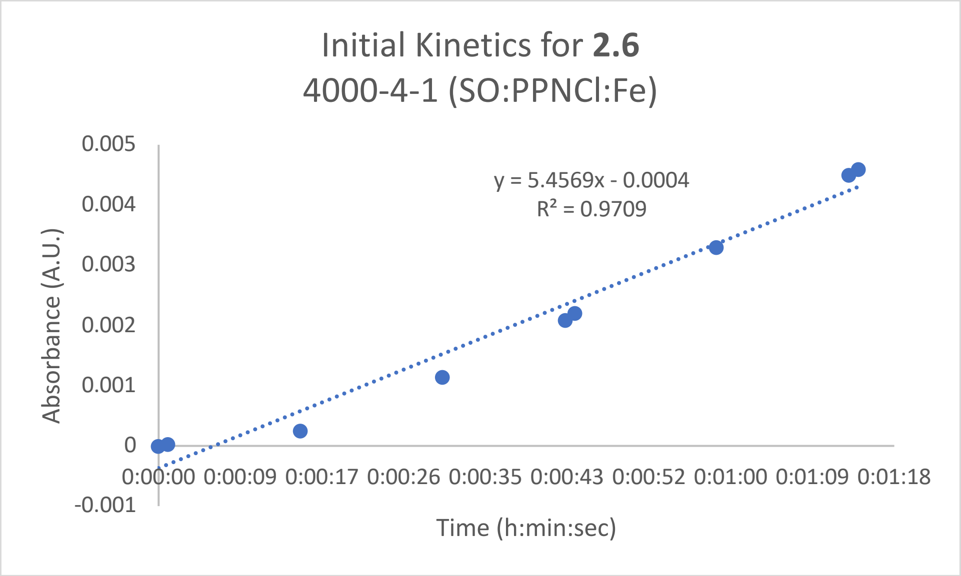

Figure A. 35. Absorbance vs. time plot for a reactant ratio of 4000:4:1 SO:PPNCl:Fe for **2.6**.

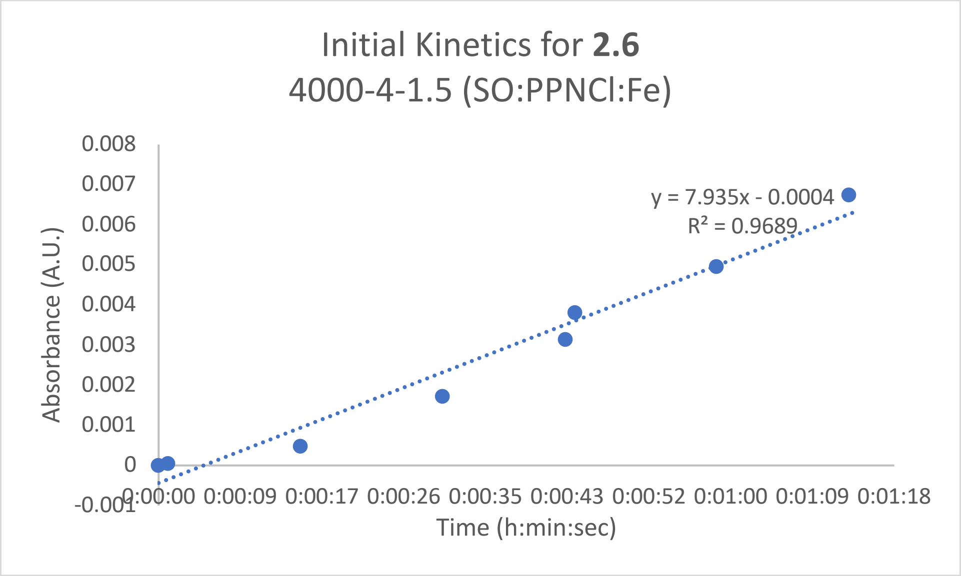

Figure A. 36. Absorbance vs. time plot for a reactant ratio of 4000:4:1.5 SO:PPNCl:Fe for **2.6**.

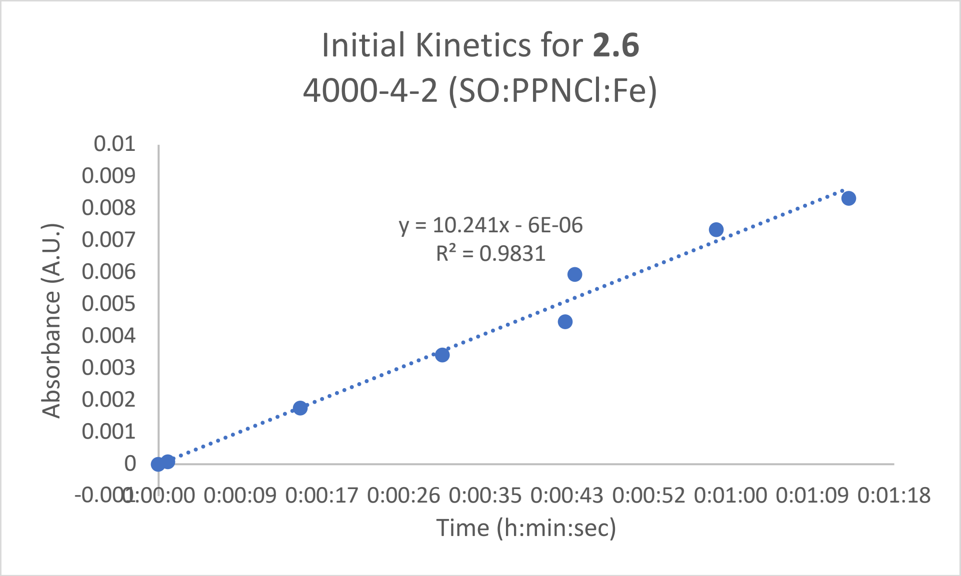

Figure A. 37. Absorbance vs. time plot for a reactant ratio of 4000:4:2 SO:PPNCl:Fe for **2.6**.

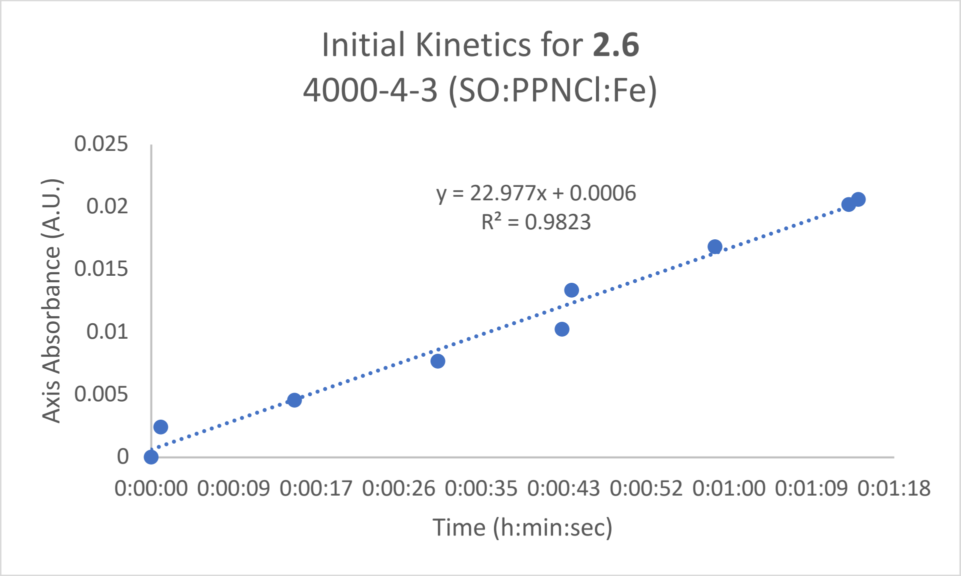

Figure A. 38. Absorbance vs. time plot for a reactant ratio of 4000:4:3 SO:PPNCl:Fe for **2.6**.

Appendix B

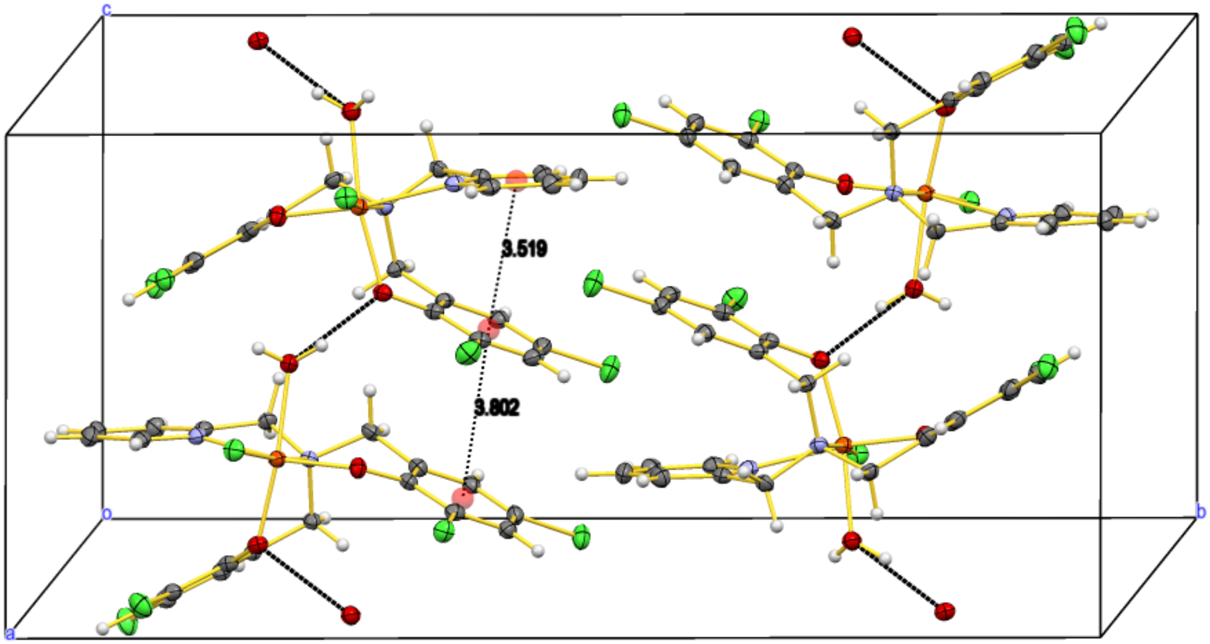

Figure B. 1. Unit cell of **3.1** showing intermolecular hydrogen bonding and π−π arene stacking.

Table B. 1. Crystallographic data and structure refinement for **3.1a**, **3.3**, **3.8** and **3.10**.

Compound	**3.1a**	**3.3**	**3.8**	**3.10**
Empirical formula	$C_{20}H_{16}Cl_5FeN_2O_3$	$C_{81}H_{92}Br_2Fe_2N_4O_8$	$C_{30}H_{46}ClFeN_2O_4$	$C_{34}H_{54}ClFeN_2O_4$
CCDC no.	1892403	1892402	1866352	1866351
Formula Weight	565.45	1521.10	589.99	646.09
Temperature/K	100	100	100	100
Crystal Color	Purple	Purple	Purple	Purple
Crystal System	Monoclinic	Monoclinic	Monoclinic	Monoclinic
Crystal Dimensions/mm^3	0.4 × 0.2 × 0.05	0.5 × 0.3 × 0.2	0.2 × 0.2 × 0.2	0.1 0.1 × 0.02
Lattice Parameters	a = 8.1439(2) Å b = 25.346(5) Å c = 11.1920(2) Å α = 90° β = 109.516(2) ° γ = 90°	a = 8.87360(10) Å b = 21.4099(3) Å c = 19.7622(3) Å α = 90° β = 97.5721(2) ° γ = 90°	a = 12.0595(7) Å b = 16.5091(9) Å c = 16.1700(11) Å α = 90° β = 105.303(7) ° γ = 90°	a = 17.1518(7) Å b = 8.4417(3) Å c = 27.2157(11) Å α = 90° β = 92.359(4) ° γ = 90°
Space group	$P2_1/c$	$P2_1/n$	$P2_1/n$	$P2_1/n$
Z value	4	2	4	4
ρ_{calc} g/cm^3	1.725	1.357	1.262	1.090
F_{000}	1140.0	1584.0	1260	1388.0
μ (MoKα)	1.333	1.521	0.607	0.484
Reflections collected	33707	48453	48019	59618
Independent reflections	5674	7043	8057	10365
R_{int}	0.0593	0.0490	0.1587	0.1564
R, wR_2 (all)	0.0799, 0.1506	0.0459, 0.1022	0.2016, 0.2154	0.1863, 0.2378
R, wR_2 [$I>2\sigma(I)$]	0.0673, 0.1427	0.0389, 0.0971	0.1232, 0.1827	0.1261, 0.2072
GOF-fit on F^2	1.162	1.043	1.103	1.062

Table B. 2. Crystallographic data and structure refinement for **3.11** and **3.14b**.

Compound	**3.11**	**3.14b**
Empirical formula	$C_{35}H_{53}ClFeNO_3$	$C_{91}H_{132}Br_2Fe_2N_2O_4$
CCDC no.	1866100	1892404
Formula Weight	627.08	1617.52
Temperature/K	100	100
Crystal Color	Purple	Purple
Crystal System	Monoclinic	Orthorhombic
Crystal Dimensions/mm^3	0.4 × 0.4 × 0.3	0.45 × 0.25 × 0.2
Lattice Parameters	a = 15.0077(7) Å b = 11.6581(5) Å c = 19.7476(9) Å α = 90° β = 103.766(5) ° γ = 90°	a = 30.2589(3) Å b = 10.26220(10) Å c = 27.2995(3) Å α = 90° β = 97.5721(2) ° γ = 90°
Space group	$P2_1/c$	$Pna2_1$
Z value	4	4
ρ_{calc} g/cm^3	1.241	1.258
F_{000}	1348.0	3440.0
μ (MoKα)	0.563	1.326
Reflections collected	14571	134622
Independent reflections	14571	22531
R_{int}	0.1031	0.0813
R, wR_2 (all)	0.0777, 0.1458	0.0768, 0.1251
R, wR_2 [I>2σ (I)]	0.0538, 0.1405	0.0542, 0.1142
GOF-fit on F^2	1.061	1.055

Table B. 3. Selected bond lengths (Å) and angles (°) for **3.1a**.

Bond or angle	Value
Fe(1)-Cl(1)	2.2748(10)
Fe(1)-O(1)	1.885(2)
Fe(1)-O(2)	1.972(2)
Fe(1)-O(3)	2.139(3)
Fe(1)-N(1)	2.262(3)
Fe(1)-N(2)	2.179(3)
O(1)-Fe(1)-Cl(1)	98.75(8)
O(1)-Fe(1)-O(2)	98.59(10)
O(1)-Fe(1)-O(3)	89.93(10)
O(1)-Fe(1)-N(1)	88.46(10)
O(1)-Fe(1)-N(2)	162.86(11)
O(2)-Fe(1)-Cl(1)	96.93(7)
O(2)-Fe(1)-O(3)	167.81(10)
O(2)-Fe(1)-N(1)	86.07(10)
O(2)-Fe(1)-N(2)	88.37(10)
O(3)-Fe(1)-Cl(1)	90.32(8)
O(3)-Fe(1)-N(1)	85.45(10)
O(3)-Fe(1)-N(2)	81.12(10)
N(1)-Fe(1)-Cl(1)	171.65(8)
N(2)-Fe(1)-Cl(1)	95.91(8)
N(2)-Fe(1)-N(1)	76.34(10)

Table B. 4. Selected bond lengths (Å) and angles (°) for **3.3**.

Bond or angle	Value
Fe(1)-Br(1)	2.4550(4)
Fe(1)-O(1)	1.8542(16)
Fe(1)-O(2)	1.8610(17)
Fe(1)-N(1)	2.2241(19)
Fe(1)-N(2)	2.134(2)
O(1)-Fe(1)-Br(1)	96.78(5)
O(1)-Fe(1)-O(2)	124.27(7)
O(1)-Fe(1)-N(1)	88.46(7)
O(1)-Fe(1)-N(2)	108.48(8)
O(2)-Fe(1)-Br(1)	97.46(5)
O(2)-Fe(1)-N(1)	86.63(7)
O(2)-Fe(1)-N(2)	123.69(8)
N(1)-Fe(1)-Br(1)	169.87(5)
N(2)-Fe(1)-Br(1)	94.32(6)
N(2)-Fe(1)-N(1)	75.76(7)

Table B. 5. Selected bond lengths (Å) and angles (°) for **3.8** and **3.10**.

Bond or angle	**3.8**	**3.10**
Fe(1)-Cl(1)	2.3068(16)	2.3118(14)
Fe(1)-O(2)	1.846(4)	1.847(3)
Fe(1)-O(1)	1.858(4)	1.856(3)
Fe(1)-N(1)	2.246(4)	2.268(4)
Fe(1)-N(2)	2.200(5)	2.184(4)
O(2)-Fe(1)-Cl(1)	95.29(12)	97.17(11)
O(2)-Fe(1)-O(1)	113.69(17)	126.59(15)
O(2)-Fe(1)-N(1)	89.38(16)	87.14(14)
O(2)-Fe(1)-N(2)	124.77(17)	117.34(15)
O(1)-Fe(1)-Cl(1)	99.41(12)	95.66(11)
O(1)-Fe(1)-N(1)	87.89(15)	86.03(14)
O(1)-Fe(1)-N(2)	119.29(17)	113.41(15)
N(1)-Fe(1)-Cl(1)	168.87(12)	173.06(11)
N(2)-Fe(1)-Cl(1)	90.69(13)	93.08(11)
N(2)-Fe(1)-N(1)	78.37(16)	80.09(14)

Table B. 6. Selected bond lengths(Å) and angles (°) for **3.11**.

Bond or angle	Value
Fe(1)-Cl(1)	2.2712(8)
Fe(1)-O(1)	2.042(2)
Fe(1)-O(2)	1.8430(19)
Fe(1)-O(3)	1.8550(19)
Fe(1)-N(1)	2.268(2)
O(1)-Fe(1)-Cl(1)	90.77(6)
O(1)-Fe(1)-N(1)	76.46(8)
O(2)-Fe(1)-Cl(1)	102.49(6)
O(2)-Fe(1)-O(1)	115.59(9)
O(2)-Fe(1)-O(3)	120.27(9)
O(2)-Fe(1)-N(1)	86.91(8)
O(3)-Fe(1)-Cl(1)	96.50(6)
O(3)-Fe(1)-O(1)	120.21(9)
O(3)-Fe(1)-N(1)	86.70(8)
N(1)-Fe(1)-Cl(1)	166.62(6)

Table B. 7. Selected bond lengths(Å) and angles (°) for **3.14a**.

Bond or angle	Value
Br(1)-Fe(1)	2.4037(9)
Fe(1)-O(1)	1.858(4)
Fe(1)-O(2)	1.872(4)
Fe(1)-N(1)	2.183(4)
Fe(1)-N(2)	2.176(4)
O(1)-Fe(1)-Br(1)	106.03(12)
O(1)-Fe(1)-O(2)	97.60(16)
O(1)-Fe(1)-N(1)	87.68(16)
O(1)-Fe(1)-N(2)	151.20(16)
O(2)-Fe(1)-Br(1)	110.98(12)
O(2)-Fe(1)-N(1)	142.89(17)
O(2)-Fe(1)-N(2)	85.80(15)
N(1)-Fe(1)-Br(1)	102.57(12)
N(2)-Fe(1)-Br(1)	99.24(11)
N(2)-Fe(1)-N(1)	73.34(16)

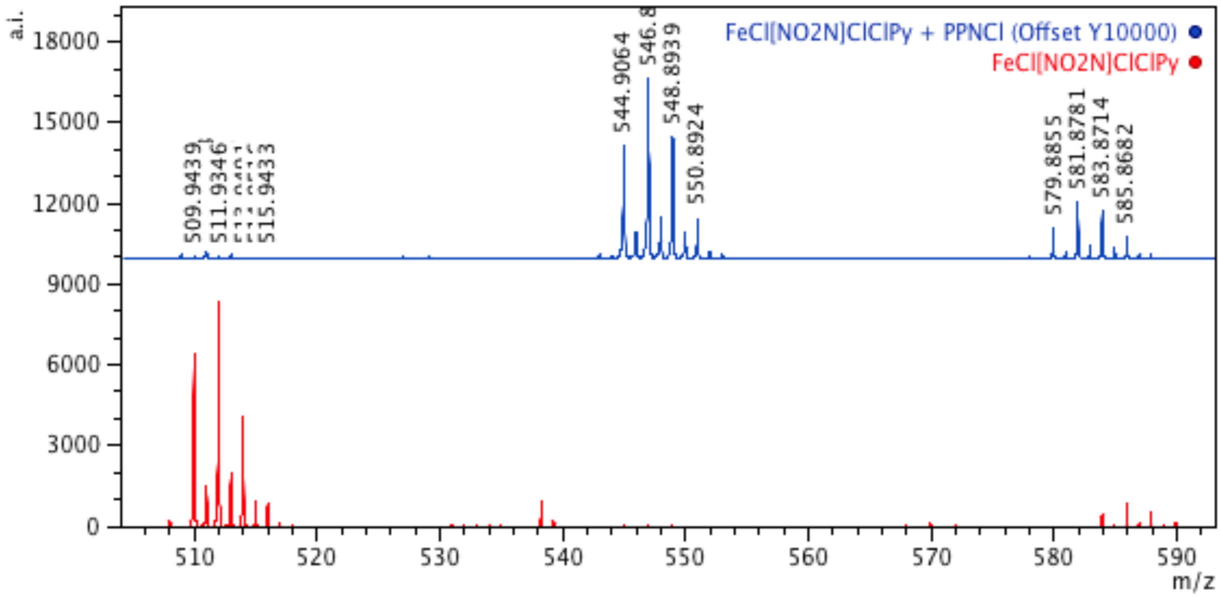

Figure B. 2. MALDI-TOF mass spectrum in negative mode of **3.1a** and PPNCl showing formation of [**3.1a**+Cl]$^-$ anion at *m/z* 581.88 (top) and mass spectrum of **3.1a** showing presence of [**3.1a**-Cl]$^+$ cation in positive mode

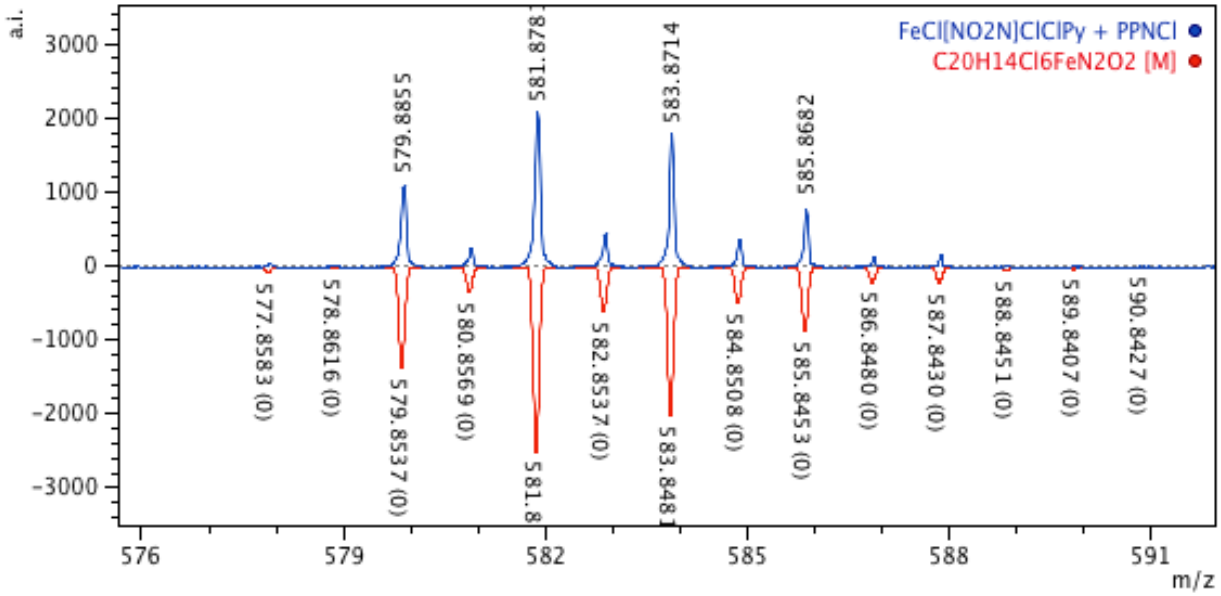

Figure B. 3. Theoretical (bottom) and experimental (top) isotopic distribution pattern of [**3.1a**+Cl]$^-$ anion

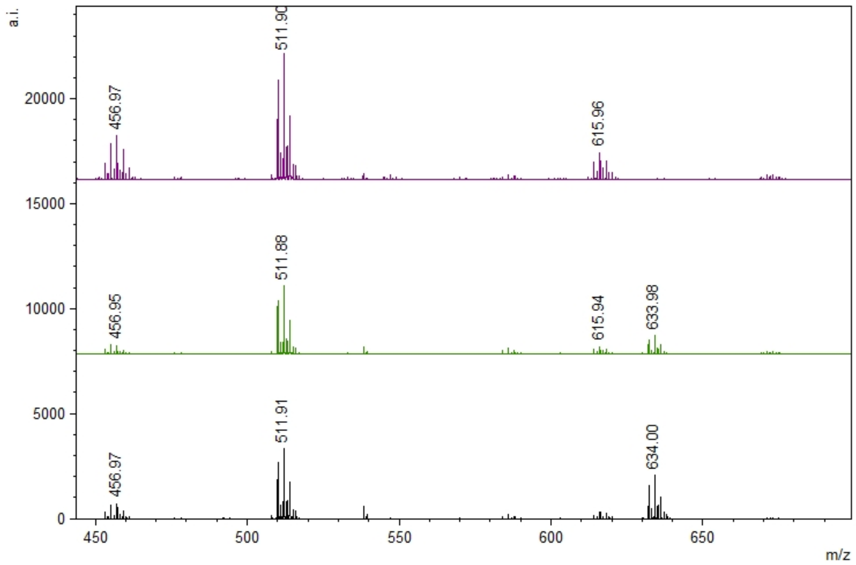

Figure B. 4. MALDI-TOF mass spectra in positive mode of **3.1a** (top) with one equivalent of DMAP (middle) and two equivalents of DMAP (bottom). Mass assigned: *m/z* 457 = [**3.1a**-FeCl]$^+$, *m/z* 512 = [3.1a-Cl]$^+$, *m/z* 616 = [**3.1a**-Cl+NEt$_3$]$^+$, *m/z* 634 = [**3.1a**-Cl+DMAP]$^+$

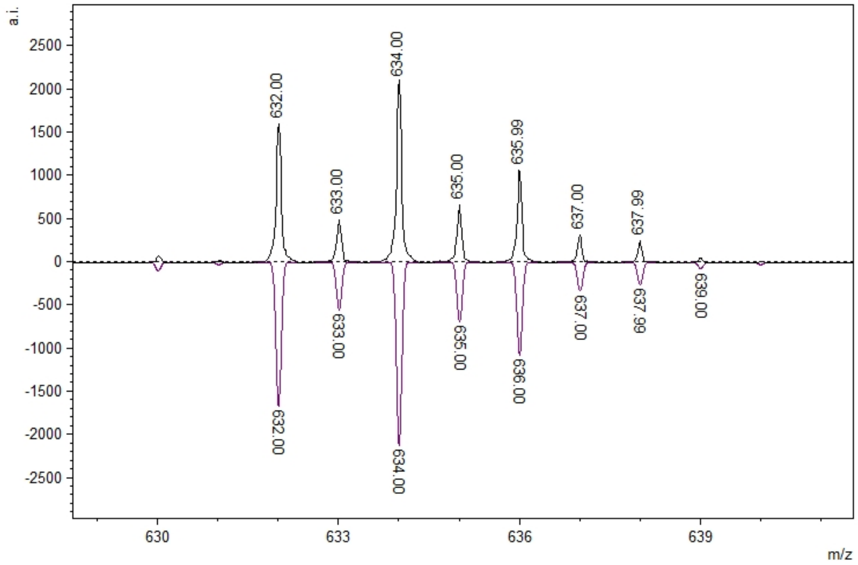

Figure B. 5. MALDI TOF mass spectrum of [**3.1a**-Cl+DMAP]$^+$. Experimental shown on top, isotopic modelling on bottom

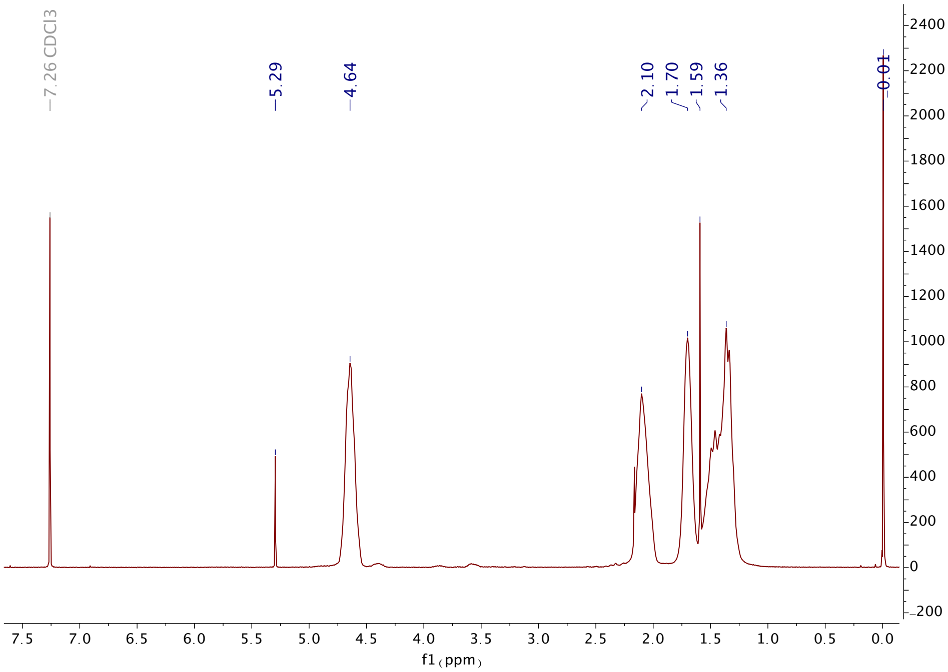

Figure B. 6. Representative ^{1}H NMR spectrum (300 MHz, 298 K, $CDCl_3$) of isolated polycyclohexene carbonate (**Table 3.1**, entry 1)

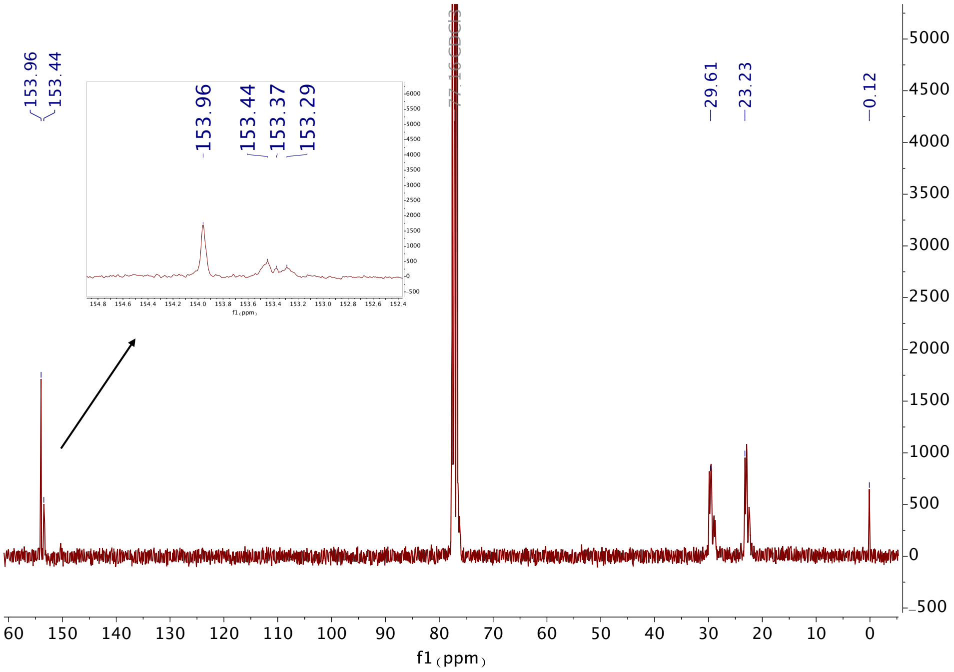

Figure B. 7. Representative ^{13}C NMR spectrum (75 MHz, 298 K, $CDCl_3$) of isolated polycyclohexene carbonate (**Table 3.1**, entry 1)

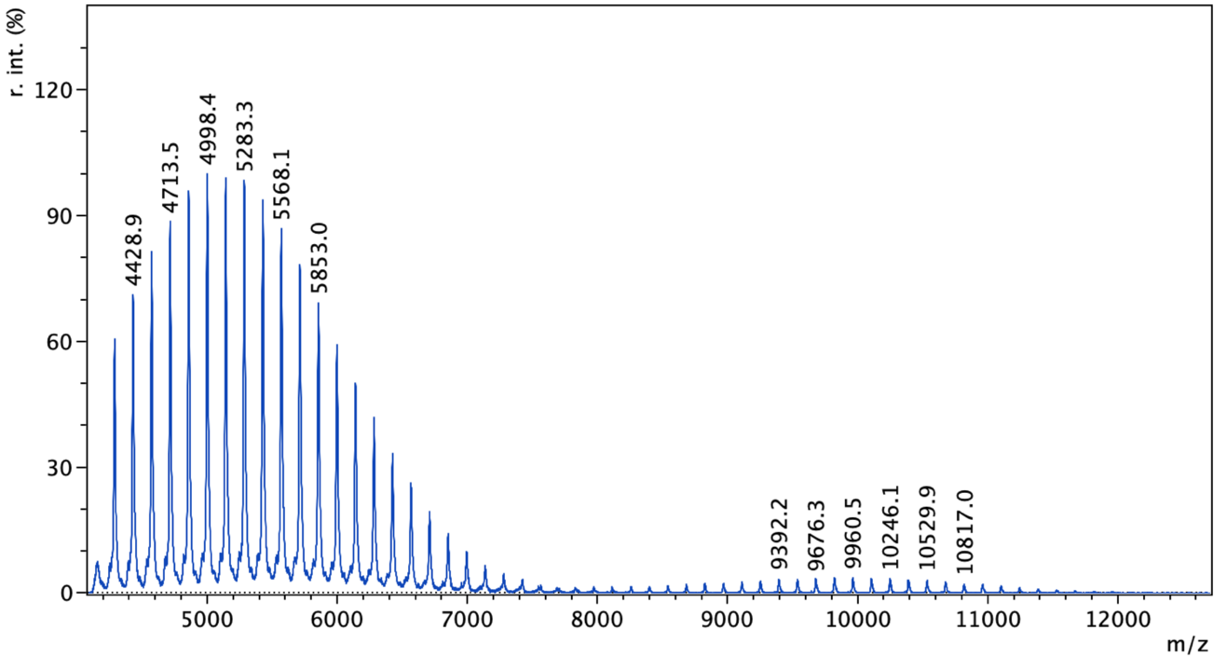

Figure B. 8. Representative MALDI-TOF mass spectrum of polycyclohexene carbonate obtained using iron complex 3.1a and PPNCl (as in **Table 3.1** entry 1). Polymer fragments identified as $Cl(C_6H_{10}CO_3)_n(C_6H_{10})OH]Na^+$.

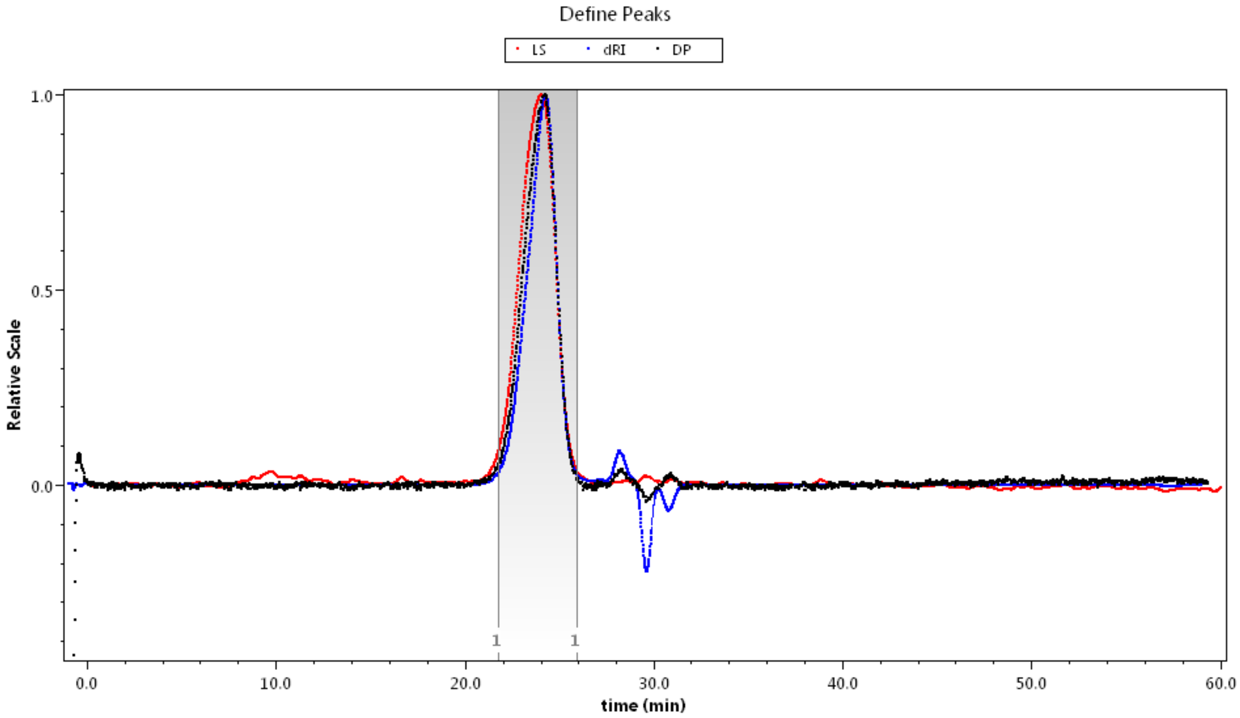

Figure B. 9. Representative GPC trace of isolated polycyclohexene carbonate (**Table 3.1**, entry 1).

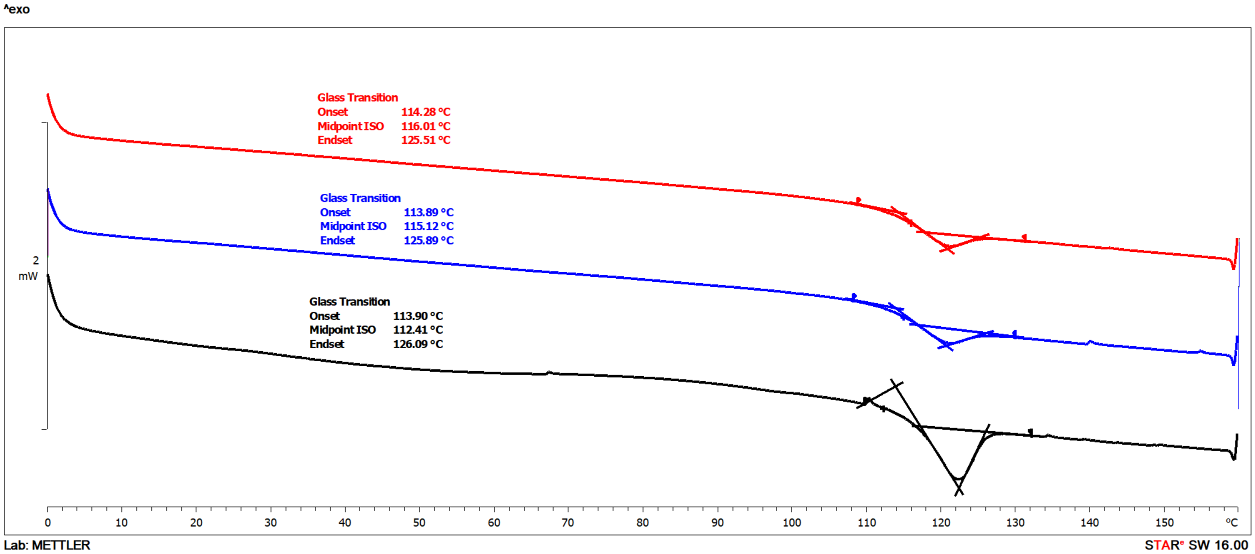

Figure B. 10. Representative DSC spectrum of isolated polycyclohexene carbonate (**Table 3.1**, entry 1)

Appendix C

Figures C1-3. Plots demonstrating reaction rates with respect to varying equivalents of BPh_3. Reactions conducted in neat propylene oxide (PO) at 20 bar CO_2, 100 °C for 3 h. Graphs show data obtained using in situ IR spectroscopy and for initial reaction period only.

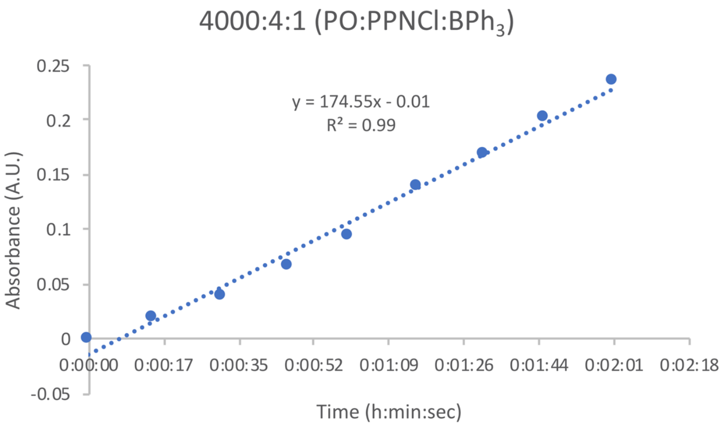

Figure C. 1. Absorbance vs. time plot for a reactant ratio of 4000:4:1 PO:PPNCl:BPh_3.

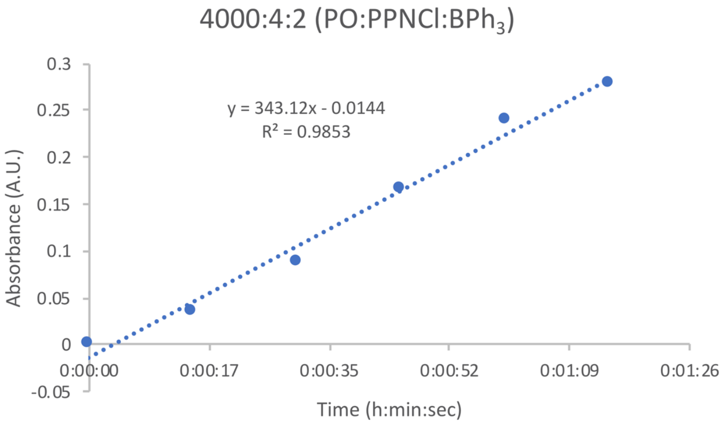

Figure C. 2. Absorbance vs. time plot for a reactant ratio of 4000:4:2 PO:PPNCl:BPh_3.

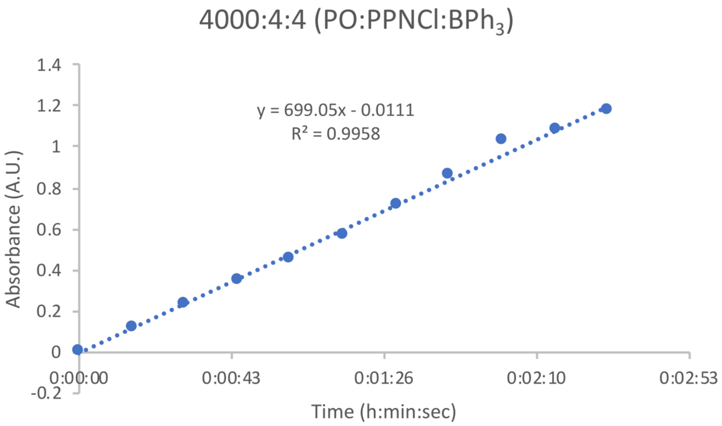

Figure C. 3. Absorbance vs. time plot for a reactant ratio of 4000:4:4 PO:PPNCl:BPh$_3$.

Table C. 1. Summary of initial reaction rates obtained from in situ IR data plotted in graphs above (Figures C1-3) for varying amounts of BPh$_3$.

Equivalents of BPh$_3$	Initial Rate (V_i)	ln ($C_{catalyst}$)	ln(V_i)
1	174.55	-7.8929	5.1622
2	343.12	-7.1997	5.8381
4	699.05	-6.5066	6.5497

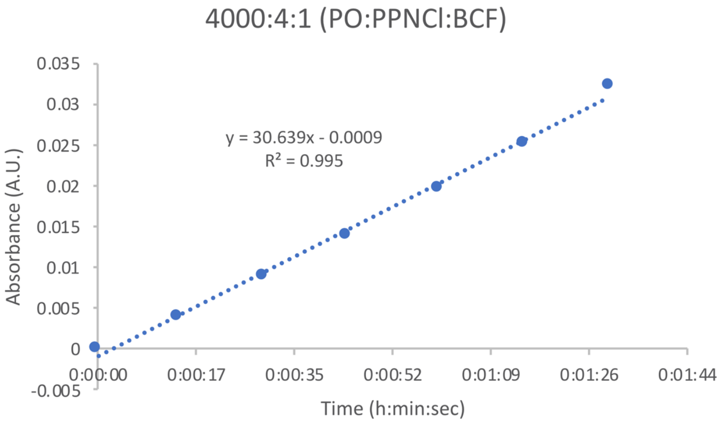

Figure C. 4. Absorbance vs. time plot for a reactant ratio of 4000:4:1 PO:PPNCl:BCF [BCF = $B(C_6F_5)_3$] for comparison with reaction rate using BPh_3 (see Figure A1). Reaction performed at 20 bar CO_2, 100 °C for 22 h. Data shown for initial reaction period only.

Figures C5-9. Plots demonstrating reaction rates with respect to varying equivalents of PPNCl (co-catalyst). Reactions were completed in 3 mL of dichloromethane in addition to propylene oxide (PO), at 20 bar CO_2, 100 °C for 3 h. Dichloromethane needed to ensure dissolution of PPNCl. Graphs show data obtained using *in situ* IR spectroscopy and for initial reaction period only.

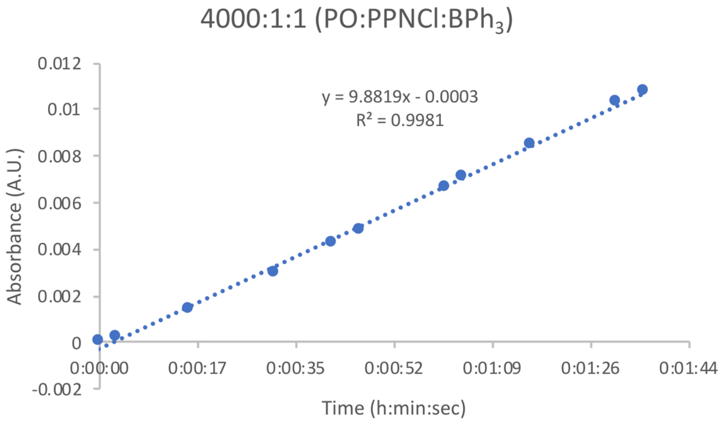

Figure C. 5. Absorbance vs. time plot for a reactant ratio of 4000:1:1 PO:PPNCl:BPh_3 in dichloromethane (3 mL).

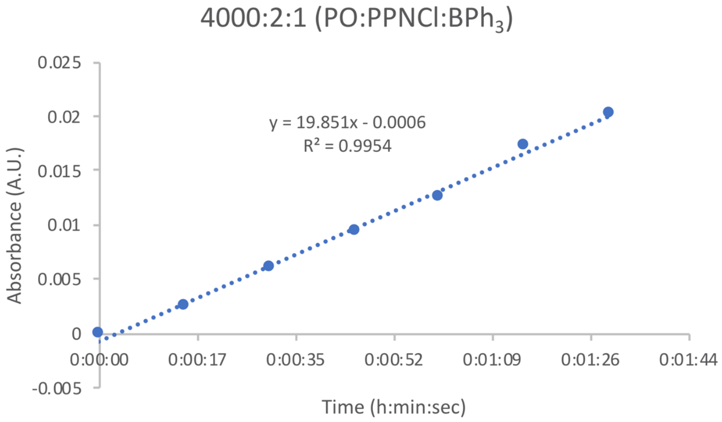

Figure C. 6. Absorbance vs. time plot for a reactant ratio of 4000:2:1 PO:PPNCl:BPh_3 in dichloromethane (3 mL).

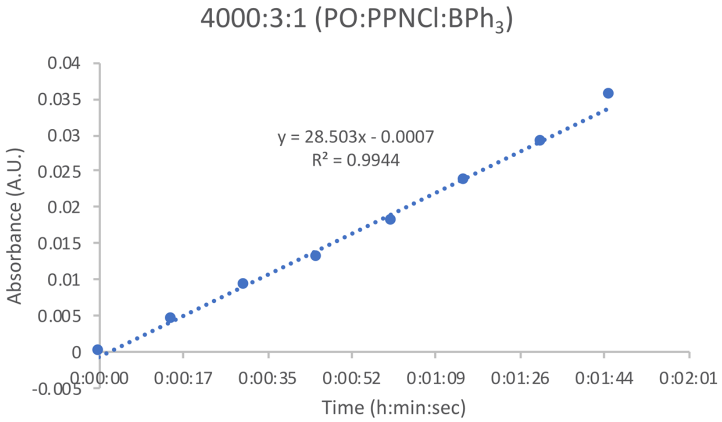

Figure C. 7. Absorbance vs. time plot for a reactant ratio of 4000:3:1 PO:PPNCl:BPh_3 in dichloromethane (3 mL).

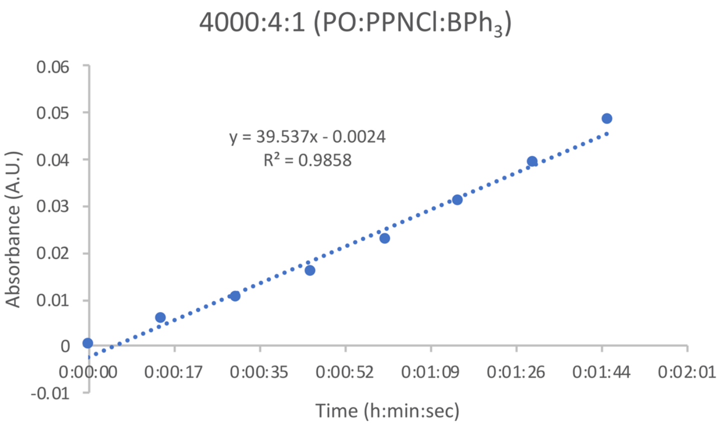

Figure C. 8. Absorbance vs. time plot for a reactant ratio of 4000:4:1 PO:PPNCl:BPh$_3$ in dichloromethane (3 mL).

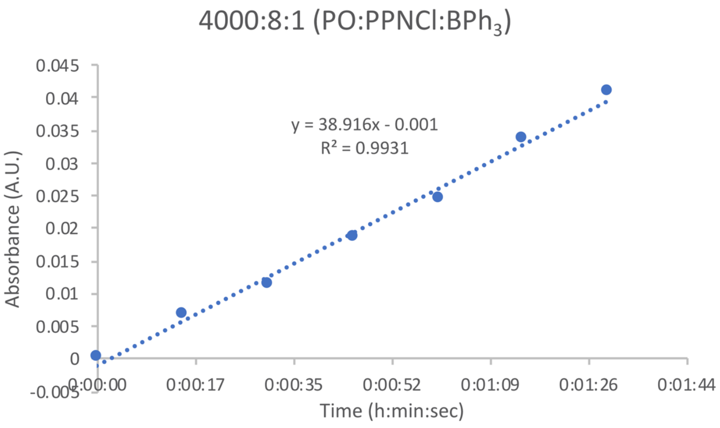

Figure C. 9. Absorbance vs. time plot for a reactant ratio of 4000:8:1 PO:PPNCl:BPh$_3$ in dichloromethane (3 mL).

Table C. 2. Summary of initial reaction rates obtained from *in situ* IR data plotted in graphs above (Figures A5-9) for varying amounts of PPNCl (varying co-catalyst loading)

Equivalents of PPNCl	Initial Rate (V_i)	ln (C_{PPNCl})	ln(V_i)
1	9.882	-8.4968	2.2907
2	19.851	-7.8037	2.9883
3	28.503	-7.3982	3.3500
4	39.537	-7.1105	3.6772
8	38.916	-6.4173	3.6614

Figures C10-12. Plots demonstrating reaction rates with respect to varying CO_2 pressure. Reactions were completed in 3 mL of dichloromethane in addition to propylene oxide (PO), at 100 °C for 3 h (4000:4:1 PO:PPNCl:BPh_3) and the specified CO_2 pressure. Graphs show data obtained using *in situ* IR spectroscopy and for initial reaction period only. Note: 20 bar CO_2 comparison is Figure C8.

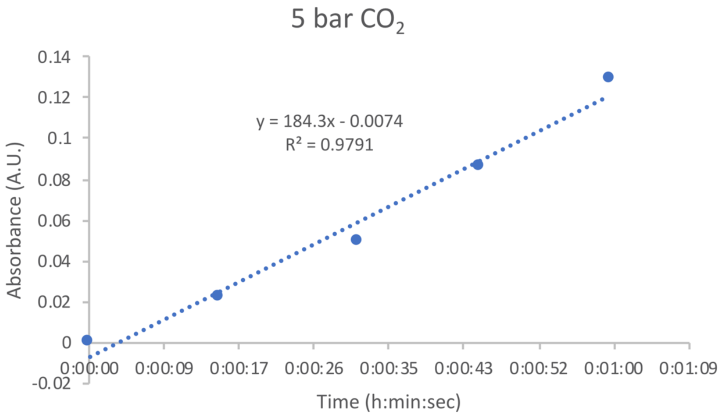

Figure C. 10. Absorbance vs. time plot for a reactant ratio of 4000:4:1 PO:PPNCl:BPh_3 in dichloromethane at a CO_2 pressure of 5 bar.

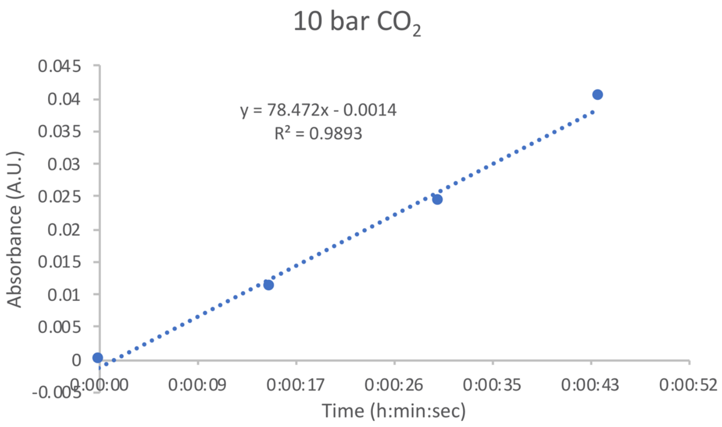

Figure C. 11. Absorbance vs. time plot for a reactant ratio of 4000:4:1 PO:PPNCl:BPh_3 in dichloromethane at a CO_2 pressure of 10 bar.

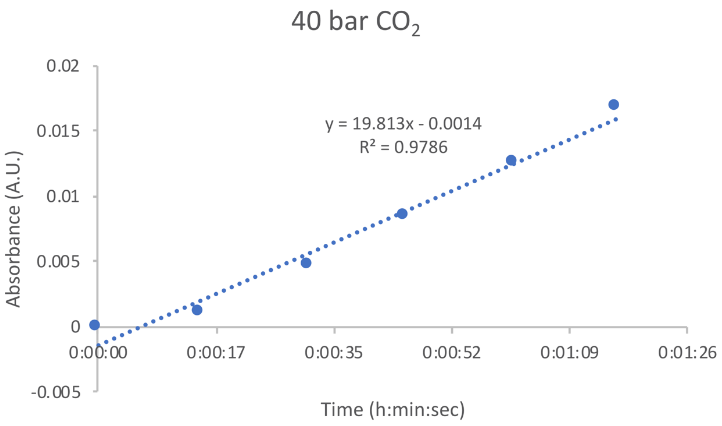

Figure C. 12. Absorbance vs. time plot for a reactant ratio of 4000:4:1 PO:PPNCl:BPh_3 in dichloromethane at a CO_2 pressure of 40 bar.

Table C. 3. Summary of initial reaction rates obtained from *in situ* IR data plotted in graphs above (Figures C8, C10-12) for varying pressures of CO_2.

CO_2 Pressure	Initial Rate (V_i)	ln (PCO_2)	ln(V_i)
5	184.300	1.6094	5.2166
10	78.472	2.3026	4.3627
20	39.537	2.9957	3.6772
40	19.81	3.6889	2.9861

Table C. 4. Homopolymerization of CHO using BPh_3 as a catalyst in the presence of PPNCl

Entry[a]	Temperature (°C)	% Conversion[b]	$M_n \times 10^{-3}$ (kg/mol), $Đ$
1	25	32	17.79, 1.72
2	40	23	18.27, 1.65
3	60	12	19.77, 1.66
4	80	14	21.16, 1.81

[a] Reaction conditions: CHO (2.5 g; 0.021 mol), PPNCl (0.118 g; 2.06×10^{-4} mol), BPh_3 (0.050 g; 2.06×10^{-4} mol), 22 h. [c] Determined by ^{1}H NMR spectroscopy.

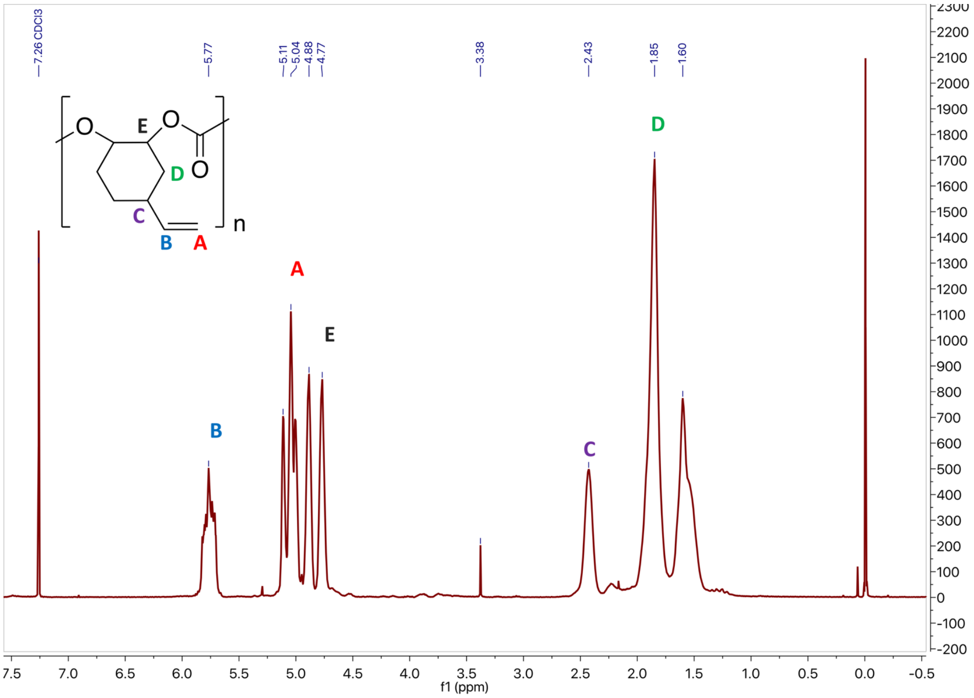

Figure C. 13. ^{1}H NMR (300 MHz, $CDCl_3$-d_1, 298 K) spectrum of isolated poly(vinylcyclohexenecarbonate) [PVCHC].

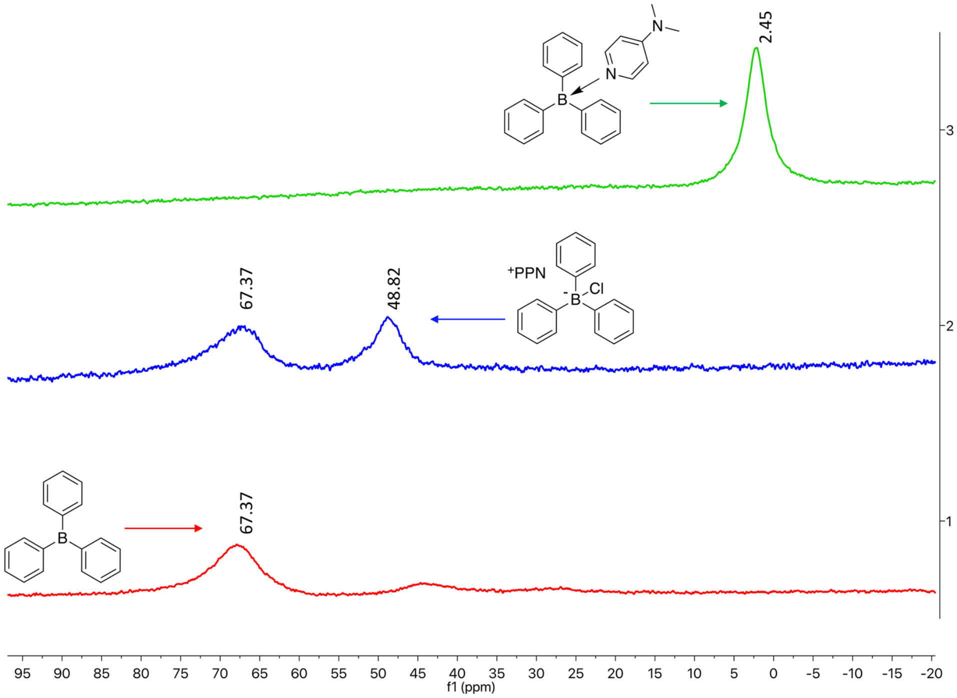

Figure C. 14. ^{11}B NMR spectra (96 MHz, CDCl$_3$-d_1, 298 K) of BPh$_3$ (red), BPh$_3$ with PPNCl (blue) and with DMAP (green) showing formation of Lewis acid/base adducts.

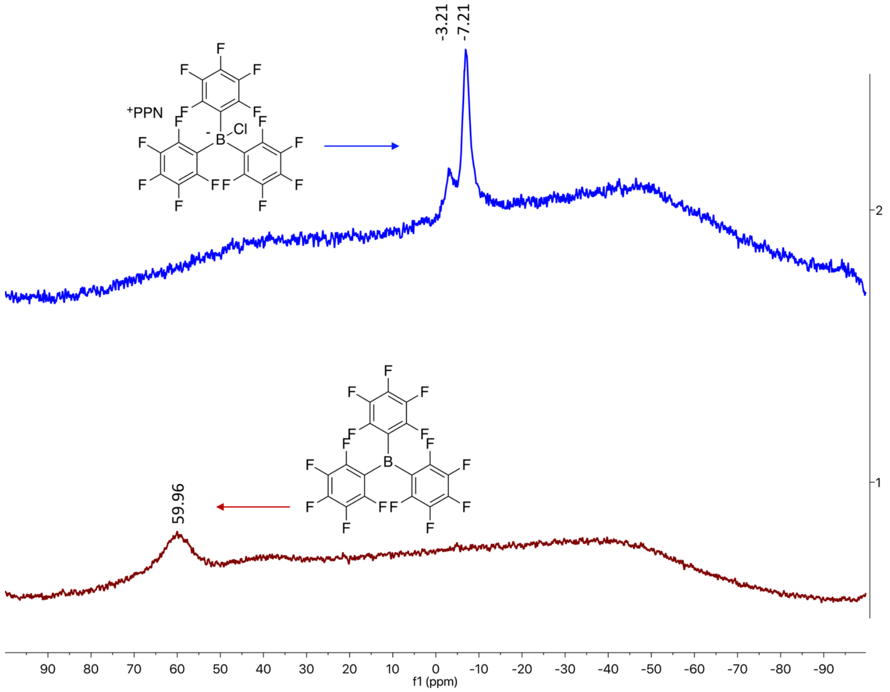

Figure C. 15. ^{11}B NMR spectra (96 MHz, CDCl$_3$-*d$_1$*, 298 K) of BCF (red) and BCF with PPNCl (blue) showing formation of Lewis acid/base adduct.

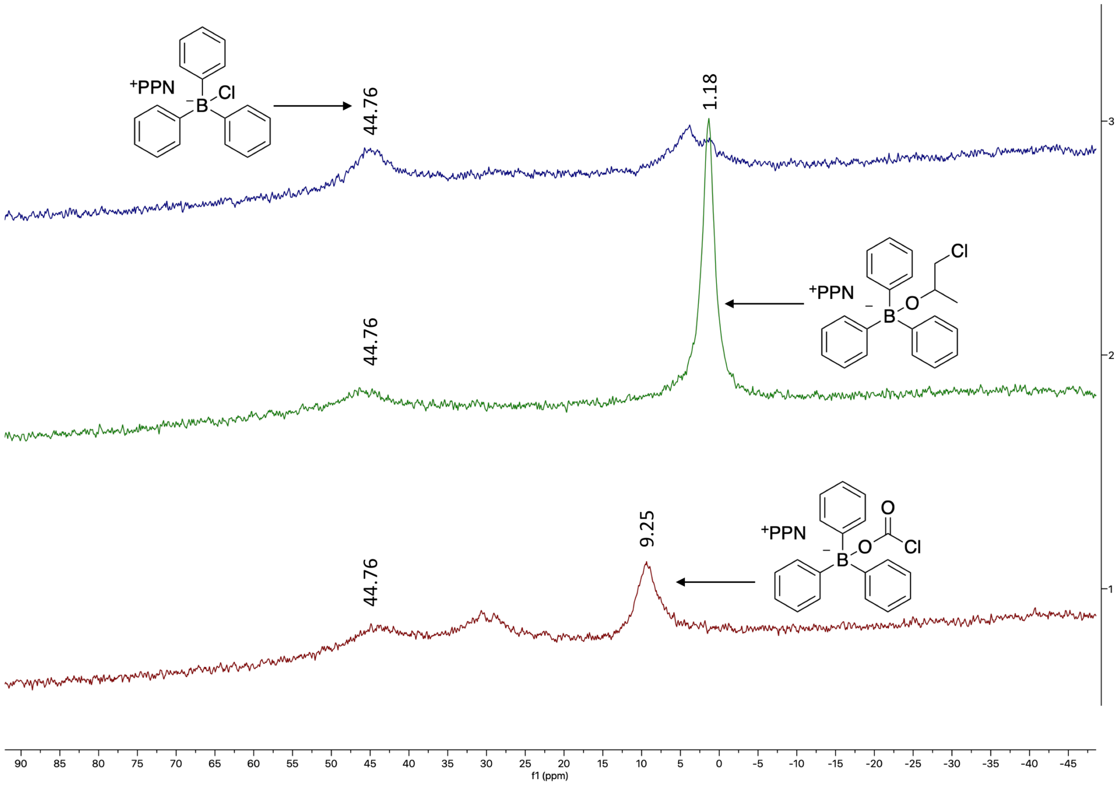

Figure C. 16. ^{11}B NMR spectra (96 MHz, CDCl$_3$-*d$_1$*, 298 K) of BPh$_3$/PPNCl + CO$_2$ (red), BPh$_3$/PPNCl + PO (green) and BPh$_3$/PPNCl + CO$_2$ adduct (i.e. that shown in red) after the addition of 1 equiv. PO (blue).

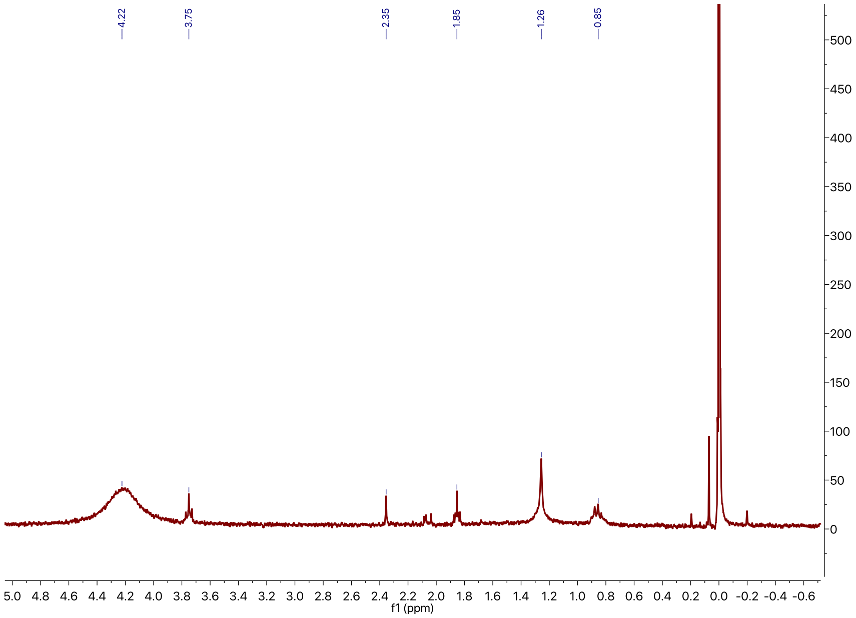

Figure C. 17. ^{1}H NMR (300 MHz, $CDCl_3$-*d_1*, 298 K) spectra of isolated polytetrahydrofuran

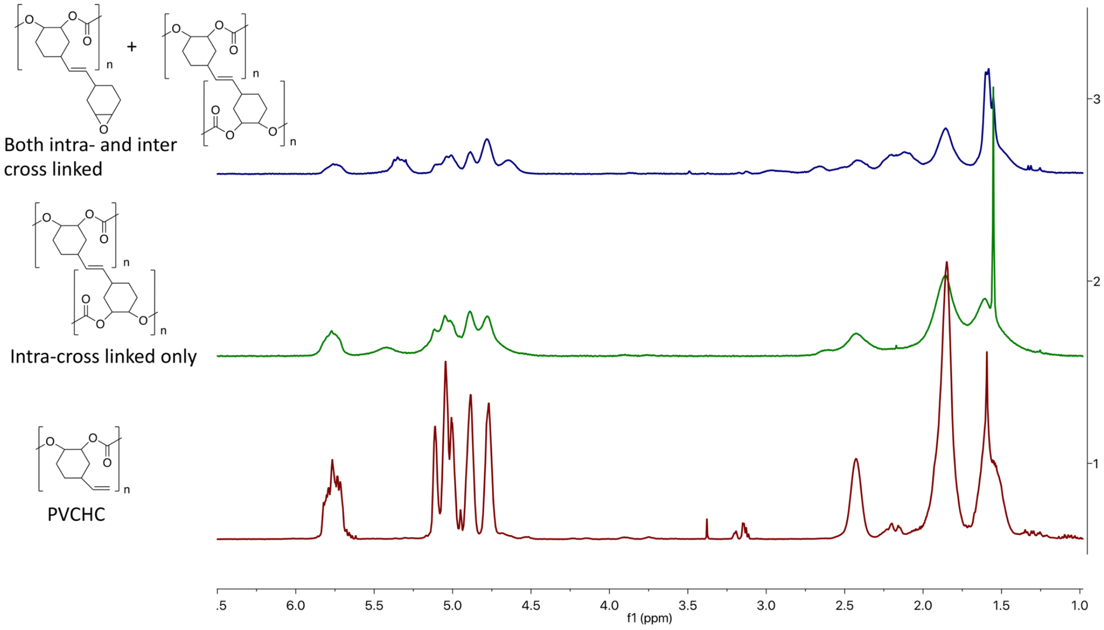

Figure C. 18. ^{1}H NMR (300 MHz, $CDCl_3$-*d_1*, 298 K) spectra of isolated PVCHC (bottom), intra-cross-linked PVCHC from two-pot process (green, middle) and cross-linked product from one-pot Grubbs reaction (blue, top).

Appendix D

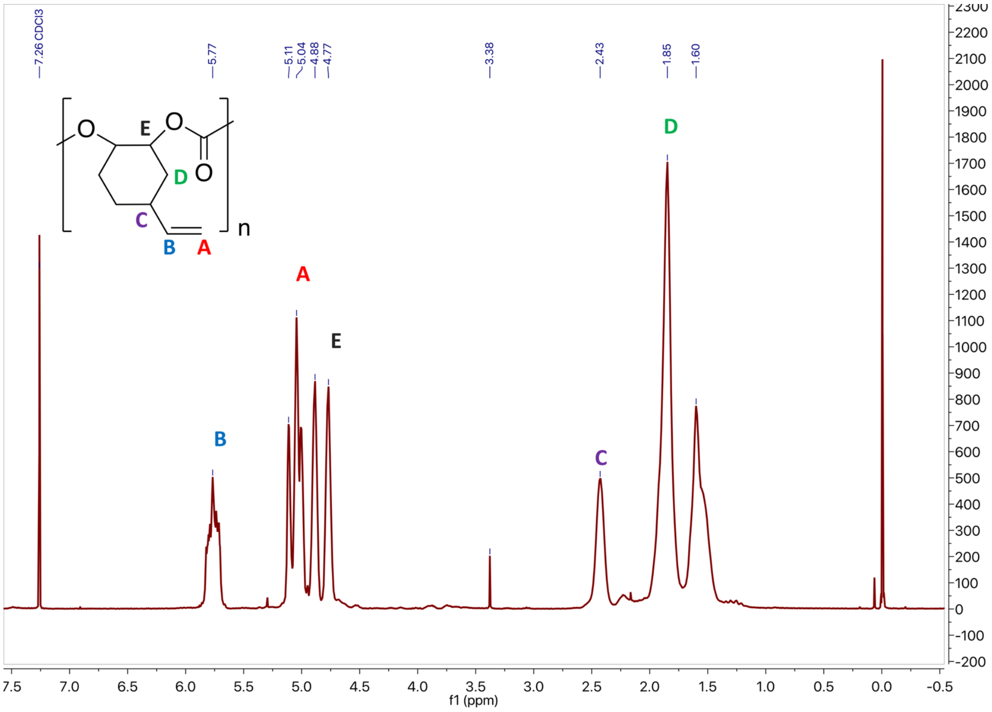

Figure D. 1. ^{1}H NMR (300 MHz, $CDCl_3$ 298 K) spectrum of isolated poly(vinylcyclohexenecarbonate) [PVCHC].

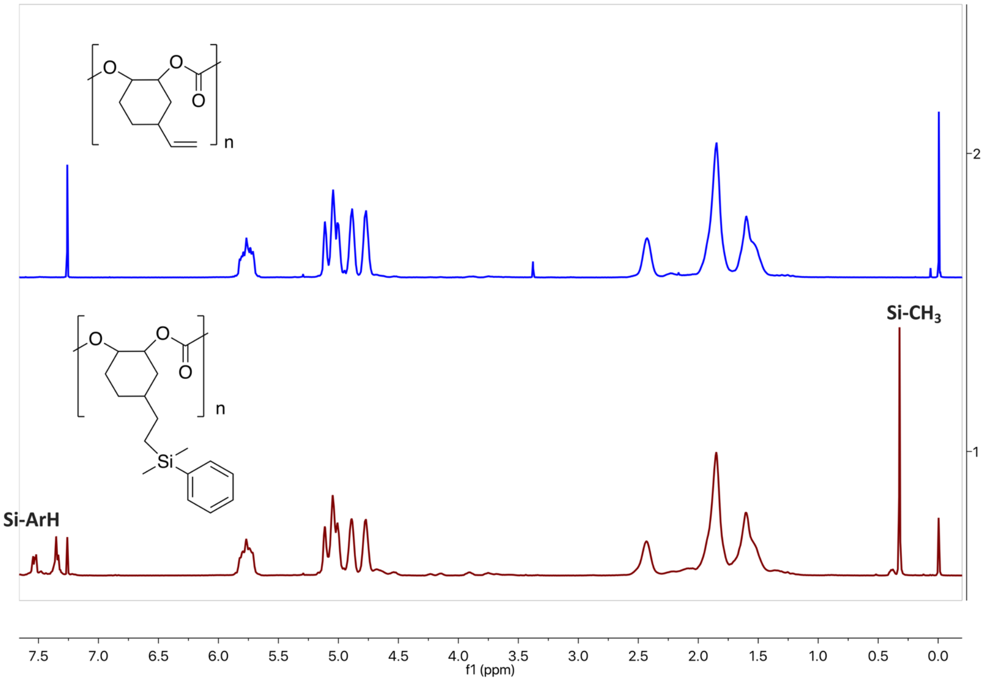

Figure D. 2. ^{1}H NMR (300 MHz, CDCl$_3$, 298 K) spectrum of isolated PVCHC (top) and isolated silylated PVCHC (bottom). 10% of vinyl groups have been silylated (see Fig. D6 for expanded view).

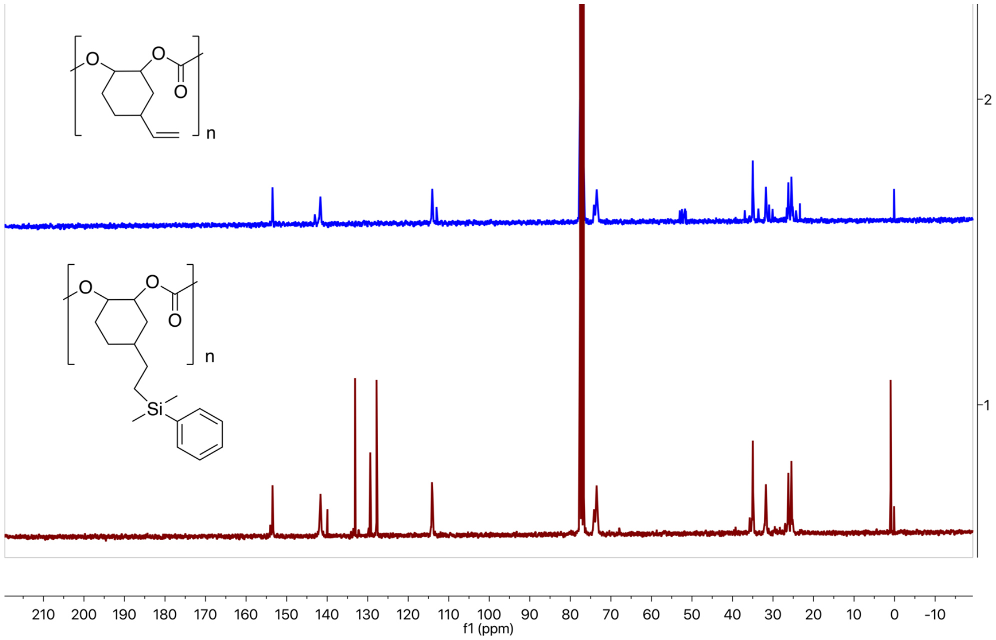

Figure D. 3. $^{13}C\{^{1}H\}$ NMR (125 MHz, $CDCl_{3}$*1*, 298 K) spectrum of isolated PVCHC (top) and isolated silylated PVCHC (bottom).

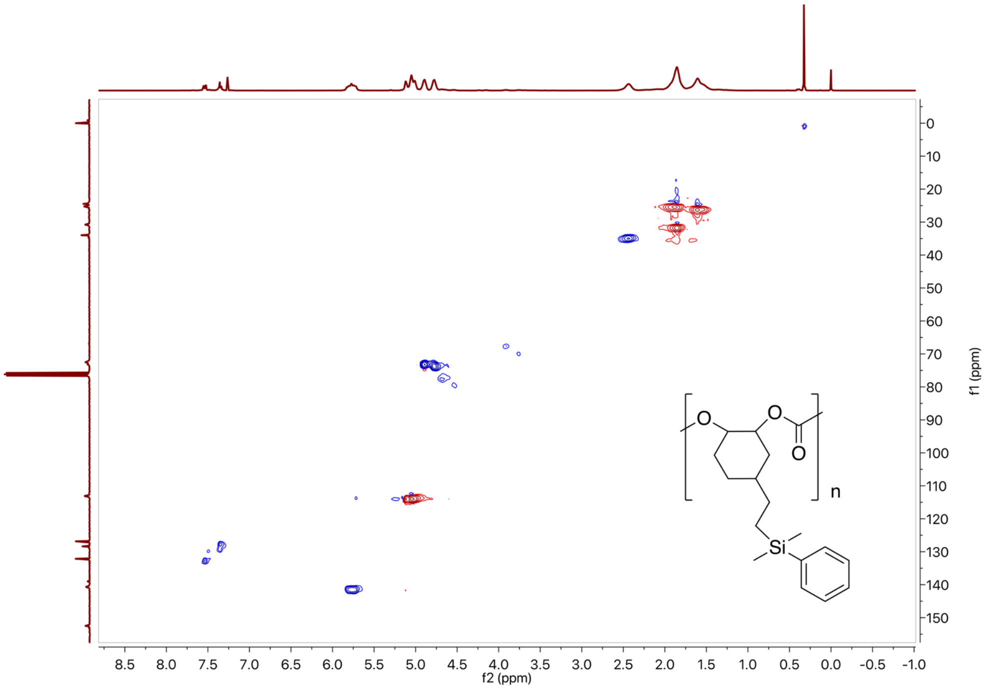

Figure D. 4. HSQC 2-D NMR spectrum of isolated silylated PVCHC. x-axis shows ^{1}H NMR spectrum (300 MHz, CDCl$_3$, 298 K) and y-axis shows ^{13}C{^{1}H} NMR spectrum (75 MHz, CDCl$_3$, 298 K) of isolated PVCHC.

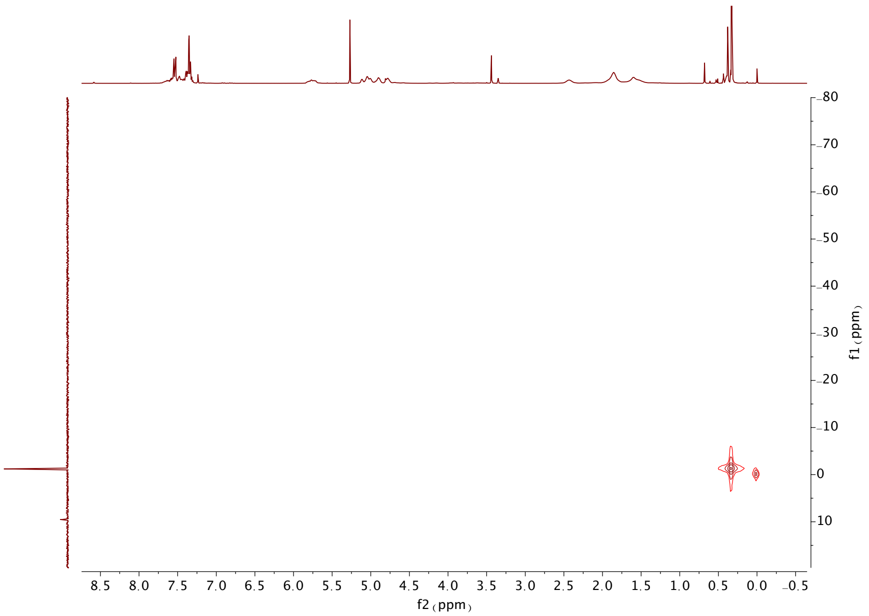

Figure D. 5. HMQC 2-D NMR spectrum of isolated silylated PVCHC. x-axis shows ^{1}H NMR spectrum (300 MHz, $CDCl_3$, 298 K) and y-axis shows ^{29}Si NMR spectrum (60 MHz, $CDCl_3$, 298 K) of the isolated polymer. J(H-Si)=10 Hz. Cross-peak at 0.0 ppm is TMS.

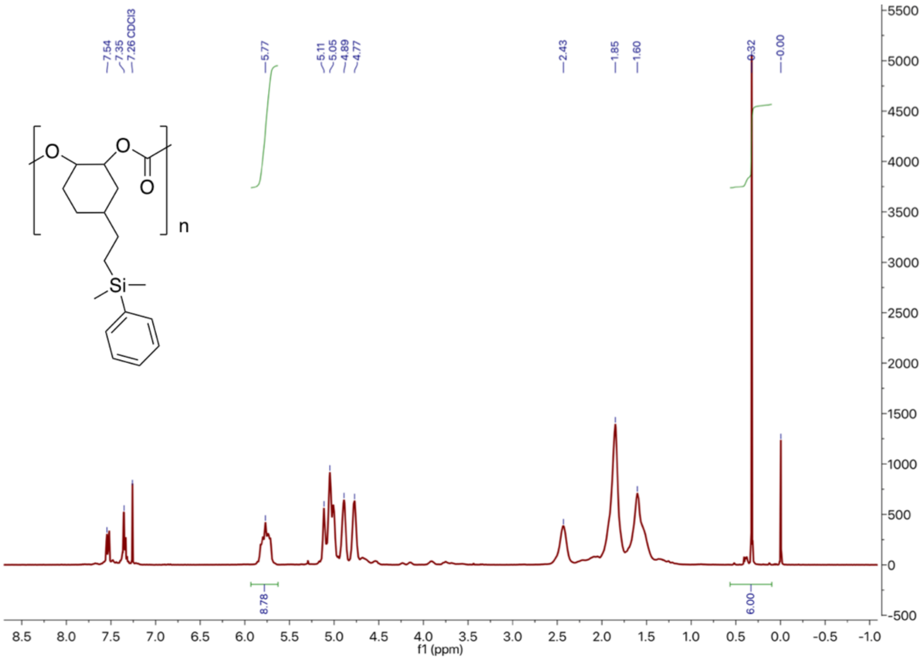

Figure D. 6. Integrated ^{1}H NMR spectrum of silylated PVCHC. Normalized 1 SiMe_2 group, 6H, which corresponds 8.78 C$H_{(B)}$ residual vinyl groups. % silyl = m/(m+n) *100% = 1/(1+8.78) *100% = 10.2% functionalization.

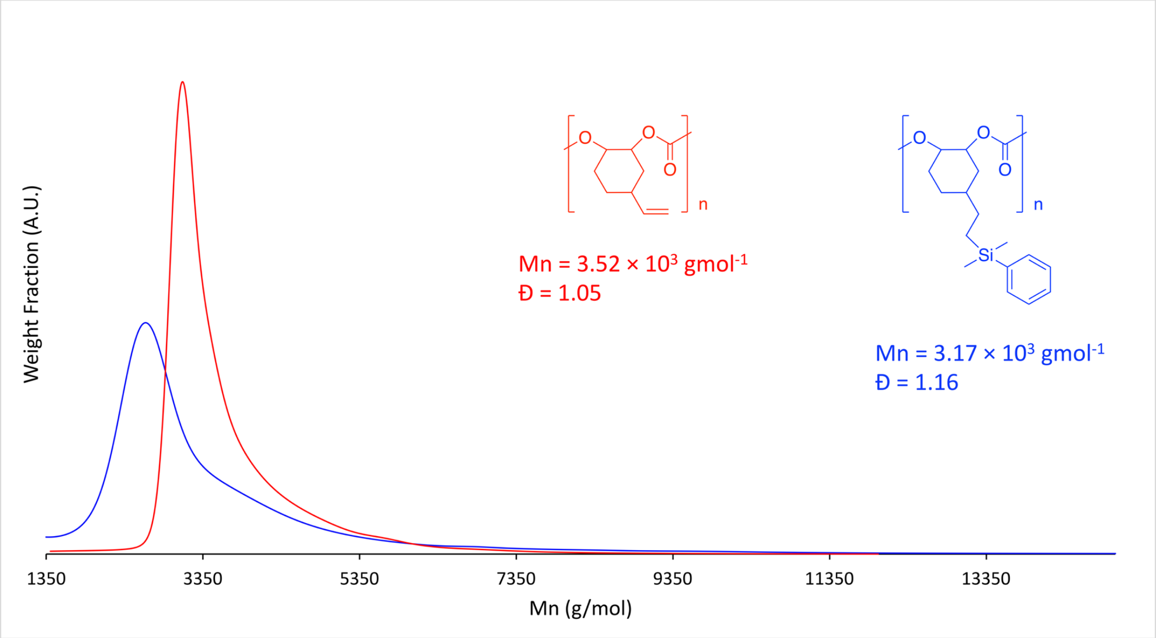

Figure D. 7. GPC chromatogram showing light scattering trace of isolated PVCHC (at 5 mol% BPh_3) and silylated PVCHC from one-pot synthesis.

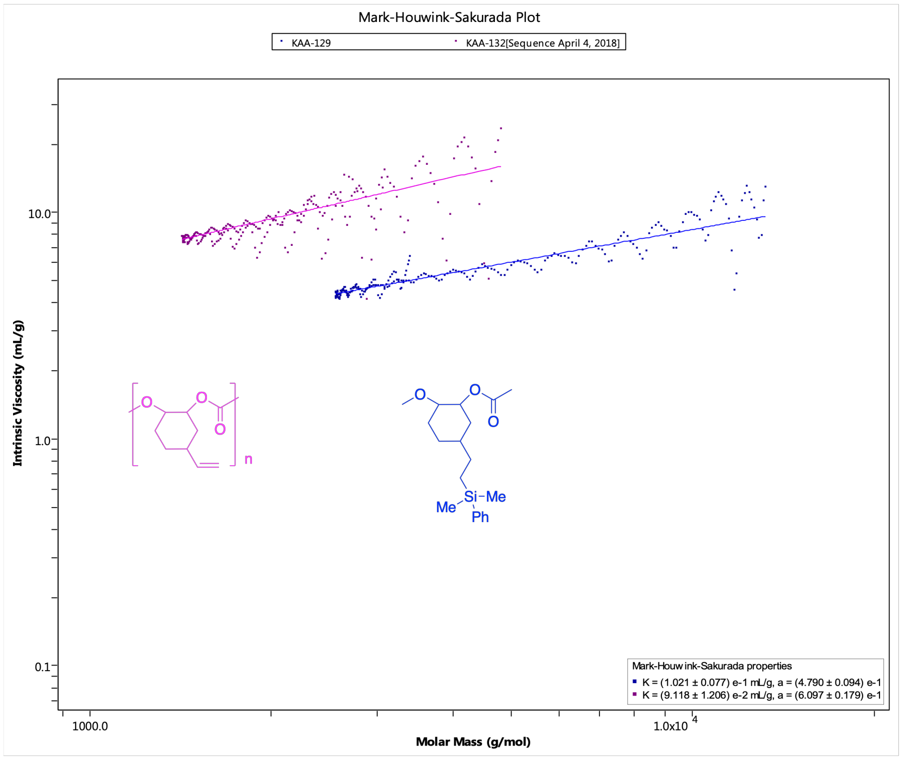

Figure D. 8. Mark-Houwink-Sakurada plot for isolated PVCHC (at 5 mol% BPh_3) and silylated PVCHC from one-pot synthesis.

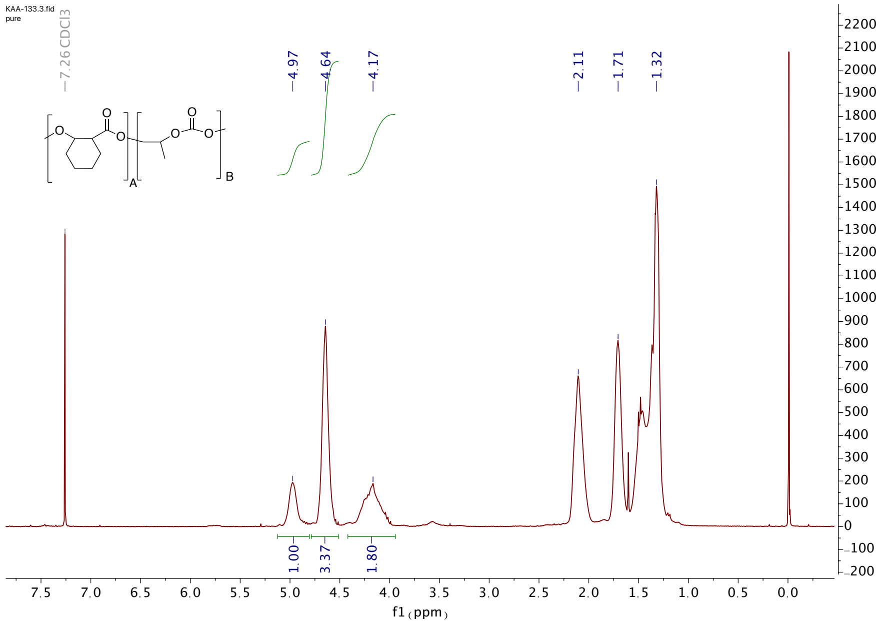

Figure D. 9. Integrated ^{1}H NMR (300 MHz, $CDCl_3$, 298 K) spectrum of PO/CHO/CO_2 terpolymer from **Table 5.1**, entry 1.

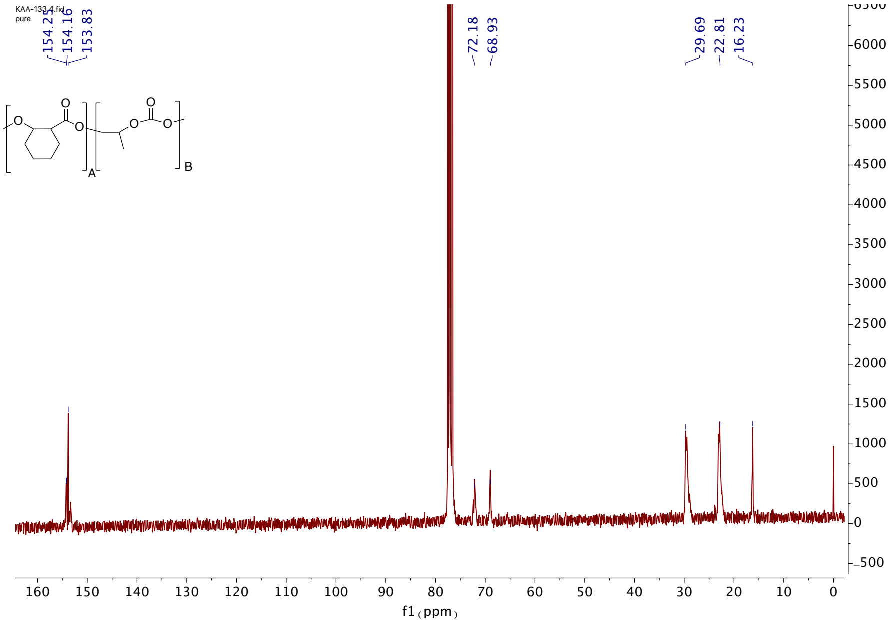

Figure D. 10. $^{13}C\{^{1}H\}$ NMR (125 MHz, $CDCl_3$, 298 K) spectrum of PO/CHO/CO_2 terpolymer from **Table 5.1**, entry 1.

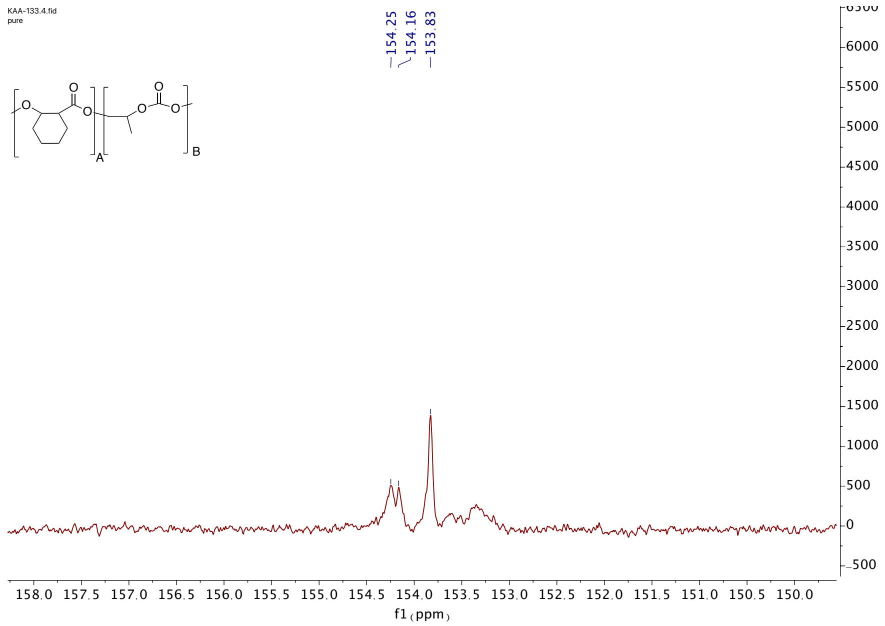

Figure D. 11. Zoom $^{13}C\{^{1}H\}$ NMR (125 MHz, $CDCl_3$, 298 K) spectrum of PO/CHO/CO_2 terpolymer from **Table 5.1**, entry 1, showing tacticity of PCHC region.

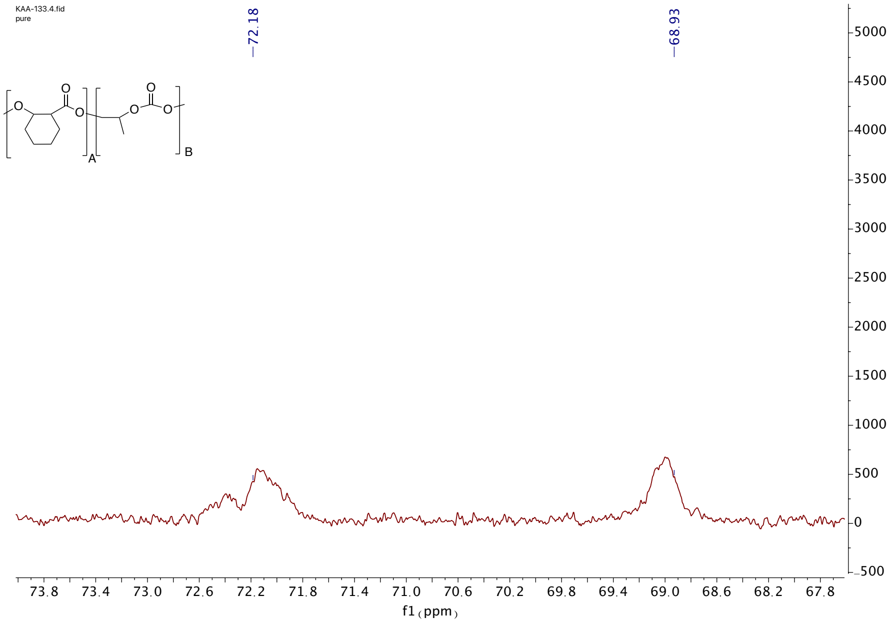

Figure D. 12. Zoom $^{13}C\{^{1}H\}$ NMR (125 MHz, $CDCl_3$, 298 K) spectrum of PO/CHO/CO_2 terpolymer from **Table 5.1**, entry 1, showing tacticity of PPC region.

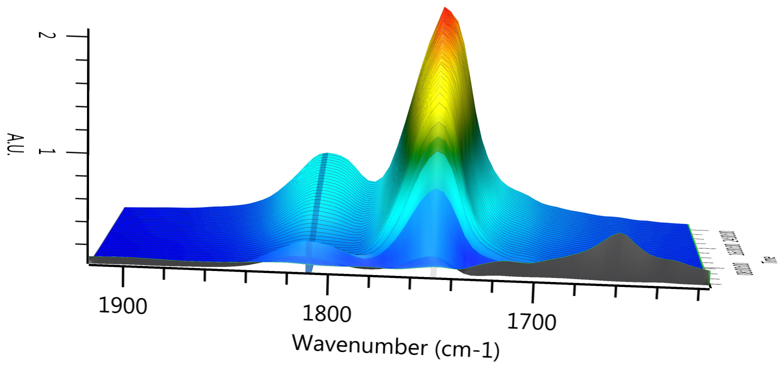

Figure D. 13. 3D React IR plot from Table 1, entry 1 showing major product is polycarbonate ($\nu = 1750\ \text{cm}^{-1}$) while cyclic carbonate ($\nu = 1809\ \text{cm}^{-1}$) is the minor product.

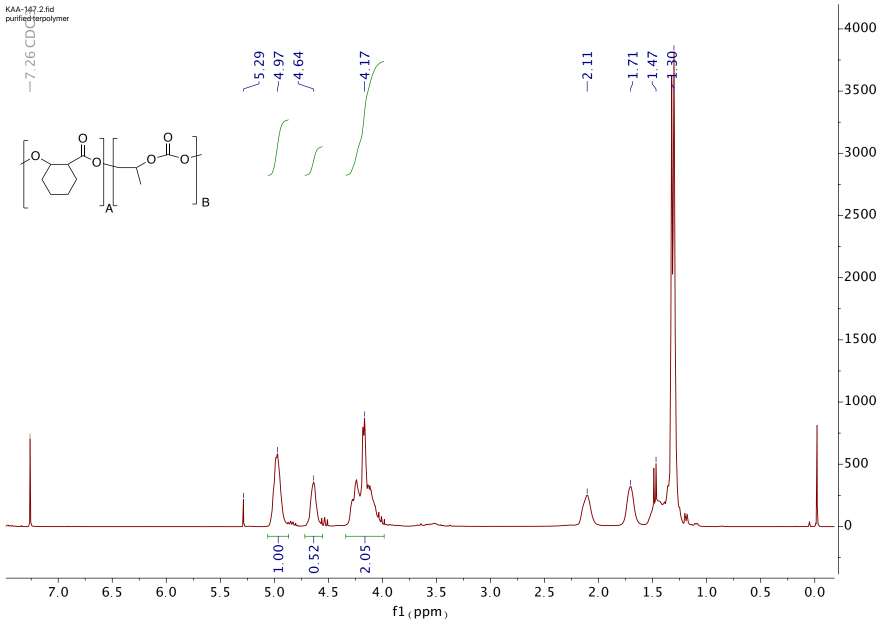

Figure D. 14. Integrated ^{1}H NMR (300 MHz, $CDCl_3$, 298 K) spectrum of PO/CHO/CO_2 terpolymer from **Table 5.1**, entry 2.

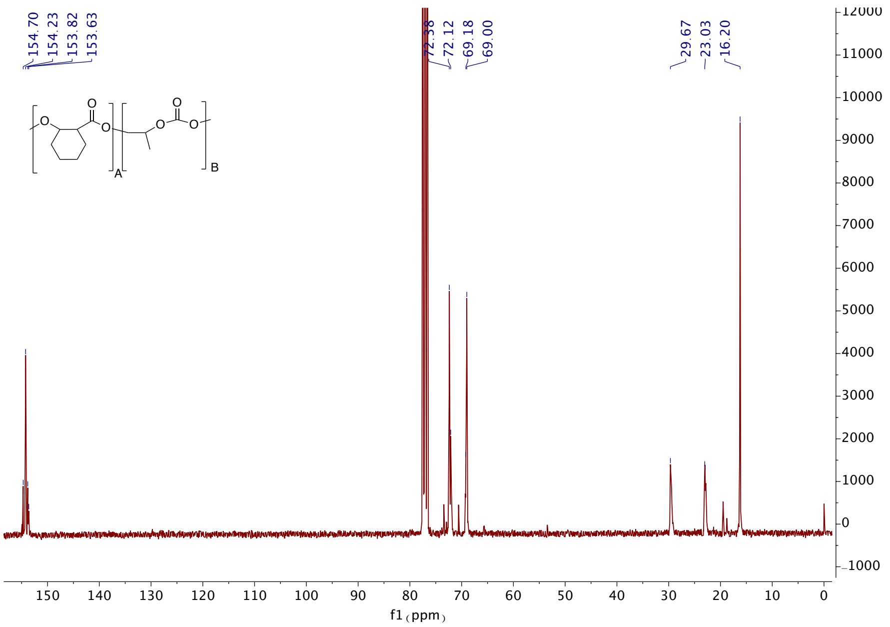

Figure D. 15. ^{13}C{^{1}H} NMR (125 MHz, CDCl$_3$-d_1, 298 K) spectrum of PO/CHO/CO$_2$ terpolymer from **Table 5.1**, entry 2.

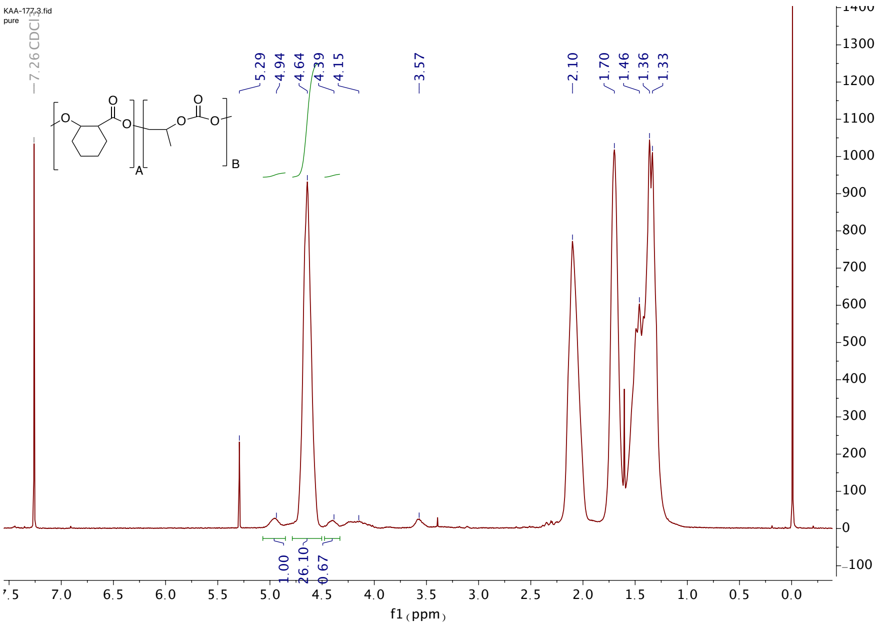

Figure D. 16. Integrated ^{1}H NMR (300 MHz, CDCl$_3$, 298 K) spectrum of PO/CHO/CO$_2$ terpolymer from **Table 5.1**, entry 3.

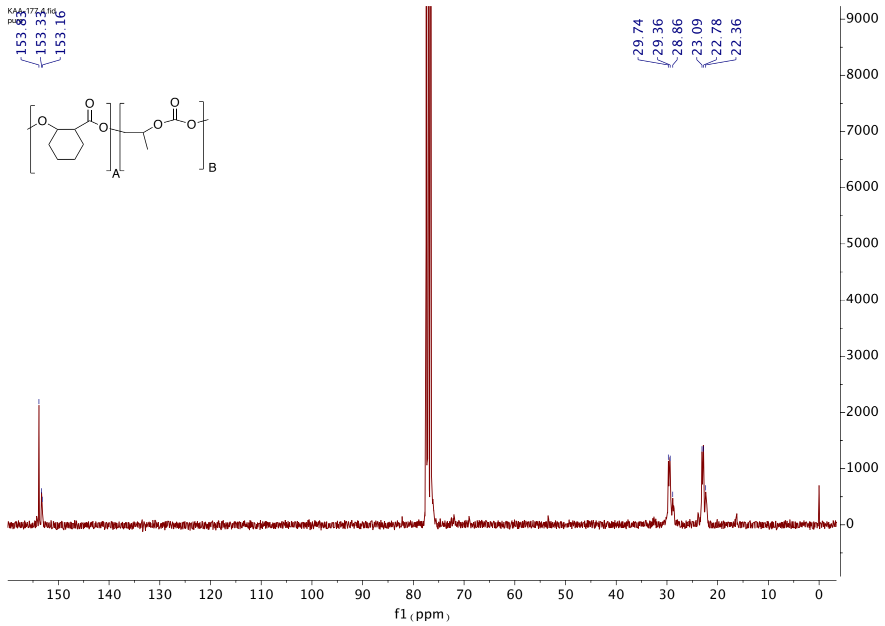

Figure D. 17. $^{13}C\{^1H\}$ NMR (125 MHz, $CDCl_3$, 298 K) spectrum of PO/CHO/CO_2 terpolymer from **Table 5.1**, entry 3.

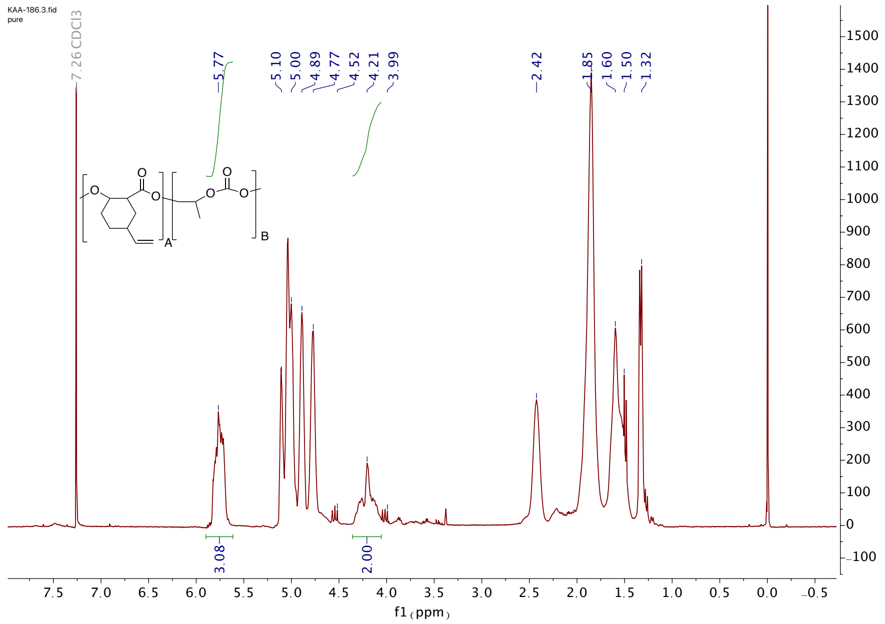

Figure D. 18. Integrated ^1H NMR (300 MHz, $CDCl_3$, 298 K) spectrum of PO/VCHO/CO_2 terpolymer from **Table 5.1**, entry 4.

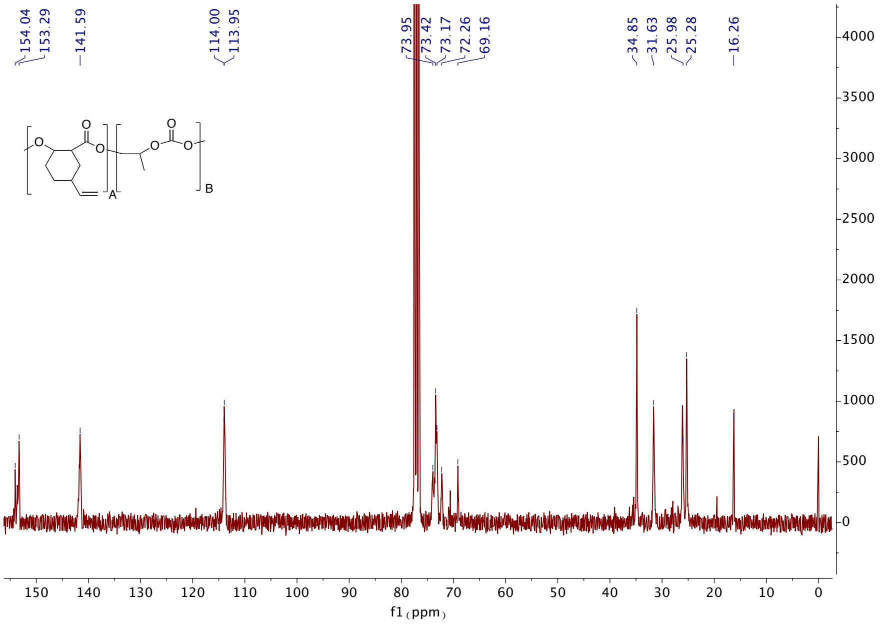

Figure D. 19. $^{13}C\{^1H\}$ NMR (125 MHz, $CDCl_3$, 298 K) spectrum of PO/VCHO/CO_2 terpolymer from **Table 5.1**, entry 4.

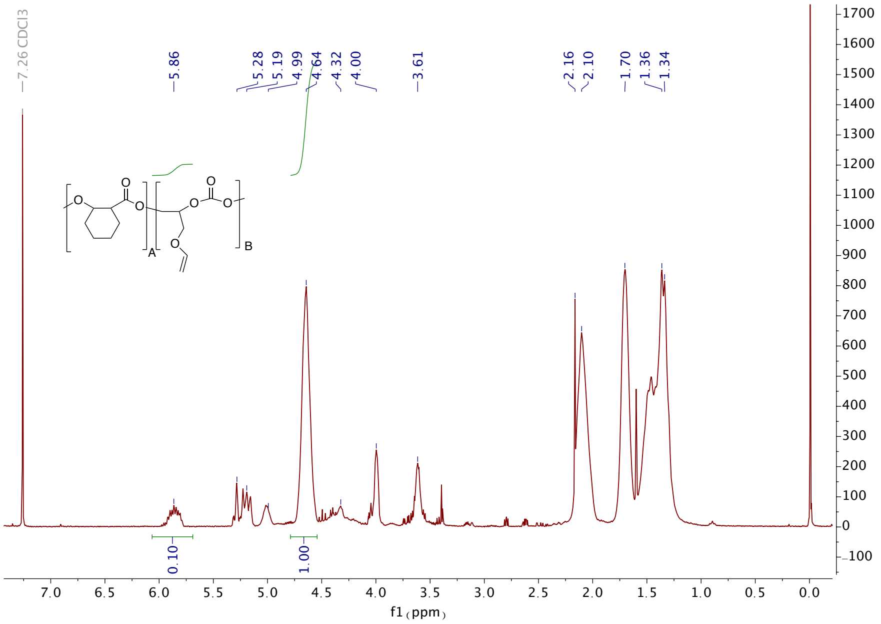

Figure D. 20. Integrated ^1H NMR (300 MHz, $CDCl_3$, 298 K) spectrum of CHO/AGE/CO_2 terpolymer from **Table 5.1**, entry 5.

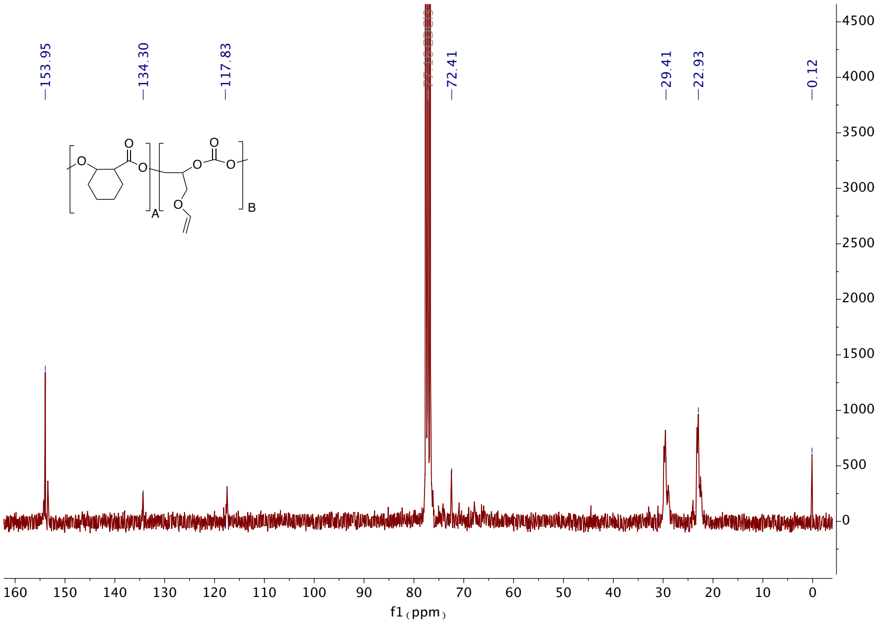

Figure D. 21. $^{13}C\{^1H\}$ NMR (125 MHz, $CDCl_3$, 298 K) spectrum of CHO/AGE/CO_2 terpolymer from **Table 5.1**, entry 5.

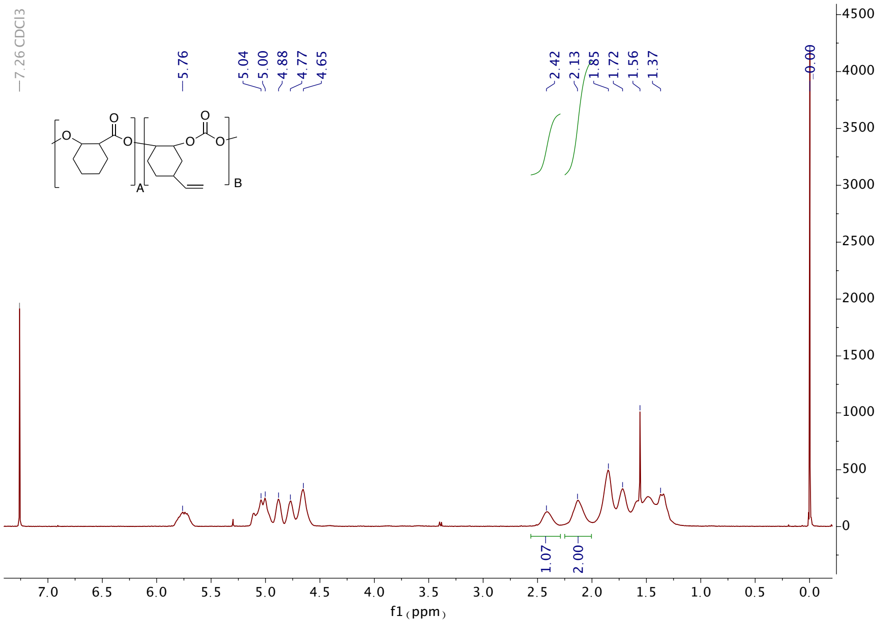

Figure D. 22. Integrated ^1H NMR (300 MHz, $CDCl_3$, 298 K) spectrum of CHO/VCHO/CO_2 terpolymer from **Table 5.1**, entry 6.

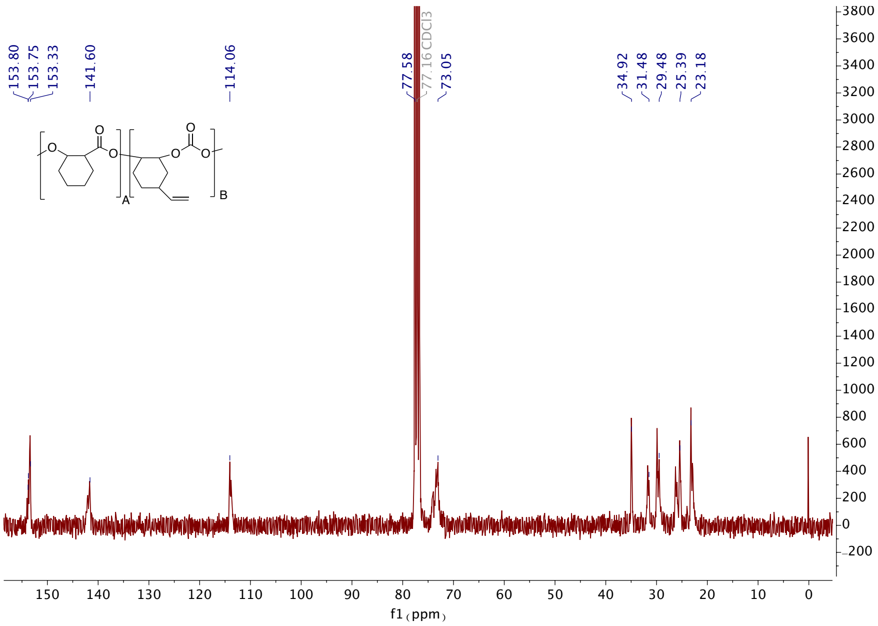

Figure D. 23. $^{13}C\{^{1}H\}$ NMR (125 MHz, $CDCl_3$, 298 K) spectrum of CHO/VCHO/CO_2 terpolymer from **Table 5.1**, entry 6.

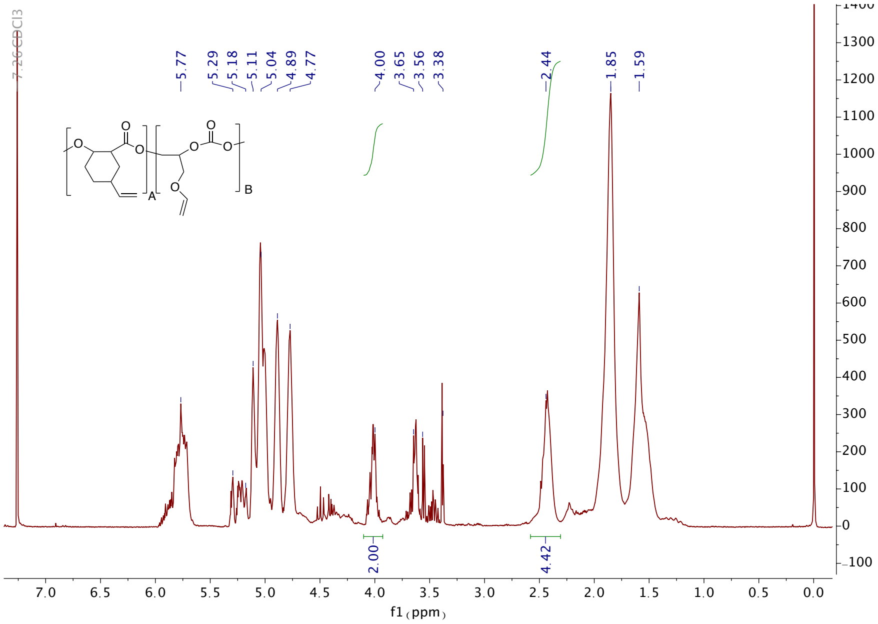

Figure D. 24. Integrated ^{1}H NMR (300 MHz, $CDCl_3$, 298 K) spectrum of VCHO/AGE/CO_2 terpolymer from **Table 5.1**, entry 7.

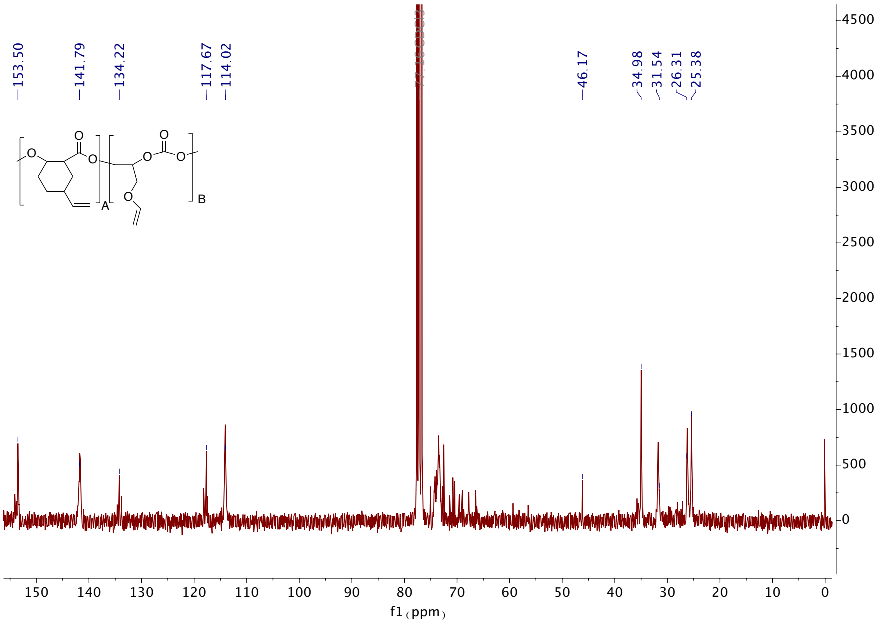

Figure D. 25. $^{13}C\{^{1}H\}$ NMR (125 MHz, $CDCl_3$, 298 K) spectrum of VCHO/AGE/CO_2 terpolymer from **Table 5.1**, entry 7.

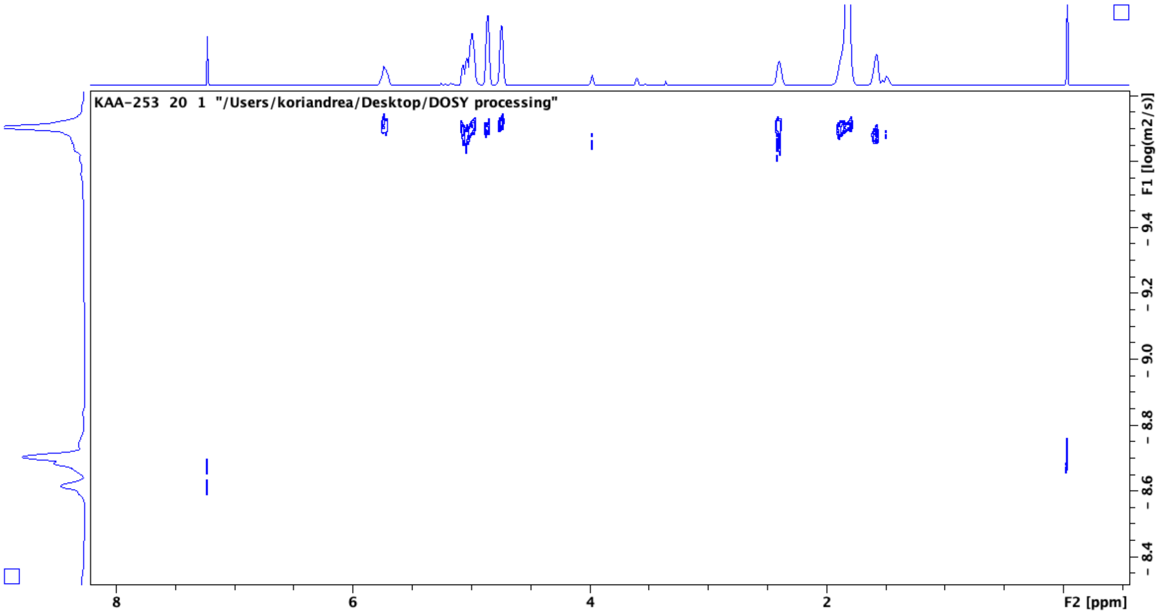

Figure D. 26. Representative DOSY NMR spectra of obtained terpolymer (CO_2/CHO/AGE) from **Table 5.1**, entry 9. (^{1}H NMR 500 MHz, $CDCl_3$, 298 K)

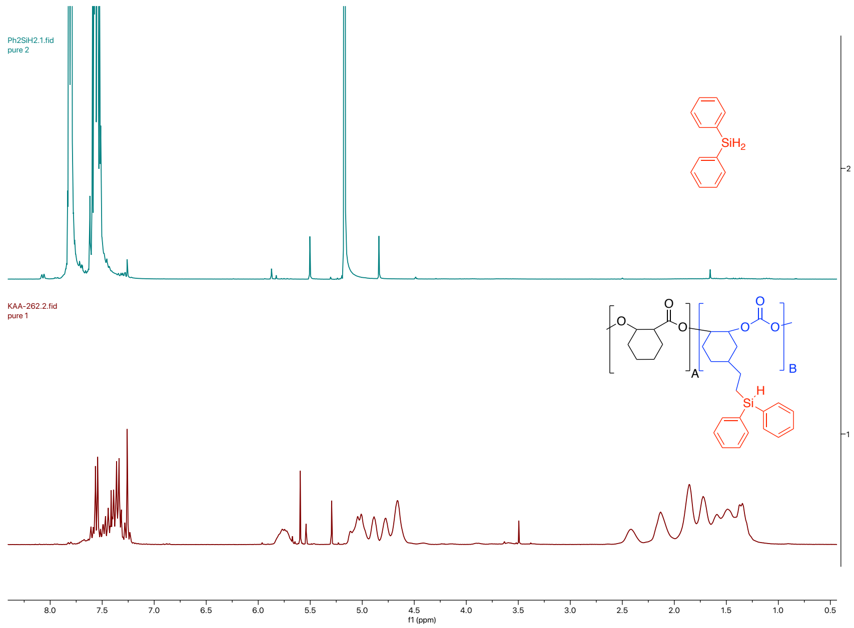

Figure D. 27. ^{1}H NMR (300 MHz, $CDCl_3$, 298 K) spectrum of pure Ph_2SiH_2 (top) and resulting functionalized terpolymer (CHO/VCHO/CO_2) (bottom). 36.4% of vinyl groups have been silylated (see Fig. D31 for expanded view).

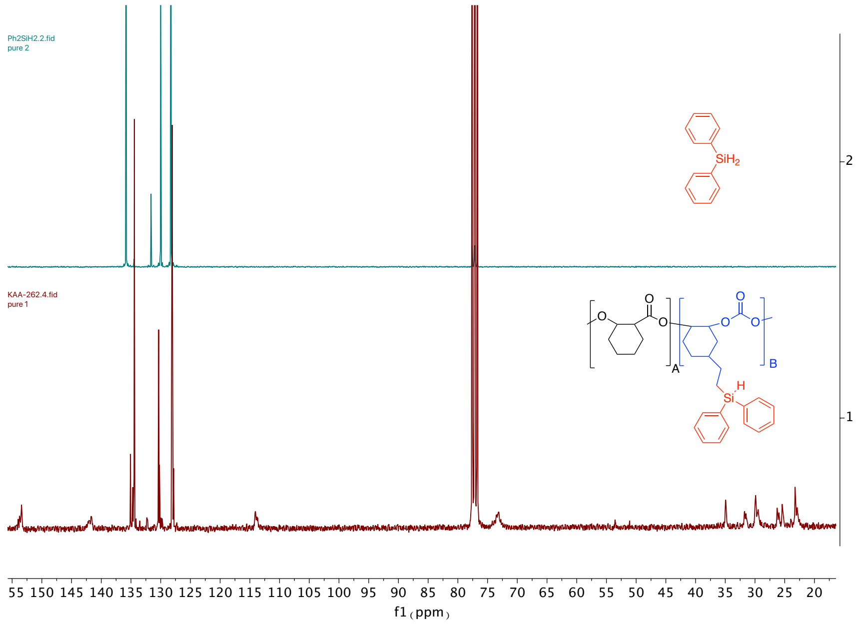

Figure D. 28. $^{13}C\{^1H\}$ NMR (125 MHz, $CDCl_3$, 298 K) spectrum of pure Ph_2SiH_2 (top) and resulting functionalized terpolymer (CHO/VCHO/CO_2) (bottom).

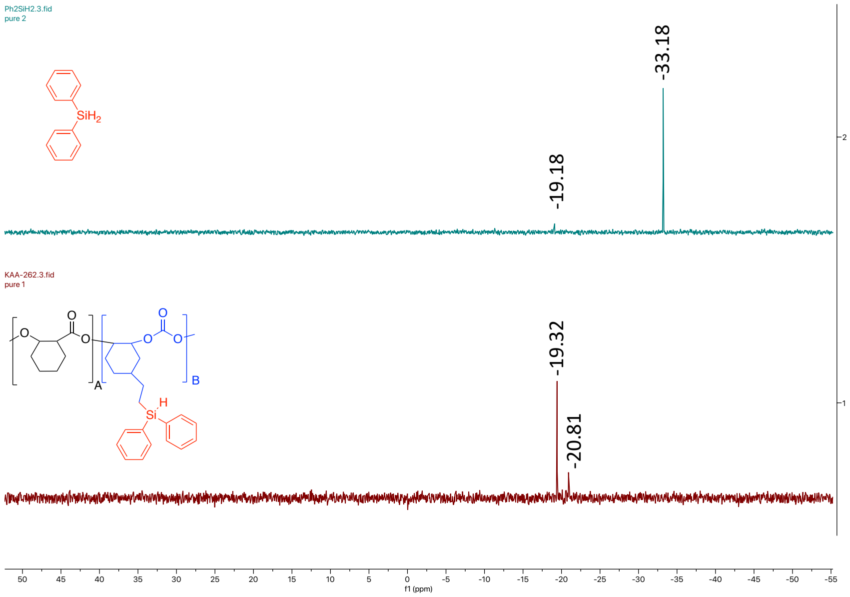

Figure D. 29. Refocused INEPT ^{29}Si NMR (60 MHz, $CDCl_3$, 298 K) spectrum of isolated PVCHC (top) and isolated silylated terpolymer (CHO/VCHO/CO_2) (bottom).

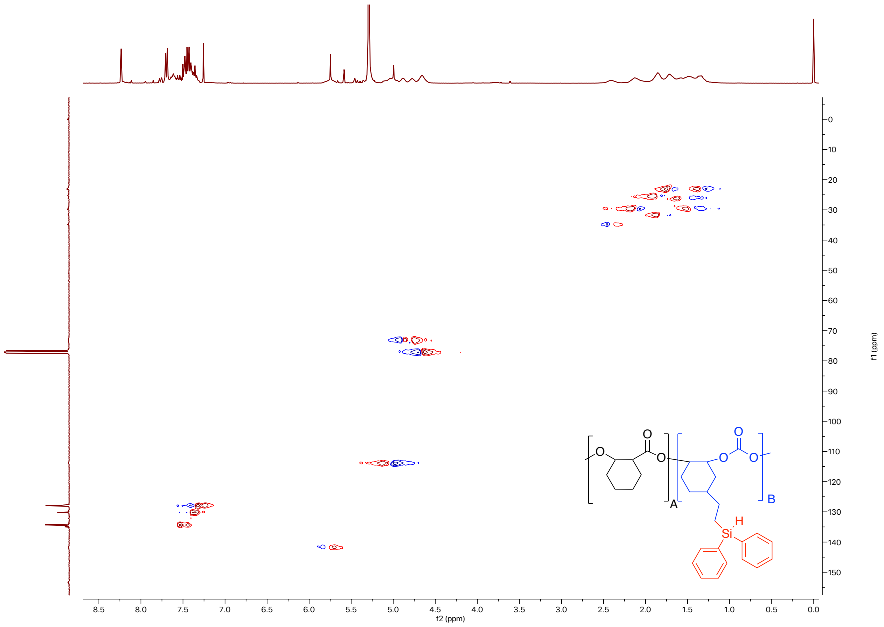

Figure D. 30. HSQC 2-D NMR spectrum of isolated silylated terpolmer (CHO/VCHO/CO_2). x-axis shows ^1H NMR spectrum (300 MHz, $CDCl_3$, 298 K) and y-axis shows $^{13}C\{^1H\}$ NMR spectrum (75 MHz, $CDCl_3$, 298 K) of the isolated polymer.

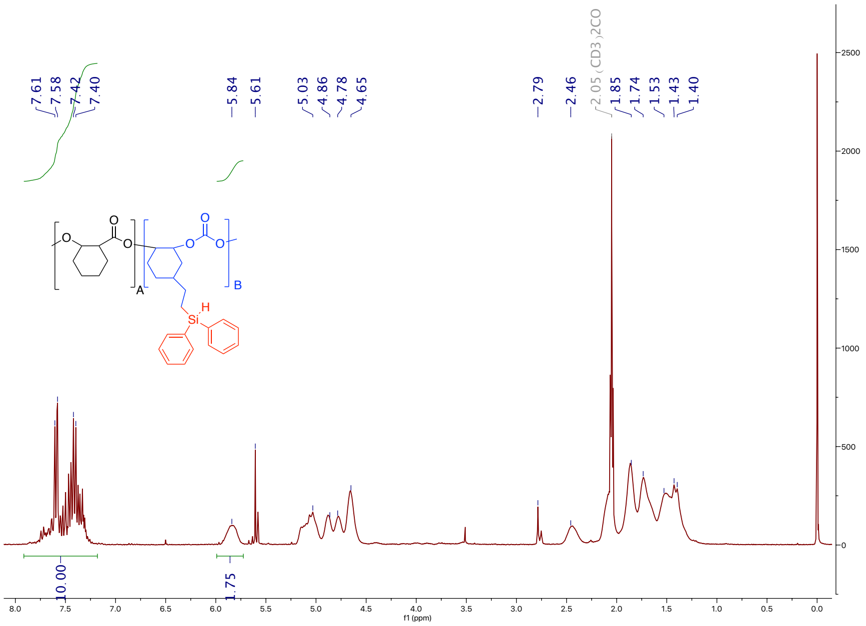

Figure D. 31. Integrated ^{1}H NMR (300 MHz, $(CD_3)_2CO$, 298 K) spectrum of silylated PVCHC. Normalized 1 Si*Ar*$_2$ group, 10H, which corresponds 1.75 C*H*$_{(B)}$ residual vinyl groups. % silyl = m/(m+n) *100% = 1/(1+1.75) *100% = 36.4% functionalization.

Figure D. 32. HMQC 2-D NMR spectrum of isolated silylated terpolmer (CHO/VCHO/CO$_2$). x-axis shows ^{1}H NMR spectrum (300 MHz, CDCl$_3$, 298 K) and y-axis shows ^{29}Si NMR spectrum (60 MHz, CDCl$_3$-d_1, 298 K) of the isolated polymer. J(H-Si)= 300 Hz

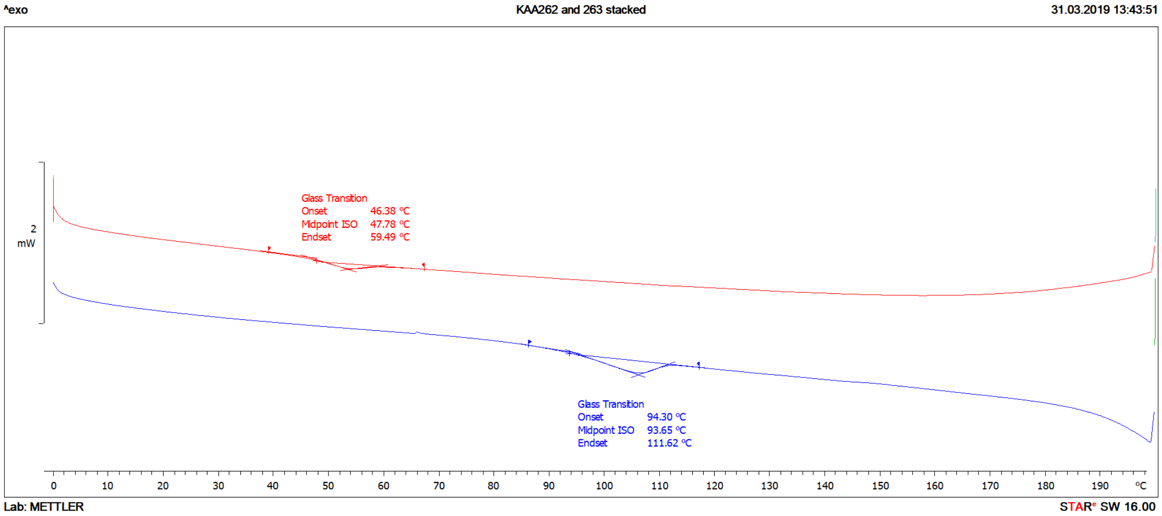

Figure D. 33. DSC of native terpolymer (CO$_2$/CHO/VCHO) from one pot reaction (blue) and after silane functionalization (red). Glass transition temperatures taken from the 3rd cycle.

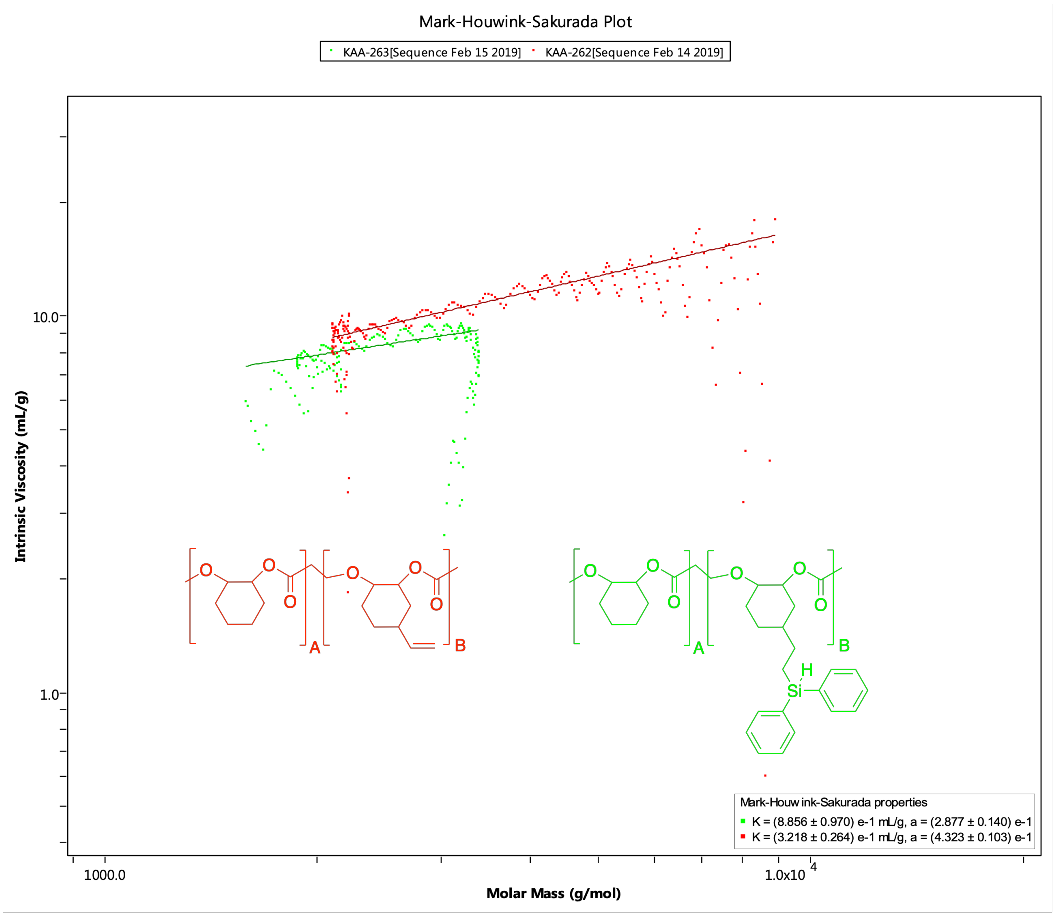

Figure D. 34. Mark-Houwink-Sakurada plot for isolated terpolymer (CHO/VCHO/CO_2) and the corresponding silylated terpolymer.

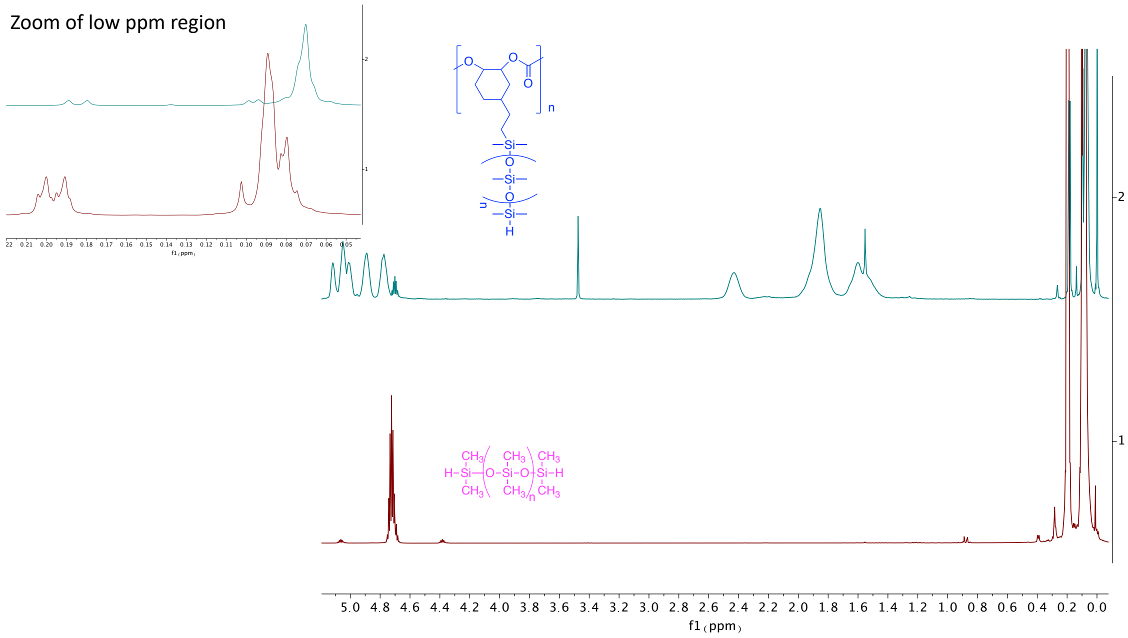

Figure D. 35. ^{1}H NMR (300 MHz, $CDCl_3$, 298 K) spectrum of pure DMS-HO3 (top) and resulting functionalized PVCHC (bottom).

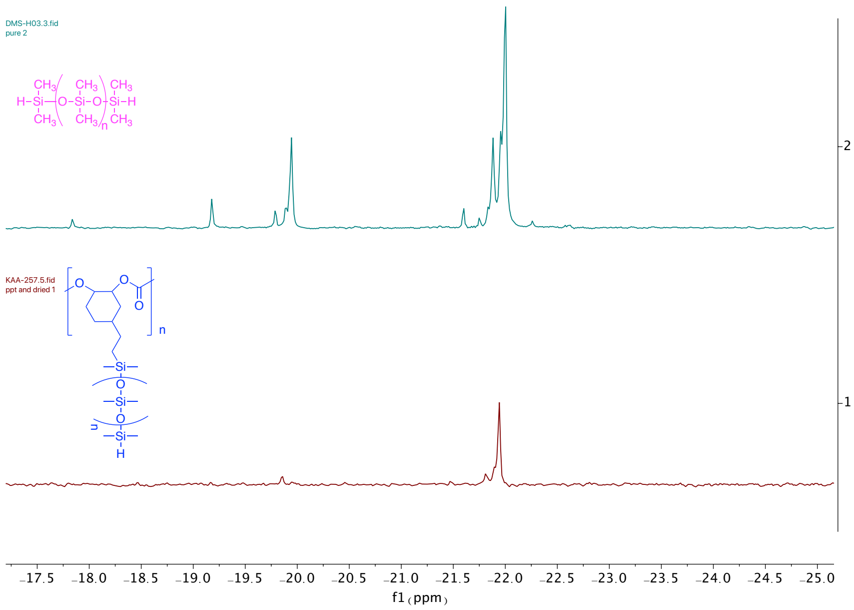

Figure D. 36. Refocused INEPT ^{29}Si NMR (60 MHz, $CDCl_3$, 298 K) spectrum of pure DMS-HO3 (top) and resulting functionalized PVCHC (bottom).

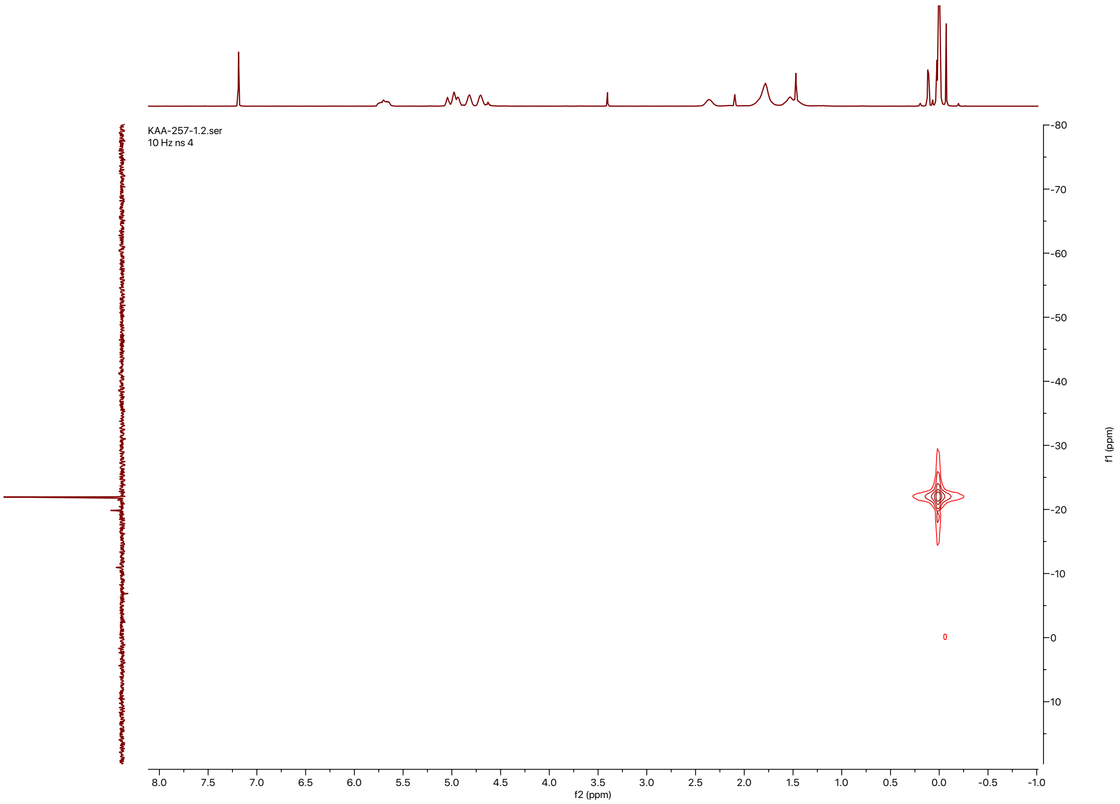

Figure D. 37. HMQC 2-D NMR spectrum of isolated DMS-HO3 functionalized PVCHC x-axis shows ^{1}H NMR spectrum (300 MHz, $CDCl_3$, 298 K) and y-axis shows ^{29}Si NMR spectrum (60 MHz, $CDCl_3$, 298 K) of the isolated polymer. J(H-Si)= 10 Hz

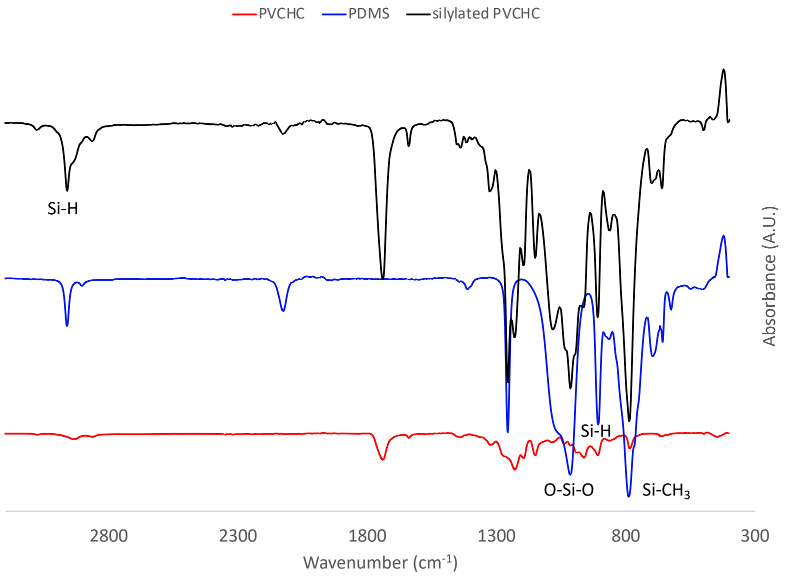

Figure D. 38. Stacked FTIR spectra of isolated PVCHC (red), DMS-HO3 (blue) and DMS-HO3 functionalized PVCHC (black)

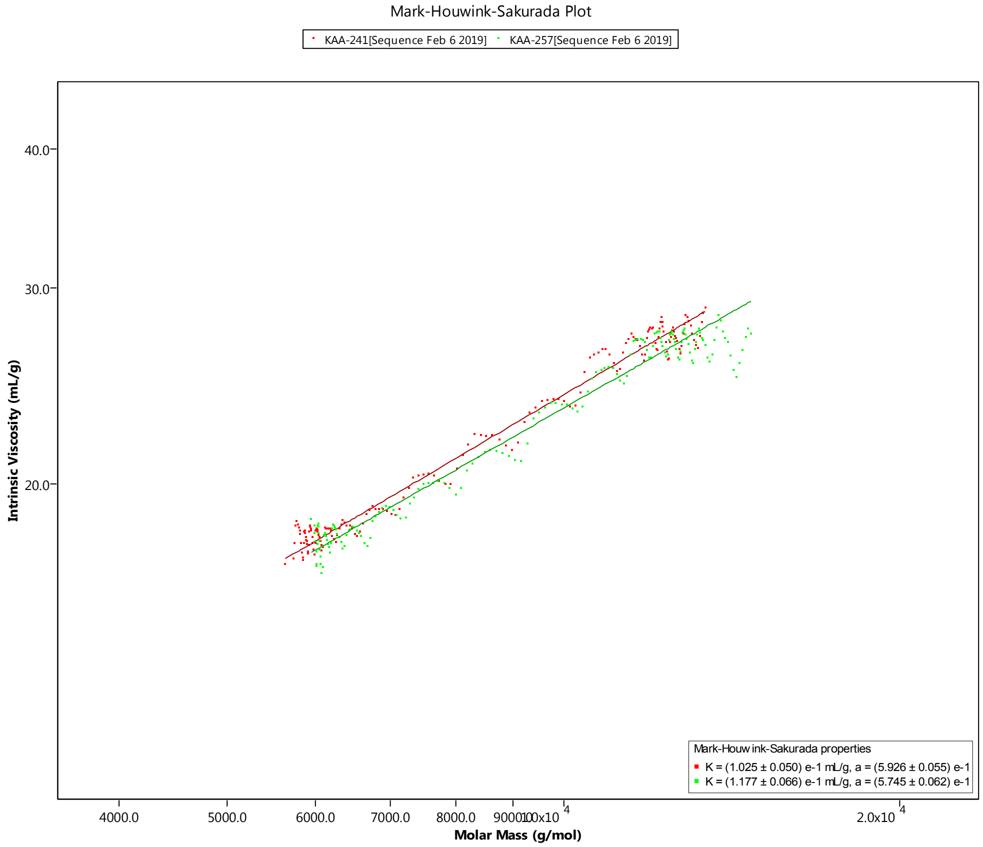

Figure D. 39. Mark-Houwink-Sakurada plot for isolated PVCHC (green) and DMS-HO3 functionalized PVCHC (red)

Appendix E

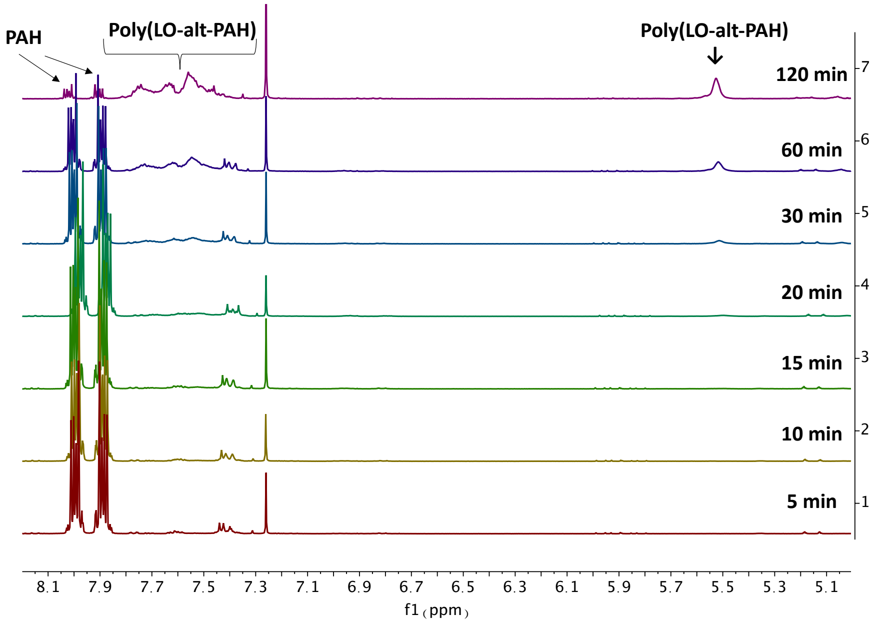

Figure E. 1. Stacked ^{1}H NMR (300 MHz, 298 K, $CDCl_3$) spectra of alternating ring-opening polymerization of LO and PAH (**Table 6.1**, entry 1)

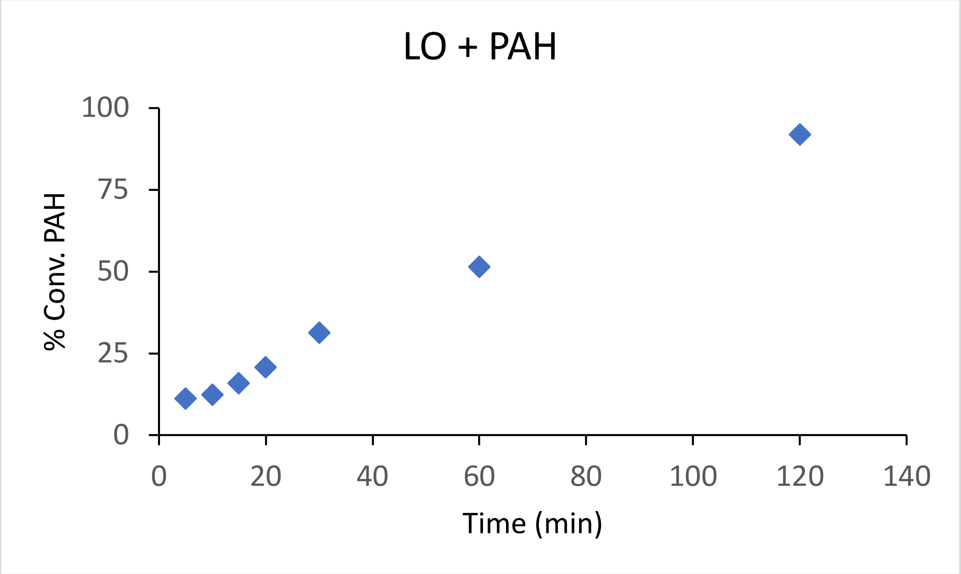

Figure E. 2. Conversion vs. time plot of alternating ring-opening polymerization of LO and PAH (**Table 6.1**, entry 1)

Table E. 1. Anhydride conversion and GPC data for alternating ring-opening polymerization of LO and PAH (**Table 6.1**, entry 1)

Aliquot Time (min)	% Conv. PAH[a]	M_n (g/mol)[b]	*Đ*[b]
5	11.2	-	-
10	12.3	-	-
15	15.8	-	-
20	20.8	-	-
30	31.2	-	-
60	51.5	4 085	1.30
120	91.9	6 051	1.16

[a]Determined from ^{1}H NMR [b]Đ, dispersity = M_w/M_n. Determined in THF by GPC equipped with a multiangle light-scattering detector. GPC data not obtained for lower conversions due to inability to isolate material

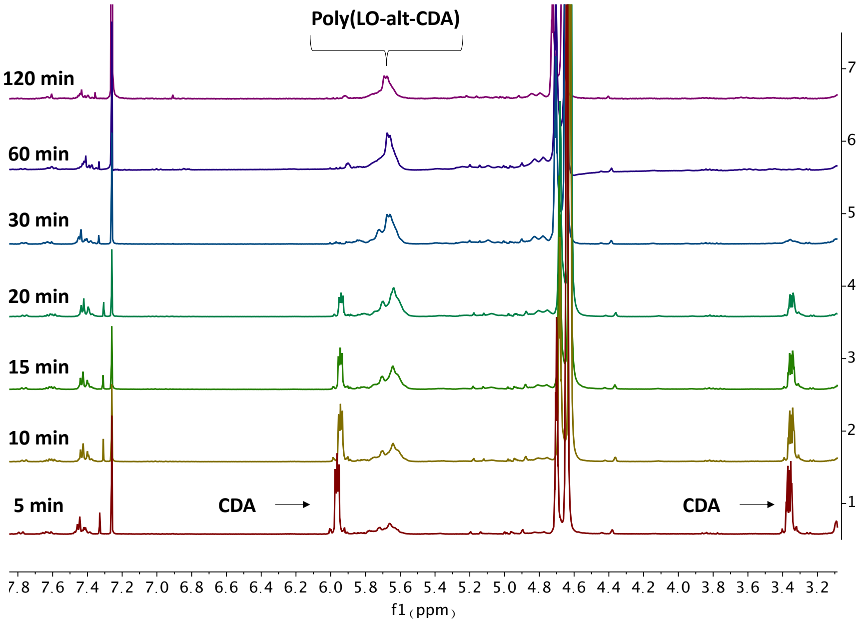

Figure E. 3. Stacked ^{1}H NMR (300 MHz, 298 K, $CDCl_3$) spectra of alternating ring-opening polymerization of LO and CDA (**Table 6.1**, entry 2)

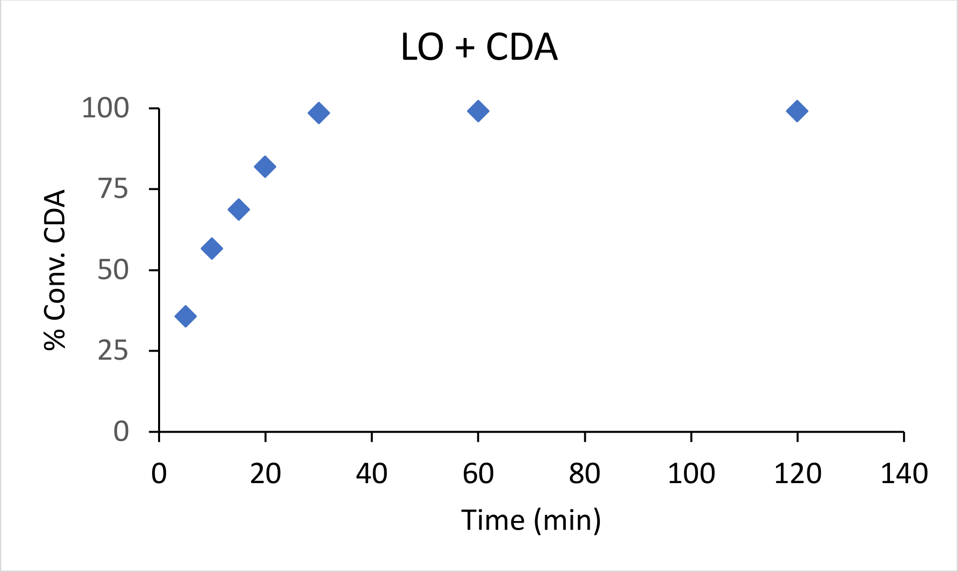

Figure E. 4. Conversion vs. time plot of alternating ring-opening polymerization of LO and CDA (**Table 6.1**, entry 2)

Table E. 2. Anhydride conversion and GPC data for alternating ring-opening polymerization of LO and CDA (**Table 6.1**, entry 2)

Aliquot Time (min)	% Conv. CDA[a]	M_n (g/mol)[b]	$Đ^b$
5	35.7	420	1.05
10	56.5	717	1.04
15	68.7	852	1.04
20	81.9	937	1.03
30	98.4	924	1.06
60	99	1 118	1.08
120	99	2 437	1.09

[a]Determined from ^{1}H NMR [b]Đ, dispersity = M_w/M_n. Determined in THF by GPC equipped with a multiangle light-scattering detector.

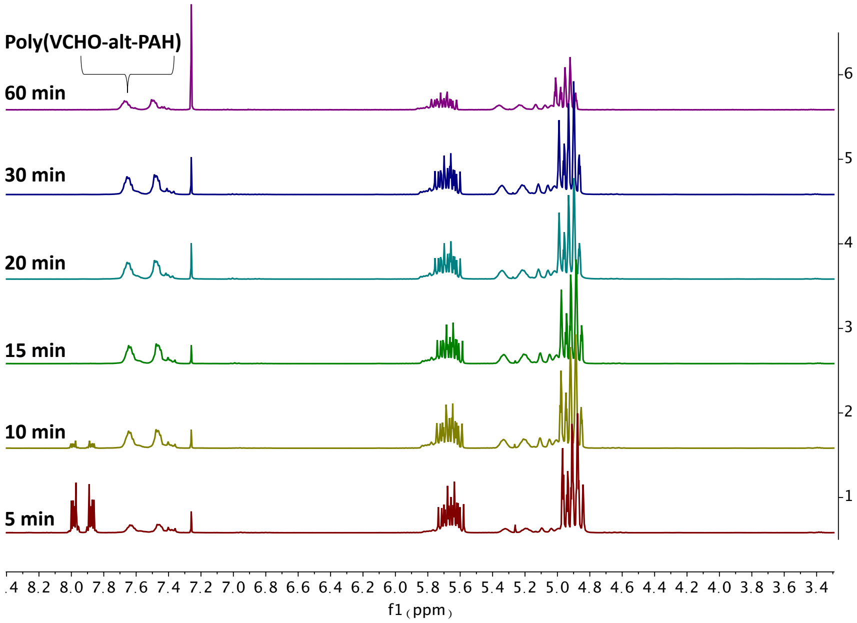

Figure E. 5. Stacked ^{1}H NMR (300 MHz, 298 K, $CDCl_3$) spectra of controlled alternating ring-opening polymerization of VCHO and PAH (**Table 6.1**, entry 3)

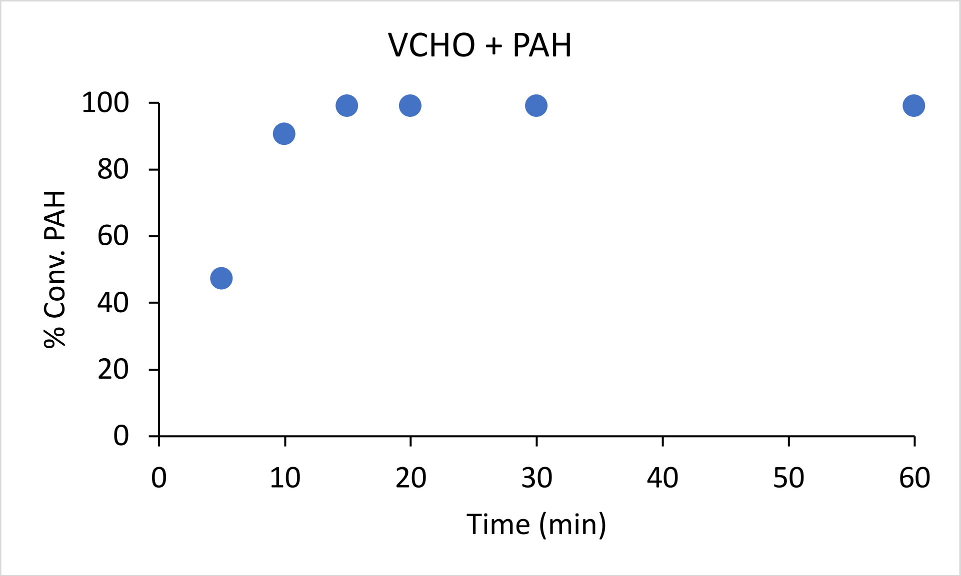

Figure E. 6. Conversion vs. time plot of controlled alternating ring-opening polymerization of VCHO and PAH (**Table 6.1**, entry 3)

Table E. 3. Anhydride conversion and GPC data for controlled alternating ring-opening polymerization of VCHO and PAH (**Table 6.1**, entry 3).

Aliquot Time (min)	% Conv. PAH[a]	M_n (g/mol)[b]	$Đ$[b]
5	47.2	9 964	1.12
10	90.5	17 140	1.14
15	99	20 290	1.14
20	99	20 680	1.17
30	99	20 260	1.17
60	99	20 260	1.17

[a]Determined from ^{1}H NMR [b]Đ, dispersity = M_w/M_n. Determined in THF by GPC equipped with a multiangle light-scattering detector.

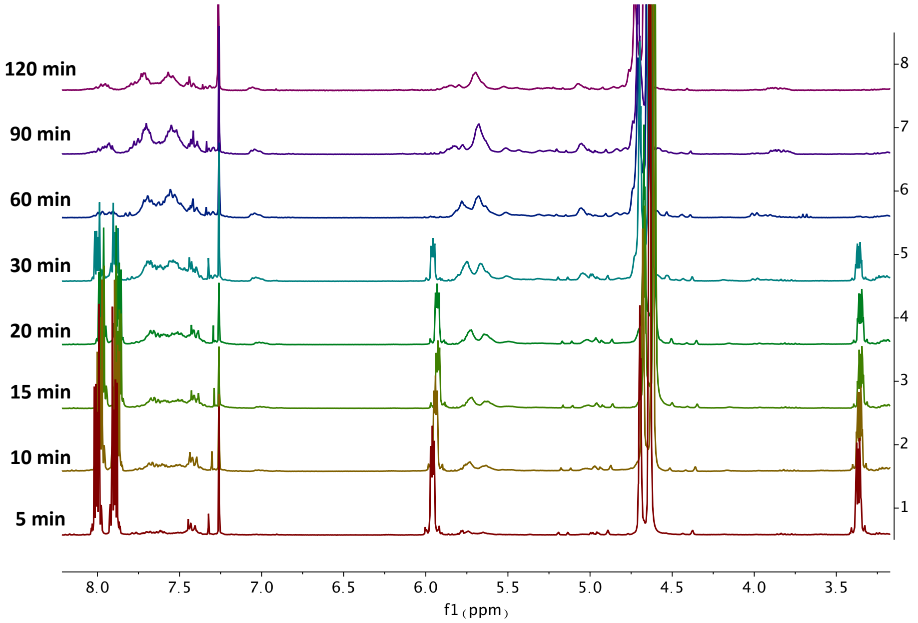

Figure E. 7. Stacked ^{1}H NMR (300 MHz, 298 K, $CDCl_3$) spectra of random alternating ring-opening polymerization of LO, PAH and CDA (**Table 6.1**, entry 7)

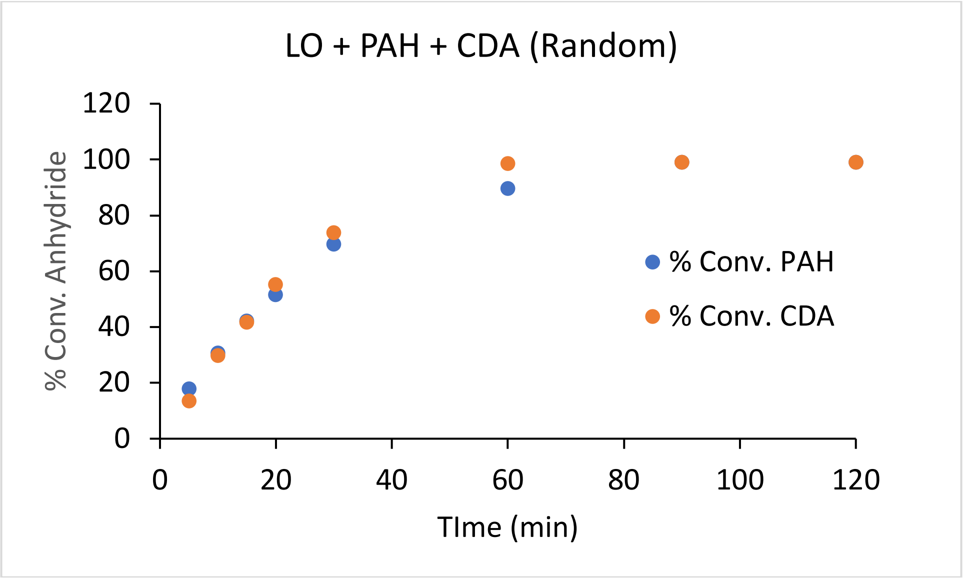

Figure E. 8. Conversion vs. time plot of random alternating ring-opening polymerization of LO and PAH (**Table 6.1**, entry 7)

Table E. 4. Anhydride conversion and GPC data for random alternating ring-opening polymerization of LO and PAH (**Table 6.1**, entry 7).

Aliquot Time (min)	% Conv. PAH[a]	% Conv. CDA[a]	M_n (g/mol)[b]	$Đ$[b]
5	17.9	13.6	626	1.04
10	30.8	29.7	568	1.03
15	42.2	41.8	790	1.03
20	51.5	55.2	825	1.05
30	69.6	73.8	881	1.06
60	89.7	98.5	1 737	1.75
90	99	99	1 737	1.75
120	99	99	1 737	1.75

[a] Determined from ^{1}H NMR [b] Đ, dispersity = M_w/M_n. Determined in THF by GPC equipped with a multiangle light-scattering detector.

Figure E. 9. 2D DOSY NMR spectra (500 MHz, 298 K, $CDCl_3$) of random alternating ring-opening polymerization of LO, PAH and CDA (**Table 6.1**, entry 7).

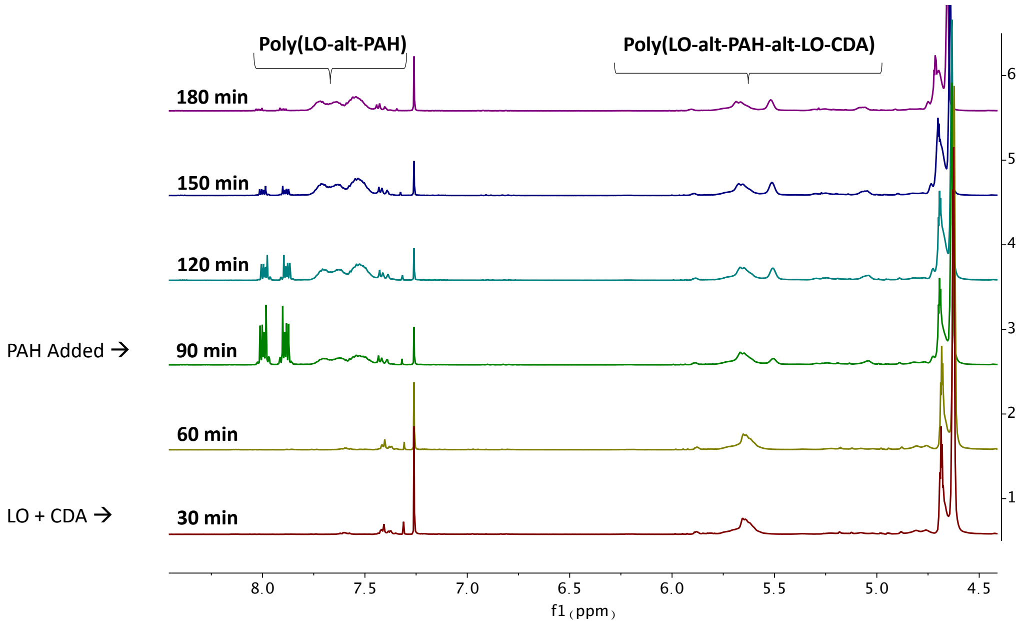

Figure E. 10. Stacked ^{1}H NMR (300 MHz, 298 K, $CDCl_3$) spectra of controlled alternating ring-opening polymerization of LO, PAH and CDA (**Table 6.1**, entry 8)

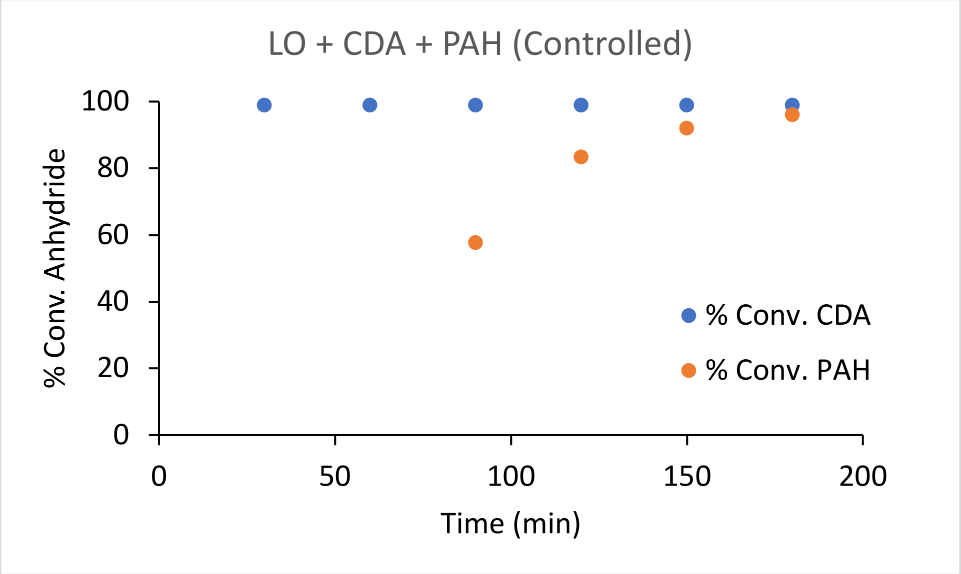

Figure E. 11. Conversion vs. time plot of controlled alternating ring-opening polymerization of LO and PAH (**Table 6.1**, entry 8)

Table E. 5. Anhydride conversion and GPC data for controlled alternating ring-opening polymerization of LO, PAH and CDA (**Table 6.1**, entry 8)

Aliquot Time (min)	% Conv. PAH[a]	% Conv. CDA[a]	M_n (g/mol)[b]	*Đ*[b]
30	-	99	880	1.1
60	-	99	920	1.1
90	58	99	1920	1.1
120	83	99	2120	1.1
150	92	99	2140	1.1
180	96	99	2100	1.2

[a] Determined from ^{1}H NMR [b] Đ, dispersity = M_w/M_n. Determined in THF by GPC equipped with a multiangle light-scattering detector.

Figure E. 12. 2D DOSY NMR spectra (500 MHz, 298 K, $CDCl_3$) of controlled alternating ring-opening polymerization of LO, PAH and CDA (**Table 6.1**, entry 8).

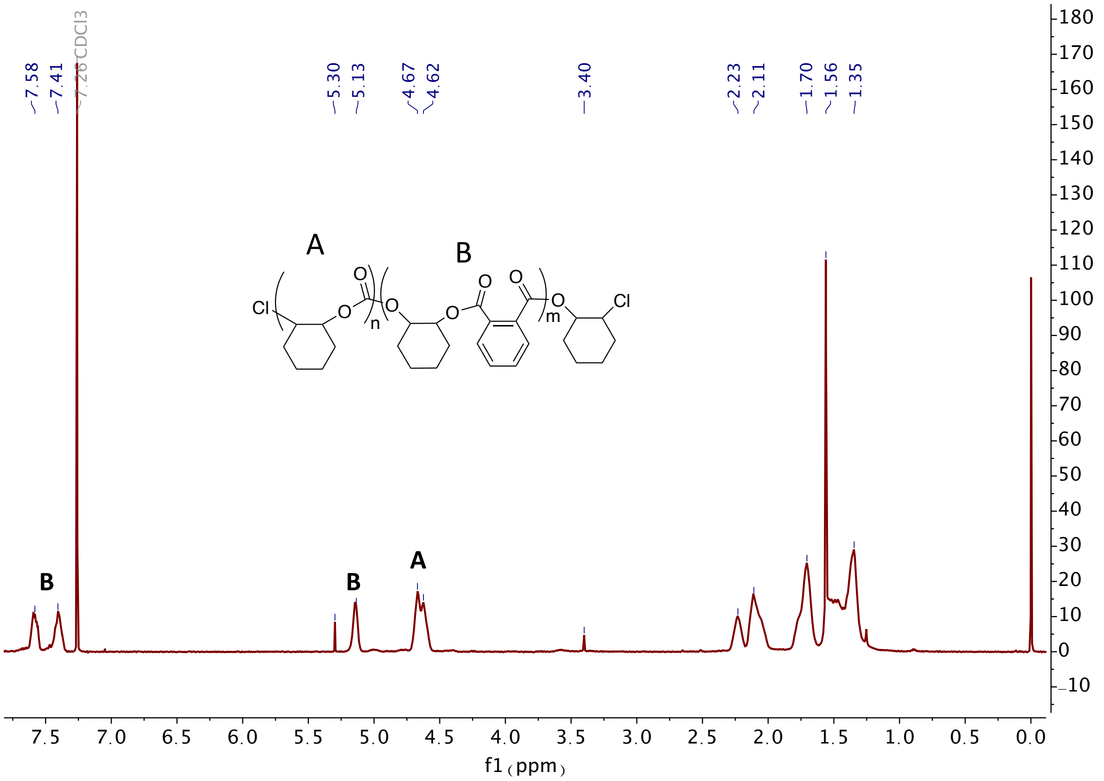

Figure E. 13. ^{1}H NMR (300 MHz, 298 K, $CDCl_3$) spectra of poly(CHC)-alt(CHO-PAH) block copolymer.

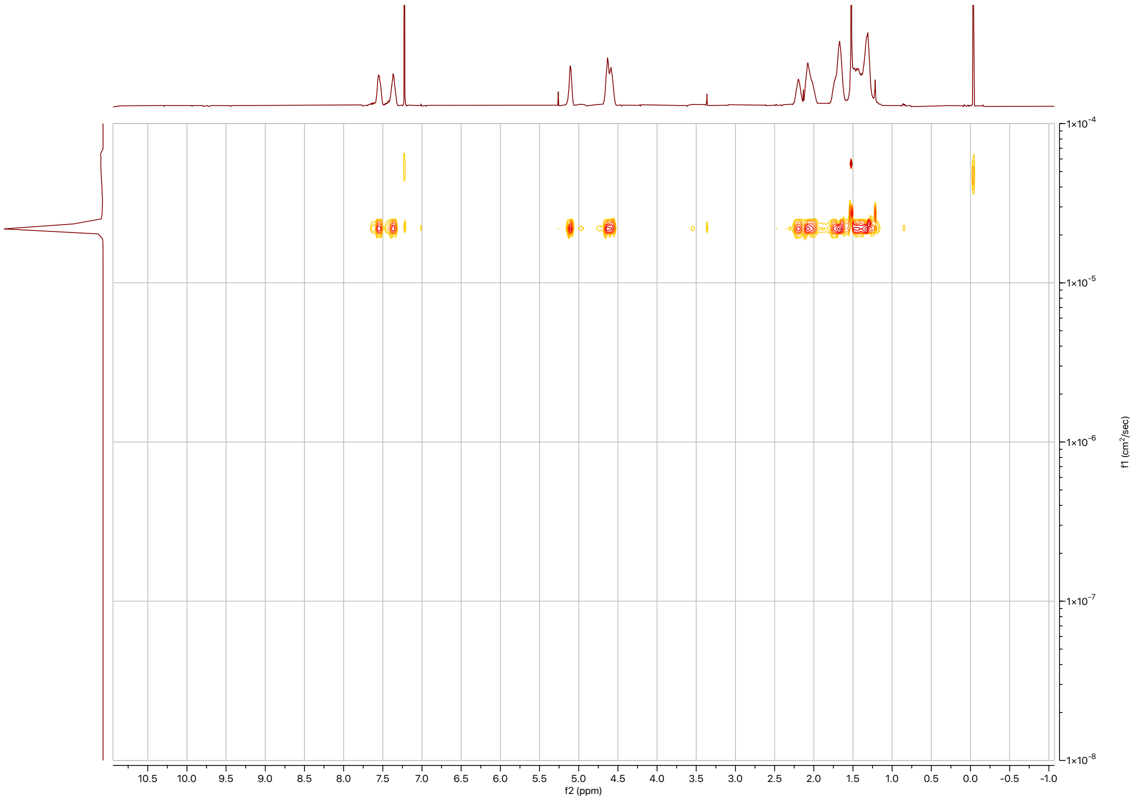

Figure E. 14. 2D DOSY NMR spectra (500 MHz, 298 K, $CDCl_3$) of poly(CHC)-alt(CHO-PAH) block copolymer.

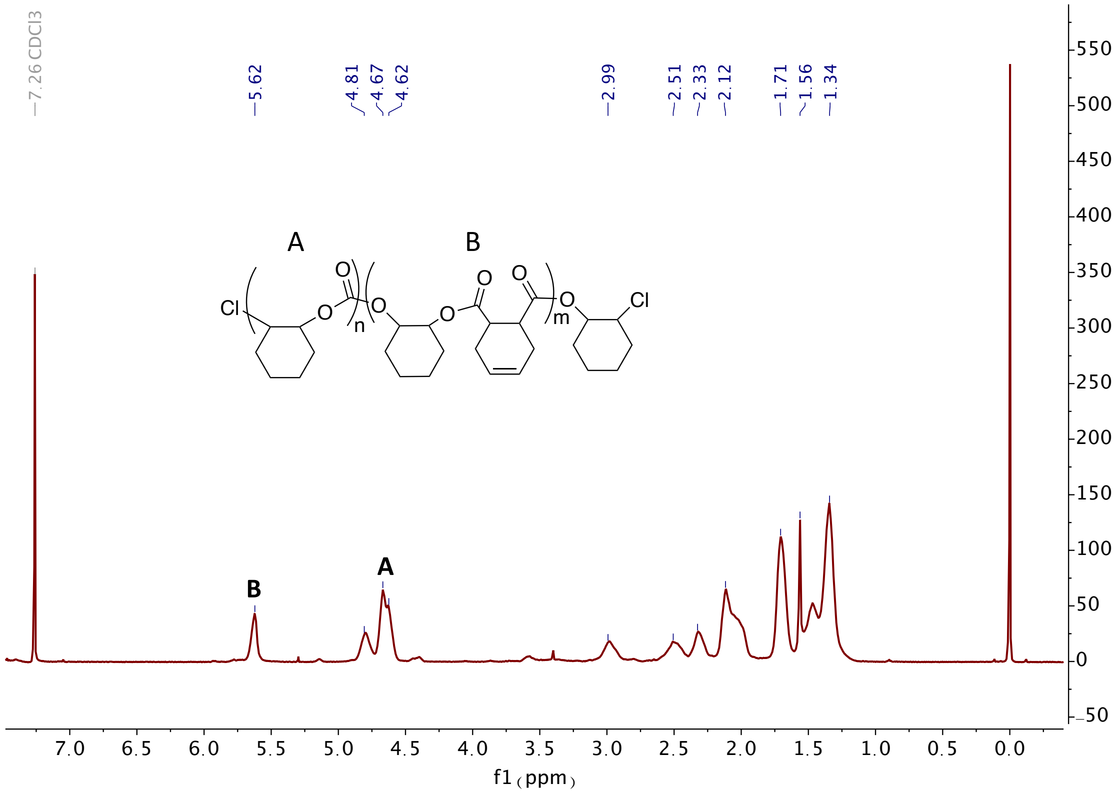

Figure E. 15. ^{1}H NMR (300 MHz, 298 K, $CDCl_3$) spectra of poly(CHC)-alt(CHO-CDA) block copolymer.

Figure E. 16. 2D DOSY NMR spectra (500 MHz, 298 K, $CDCl_3$) of poly(CHC)-alt(CHO-CDA) block copolymer.

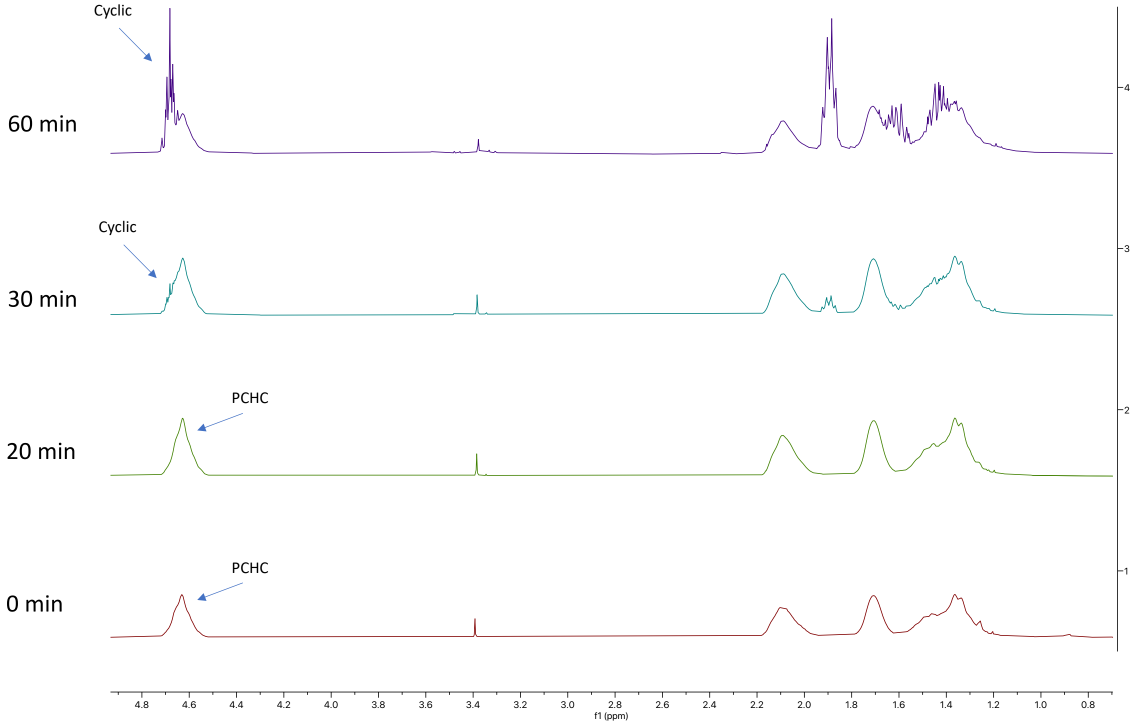

Figure E. 17. Stacked ^{1}H NMR (300 MHz, 298 K, $CDCl_3$) spectra of BCF catalyzed PCHC degradation experiments

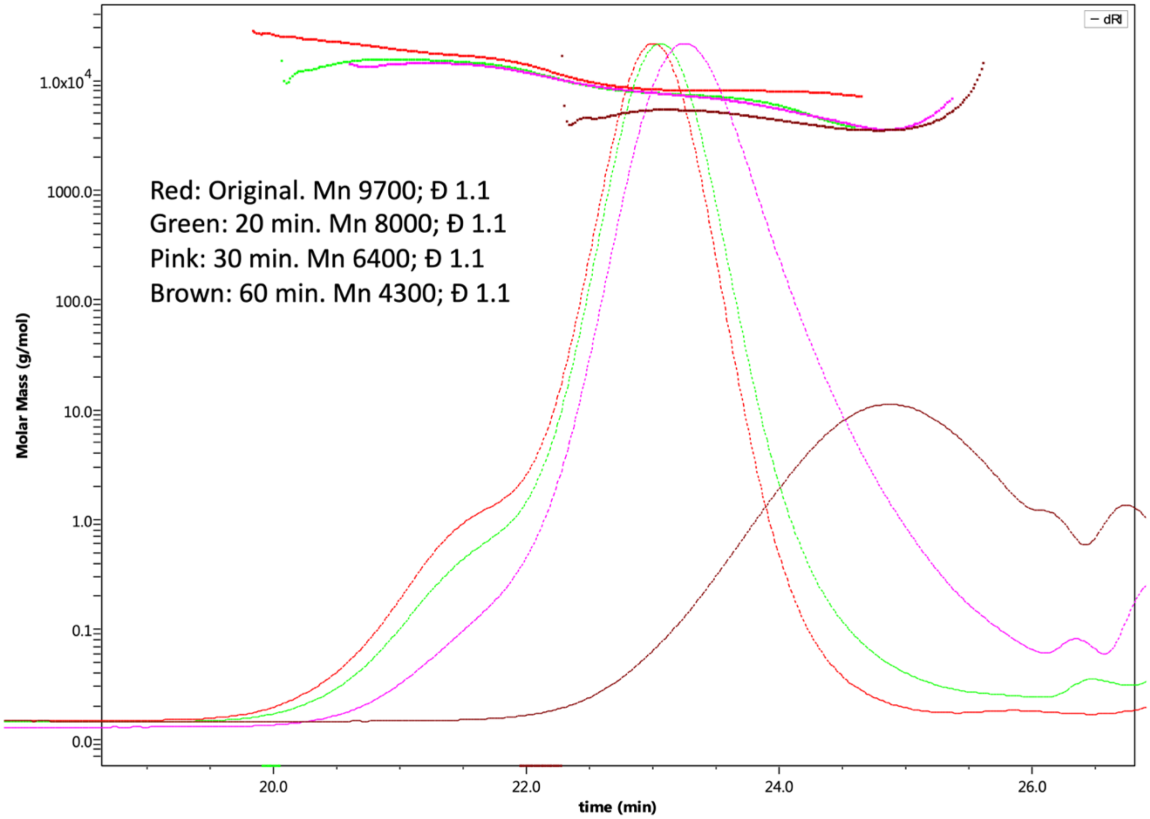

Figure E. 18. GPC overlay of BCF catalyzed PCHC degradation experiments.